Project Submission Form

Student name: Kieran Joyce

Student number: 53693104

Project title: Green Photochemistry: Solar synthesis of fine chemicals, development of novel porphyrin nano structured solid supported sensitizers and implementation of a novel photochemical microflow reactor.

Supervisor: Dr. Kieran Nolan

Declaration

I hereby certify that this material, which I now submit for assessment on the programme of study leading to the award of Doctor of Philosophy is entirely my own work, that I have exercised reasonable care to ensure that the work is original, and does not to the best of my knowledge breach any law of copyright, and has not been taken from the work of others save and to the extent that such work has been cited and acknowledged within the text of my work.

Signed: _____

ID No.: _____

Date: _____

Table of Contents

Project Submission Form i

Table of Contents ii

Dedication vii

Acknowledgements vii

Abstract ix

Chapter 1: Literature survey 1

1.1 Singlet oxygen 2

1.2 Sensitizers 8

1.3 Photooxygenation reactions 16

1.4 Green chemistry & photochemistry 26

1.5 Solar reactor technology 29

1.6 Thesis proposal 33

1.7 References 36

Chapter 2: Heterogeneous dye sensitized photooxygenation of 1,5-dihydroxynaphthalene, α-terpinene and β-citronellol 38

2.1 Introduction 39

2.2 Laboratory scale photooxygenation of 1,5-DHN, β-citronellol and α-terpinene 40

2.3 Solar dye sensitized photooxygenations 56

2.4 Conclusion 71

2.5 Experimental 74

2.6 References 90

Chapter 3: Heterogeneous dye sensitized photooxygenations: Immobilisation of sensitizers onto Merrifeld resins…….....91

3.1 Introduction 92

3.2 Results and discussion.....94

3.3 Conclusion.....112

3.4 Experimental 114

3.5 References 122

Chapter 4: Heterogensous dye sensitized photooxygenation of α-terpinene: Immobilisation of TCPP and TCPPZn onto silica nano particles…... 123

4.1 Introduction 124

4.2 Results and discussion.....129

4.3 Conclusion.....159

4.4 Experimental 161

4.5 References 170

Chapter 5: Design and implementation of a novel photochemical microflow bubble reactor for dye sensitized photooxygenations…….....171

5.1 Introduction 172

5.2 Development of photochemical microflow reactor.....177

5.3 Results and discussion.....180

5.4 Conclusion.....201

5.5 Experimental 203

5.6 References 209

Chapter 6: Heterogeneous dye sensitized photooxygenations utilizing a novel photochemical microflow bubble reactor…….....210

6.1 Introduction 211

6.2 Results and discussion.....220
6.3 Conclusion.....241
6.4 Experimental.....243
6.5 References.....248
Thesis Conclusion.....249
Appendix.....252

Abbreviations

°C	Degrees Celsius
^{13}C NMR	Carbon thirteen nuclear magnetic resonance
^{1}H NMR	Proton nuclear magnetic resonance
AGR	Average global radiation
APTES MNPs	APTES encapsulated magnetic nano particles
APTES SNP's	APTES encapsulated silica nano particles
APTES	(3-aminopropyl)-triethoxysilane
cm^{-1}	Wavenumber
DCM	Dichloromethane
DLS	Dynamic light scattering
DMF	Dimethyl formamide
DMSO	Dimethyl sulfoxide
DMSO-d6	Deuterated dimethyl sulfoxide
e.g.	For example
EDC	1-Ethyl-3-(3-dimethylaminopropyl)carbodiimide
et al.	and others
EtOAc	Ethyl acetate
EtOH	Ethanol
Fe_3O_4	Iron oxide
FeSEM	Field emission scanning electron microscopy
g	Gram
Hrs	Hours
Hz	Hertz
IPA	Isopropyl alcohol
IR	Infrared
J	Joule
L	Liter
MeOH	Methanol
Min	Minutes

mM	Milli molar
mmol	Millimole
MNPs	Magnetic nano particles
mol	Mole
MR	Merrifield resin
NHS	N-hydroxysuccinimide
nm	Nano meters
OA	Oleic acid
ppm	Parts per million
PS	Particle size
PTC	Parabolic trough collector
RB	Rose Bengal
SEM	Scanning electron microscopy
STY	Space time yield
TAA	tert-Amyl alcohol
TCPP APTES MNPs	TCPP functionalised MNPs
TCPP APTES SNPs	TCPP functionalised APTES SNP’s
TCPP	meso-Tetra-(4-carboxyphenyl)porphine
TEOS	Tetraethyl ortho silicate
TLC	Thin layer chromatography
UV/Vis	Ultraviolet-visible spectroscopy
VOC	Volatile organic compounds
α	Alpha
β	Beta
λ	Wavelength (nm)
μL	Microliter

Dedication

Dedicated to Mam, Dad and Elaine; three people in my life who at different stages ensured failure was never an option.

Acknowledgements

Firstly, I would like to thank Dr. Kieran Nolan for his guidance, patience and supervision throughout this project. Secondly, I would like to thank the Environmental Protection Agency for their funding under the STRIVE initiative.

I would also like to thank the technical staff; Veronica, Damien, Vinny, Ambrose, Mary and Catherine. Without their efforts and patience the bulk of the work required for this project could not have been accomplished.

I would also like to thank all of the friends who I have made over the years here at DCU (you know who you are). Wihtout you guys to distract me from all the negative results this thesis would have never been written.

Finally, and most importantly I would like to thank Elaine. Without your unwavering support and love this really would not have been possible. Now, let the next adventure begin!

Abstract

This work describes the homogeneous dye sensitized photooxygenations of 1,5-dihydroxynaphthalene (1,5-DHN), β-citronellol and α-terpinene in a series of low molecular weight alcohols under both artificial light (500 W halogen lamp) and natural light (sunlight) conditions. The reactions were assessed for greenness using the twelve principles of green chemistry and several key factors were identified as having a significant negative impact on this greenness. These were primarily, waste generation due to column chromatography, high water wastage due to essential cooling and high electrical energy demand.

Upon identification of these factors, sensitizers were covalently bound to a series of solid supports including; Merrifield resins, silica nano particles and magnetic iron oxide nano particles. Covalent immobilisation of sensitizers onto these solid supports allowed for their facile removal from the reaction mixture post irradiation via centrifugation or external magnetic field. This subsequently eliminated column chromatography. Recyclability studies were also performed.

Furthermore, a low energy demanding photochemical microflow bubble reactor was developed. This system, in addition to the elimination of water cooling also saw significant increases in percent conversions to products under homogeneous conditions. Furthermore, in conjunction with silica and iron oxide solid support sensitizers superior energy efficiencies and space time yields were also achieved.

Chapter 1

Literature survey

1.1 Singlet oxygen

1.1.1 History of singlet oxygen

Gaseous singlet oxygen was first discovered by astrophysicists in 1924 however it wasn't until 1931 that Hans Kautsky postulated that the reactive intermediate in dye photosensitized reactions was an activated species of molecular oxygen.[1] Kautsky adsorbed trypaflavine (a dye) and leucomalachite green (an oxygen acceptor compound) onto SiO_2 gel beads between 0.23 and 1.2 mm in diameter. These were then mixed and irradiated in the presence of oxygen. Kautsky noticed that the leucomalachite green was converted to malachite green. As there was no solvent present Kautsky concluded that a chemically active gas must have been responsible for the reaction.[2] He postulated that the dye absorbed light and transferred the energy to oxygen converting it to an activated form allowing it to undergo a chemical reaction with the oxygen acceptor (Scheme 1.1).

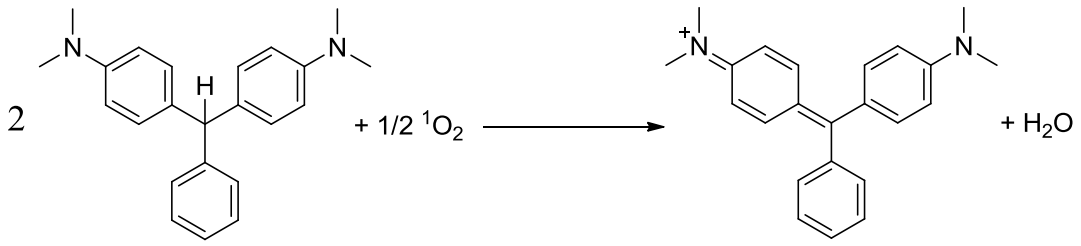

Scheme 1.1: Kautsky's reaction for activated oxygen.

Unfortunately, Kautsky's theory was widely rejected due to lack of direct evidence and with the advent of World War II his theory along with research into this area was largely forgotten. However, in 1963 Kahn [3] *et al* published a paper entitled *"Red chemiluminescence of molecular oxygen in aqueous media"* which built upon the work of H.H Siegler.[4] While spectroscopically measuring the reaction of hydrogen peroxide with sodium hypochlorite Siegler reported a newly found chemiluminescence. Kahn *et al* investigated this faint red chemiluminescence further and identified two separate peaks at 6334 and 7032 Å with a base width of 100 and 125 Å respectively. These two peaks were attributed to the ground state ($^3\Sigma$) and the first excited singlet state ($^1\Delta$) of molecular oxygen.

1.1.2 Molecular orbital theory of singlet oxygen

Oxygen (O_2) is a diatomic molecule and is electronically unique in terms of diatomic molecules as each oxygen atom has an equal number of valence electrons. As a consequence of this the Highest Occupied Molecular Orbital (HOMO) of O_2 in its ground state holds two spin parallel electrons (Figure 1.1).[5] Consequently, molecular oxygen is a ground state triplet. This is unusual for diatomic molecules, nitrogen for example finds its ground state in its singlet form as too does hydrogen and the halogens. Figure 1.1 below shows the electronic configuration of ground state oxygen and nitrogen.

However, the ground state of oxygen can be converted by electronic excitation to the more reactive singlet form which is also diamagnetic (Figure 1.2).

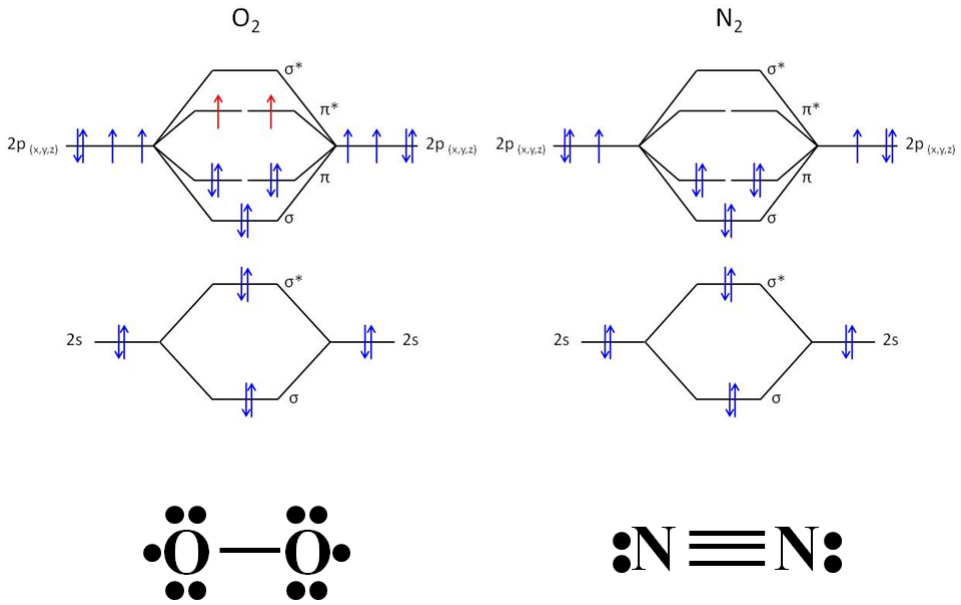

Figure 1.1: Electronic configuration and Lewis structures of ground and excited state molecular oxygen and nitrogen.

Molecular oxygen has two low lying singlet excited states $^1\Delta$ and $^1\Sigma$ which are 94 and 132 kJ/mol higher in energy than the ground triplet state ($^3\Sigma$). Both of the excited singlet states of oxygen are chemically reactive but the short life time of the higher state $^1\Sigma$ means that almost all reactions of singlet oxygen involve the lower

excited state $^1\Delta$. The electronic configuration of the HOMO for ground ($^3\Sigma$) and excited states ($^1\Delta$ and $^1\Sigma$) are shown Figure 1.2.

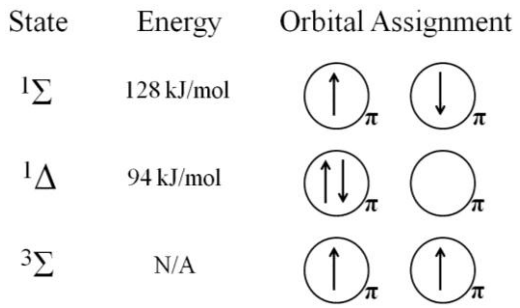

Figure 1.2: HOMO electronic configurations for ground and excited state oxygen.

1.1.3 Methods of singlet oxygen generation

There are several methods of singlet oxygen generation including; chemical and thermal methods, photolytic decomposition of ozone, electric discharge and dye sensitization.

1.1.3.1 Chemical generation of singlet oxygen

Chemical production of singlet oxygen ($^1O_2$) usually involves the reaction of hydrogen peroxide with hypochlorites or hypobromites to yield singlet oxygen quantitively (Scheme 1.2).[6,7]

$$H_2O_2 + NaOCl \rightarrow H_2O + NaCl + {}^1O_2$$

Scheme 1.2: Production of $^1O_2$ from the reaction of H_2O_2 with sodiumhypochlorite.

An alternative to using hypochlorite has become available in the form of molybdate ions in a water in oil (W/O) microemuslion (Scheme 1.3). The molybdate ions act as a catalyst to form singlet oxygen from hydrogen peroxide according to the equation in Scheme 1.3.[8] Both of these methods are attractive owing to the fact that the yield of singlet oxygen in each case is quantitative.

$$2H_2O_2 + MoO_4^{2-} \rightarrow 2H_2O + {}^1O_2$$

Scheme 1.3: Production of $^1O_2$ from the reaction of H_2O_2 with molybdate anions.

1.1.3.2 Thermal generation of singlet oxygen

Thermal production of singlet oxygen usually involves the decomposition of various endoperoxides at elevated temperatures. 9,10-Anthracene endoperoxides are one common source for the production of singlet oxygen in this manner.[9-11] Another source is 3,3'-(1,4-naphthylidene) diproprionate ($NDPO_2$, Scheme 1.4).[12]

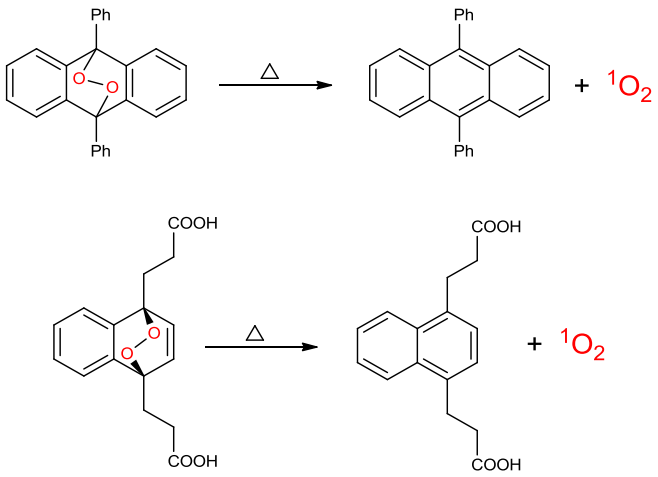

Scheme 1.4: Thermal decomposition of an anthracene derivative and $NDPO_2$ to yield $^1O_2$.

1.1.3.3 Photolytic decomposition of ozone

Photolytic decomposition of ozone also produces singlet oxygen in high yields. However, the initial cost of generating ozone is high and the process as a whole is not cost effective. Other reports demonstrate the reaction of ozone with certain organic compounds to yield organic trioxides and tetraoxides which then readily decompose to liberate singlet oxygen.[13] Again however, the initial cost of the ozone generation nullifies the cost efficiency of the process.

1.1.3.4 Dye sensitized generation of singlet oxygen

Singlet oxygen was generated solely via dye sensitized methods throughout this thesis. Consequently, we will focus on this method throughout the remainder of this text and the mechanism of this process will be discussed further in this section.

All photochemical reactions, including dye sensitized photooxygenations are governed by the Grotthus-Draper and the Stark-Einstein laws.

The Grotthus-Draper law states that light must be absorbed by a molecule in order for a photochemical change to take place.[14]

The Stark-Einstein law states that a molecule need only absorb one quantum of light and all of its photochemical processes arise from the resulting excited state.

The Jablonski diagram (Figure 1.3) illustrates these two laws and the resulting phenomena that arise from the absorption of a photon of light by a dye or sensitizer molecule.

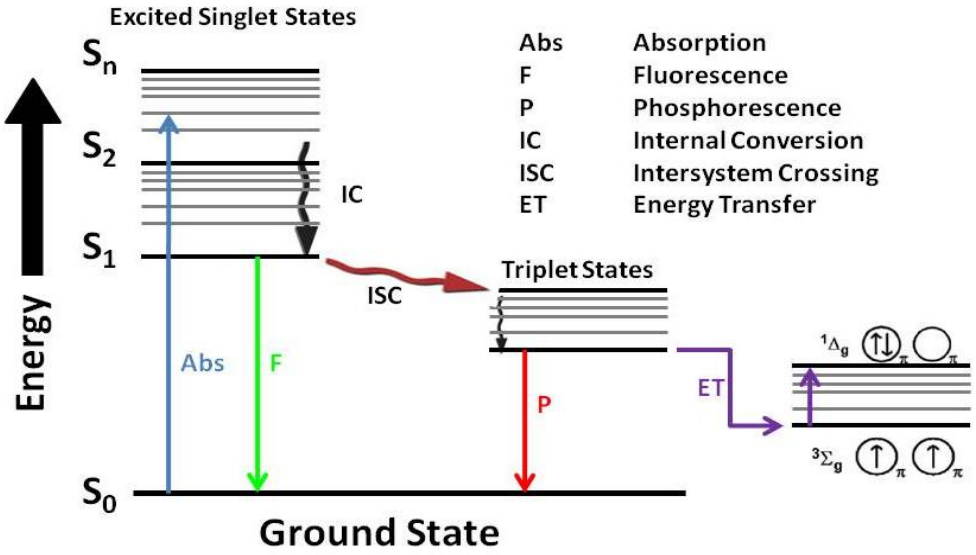

Figure 1.3: Jablonksi diagram.

For a dye sensitized photooxygenation to occur a dye or sensitizer molecule must first absorbe a photon of light. The energy gained during this process promotes an electron from the HOMO of its ground singlet state (S_0) to an excited singlet state (S_n) depending on the energy of the incident photon. From this excited singlet state a physical radiationless process know as internal conversion occurs. Dissipation of the gained energy to the surrounding solvent molecules through bond vibrations returns the excited state electron back down to its first excited singlet state (S_1). This

process is also known as vibrational relaxation.[15,16] From this first excited singlet state two separate phenomena can occur; fluorescence or intersystem crossing (ISC). Fluorescence is a radiative process that involves the return of the excited electron to its ground singlet state with the emission of a photon of light proportional to the energy difference between the first excited and ground singlet states. For this reason the light emitted by a molecule is rarely if ever the same wavelength of the incident photon.[17] Intersystem crossing (ISC) is a radiationless transition between two electronic states having different multiplicities. This results in another vibrationally excited molecule but in a lower electronic state.[18] Although ISC is quantum mechanically forbidden, it occurs due to spin-orbit and spin-spin coupling. Spin-orbit coupling is a phenomenon where by the magnetic field generated by the electron orbital motion generates enough torque to flip the spin of the electron.[18] Spin-spin coupling is the interaction between the magnetic fields of two orbiting electrons. However, it should be noted that spin-spin coupling is negligible in comparison to spin-orbit coupling. Overall, ISC results in either; 1) direct conversion of the first excited singlet state to the first excited triplet state ($S_1 \rightarrow T_1$) or, 2) conversion of the first excited singlet state to a high energy triplet state ($S_1 \rightarrow T_n$).

Once a dye or sensitizer molecule is in its excited triplet state two process can occur; phosphorescence or chemical quenching. Phosphorescence is a radiative process where the excited triplet state is returned to its ground singlet state with the emission of a photon of light equal to the energy difference between the first excited triplet state and the ground singlet state. Phosphorescence is longer lived than fluorescence since it is a forbidden process resulting in long life times for the triplet state. Chemical quenching is the transfer of the excess energy of the excited triplet state to another molecule (via a collision) resulting in the return of the excited triplet state to the ground singlet state. If ground triplet state molecular oxygen is the molecule that collides with the excited triplet state sensitiser it can become excited to its reactive singlet state and can then undergo a variety of photooxygenation reactions.

1.2 Sensitizers

1.2.1 Rose Bengal (RB)

Rose Bengal (CAS No: 152-74-9) or 4,5,6,7-tetrachloro-2′,4′,5′,7′-tetraiodofluorescein is a common xanthene based dye (Figure 1.4). Its name has connections to the red symbolic spot worn at the part of the hair by Bengali women to symbolize marriage.

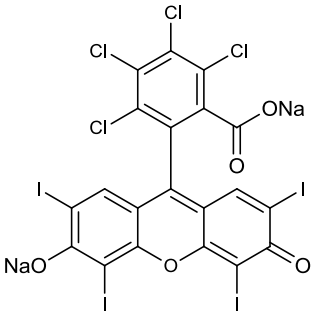

Figure 1.4: Structure of rose Bengal disodium salt.

The disodium salt form of rose Bengal (CAS No: 632-69-9) is commercially available (it is this form of the dye that was used during this work). Rose Bengal disodium salt is highly soluble in polar solvents making it an ideal candidate for use as a sensitizer for dye sensitized photooxygenations. In addition, it absorbs strongly within the visible region again making it an ideal sensitizer when using either solar or artificial "white" light (Figure 1.5). The wavelength of maximum absorbance (λ-max) and the extinction coefficient (ε) are both solvent dependant. Rose Bengal has a λ-max at 556 nm with an extinction coefficient of 135,000 $M^{-1}cm^{-1}$ in methanol.[19] Table 1.1 shows the λ-max value for rose Bengal disodium salt in a variety of solvents of importance to this work.

Table 1.1: λ-max values for rose Bengal disodium salt in various solvents.

Solvent	H_2O	EtOH	MeOH	Acetone	IPA
λ-max (nm)	546	558	556	562	562

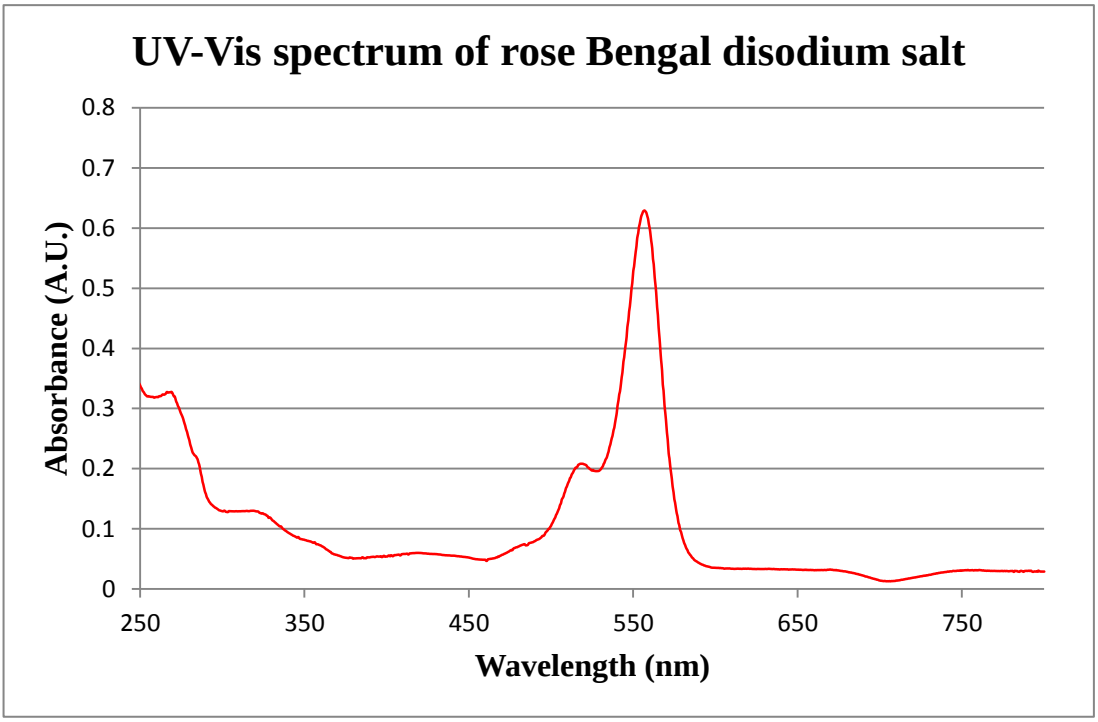

Figure 1.5: UV-Vis spectrum of rose Bengal disodium salt in methanol.

Rose Bengal disodium salt, when irradiated produces almost exclusively singlet oxygen due to the high level of intersystem crossing to its triplet state where it is quenched by molecular oxygen. This makes it ideal for Type II photooxygenations. Singlet oxygen quantum yields (Φ^1O_2) of up to 81 % have been reported for rose Bengal disodium salt in methanol.[20] Rose Bengal is also reported to have singlet oxygen quantum yields between 0.75 and 0.8 in H_2O and up to 0.76 in ethanol.[21, 22] Due to these physical properties rose Bengal is primarily used as an inexpensive, robust sensitizer during dye sensitized photooxygenations.[23-25]

1.2.2 Methylene blue (MB)

Methylene blue (CAS No: 61-73-4) or 3,7-bis(dimethylamino) phenazathionium chloride is a typical phenothiazine dye (Figure 6). It has a deep green/black colour while in its solid form but it provides a deep blue colour in solution. Similar to rose Bengal, methylene blue also absorbs strongly in the visible region. However, unlike rose Bengal, methylene blue has two distinct absorption bands with λ-max values of approximately 290 and 650 nm (Figure 1.7).

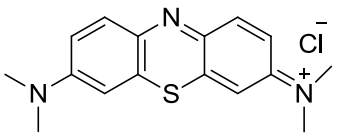

Figure 1.6: Structure of methylene blue (MB).

Methylene blue has a λ-max of 664 nm in H_2O with an extinction coefficient of 76,000 $M^{-1}cm^{-1}$.[26] In isopropyl alcohol (IPA), methylene blue has extinction coefficients of 73,680 and 97,200 $M^{-1}cm^{-1}$ at 275 and 640 nm, respectively. Methylene blue has also been reported to have singlet oxygen quantum yields of 0.50 – 0.57 in methanol and up to 0.57 in dichloromethane.[27-29] These relatively high singlet oxygen quantum yields in conjunction with good solubility in polar solvents makes methylene blue another ideal candidate for the use as a sensitizer in dye sensitized photooxygenations.

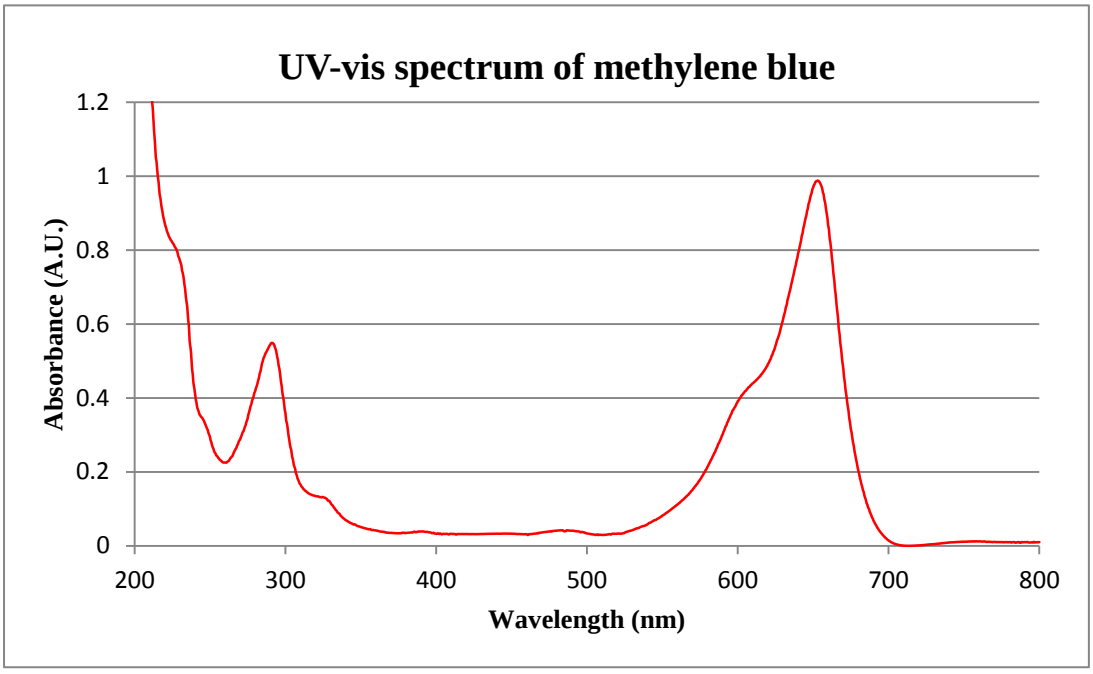

Figure 1.7: UV-Vis spectrum of methylene blue in methanol.

1.2.3 Tetraphenylporphyrin (TPP)

Tertaphenyl porphyrin (CAS No: 917-23-7) is a synthetic heterocyclic compound similar to naturally occurring porphyrins. Porphyrins are dyes and cofactors found in haemoglobin and cytochromes and are related to chlorophyll and vitamin B_{12}. Natural porphyrins are generally complicated molecules showing low symmetry and usually contain polar substituents. In contrast, tetraphenyl porphyrin is a symmetrically substituted porphyrin derivative that is very hydrophobic. This hydrophobicity results in the fact that TPP is usually only soluble in non-polar solvents such as chloroform or dichloromethane. The first report for the synthesis of porphyrins was put forward by Rothemund.[30] In this process pyrrole and formaldehyde were heated to 150 °C in a sealed tube for 36 hours in a solution of pyridine to produce porphyrin. Substituted aldehydes such as benzaldehyde could be used to synthesize TPP however, yields were typically low (<10 %). Adler and Longo *et al* revisited the work of Rothemund and modified the procedure, replacing the pyridine with propionic acid.[31] By refluxing pyrrole and benzaldehyde in propionic acid TPP could be synthesized in 30 minutes with yields of 20-25 %; however, the product often contained up to 5 % chlorin which was extremely difficult to remove (Scheme 1.5). In 1987 Lindsey *et al* further improved the synthesis of TPP by reacting equimolar amounts of pyrrole, benzaldehyde and triethyl orthoacetate in anhydrous DCM under a N_2 atmosphere for 1 hour at room temperature. The reaction is catalysed by the addition of boron trifluoroetherate or trifluoro acetic acid to form tetraphenylporphyrinogen. After one hour an oxidising agent such as 2,3-dichloro-5,6-dicyanobenzoquinone (DDQ) or 2,3,5,6-tetrachlorobenzoquinone (p-chloranil) is added and the solution refluxed for 1 hour. This oxidising agent converts the tetraphenylporphrinogen to the aromatic porphyrin (Scheme 1.5). Using this method Lindsey was able to obtain yields of up to 50 %.[32]

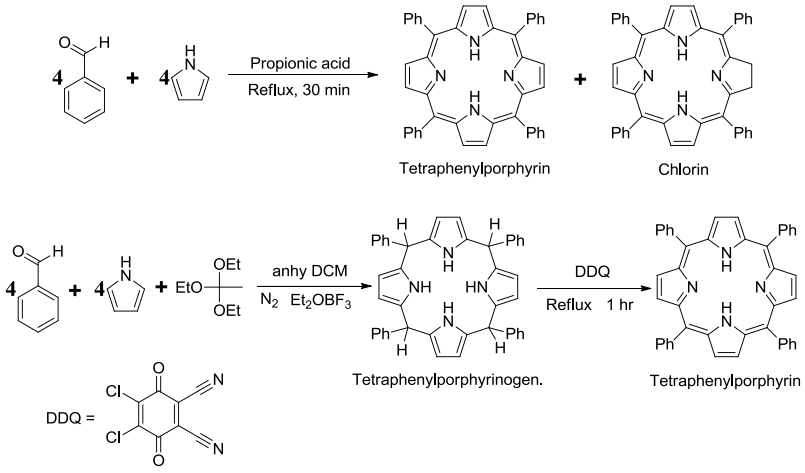

Scheme 1.5: Synthesis of TPP via the Adler and Lindsey methods.

Similar to rose Bengal and methylene blue TPP also absorbs strongly in the visible region (Figure 1.8). The λ-max for TPP is found at 417 nm (Soret band) in chloroform with four additional absorbance bands (Q-bands) at 514, 549, 589 and 644 nm respectively.[33] Table 1.2 shows the Soret and Q bands for TPP in various other solvents.

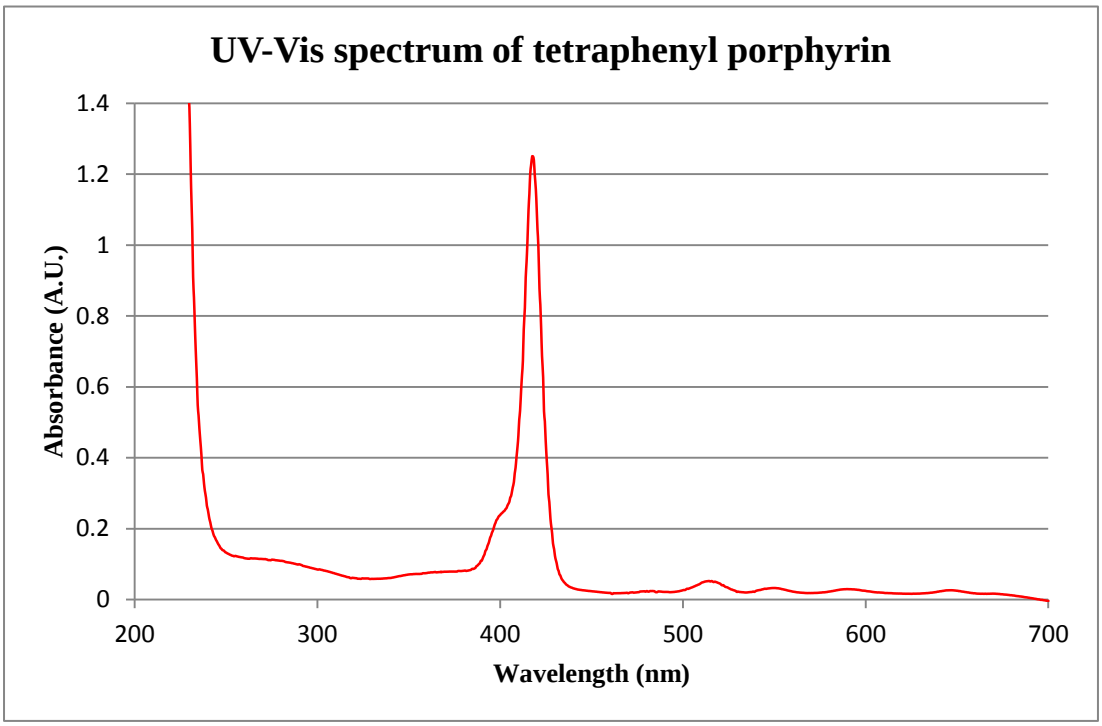

Figure 1.8: UV-vis spectrum of TPP in DCM.

Table 1.2: Soret and Q bands for TPP in various solvents.

Solvent	λ-max (Soret band)	Q_1	Q_2	Q_3	Q_4
DMF	417	514	550	593	646
CH_2Cl_2	415	514	549	589	645
$CHCl_3$	417	514	549	589	644

TPP also exhibits a strong extinction coefficient between 230,000 – 270,000 $M^{-1}cm^{-1}$ depending on the solvent. In addition to this TPP has been reported to show high quantum yields of intersystem crossing (Φ_{isc}) and singlet oxygen production. Quantum yields of intersystem crossing of 0.82 and singlet oxygen quantum yields of up to 0.63 have been reported for TPP in benzene.[34]

TPP can also coordinate to [2^+] metal ions. The chelation of either zinc or palladium ions to the porphyrin centre have been reported to increase the quantum yields of both intersystem crossing and singlet oxygen production (Table 1.3).[34]

Table 1.3: Quantum yields of ISC and $^1O_2$ production for TPP, TPPZn(II) and TPPPd(II).

Porphyrin	Φ_{isc}	Φ^1O_2
TPP	0.82	0.63
TPP(Zn)	0.88	0.83
TPP(Pd)	1.00	0.88

1.2.4 Meso-tetra-(4-carboxyphenyl) porphyrin (TCPP)

Meso-tetra-(4-carboxyphenyl) porphyrin (TCPP) (CAS No: 14609-54-2) is a water soluble derivative of TPP. The addition of four polar carboxylic moieties at the meso position also allows for solubilisation of TCPP in alcoholic solvents. Using 4-formyl benzaldehyde, TCPP can be synthesized by either the Rothemund/Adler or Lindsey method. Yields of up to 25 % can be achieved by the Rothemund/Adler method (Scheme 1.6).

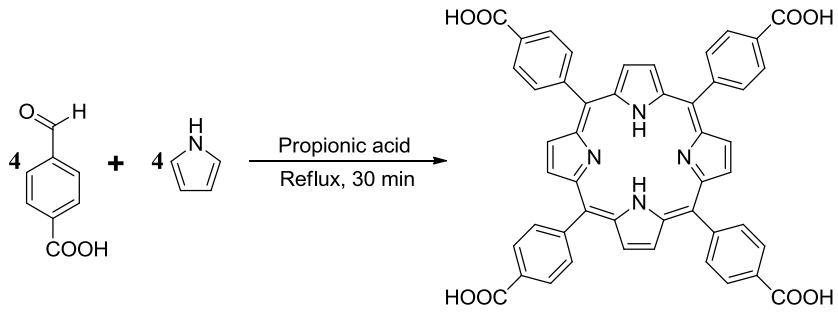

Scheme 1.6: The Rothmund/Adler synthesis of TCPP.

Similar to tetraphenyl porphyrin TCPP also shows a measured λ-max (Soret band) at 415 nm and four distinct Q bands at 514, 545, 590 and 645 respectively in IPA. It has an extinction coefficient of 375,000 $M^{-1}cm^{-1}$ with regards to the Soret band. Figure 1.9 shows the UV-Vis spectrum of TCPP in methanol.

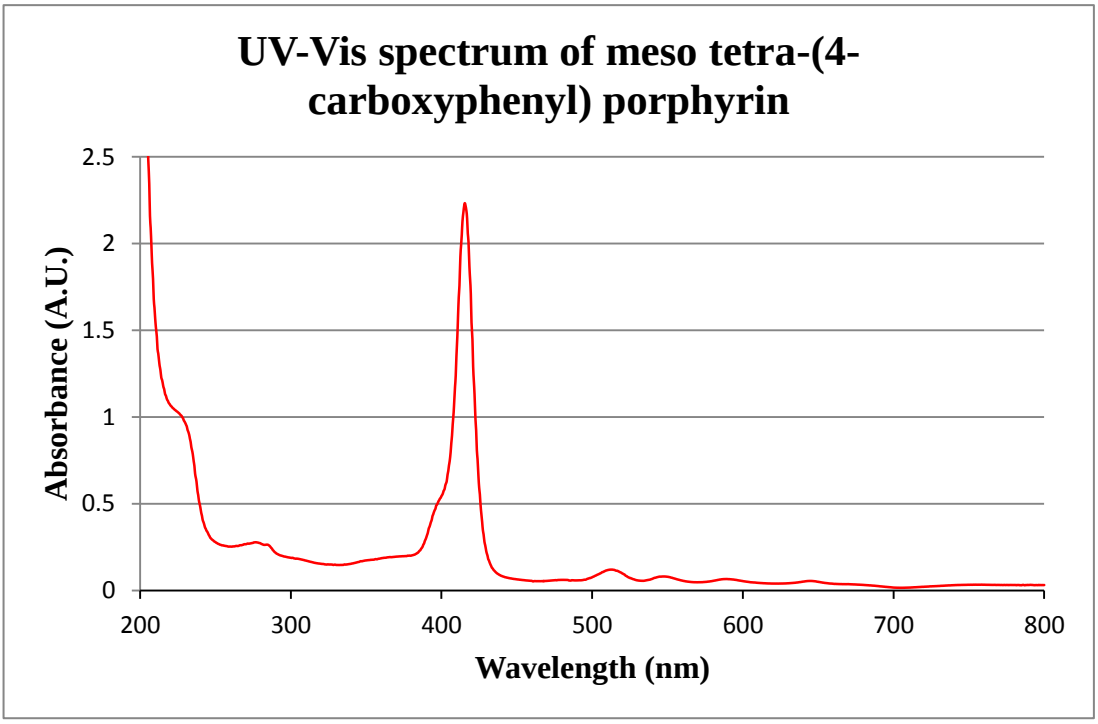

Figure 1.9: UV-Vis spectrum of TCPP in methanol.

Singlet oxygen quantum yields of up to 0.58 have been reported for TCPP in water.[34] Table 1.4 shows the λ-max, extinction coefficient and the Q bands for TCPP dissolved in water, ethanol and IPA.[35, 36]

Table 1.4: λ-max for Soret and Q bands of TCPP in various solvents.

Solvent	λ-max (soret band)	Q_1	Q_2	Q_3	Q_4	ε
H_2O	418	515	549	591	646	3.94×10^5
EtOH	419	514	548	588	645	-
IPA	430	514	545	590	645	8.7×10^4

1.3 Photooxygenation reactions

Photooxygenation reactions are defined by IUPAC as "light induced oxidation reactions where molecular oxygen is incorporated into the final product(s)".[18] Singlet oxygen can undergo three main types of photooxygenation; Type I, II and III. All three reaction mechanisms result in the incorporation of molecular oxygen into the products.

1.3.1 Type I Photooxygenations

Type I photooxygenations involve the interaction of the triplet excited state sensitizer, Sens(T_1) with the substrate (Sub) to produce substrate and sensitizer radicals (Scheme 1.8). This usually occurs via homolytic cleavage of a C-H bond on the substrate. The radical substrate can then further react with ground or triplet state oxygen to produce a substrate-O_2 radical which can subsequently react with either another substrate molecule, propagating the reaction, or with a sensitizer radical resulting in termination. This process allows for chain propagation and as such quantum yields for this type of photooxygenation can often exceed unity.

$$\text{Sens}(S_0) + h\nu \rightarrow \text{Sens}(S_1) \rightarrow \text{Sens}(T_1) \qquad \text{(excitation and ISC)}$$

$$\text{Sens}(T_1) + \text{R-H} \rightarrow {}^{\bullet}\text{SensH} + {}^{\bullet}\text{R} \qquad \text{(initiation)}$$

$${}^{\bullet}\text{R} + O_2({}^3\Sigma) \rightarrow \text{R-O-O}^{\bullet}$$

$$\text{R-O-O}^{\bullet} + \text{R-H} \rightarrow \text{R-O-O-H} + {}^{\bullet}\text{R} \qquad \text{(propagation)}$$

$$\text{R-O-O}^{\bullet} + {}^{\bullet}\text{SensH} \rightarrow \text{R-O-O-H} + \text{Sens}(S_0) \qquad \text{(termination)}$$

Scheme 1.7: Type I photooxygenation mechanism.

1.3.2 Type II photooxygenations

Type II photooxygenations begin with the initial excitation of the sensitizer ($S_0 \rightarrow S_1$) followed by intersystem crossing (ISC) to its triplet excited state ($S_1 \rightarrow T_1$). The sensitizer then transfers its energy directly to ground state molecular oxygen, $O_2({}^3\Sigma)$, in a radiation-less process. The excited singlet state oxygen ($O_2{}^1\Delta$) is then capable

of reacting with the substrate in a variety of ways to yield products with molecular oxygen incorporated into them (Scheme 1.8). Cycloadditions such as [4+2] and [2+2] are the most common mechanisms by which molecular oxygen becomes incorporated into the product. Singlet oxygen can also undergo a Schenck "ene" reaction with alkenes to produce hydroperoxides. The final products of both Type I and Type II reactions are often the same. However, in most cases the final products are attributable to Type II processes due to the high quantum yield of sensitizer triplet state quenching by molecular oxygen and the high reactivity of the resulting singlet oxygen species.

$$Sens(S_0) + h\nu \rightarrow Sens\ (S_1) \rightarrow Sens\ (T_1) \qquad \text{(excitation and ISC)}$$

$$Sens(T_1) + O_2(^3\Sigma) \rightarrow Sens(S_0) + O_2{}^1\Delta$$

$$O_2{}^1\Delta + Substrate \rightarrow Product$$

Scheme: 1.8: Type II photooxygenation mechanism.

1.3.3 Type III photooxygenations

Type III photooxygenations involve an electron transfer between the singlet excited state sensitizer (S_1) and the substrate to generate a sensitizer radical anion and a substrate radical cation (Scheme 1.9). In general the excited state sensitizer is the electron acceptor during this process. Although ground state molecular oxygen, $O_2(^3\Sigma)$, is capable of reacting with either the sensitizer radical anions or the substrate radical cations the reaction with the sensitizer radical anions dominates due to the much greater speed of this reaction resulting in the formation of superoxide anions ($O_2^{\bullet -}$). These superoxide anions then react with substrate radical cations to produce oxygenated products.

$$Sens(S_0) + h\nu \rightarrow Sens\ (S_1) \quad \text{(excitation)}$$

$$Sens(S_1) + Substrate \rightarrow Sens^{\bullet -} + Substrate^{\bullet +}$$

$$Sens^{\bullet -} + O_2(^3\Sigma) \rightarrow Sens(S_0) + O_2^{\bullet -}$$

$$O_2^{\bullet -} + Substrate^{\bullet +} \rightarrow \text{Oxygenated product}$$

Scheme 1.9: Type III photooxygenation mechanism.

Although Type I, II and III photooxygenations compete with one another the final products are generally the same. Furthermore, the majority of product(s) formed are done so via the Type II mechanism. This is due to long triplet life times of the sensitizer and high quantum yields of singlet oxygen. For these reasons we will only concentrate on Type II photooxygenations throughout the remainder of this text.

1.3.3.1 Type II photooxygenation mechanisms

[4+2] photooxygenations

The mechanism of the [4+2] cycloaddition of singlet oxygen to conjugated dienes can be explained by a concerted Diels Alder process. In general the reaction is stereospecific and the presence of an electron donor group on the diene greatly increases the rate of reaction. Under this guise the singlet oxygen acts as the dienophile and adds to the less sterically hindered side of the conjugated diene resulting in the formation of an endoperoxide (Scheme 1.10). Such endoperoxides are often unstable and can decompose back to the diene (9,10-diphenylanthracene) under thermal conditions with the liberation of singlet oxygen (Section 1.1.3.2).[37] Subsequent reactions are also possible with the formation of new products as is the case with juglone formation.

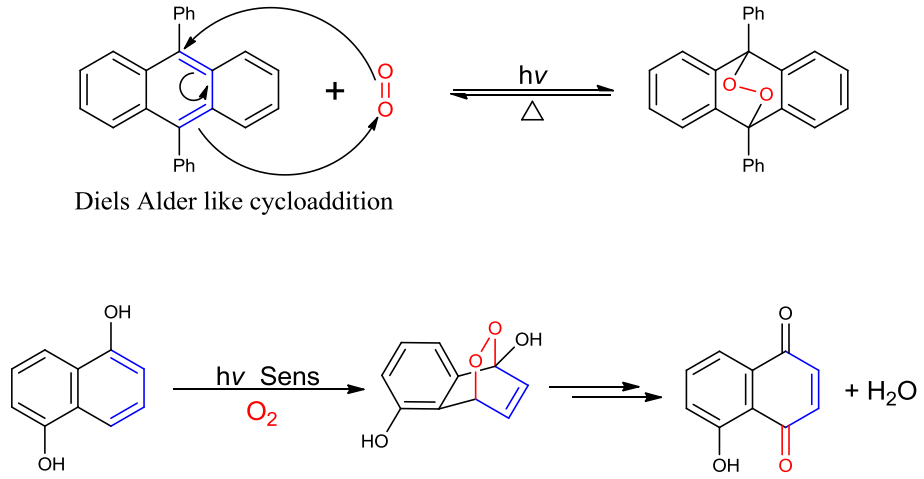

Scheme 1.10: [4+2] photooxygenation of 9,10-diphenylanthracene and 1,5-dihydroxynaphthalene.

Juglone can be found naturally in the leaves, roots, bark and husks of the black walnut tree (Juglans nigra) and other related plants. Within these plants it acts as an allelopathic compound (inhibits the growth of other plants) and as such it is sometimes used as a herbicide. However, juglone is more often used as a dye for textiles and inks and is also used as a colouring agent within the food and cosmetic industries.

A further example of a [4+2] photooxygenation is the dye sensitized photooxygenation of α-terpinene to ascaridole (Scheme 1.11). First isolated from chenopodium oil (American wormseed) by Huthig in 1908, ascaridole is a bicyclic monoterpene with an unusual bridging peroxide functionality. However, the correct structure was not elucidated until 1912 by Otto Wallach.[38 a-b] Soon after its isolation ascaridole was determined to have anthelmintic properties and was used to treat intestinal worm infections in both humans and livestock.[39] The first laboratory synthesis of ascaridole was reported by Schenck in 1944.[40] He used chlorophyll isolated from spinach leaves to perform the dye sensitized photooxygenation of α-terpinene to synthesize ascaridole on an industrial scale. Today, ascaridole is not used to treat humans due to its negative side effects but it is still used to treat livestock throughout the Central American countries. Additionally, it is still used in low concentrations within the perfume industry and also, to some extent, as a flavour compound.

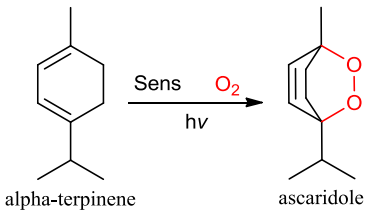

Scheme 1.11: The dye sensitized photooxygenation of α-terpinene to ascaridole.

The bridged endoperoxide functionality of ascaridole is unstable and even explosive at temperatures above 150 °C. Ascaridole can slowly decompose in air to give another natural compound para-cymene. This process can be safely achieved in the laboratory by reduction of ascaridole to the corresponding diol followed by dehydration to p-cymene (Scheme 1.12).

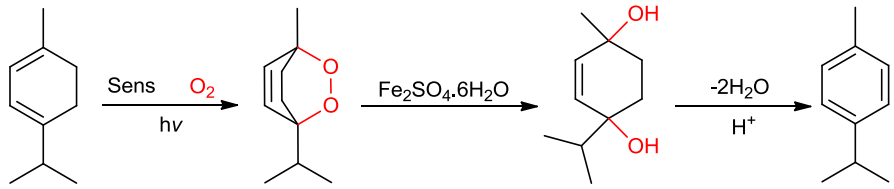

Scheme 1.12: Three step synthesis of p-cymene.

Despite evidence for a concerted mechanism for Type II photooxygenations, evidence also exists for a non-concerted process during dye sensitized photooxygenations. In 1976 Dewar and co-workers calculated that the reaction pathway through perepoxide and zwitterionic intermediates would be lower in energy than that of a concerted [4+2] cycloaddition reaction between singlet oxygen and 1,3-butadiene.[41] These calculations are reinforced by the experimental findings of Delogu and co-workers.[42] They observed the formation of an unexpected anti cycloadduct in high yield during the dye sensitized photooxygenation of bisdialine (Scheme 1.13). These results are inconsistent with a concerted mechanism but could be explained by the formation of a perepoxide intermediate which could then open up into a zwitterion allowing for the formation of both the syn and anti product.[42]

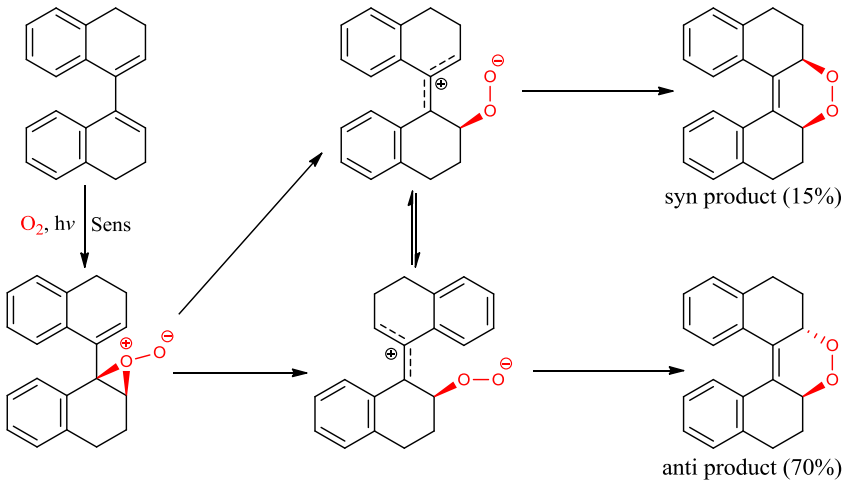

Scheme 1.13: Dye sensitized photooxygenation of bisdialine.

This data suggests that the reaction of singlet oxygen with conjugated dienes may not always follow a concerted [4+2] cycloaddition mechanism. The actual mechanism followed is substrate dependant, which is of no surprise, considering the very broad scope of molecules containing conjugated dienes capable of reacting with singlet oxygen. However, in most cases and those noted in this thesis, the final product(s) remain the same despite the mechanism and so adoption of a concerted mechanism is an adequate description of the photochemical process.

[2+2] Photooxygenations

The [2+2] cycloaddition of singlet oxygen to sufficiently activated alkenes was initially thought to follow a concerted mechanism in accordance with the Woodward-Hoffman rules. However, today it is generally accepted that the reaction proceeds through a zwitterionic intermediate resulting in a [2+2] cycloadduct (Scheme 1.14). Upon excitation singlet oxygen initially forms an exiplex with the alkene followed by formation of a zwitterion. This then rearranges to the [2+2] cycloadduct, in this case a dioxetane ring.

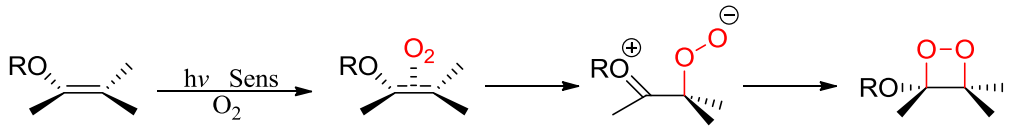

Scheme 1.14: The mechanism of addition of singlet oxygen to alkenes.

It should be stated for an alkene to be activated for the addition of singlet oxygen an electron withdrawing group (EWG) must be present alpha to the double bond.

The dioxetane rings that are formed through this process are often very unstable and readily decompose to give carbonyl compounds by a two step process involving a diradical intermediate (Scheme 1.15). The energy released is substantially greater than that required to populate either the (n,π*) singlet or triplet states of the carbonyl products and results in the emission of light. In general, the formation of triplet state carbonyl compounds is approximately 10 times greater than that of singlet state carbonyl compounds and as such the light emission detected is primarily due to phosphorescence.[37]

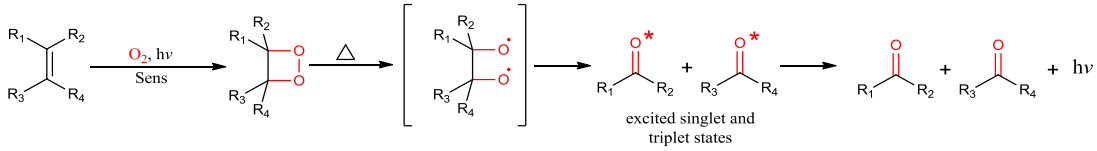

Scheme 1.15: Dioxetane formation and chemiluminescent decomposition.

The Schenck "ene" reaction

The Schenck "ene" reaction is very similar to the well known ene or Alder-ene reaction between alkenes with an allylic hydrogen and an enophile (sufficiently activated [EWG] π bonded molecule). However, in the Schenck "ene" reaction the enophile is exclusively singlet oxygen producing compounds with a hydroperoxide moiety (Scheme 1.16).

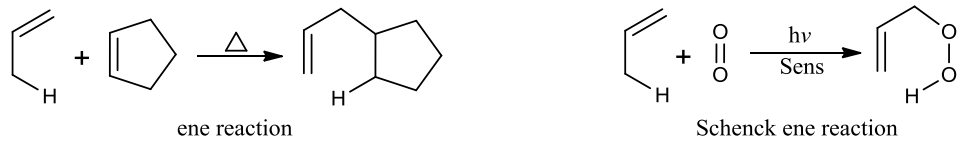

Scheme 1.16: The ene and Schenck ene reactions.

The Schenck "ene" reaction follows a concerted mechanism governed by the Woodward-Hoffman rules. The reaction is stereospecific and occurs suprafacially involving the abstraction of an allylic hydrogen. This results in the formation of a new σ bond and a 1,5-hydrogen shift. The frontier molecular orbital interaction occurs between the HOMO of the ene and the LUMO of the enophile (singlet oxygen). The HOMO of the ene is the combination of the π bonding orbital and the C-H bonding orbital of the allylic hydrogen (Scheme 1.17).

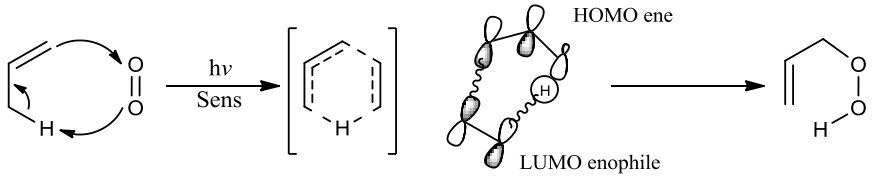

Scheme 1.17: The concerted Schenck "ene" reaction mechanism.

Consistent with this concerted pathway stereochemistry is conserved in the products and no cis-trans isomerisation occurs during the reaction. This allows for the introduction of a variety of functionalities at the allylic position in certain molecules. In addition, singlet oxygen favours attack from the less sterically hindered face of the substrate. The dye sensitized photooxygenation of β-citronellol is a good example of this Schenck "ene" reaction that is performed on a multi tonne scale annually by Symrise Ltd during the production of rose oxide.

Rose oxide is a natural compound derived mainly from the essential oil of Bulgarian roses.[43] It has four unique stereoisomers each of which has a different odour threshold measured in parts per billion (Figure 1.10). It is the *l*-cis(2S,4R) or (-)-cis form of rose oxide that it of greatest commercial value due to its use in high end perfumes. It requires over 3000 kg of Bulgarian roses to isolate only 1 kg of this

natural stereoisomer.[44] However, the four stereoisomers can be synthesized via a three step process beginning with the dye sensitized photooxygenation of β-citronellol (Scheme 1.18).

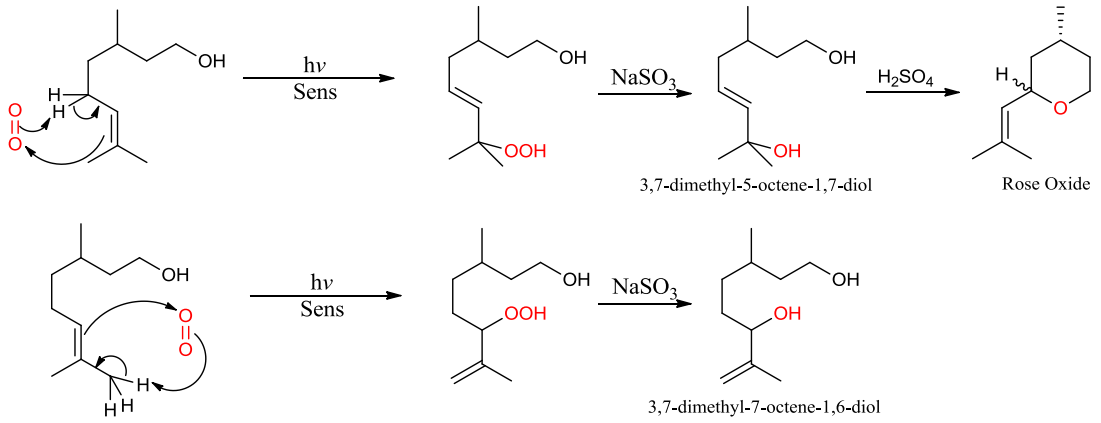

Scheme 1.18: The dye sensitized photooxygenation of β-citronellol to its corresponding hydroperoxides.

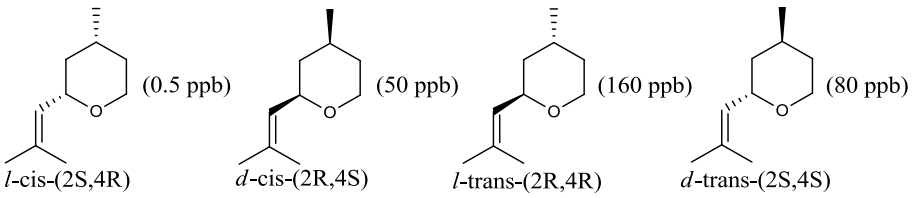

Figure 1.10: Four stereoisomers of rose oxide showing odour threshold.

As with [4+2] and [2+2] cycloadditions involving singlet oxygen there is also evidence that the ene reaction does not follow a concerted mechanism but rather a stepwise process involving perepoxide intermediates. During the [4+2] dye sensitized photooxygenation of 5-isopropyl-1,3-cyclohexadiene Davis *et al* [45] reported the formation of an ene product in addition to the [4+2] cycloadduct. The formation of these two products led to the conclusion that the two products came from the same intermediate, a perepoxide (Scheme 1.19).

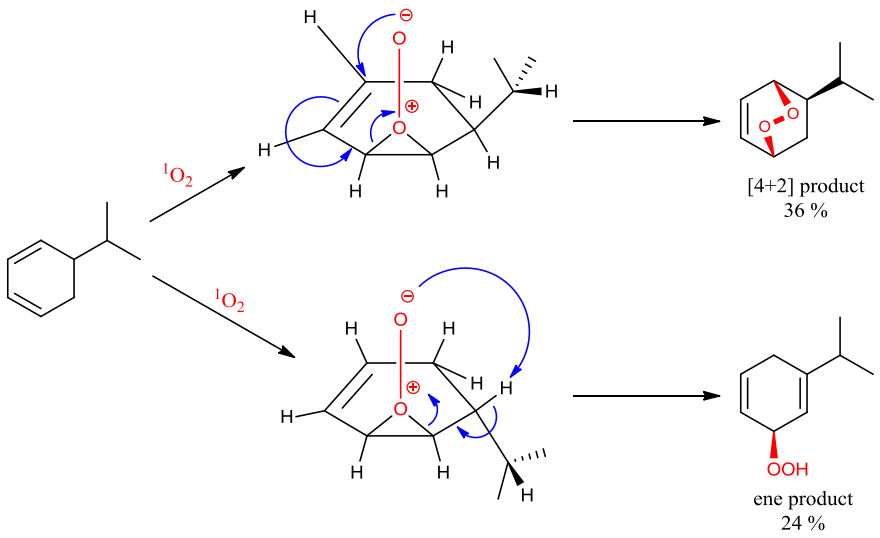

Scheme 1.19: Competing mechanisms showing [4+2] and ene products.

Photooxygenations are known to be complicated by the competition of the ene reaction with [4+2] and [2+2] cycloadditions in molecules where an allylic hydrogen is present. Matsumoto *et al* reported the formation of both ene and [2+2] products from the reaction of singlet oxygen with styrene derivatives (Scheme 1.20).[46]

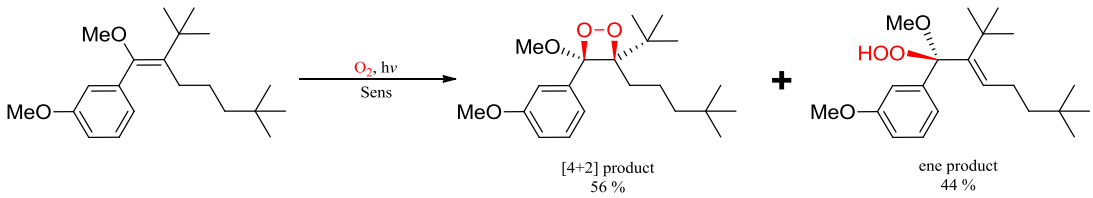

Scheme 1.20: Competing [4+2] and ene mechanisms.

It is clear that while the Woodward-Hoffman rules for pericyclic reactions can adequately explain the incorporation of molecular oxygen into a substrate via [4+2], [2+2] and Schenck ene mechanisms, there does exist some examples where these concerted mechanisms are not sufficient. However, these examples are few in number and it is generally accepted that the vast majority of [4+2] and ene reactions follow a concerted mechanism unless the final products indicate otherwise. Interestingly, the mechanism for the formation of dioxetanes has been debated more strongly. However, depending on the substrate and/or the final product(s) either a concerted [2+2] mechanism or a step wise process involving zwitterionic intermediates are acceptable.

1.4 Green chemistry & photochemistry

The concept of green or environmentally safe chemistry has been around for several decades but it wasn't until 1998 that Anastas and Warner defined green chemistry as the *"utilization of a set of principles that reduces or eliminates the use or generation of hazardous substances in the design, manufacture and application of chemical products."* [47] This set of principles consisted of 12 rules which are as follows:

1. It is better to prevent waste than to treat or clean up waste after it is formed.
2. Synthetic methods should be designed to maximise the incorporation of all materials used in the process into the final product.
3. Wherever practicable, synthetic methodologies should be designed to use and generate substances that possess little or no toxicity to human health and the environment.
4. Chemical products should be designed to preserve efficacy of function while reducing toxicity.
5. The use of auxiliary substances (e.g. solvents, separation agents, etc) should be made unnecessary wherever possible and, innocuous when used.
6. Energy requirements should be recognised for their environmental and economic impacts and should be minimised. Synthetic methods should be conducted at ambient temperature and pressure.
7. A raw material of feedstock should be renewable rather than depleting wherever technically and economically practicable.
8. Unnecessary derivatisation (blocking group, protection/deprotection, temporary modification of physical/chemical processes) should be avoided wherever possible.
9. Catalytic reagents (as selective as possible) are superior to stoichiometric reagents.
10. Chemical products should be designed so that at the end of their function they do not persist in the environment and break down into innocuous degradation products.

11. Analytical methodologies need to be further developed to allow for real-time, in-process monitoring and control prior to the formation of hazardous substances.

12. Substances and the form of a substance used in a chemical process should be chosen so as to minimise the potential for chemical accidents, including releases, explosions and fires.

Today, with depleting levels of fossils fuels, and rising average global temperatures it has become necessary to switch from fossil fuels and move towards green, renewable and sustainable energy sources. Although it is not possible to reverse the negative effects humans have had on this planet, it is imperative that to prevent any further long lasting damage. It is becoming important that the chemical and pharmaceutical industries move towards "*green chemistry*". By implementing the twelve principles of green chemistry it will be possible to reduce or even eliminate the use of toxic reagents, prevent the generation of waste and reduce or eliminate the need for solvents and high energy demanding processes within these industries.

As previously outlined light can be used to initiate an abundance of chemical reactions, some of which would otherwise require the use of harsh or toxic chemical reagents. One such example of this is the photooxygenation of 1,5-dihydroxynaphthalene to juglone. Traditional syntheses of juglone from 1,5-dihydroxynaphthalene required the use of harsh and toxic oxidants such as iodic or chromic acids.[48] However, under photochemical conditions the use of these toxic reagents is eliminated (Scheme 1.21). Furthermore the only side product produced during the reaction is water.

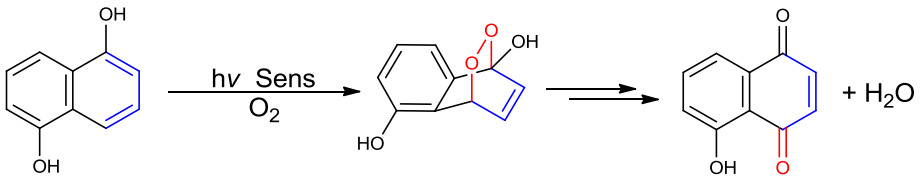

Scheme 1.21: Dye sensitized photooxygenation of 1,5-dihydroxynaphthalene to juglone.

Solar chemistry is a niche area of photochemistry that focuses on the initiation of photochemical reactions using solar radiation. In this manner it is considered to be a

further step towards “green” chemistry as it eliminates the need for energy demanding lamps (halogen, mercury and xenon) and replaces them with the ultimate renewable resource, solar radiation. Although a niche area of photochemistry, the research field of solar chemistry has grown rapidly in the last few years. As a direct result of this increased level of interest and research an abundance of solar technology has been developed to capture and utilise the sun’s rays for a variety of applications. These applications range from photovoltaic solar panels for electricity generation, water heating systems and waste water treatment systems to chemical synthesis technologies. As this work is concerned with the photochemical synthesis of several fine chemicals using solar light, the developing technology in this area of research will be discussed further.

1.5 Solar reactor technology

The earliest photochemical reactions were performed outdoors by Ciamician, Schenck and other early photo-chemists in uncooled flasks using natural sunlight (Figure 1.11). However, it was soon realised that this approach was impractical and with the development of new lamp technologies photochemistry moved "indoors" back into the laboratory.

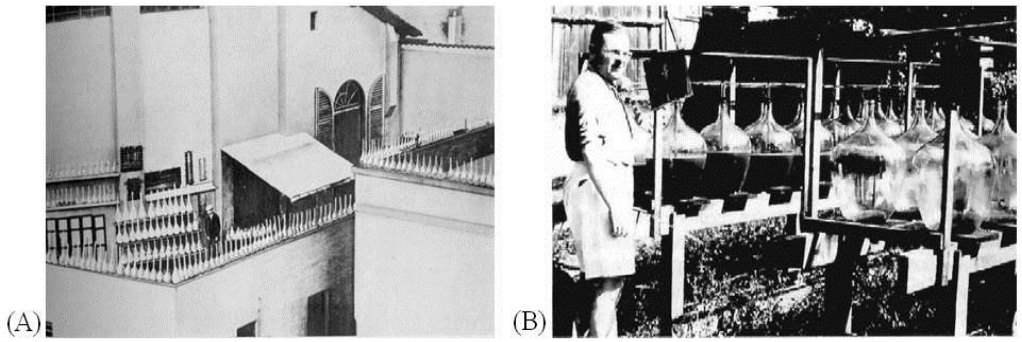

Figure 1.11: A) Ciamician's laboratory in Bologna, ca. 1912, and B) Schenck's production of ascaridole in Heidelberg, ca 1949.

1.5.1 Non concentrating solar reactors

A Schlenk flask can be used as a basic non concentrating solar reactor. However, more sophisticated designs such as those at the German Aerospace Centre (DLR) have been developed such as the flatbed reactor. Flatbed reactors are advantageous in the fact that they are designed to maximise the surface area exposed to the sun's incident rays. In addition, they are designed to have a short path length (~1 cm) to allow for irradiation of the entire reaction solution simultaneously. Also, as can be seen from Figure 1.12 internal cooling tubes can also be fitted during the construction process.

These types of non-concentrating reactors utilise both direct and diffuse light and are ideal for use in countries such as Germany or Ireland where up to 60 % of the light received annually is diffuse in nature.

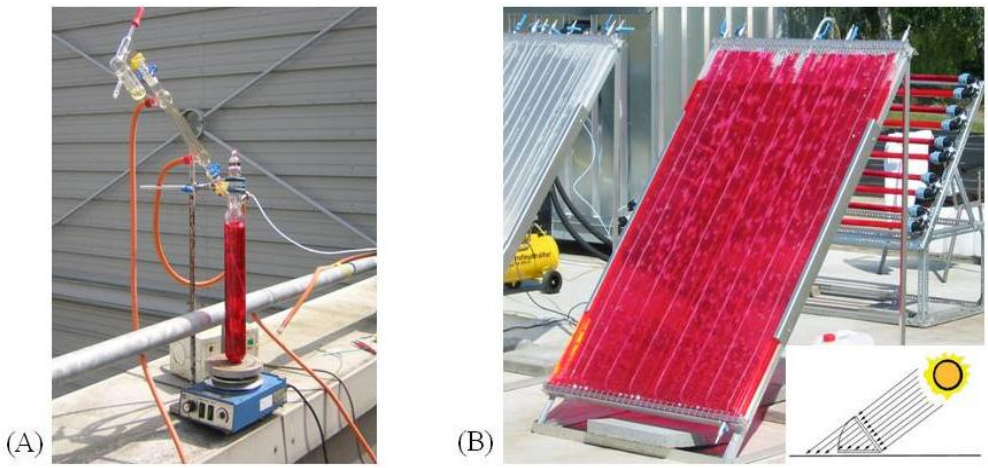

Figure 1.12: A) Schlenk flask set up for solar irradiation and B) flatbed reactor at the DLR in Cologne Germany.

In order to maximise the energy transfer from the sun to the reaction solution the angle of incidence of the sun rays to the surface of the flatbed reactor should be 90 °. As a general rule of thumb this can be achieved by adjusting the tilt of the flatbed reactor from the horizontal at an angle equal to the latitude of its current location plus 15 ° in winter and minus 15 ° in summer.

Other non-concentrating solar reactors include free falling film reactors, pressurised flat plate reactors and solar ponds.[49-51] The latter, as the name suggests, consists of an open pool exposed to the atmosphere and irradiated by the sun. Free falling film reactors have the reaction solution pass over a flat tilted surface coated with a catalyst and pressurised flat plate reactors seal the reaction solution from the atmosphere between two glass or pyrex plates.

1.5.2 Concentrating solar reactors

1.5.2.1 Parabolic trough collectors (PTCs)

Originally designed for solar thermal applications, parabolic trough collectors (PTCs) consist of a reflective parabolic trough with an energy absorbing tube centred at the focus of this parabola. In this way the parabola reflects all direct or perpendicular incident rays onto the energy absorbing tube with a concentration factor of up to 10. However, PTCs suffer from the disadvantage of only reflecting direct or perpendicular incident rays onto the centre tube. If the PTC is not aligned

with the suns azimuth and elevation, the efficiency of the system drops significantly. In order to address this issue, the PTCs (installed at the DLR in Cologne) are fitted onto dual axis mounting systems controlled by computer. This system continually monitors the sun's position and adjusts the position of the PTR accordingly to maintain an optimised incident angle (Figure 1.13).

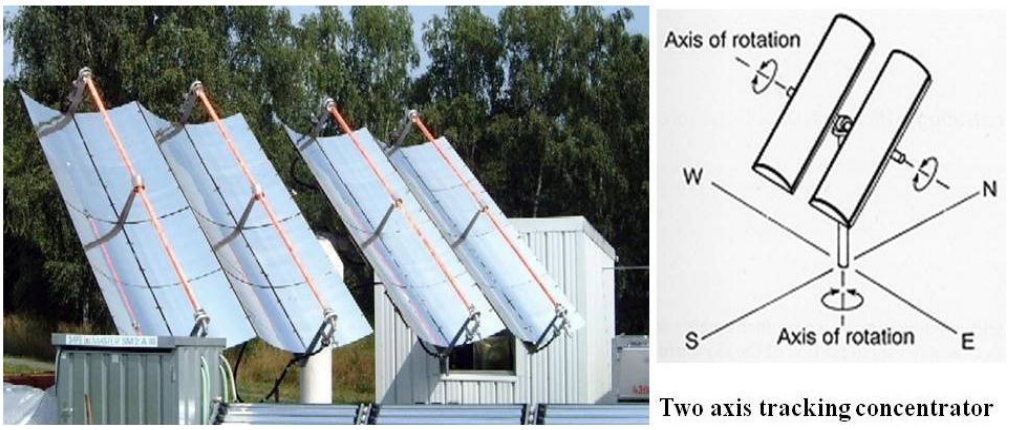

Figure 1.13: Parabolic trough collectors showing dual axis tracking.

The first photochemical application of the PTCs was the treatment of waste water. In order to adapt the PTCs for this purpose the central heat absorbing tube was replaced with a simple clear pyrex tube to allow for irradiation of the reaction solution. However, PTCs have since been adapted for synthetic photochemical reactions such as the PROPHIS loop at the DLR in Cologne, Germany. Here they have successfully performed the dye sensitized photooxygenations of β-citronellol and 1,5-dihydroxynaphthealene on a muliti-litre scale (up to 80 L).[25]

1.5.2.2 Compound parabolic trough collectors (CPC's)

Similar to PTCs, compound parabolic trough collectors (CPCs) were originally designed for solar thermal applications and were later adapted for waste water treatment and synthetic photochemistry. CPCs consist of a series of linked tubes each with two sections of reflective parabolic trough mounted below them. They can be seen as a combination of concentrating PTCs and non-concentrating systems such as the flatbed reactor. Similar to flatbed reactors they are static collectors and should be tilted from the horizontal accordingly. Unlike flatbed reactors, CPCs also

incorporate two modified sections of reflective parabolic trough mounted below the tubes. The addition of these two sections of reflective parabolic trough allows the CPC to utilize both direct and diffuse light. The modified parabolic trough can be seen in Figure 1.14 showing how both direct and diffuse light can be utilised by the system.

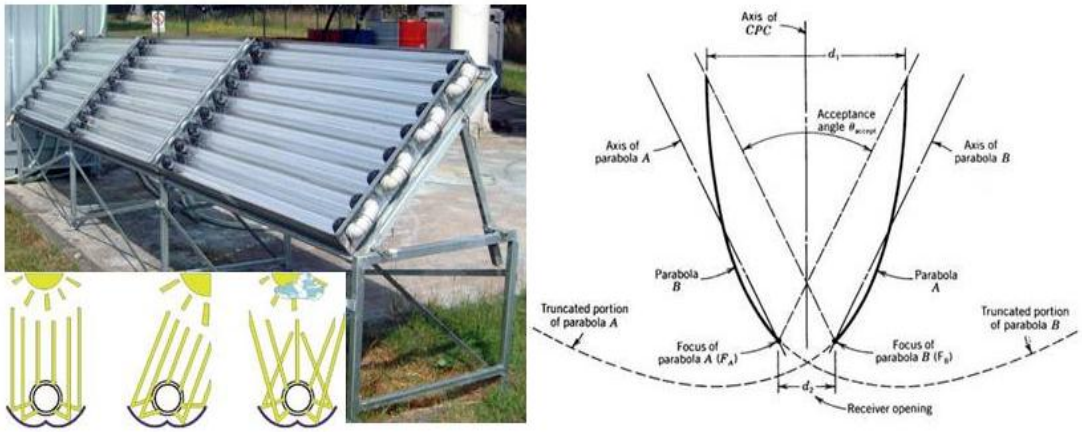

Figure 1.14 Compound parabolic trough showing two component parabolic trough sections.

Due to their utilisation of both diffuse and direct light CPCs are the ideal choice of solar reactor for use in locations of low annual levels of direct sunlight such as Ireland or Germany. The efficiency of traditional PTCs would suffer greatly at these locations and would only offer optimal yields several days a year due to the weather conditions. In addition to this the initial setup costs of a CPC would be significantly lower than that of a PTC.

1.6 Thesis Proposal

The dye sensitized photooxygenations of α-terpinene and β-citronellol are well documented within the literature and are already considered to be "green" or environmentally friendly reactions (Scheme 1.22). This is due to 100 % atom economy seen in the final products of the reactions. Although the synthesis of juglone provides 91 % atom economy the only side product of the reaction is water and as a result the reaction is also considered to be a "green" reaction.

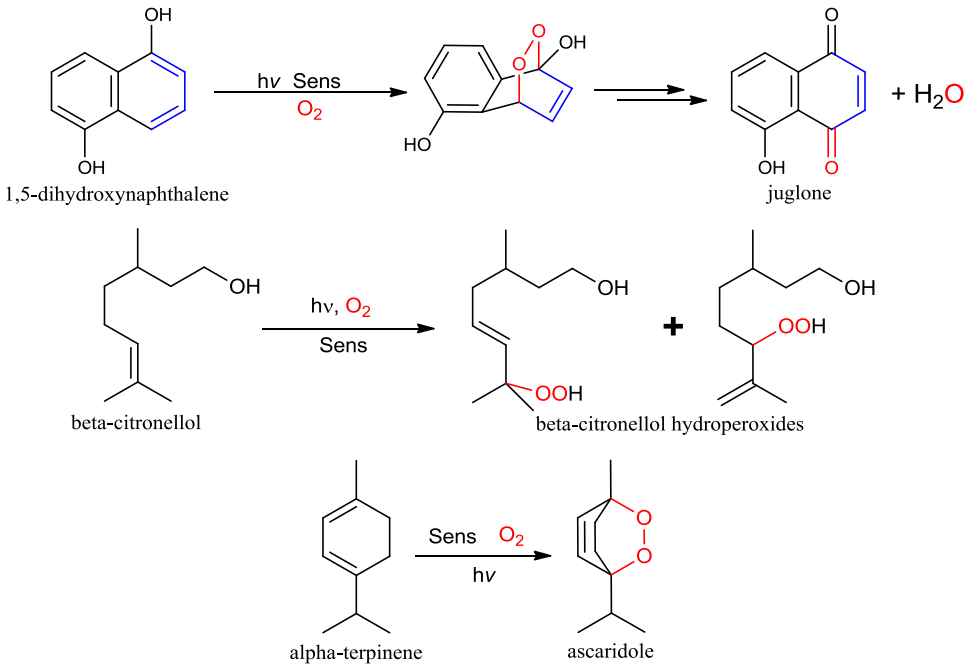

Scheme 1.22: Photooxygenation of 1,5-dihydroxynaphthalene, β-citronellol and α-terpinene.

Despite the general consensus of "greenness" within the literature for these reactions, it may be possible to significantly improve these reactions with respect to energy consumption and waste production. To achieve these goals the following parameters were to be investigated:

1) Can these three reactions be performed with a 500 W halogen lamp using various sensitizers (RB, MB, TPP and TCPP), and if so is the process really green?

Can the dye sensitized photooxygenations of 1,5-dihydroxynaphthalene, α-terpinene and β-citronellol be further improved using the twelve principles of green chemistry? To achieve this goal it will be first necessary to determine the best sensitizer (RB, MB, TPP and TCPP) and solvent (acetone, ethyl acetate and a variety of alcohols) for the optimization of singlet oxygen quantum yields. The results of these initial laboratory scale experiments will define the optimum reaction solvent and sensitizer for the targtted dye sensitized photooxygenation reactions.

2) Could the same photooxygenations be performed successfully under Irish solar conditions, reducing energy consumption, and if so is the setup of a multi liter scale pilot plant feasible?

In this work the target reactions will be performed using both Schlenck and flatbed reactors under Irish solar conditions. The flatbed reactors are large volume (4-8 L) solar reactors and are designed to allow for a high surface area to volume ratio. Correct alignment of these flat bed reactors with the suns incident rays should provide superior yields and/or conversion rates over the traditional Schlenk flasks. The results of these experiments will help to determine if a multi liter scale pilot plant could be set up at DCU for the solar synthesis of several fine chemicals.

3) Can the sensitizers be immobilized onto solid supports in order to eliminate purification and if so would they lose efficacy?

In accordance with the twelve principles of green chemistry only catalytic amounts of sensitizer are required for dye sensitized photooxygenation reactions under homogeneous conditions. However, it may be possible to immobilize selected sensitisers onto a series of different solid supports. This ‘hetergeneous approach’ would offer two key advantages over traditional homogeneous reaction conditions: Firstly, the sensitizer can be easily removed (filtration or centrifugation) and recycled. Secondly, as in the case of the photooxygenation of α-terpinene and β-citronellol, purification could be eliminated entirely. In order to do investigate the possibility of developing heterogeneous senesitisers three classes of solid supports

will be initially screened. These supports are; 1) Merrifield resins, 2) silica beads (200-300 nm) and 3) magnetic nano particles - iron oxide nano particles (~20 nm)

The results of these experiments will determine if the immobilization of sensitizers onto solid supports are feasible for dye sensitized photooxygenations.

4) Could a low energy consuming, low cost continuous flow system be developed and if so could it be used in conjunction with the solid supported sensitizers?

Recently, a low energy cost effective, continuous flow system has been developed by the Nolan group at DCU. This continuous flow system can irradiate up to 5 ml of solvent simultaneously allowing for gram scale synthesis and the light source ia a low energy fluorescent bulb, eliminating the high energy demand of the halogen, mercury and rayonet lamps. Furthermore, utilization of a low energy fluorescent bulb significantly reduces the thermal energy generated by the light source, eliminating the need for water cooling. This new photoreactor technology will be evaluated using the optimized photooxygenation reactions developed in point 1 and 3 above and the results will be compared to the solar experiments in point 2 to determine the 'Greenest' of these methodologies.

1.7 References

(1) Kautsky, H.; De Bruijn, H. *Naturwiss* **1931**, *19*, 1043.

(2) Kautsky, H. *Trans. Faraday. Soc.* **1939**, *35*, 216.

(3) Khan, A. U.; Kasha, M. *J. Chem. Phys.* **1963**, *39*, 2105.

(4) Seliger, H. H. *Anal. Biochem.* **1960**, *1*, 60-65.

(5) Kearns, D. R. *Chem. Rev.* **1971**, *71*, 395-427.

(6) Khan, A. U.; Kasha, M. *J. Chem. Phys.* **1963**, *39*, 2105-2106.

(7) Maetzke, A.; Knak Jensen, S. J. *Chemical Physics Letters* **2006**, *425*, 40-43.

(8) Aubry, J.M.; Bouttemy, S. *J. Am. Chem. Soc.* **1997**, *119*, 5286-5294.

(9) Balci, M. *Chem. Rev.* **1981**, *81*, 91-108.

(10) Turro, N. J.; Chow, M.; Rigaudy, J. *J. Am. Chem. Soc.* **1979**, *101*, 1300-1302.

(11) Turro, N. J.; Ramamurthy, V.; Liu, K. C.; Krebs, A.; Kemper, R. *J. Am. Chem. Soc.* **1976**, *98*, 6758-6761.

(12) Di Mascio, P.; Sies, H. *J. Am. Chem. Soc.* **1989**, *111*, 2909-2914.

(13) Stary, F. E.; Emge, D. E.; Murray, R. W. *J. Am. Chem. Soc.* **1976**, *98*, 1880-1884.

(14) Rohatgi-Mukherjee, K. K. In *Introducing Photochemistry;* Fundamentals of Photochemistry; New Age International Publishers: India, 1986; pp 3-4.

(15) Becker, R. S.; Dolan, E.; Balke, D. E. *J. Chem. Phys.* **1969**, *50*, 239-245.

(16) Pecourt, J. L.; Peon, J.; Kohler, B. *J. Am. Chem. Soc.* **2001**, *123*, 10370-10378.

(17) Gentemann, S.; Medforth, C. J.; Forsyth, T. P.; Nurco, D. J.; Smith, K. M.; Fajer, J.; Holten, D. *J. Am. Chem. Soc.* **1994**, *116*, 7363-7368.

(18) Verhoeven, J. W. *Pure Appl. Chem.* **1996**, *68*, 2223-2286.

(19) Rauf, M. A.; Graham, J. P.; Bukallah, S. B.; Al-Saedi, M. A. S. *Spectrochimica Acta Part A: Molecular and Biomolecular Spectroscopy* **2009**, *72*, 133-137.

(20) Escalada, J. P.; Gianotti, J.; Pajares, A.; Massad, W. A.; Amat-Guerri, F.; Garca, N. A. *J. Agric. Food Chem.* **2008**, *56*, 7355-7359.

(21) Lambert, C. R.; Kochevar, I. E. *J. Am. Chem. Soc.* **1996**, *118*, 3297-3298.

(22) Lamberts, J. J. M.; Schumacher, D. R.; Neckers, D. C. *J. Am. Chem. Soc.* **1984**, *106*, 5879-5883.

(23) Bernhard, J. M. *Micropaleontology* **2000**, *46*, 38-46.

(24) Oelgemoller, M.; Healy, N.; de Oliveira, L.; Jung, C.; Mattay, J. *Green Chem.* **2006**, *8*, 831-834.

(25) Oelgemoller, M.; Jung, C.; Ortner, J.; Mattay, J.; Zimmermann, E. *Green Chem.* **2005**, *7*, 35-38.

(26) Antony, T.; Atreyi, M.; Rao, M. V. R. *Chem. Biol. Interact.* **1995**, *97*, 199-214.

(27) Yoshiharu, U. *Chem. Lett.* **1973**, *2*, 743.

(28) Detty, M. R.; Merkel, P. B. *J. Am. Chem. Soc.* **1990**, *112*, 3845-3855.

(29) Chaon, J. N.; Jamieson, G. R.; Sinclair, R. S. *Chem. Phys. Lipids* **1987**, *43*, 81-99.

(30) Rothemund, P. *J. Am. Chem. Soc.* **1936**, *58*, 625-627.

(31) Adler, A. D.; Longo, F. R.; Finarelli, J. D.; Goldmacher, J.; Assour, J.; Korsakoff, L. *J. Org. Chem.* **1967**, *32*, 476-476.

(32) Lindsey, J. S.; Schreiman, I. C.; Hsu, H. C.; Kearney, P. C.; Marguerettaz, A. M. *J. Org. Chem.* **1987**, *52*, 827-836.

(33) Carvalho, C. M. B.; Neves, M. G. P. M. S.; Tomel, A. C.; Paz, F. A. A.; Silva, A. M. S.; Cavaleiro, J. A. S. *Org. Lett.* **2011**, *13*, 130-133.

(34) Redmond, R. W.; Gamlin, J. N. *Photochem. Photobiol.* **1999**, *70*, 391-475.

(35) Diaz-Uribe, C. E.; Daza, M. C.; Martínez, F.; Páez-Mozo, E. A.; Guedes, C. L. B.; Di Mauro, E. *J. Photochem. Photobiol. A.* **2010**, *215*, 172-178.

(36) Castriciano, M. A.; Romeo, A.; Angelini, N.; Micali, N.; Longo, A.; Mazzaglia, A.; Scolaro, L. M. *Macromolecules* **2006**, *39*, 5489-5496.

(37) Gilbert, A.; Baggot, J. In *Photo-oxygenation reactions;* Essentials of molecular photochemistry; 1991; pp 501.

(38) a) Wallach, O. *Justus Liebigs Ann. Chem.* **1912,** *392*, 45-75, b). Nelson, E. K. *J. Am. Chem. Soc.* **1913**, *35*, 84-90.

(39) Hammond, J. A.; Fielding, D.; Bishop, S. C. *Veterinary Research Communications* **1997**, *21*, 213-228.

(40) Schenck, G. O. *Ind. Eng. Chem.* **1963**, *55*, 40-43.

(41) Dewar, M. J. S.; Thiel, W. *J. Am. Chem. Soc.* **1977**, *99*, 2338-2339.

(42) Delogu, G.; Fabbri, D.; Fabris, F.; Sbrogio, F.; Valle, G.; De Lucchi, O. *J. Chem. Soc. , Chem. Commun.* **1995**, *27*, 1887-1888.

(43) Seidel, C. F.; Stoll, M. *Helv. Chim. Acta* **1959**, *42*, 1830-1844.

(44) Alsters, P. L.; Jary, W.; Nardello-Rataj, V.; Aubry, J. *Org. Process Res. Dev.* **2010**, *14*, 259-262.

(45) Davis, K. M.; Carpenter, B. K. *J. Org. Chem.* **1996**, *61*, 4617-4622.

(46) Matsumoto, M.; Kobayashi, H.; Matsubara, J.; Watanabe, N.; Yamashita, S.; Oguma, D.; Kitano, Y.; Ikawa, H. *Tetrahedron Lett.* **1996**, *37*, 397-400.

(47) Anastas, P. T.; Kirchhoff, M. M. *Acc. Chem. Res.* **2002**, *35*, 686-694.

(48) Hashemi, M. M.; Akhbari, M. *Russian Journal of Organic Chemistry* **2005**, *41*, 935-936.

(49) Giménez, J.; Curcó, D.; Queral, M. A. *Catalysis Today* **1999**, *54*, 229-243.

(50) Giménez, J.; Curcó, D.; Marco, P. *Water Science and Technology* **1997**, *35*, 207-213.

(51) Goslich, R.; Dillert, R.; Bahnemann, D. *Water Science and Technology* **1997**, *35*, 137-148.

Chapter 2:

Homogeneous dye sensitized photooxygenations of 1,5-dihydroxynaphthalene, α-terpinene and β-citronellol.

2.1 Introduction

The aim of the work described in this chapter is to evaluate the photooxygenations of 1,5-dihydroxynaphthalene (1,5-DHN), α-terpinene and β-citronellol and to highlight how the *twelve principles of green chemistry* [1] can be applied to assess and improve these three reactions. The reactions were first performed indoors under artificial light and then repeated outdoors under solar conditions. The results of both "indoor" and solar photooxygenations were compared and assessed for their "greenness" with respect to: a) energy consumption, b) water usage and c) purification methods.

Initially the dye sensitized photooxygenation of 1,5-dihydroxynaphthalene to juglone was selected as a model reaction and was optimized and validated on a laboratory scale (50-100 ml Schlenk flask) using a 500 W halogen lamp as the light source and rose Bengal as sensitizer (Scheme 2.1).

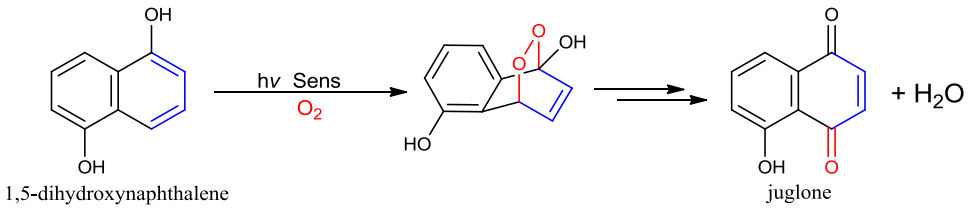

Scheme 2.1: Dye sensitized photooxygenation of 1,5-DHN to juglone.

Once optimized and validated the same synthetic conditions were then employed for the dye sensitized photooxygenations of both α-terpinene and β-citronellol.

It should be noted that the reduction of ascaridole to its corresponding diol and subsequent dehydration to p-cymene are well documented within the literature and will not be dealt with further in this text.[2-4] The aim of this work is to assess the initial photochemical step using the twelve principles of green chemistry and to optimise the process in its entirety to be as environmentally friendly as possible.

2.2 Laboratory scale photooxygenations of 1,5-DHN, β-citronellol and α-terpinene

2.2.1 Dye sensitized photooxygenation of 1,5-dihydroxynaphthalene, optimisation and validation

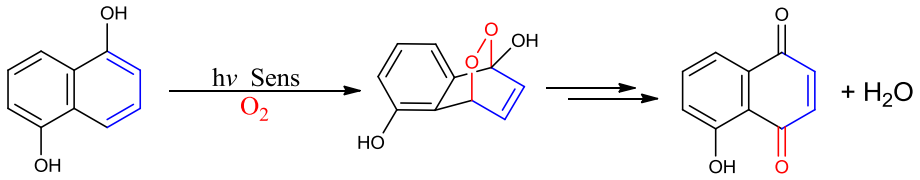

Scheme 2.2: The dye sensitized photooxygenation of 1,5-DHN to juglone.

2.2.1.1 Validation of the dye sensitized photooxygenation of 1,5-DHN (Experiments 1-13)

Like all dye sensitized photooxygenations the photooxygenation of 1,5-DHN to juglone requires three separate parameters for the reaction to proceed. These are namely a light source, a sensitizer (in this case rose Bengal) and a supply of oxygen. In order to prove that all three of these requirements must be met for a dye sensitized photooxygenation to occur a series of validation experiments were performed. During this set of experiments one of each of the required parameters was removed and the dye sensitized photooxygenation of 1,5-DHN attempted. The results of these experiments confirmed that all three parameters; light source, sensitizer and oxygen must be present for the reaction to proceed (Section 2.5.5). If any one of these three conditions is not met the synthesis of juglone via a dye sensitized photooxygenation process is impossible.

It should be noted that the results of the sensitizer free experiments showed that in the absence of a sensitizer low yields of juglone could still be obtained. This is due to self sensitization of the starting material, 1,5-DHN. The results of the sensitizer free experiments are in agreement with Duchstein *et al* [5] who reported yields of juglone of up to 20 % in acetonitrile when using a halogen lamp ($\lambda > 360$ nm). Duchstein also reported yields of up to 15 % when using a high pressure mercury lamp (< 360 nm). Murtinho *et al* [6] reports yields of up to 28 % while using a

tungsten lamp and Luiz *et al* [7] reports that 1,5-dihydroxynaphthalenes are good self sensitizers at 337 nm.

Once the dye sensitized photooxygenation of 1,5-DHN was validated, the process was then optimised with regards to solvent selection.

2.2.1.2 Solvent optimisation (Experiments 14-20)

Previous studies on the photochemical synthesis of juglone reported the use of a variety of halogenated solvents, in particular dichloromethane (DCM) and chloroform ($CHCl_3$). The reason behind their favoured use lies in the relatively long life times of singlet oxygen in these solvents (Appendix A1). Values from the literature show that the life times of singlet oxygen in halogenated solvents can range from 75 μs to 900 μs depending on the solvent.[8-12]

Despite this obvious advantage these solvents are highly toxic to the environment with some reports claiming that they may even be toxic to the human liver.[13] In addition, the disposal of such halogenated solvents continues to rise in cost. With this in mind, improved, environmentally friendly and cost effective solvents had to be evaluated.

A recent paper published by the Pfizer Global Research and Development team in Green Chemistry [14] outlined a solvent selection guide for medicinal chemistry (Figure 2.1). Pfizer placed selected solvents into one of three categories – preferred, usable and undesired. With reference to this guide the halogenated solvents were replaced with the more environmentally friendly short chain alcohols as they provided sufficient solubilisation of both 1,5-DHN and rose Bengal.

Preferred	Usable	Undesirable
Water	Cyclohexane	Pentane
Acetone	Heptane	Hexane(s)
Ethanol	Toluene	Di-isopropyl ether
2-Propanol	Methylcyclohexane	Diethyl ether
1-Propanol	Methyl-*t*-butyl ether	Dichloromethane
Ethyl acetate	Isooctane	Dichloroethane
Isopropyl acetate	Acetonitrile	Chloroform
Methanol	2-methyl THF	Dimethyl formamide
Methyl ethyl ketone	Tetrahydrofuranone	*N*-methylpyrrolidine
1-Butanol	Xylenes	Pyridine
t-Butanol	Dimethyl sulfoxide	Dimethyl acetate
	Acetic acid	Dioxane
	Ethylene glycol	Dimethoxyethane
		Benzene
		Carbon tetrachloride

Figure 2.1: The Pfizer solvent selection guide for medicinal chemistry.

The singlet oxygen lifetimes of the various alcohols were readily available in the literature (Appendix A1) and ranged from 9 to 34 μs.[12, 15-19] Results from the literature show that as the chain length and branching of the alcohol increases so too does the singlet oxygen lifetime. Tert-butanol (t-Bu) has the longest lifetime (34 μs) but was unsuitable as a solvent due to its high melting point of 25 °C. t-Butanol was however, substituted with tert-amyl alcohol (TAA) or 2-methyl-2-butanol a similar branched alcohol which was supplied by Dr Peter Dunn of Pfizer. In order to determine the suitability of this solvent for dye sensitized photooxygenations a series of experiments were performed (Experiments 14-20, Table 2.1). 1,5-DHN (10 mM) and rose Bengal (0.25 mM) were dissolved in 50 ml of solvent and irradiated for 4 hours in front of a 500 W halogen lamp. ^{1}H NMR (acetone-d_6) was used to determine the percent conversion of 1,5-DHN to juglone after 4 hours (Figure 2.2).

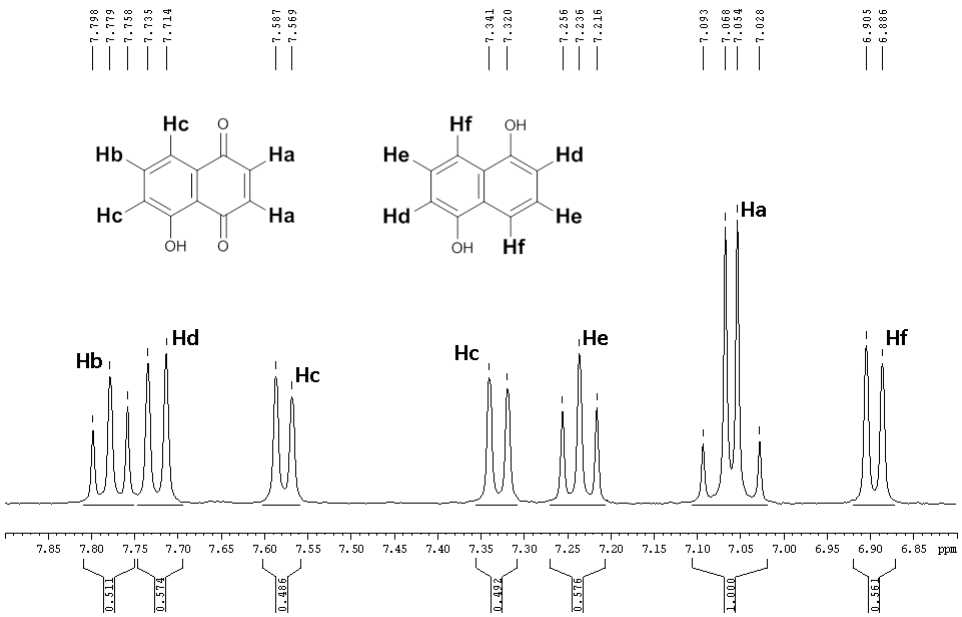

Figure 2.2: ^{1}H NMR spectrum of crude reaction sample showing 66 % conversion.

The dye sensitized photooxygenation of 1,5-DHN was also performed using methanol, ethanol and IPA. In addition, acetone and ethyl acetate were used as these too were considered to be green solvents. Water, the ultimate green solvent was also used. The results (Table 2.1) clearly demonstrate that TAA provides the greatest percentage conversion to juglone. Although singlet oxygen lifetimes could not be found for TAA in the literature it is assumed that the life time would lie somewhere between that of IPA and *t*-Bu.

Table 2.1: Synthesis of juglone in various "green" solvents.

Exp No	Solvent	Time (hr)	Conversion (%)	$^{1}O_2$ Lifetime
14	MeOH	4	22	9-10
15	EtOH	4	30	11-15
16	IPA	4	32	22
17	TAA	4	39	--
18	Acetone	4	14	25-50
19	Ethyl acetate	4	9.5	45-50
20	H_2O	4	11	4.0-4.2

2.2.1.3 Light intensity

The intensity of the light received at the Schlenk flask significantly affected the final yield of the reaction. A greater light intensity dramatically increases the number of photons capable of initiating a photochemical reaction. This light intensity can be easily adjusted by changing the distance between the light source and the Schlenk flask. In order to quantify how light intensity is related to this distance a series of light intensity measurements (Lux) were taken using a data logging light meter (ATP LX-8809A) at various distances from the 500 W halogen lamp. The results show that light intensity is inversely proportional to the square of the distance from the light source. i.e. light intensity = $1/d^2$ (Table 2.2). The results of Table 2.2 were also graphed in order to show this relationship and its linearity in the range of distances measured (Figure 2.3).

Table 2.2: Light intensities (lux) at given distances from the light source.

Distance (cm)	Lux	d^2 (cm^2)	$1/d^2$ ($1/cm^2$)
40	10700	1600	0.000625
38	11550	1444	0.000693
36	12350	1296	0.000772
34	13250	1156	0.000865
32	14950	1024	0.000977
30	16050	900	0.001111
28	17760	784	0.001276
26	19300	675	0.001479
24	21500	576	0.001736
22	24000	484	0.002066
20	26600	400	0.002500
19	28800	361	0.002770
18	30450	324	0.003086

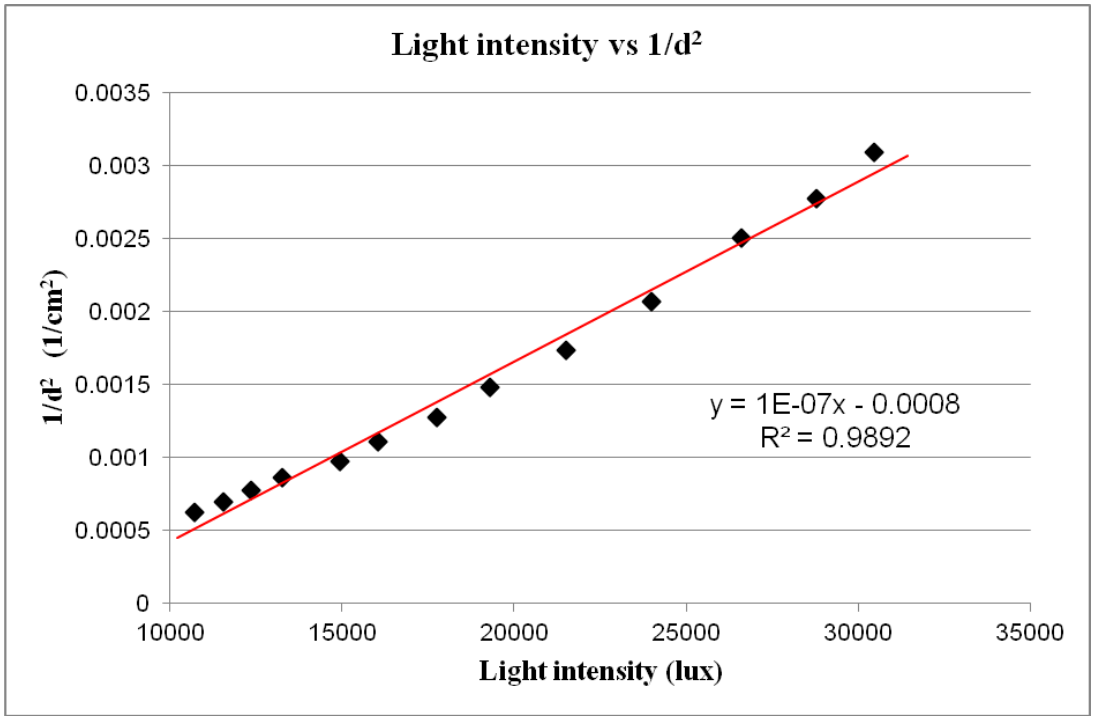

Figure 2.3: Light intensity vs $1/d^2$.

In order for the results of subsequent experiments to be directly comparable, the distance of the Schlenk flask to the light source was set at 27 cm for all experiments. This distance was adopted as it provided us with the shortest distance (greatest light intensity) between the reaction mixture and the light source without a resulting rise in temperature of the reaction mixture caused by thermal energy generated by the halogen lamp. The utilization of a cold finger allowed us to regulate the temperature between 15-25 °C.

2.2.1.4 Electrical energy usage

To account for all of the electrical energy required for the photooxygenation of 1,5-DHN to juglone a plug in energy meter was employed. The meter was used to measure the amount of energy in kilo joules per hour (kJ/hr) for each piece of electrical equipment used during the synthetic process (Appendix A2). An energy consumption of 1556.4 kJ/hr was recorded for the 500 W halogen lamp. This could then be used later to determine energy savings, when using sunlight as a light source.

2.2.1.5 Optimised dye sensitized photooxygenation of 1,5-DHN (Experiments 21-23)

Once validated and optimised juglone could be readily synthesized from 1,5-DHN (10 mM) under artificial light conditions (500 W halogen lamp, 27 cm distance) using rose Bengal as sensitizer (0.25 mM) in 50 ml of TAA (Experiment 21-23) Percentage conversions of up to 65 % were realized in only three hours (Table 2.3).

Table 2.3: Dye sensitized photooxygenation of 1,5-DHN to juglone (optimised).

Exp No	Solvent	Sensitizer	Time (hr)	Conversion (%)
21	TAA	RB	3	65
22	TAA	RB	3	66
23	TAA	RB	3	60

2.2.2 Photooxygenations of α-terpinene and β-citronellol

2.2.2.1 Photooxygenation of α-terpinene (Experiments 24-26 & 29-31)

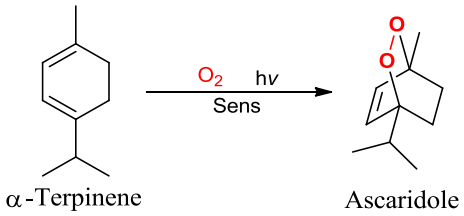

Scheme 2.3: Dye sensitized photooxygenation of α-terpinene to ascaridole.

Although the dye sensitized photooxygenation of α-terpinene is known to be a fast reaction, determination of the rate of conversion by ^{1}H NMR can be difficult. This is due to the volatility of α-terpinene itself. In order to determine the percentage conversion of a crude sample by ^{1}H NMR the solvent must first be removed. However, the removal of high boiling point solvents such as TAA or IPA under vacuum results in the simultaneous removal of any remaining α-terpinene preventing accurate determination of percentage conversion. Consequently, the dye sensitized photooxygenation of α-terpinene was initially attempted using acetone as the solvent (Experiments 24-26). α-Terpinene (104 mM) and sensitizer (0.25 mM) were dissolved in 50 ml of acetone and irradiated using a 500 W halogen lamp at a

distance of 27 cm for three hours. It was assumed the lower boiling point of acetone would allow for its removal under mild vacuum conditions without the simultaneous removal of α-terpinene. Unfortunately, results showed this not to be the case. ^{1}H NMR therefore is not suitable for the accurate determination of percent conversion of crude samples.

In order to determine the percent conversion of these reactions column chromatography (95:5 cyclohexane / ethyl acetate) was employed and isolated yields of 58 and 42 % were obtained for rose Bengal and methylene blue respectively (Table 2.4). Tetraphenyl porphyrin (TPP), synthesized by the Adler method (Scheme 2.4), was also tested (Experiment 27). Isolated yields of up to 61 % were obtained using TPP as sensitizer with acetone as solvent (Table 2.4). Due to this superior yield, a water soluble derivative of TPP was also synthesized according to the Adler method (Scheme 2.4, Experiment 28). meso-Tetra-(4-carboxyphenyl) porphyrin (TCPP) was synthesized as TPP was not soluble in alcoholic solvents.

Table 2.4: Synthesis of ascaridole using RB, MB and TPP in acetone.

Exp No	Sensitizer (0.25 mM)	Time (hr)	% yield
24	RB	2	58
25	MB	2	42
26	TPP	2	61

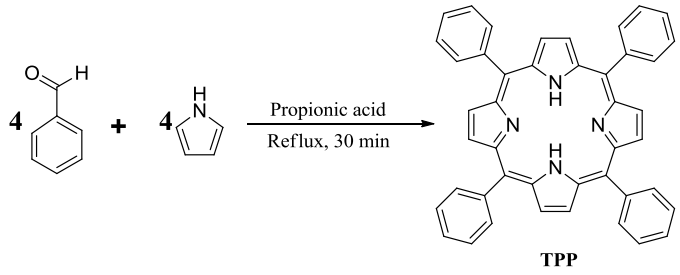

TPP

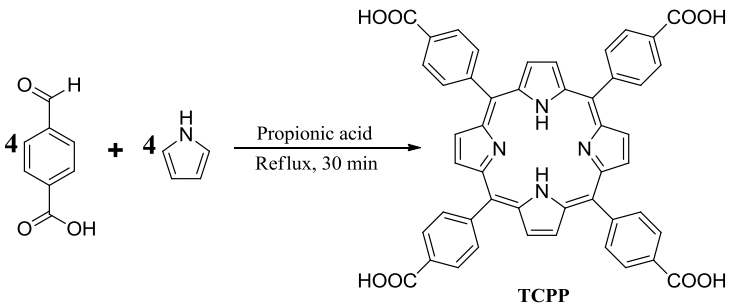

TCPP

Scheme 2.4: Synthesis of TPP and TCPP via the Adler method.

A UV-Vis assay was conducted to develop a real time process method for analysis for the rate of conversion of α-terpinene to ascaridole in both IPA and TAA. Ascaridole itself has a weak absorption band in the same region of the UV-Vis spectrum as α-terpinene. However, it has a measured extinction coefficient (ε) of 32.89 $M^{-1}.cm^{-1}$ at 265.5 nm in IPA. In contrast, α-terpinene has a measured extinction coefficient of 7810 $M^{-1}.cm^{-1}$ (Figure 2.4) at 275nm in IPA. This is approximately 240 times greater than that of ascaridole. For this reason the change in concentration of α-terpinene can be easily monitored by UV-Vis. A set of calibration curves to measure α-terpinene concentration in IPA, TAA and ethanol were generated (Table 2.5, Figures 2.5 – 2.7).

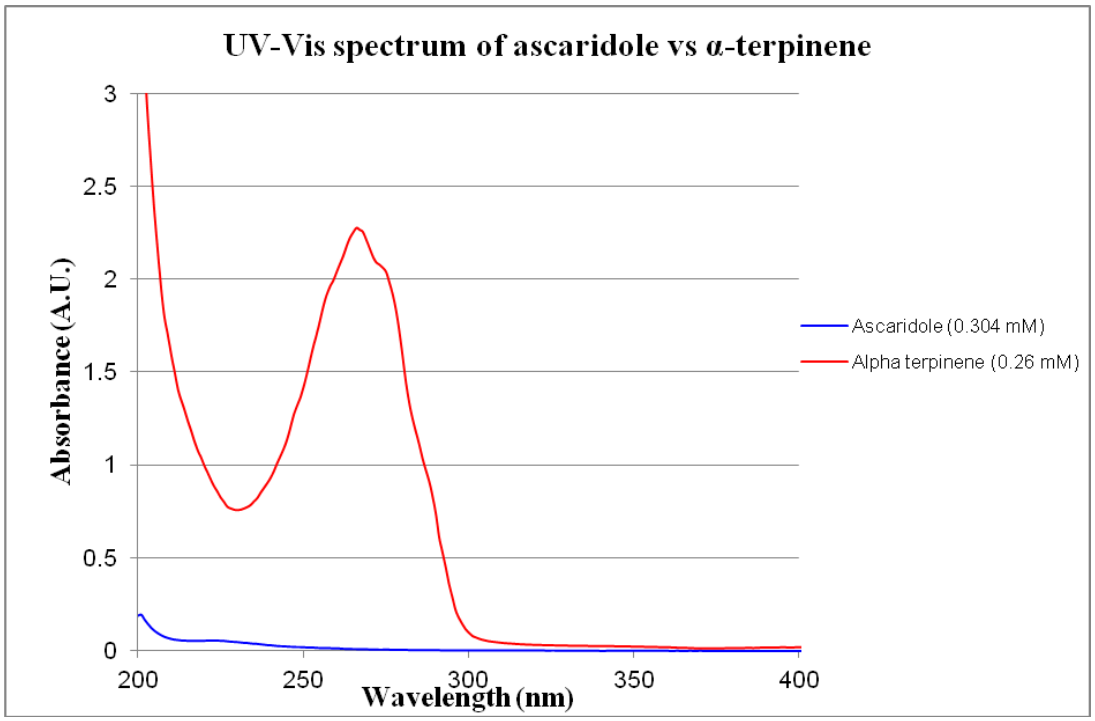

Figure 2.4: UV-Vis spectrum of α-terpinene and ascaridole in IPA.

Table 2.5: Absorbance values of α-terpinene in IPA, TAA and EtOH at various concentrations.

	***iso*-propyl alcohol**		***tert*-amyl alcohol**		**Ethanol**	
Conc (mM)	**λ-max (nm)**	**Average Absorbance**	**λ-max (nm)**	**Average Absorbance**	**λ-max (nm)**	**Average Absorbance**

0.2600	265.5	2.0083	267	2.0233	266	1.9712
0.1300	265.5	1.0129	267	1.0243	266	1.0122
0.0650	265.5	0.5077	267	0.5299	266	0.5689
0.0325	265.5	0.2513	267	0.2808	266	0.3026
0.0163	265.5	0.1372	267	0.1251	266	0.1731

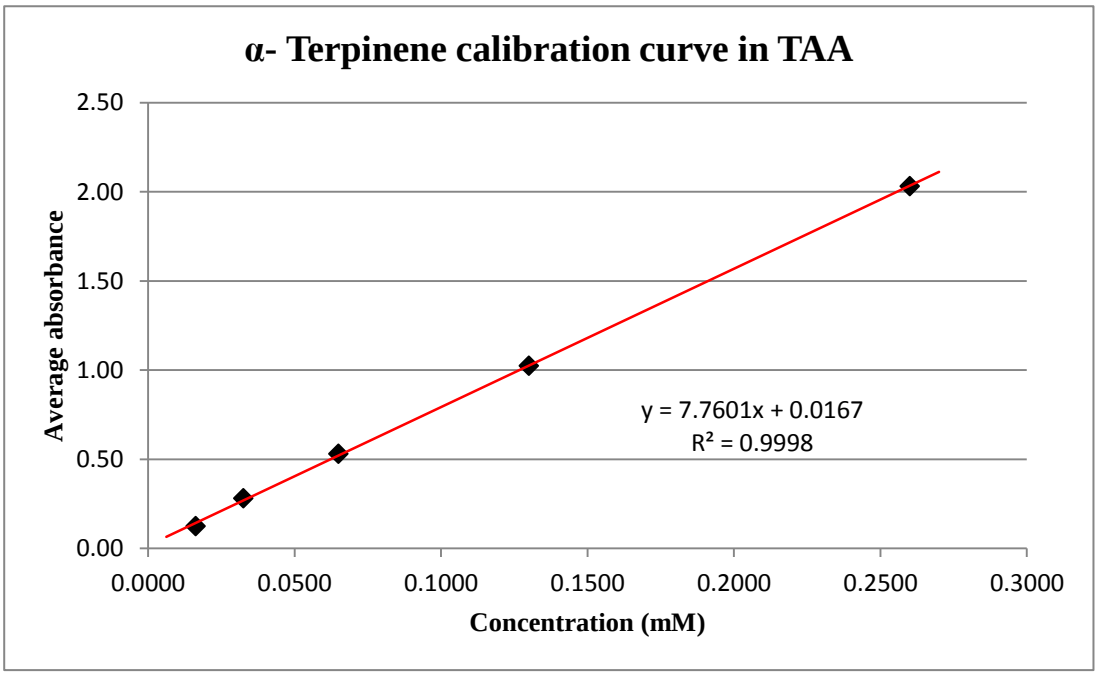

Figure 2.5: Calibration curve for α-terpinene in TAA.

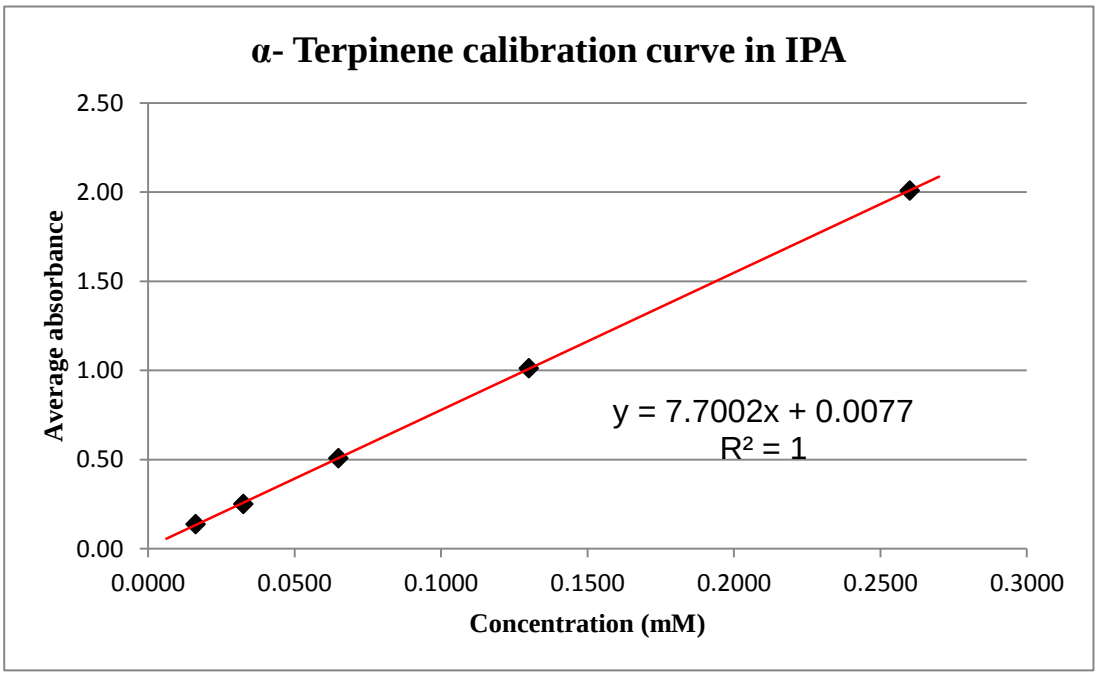

Figure 2.6: Calibration curve for α-terpinene in IPA.

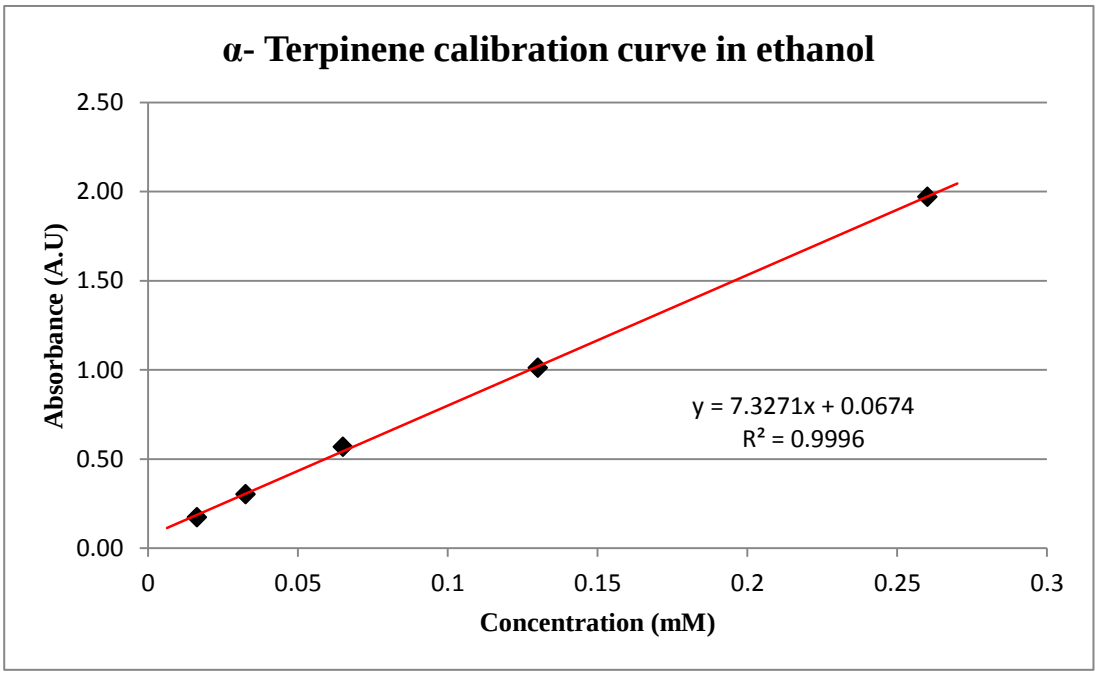

Figure 2.7: Calibration curve for α-terpinene in ethanol.

Utilisation of this method of analysis allowed for the accurate determination of the rate of conversion of α-terpinene to ascaridole in TAA. In a set of experiments, α-terpinene (104 mM) and sensitizer (0.25) mM were dissolved in 50 ml of TAA and irradiated at a distance of 27 cm using a 500 W halogen lamp for two hours (Experiments 29-31). Rose Bengal gave a conversion of 97 % in just two hours. Interestingly, methylene blue performed poorly and failed to provide conversions above 15 % (Figure 2.8). This was attributed to photo-bleaching as methylene blue quickly lost its colour in the reaction mixture. TCPP provided complete conversion in two hours. Comparison of these results with those obtained in acetone (Table 2.4) shows that TAA, in case of rose Bengal and TCPP is a superior solvent for the dye sensitized photooxygenation of α-terpinene.

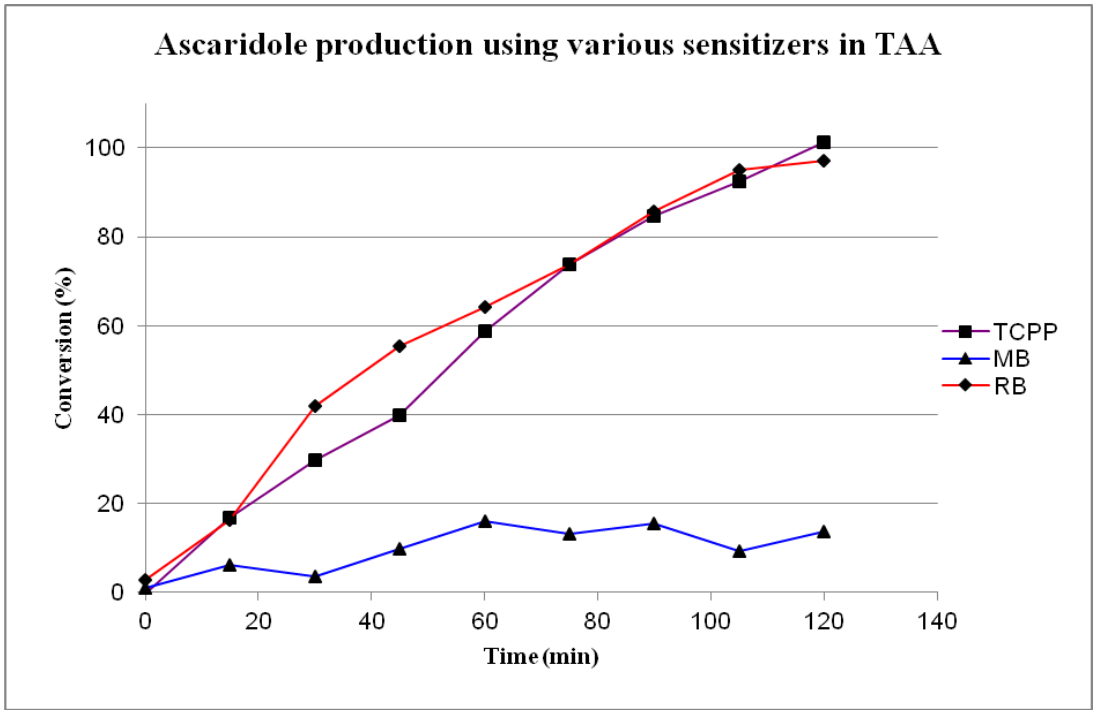

Figure 2.8: Dye sensitized photooxygenation of α-terpinene in TAA using TCPP, MB and RB.

2.2.2. Photooxygenation of β-citronellol (Experiments 32-38)

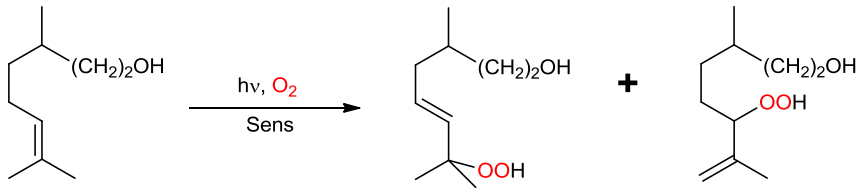

Scheme 2.5: Dye sensitized photooxygenation of β-citronellol.

The dye sensitized photooxygenation of β-citronellol was performed based upon the optimised conditions determined for the synthesis of juglone (Experiments 32-34). Briefly, β-citronellol (104 mM) and sensitizer (0.25 mM) were dissolved in 50 ml of TAA and irradiated at a distance of 27 cm from a 500 W halogen lamp for two hours. ^{1}H NMR ($CDCl_3$) was used to determine the percent conversion. Using rose Bengal as the sensitizer ^{1}H NMR showed a 44 % conversion of β-citronellol to its corresponding hydroperoxides in 2 hours (Figure 2.9). Further investigation involved repeating the experiment with methylene blue and TCPP as sensitizers, which gave percent conversions of 52 and 51 % respectively (Table 2.6).

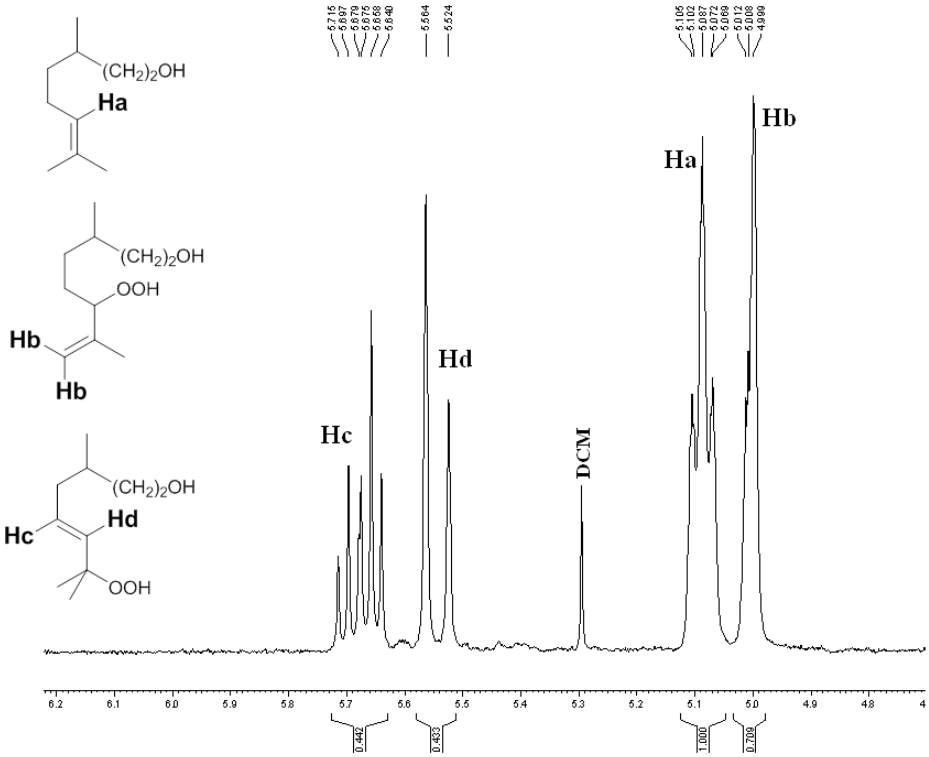

Figure 2.9: ^{1}H NMR spectrum showing 44 % conversion of β-citronellol to its corresponding hydroperoxides.

Table 2.6: Dye sensitized photooxygenation of β-citronellol in TAA using RB, MB and TCPP.

Exp No.	Solvent	Sensitizer (0.25 mM)	Time (hr)	Conversion (%)
32	TAA	RB	2	44
33	TAA	MB	2	52
34	TAA	TCPP	2	51

The experiments were repeated using acetone as the solvent due to the increased solubility of both the starting material and the sensitizers. Percentage conversions of 62, 90 and 60 % were achieved for rose Bengal, methylene blue and TCPP respectively after 2 hours of irradiation (Table 2.7) in acetone. Due to its solubility in acetone TPP was also used as sensitizer which gave a conversion rate of 86 % after 2 hours of irradiation.

Table 2.7: Dye sensitized photooxygenation of β-citronellol with various sensitizers in TAA and acetone.

Exp No.	Solvent	Sensitizer (0.25 mM)	Time (hr)	Conversion (%)
35	Acetone	RB	2	62
36	Acetone	MB	2	90
37	Acetone	TCPP	2	60
38	Acetone	TPP	2	86

The results indicate that acetone; in the case of the photooxygenation of β-citronellol is a superior solvent compared to TAA. This may be attributed to increased solubility of both β-citronellol and the sensitizers in acetone. A sensitizer concentration of 0.25 mM in TAA represents a saturated solution and often prolonged periods of sonication are required to solubilise all of the sensitizer. In contrast, the sensitizers are readily soluble in acetone. This is especially true for methylene blue and is reflected in a significant percent conversion of 90 % after two hours of irradiation. Despite this increased solubility of sensitizer and resulting significant increase in percentage conversion the use of acetone as solvent gave rise to a separate issue. Due to the low boiling point and high volatility of acetone it readily evaporated during the reaction as a result of the constant air bubbling. Consequently, the Schlenk flask had to be regularly "topped up" during the reaction as the acetone levels dropped. For this reason acetone is considered not to be an ideal solvent for dye sensitized photooxygenations when using a Schlenk flask apparatus.

2.2.3 Green issues with laboratory scale dye sensitized photooxygenations.

The dye sensitized photooxygenations of 1,5-DHN, α-terpinene and β-citronellol are considered to be "green" synthetic processes as they satisfy many of the twelve principles of green chemistry (Table 2.8).

Table 2.8: Compliance of dye sensitized photooxygenations with the twelve principles ofgreen chemistry.

Rule	Description	Compliant	Details
1	Waste should be prevented and innocuous when generated	YES	In the case of the photooxygenation of 1,5-DHN water is the only by-product.
2	Incorporation of all materials into final product	YES	In the case of the photooxygenation of α-terpinene and β-citronellol 100 % atom economy is observed
6	Energy requirements should be minimised	YES	Elevated temperatures are not required. Ambient conditions are sufficient
7	Renewable feedstock	YES	α-Terpinene and β-citronellol are natural compounds and as such are renewable
11	Analytical methods should be employed for real time, in-process monitoring	YES	In the case of photooxygenation of α-terpinene UV-Vis spectroscopy was employed
12	Reagents used should be chosen to minimise potential for accidents	YES	The use of air is sufficient instead of O_2.

Despite already being considered "green" several factors were identified during the dye sensitized photooxygenation of these three compounds that did not comply with the twelve principles of green chemistry. These were namely:

- The light source (high energy demand)
- The requirement for column chromatography in order to remove the sensitizer from the crude product
- The need for water cooling during the irradiation process.

A 500 W halogen lamp was chosen as our light source as it gave a high intensity emission spectrum that ranged from 360 – 1100 nm (Appendix C). This broad emission spectrum allowed for the use of a variety of different sensitizers. Despite

this advantage the energy demand of the lamp (1556.4 kJ/hr) is high. In comparison, the only other electrical device required, the single pump to supply a stream of air, uses only 5.2 kJ/hr. This large energy demand conflicts directly with rule 6 of the 12 principles. Solar dye sensitized photooxygenations of these three compounds would eliminate the high energy light source resulting in a direct saving of 1556.4 kJ of electrical energy per hour.

The removal of the sensitizer from the crude reaction solution was achieved by column chromatography. This is in conflict with rules 1 and 5 of the 12 principles. Utilisation of sensitizers immobilised onto solid supports may provide a solution to this problem.

Throughout the irradiation process the 500 W halogen lamp generated a considerable amount of thermal energy resulting in the eventual evaporation of the reaction solvent. In order to prevent this from occurring water cooling via a cold finger was adopted. Consequently, this resulted in the comsumption of up to 4 L/min or 240 L/hr of water during the irradiation process. The cold finger works in a similar fashion to a Liebig condenser and requires constant running cold water. Water is a precious commodity and at present the supply of clean water is expensive and demands a large carbon footprint. In order for subsequent dye sensitized photooxygenations to be in compliance with the twelve principles of green chemistry the utilisation of water cooling would ideally have to be reduced or eliminated.

2.3 Solar dye sensitized photooxygenations

2.3.1 Average global radiation (AGR): diffuse and direct solar irradiation.

Dublin City University (DCU) is located 167 m above sea level at latitude 53° 23' 28'' N and longitude 6° 12' 19'' W. Although on-site weather monitoring facilities are not available at DCU to collect meteorological data the Irish Meteorological Service (MET Eireann) has such a station established at Dublin airport which is 4.5 km from DCU (Figure 2.10).

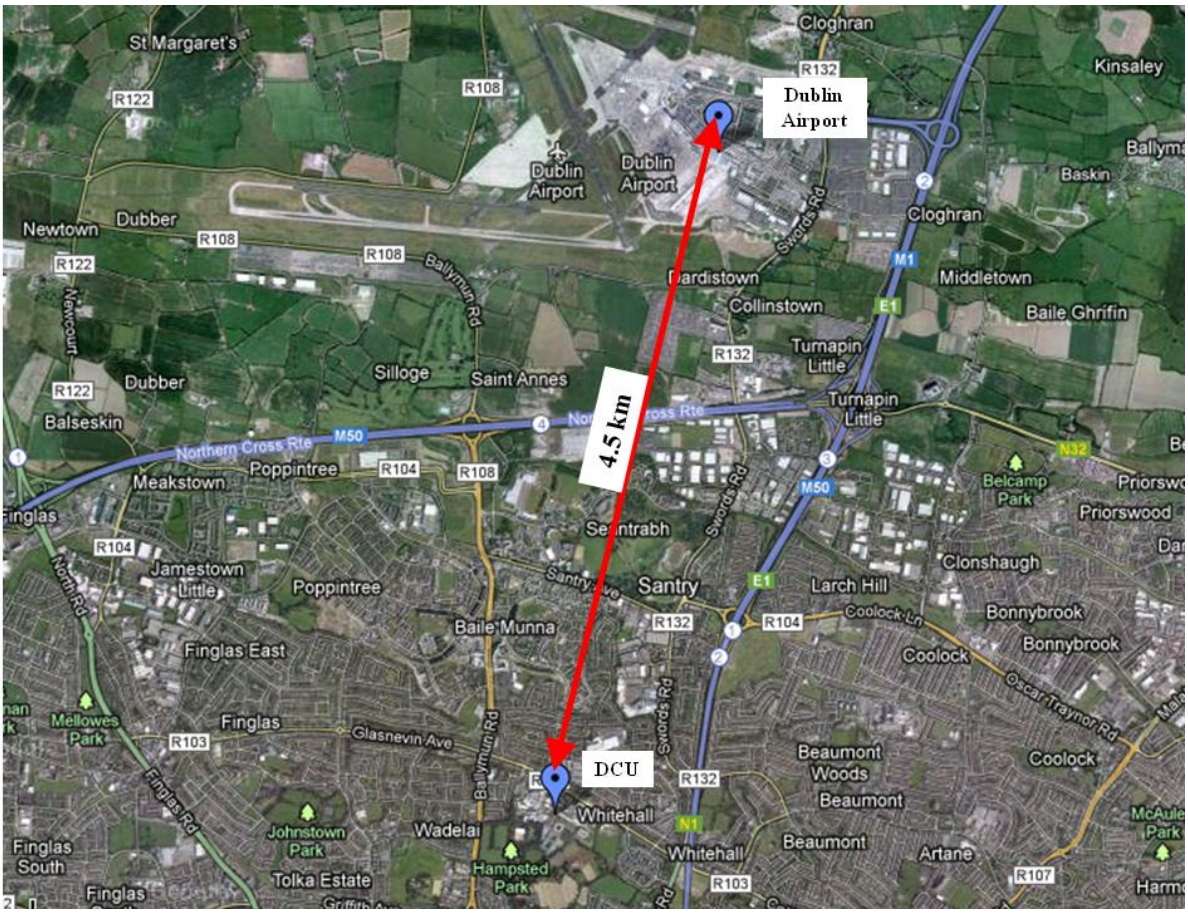

Figure 2.10 Map showing distance from DCU to Dublin airport.

This station receives an average of 1437.8 hours of sunlight per annum based on data collected from 1978 to 2008. The overall amount of solar radiation received at this and other weather stations around the country is measured in J/cm^2. The mean

global radiation received at Dublin airport, Birr and Kilkenny is shown below in Table 2.9.

Table 2.9: Total average global radiation received at Dublin airport, Birr and Kilkenny weather stations (1981-2000).

	Jan	Feb	March	April	May	June	July	Aug	Sep	Oct	Nov	Dec	Annual
Dublin Airport	7007	12363	24402	37364	49216	51417	51598	42616	29695	10824	8711	5327	337740
Birr	6916	12437	23357	37677	50535	48772	46967	40930	29374	17483	8848	5468	328764
Kilkenny	7153	12556	24869	31974	52014	50815	50654	41413	29799	18062	9127	5704	341340

It is important to note that on an annual basis approximately 57 % of the total global radiation received at these weather stations arrives during the months of May to August. If we include the month of April in this calculation the amount of global radiation received increases to 68 %. This is an indication that while solar dye sensitized photooxygenations may be possible at DCU they may only be feasible during the months of April to August. During the other months of the year there may not be enough solar radiation available to efficiently perform dye sensitized photooxygenations.

Solar radiation that reaches the Earth's surface arrives in two separate forms; direct and diffuse radiation (Figure 2.11). Direct solar radiation occurs mainly on very sunny days with little or no cloud cover. In this way the solar rays can travel uninterrupted from the sun to the reaction apparatus. Diffuse radiation on the other hand, comprising up to 60 % of the annual solar radiation received in Ireland, arrives at the reaction apparatus from all angels due to light scattering in the atmosphere. On overcast days practically all of the solar radiation received at DCU is diffuse in nature.

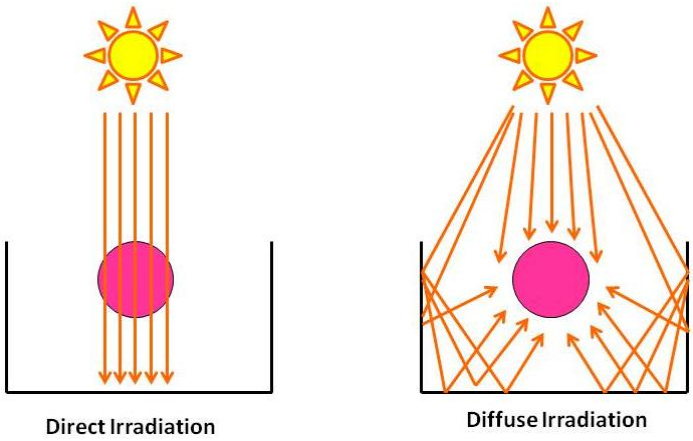

Figure 2.11: Direct and diffuse solar irradiation.

While conducting solar dye sensitized photooxygenations at DCU the solar conditions were recorded under four headings and were later compared to data received from MET Eireann for the same time period. This quantified the mean solar radiation received and determined the percentage diffuse radiation. These four headings were referred to as direct sun, partial cloud, partial sun and overcast. Comparatively, the results obtained from solar photooxygenations could be based upon the mean global solar radiation received and the percentage direct and diffuse radiation for each of the above headings. Table 2.10 below illustrates the Average Global Radiation (AGR) received per hour for each of the headings. The table also illustrates how much of the solar radiation received was in the form of diffuse light.

Table 2.10: MET Eireann solar radiation data.

Sunlight Description	Global Radiation (J/cm^2/hr)		% Diffuse Radiation
	Average	Range	
Direct sun	238	141-323	< 39
Partial cloud	190	117-291	40-54
Partial sun	183	142-221	55-69
Overcast	130	51-203	>70

2.3.2 Laboratory scale solar dye sensitized photooxygenations

Dye sensitized solar photooxygenations were initially performed using 100 ml Schlenk flasks identical to those used in the laboratory. The experiments were set up in the same manner as in the laboratory including water cooling but in the absence of the 500 W halogen lamp (Figure 2.12).

Figure 2.12: Laboratory scale solar dye sensitized photooxygenation of 1,5-DHN.

2.3.2.1 Solar dye sensitized photooxygenation of 1,5-DHN (Experiments 39-44)

Under optimised conditions outlined for the synthesis of juglone, the solar dye sensitized photooxygenation of 1,5-dihydroxypaphthalene was performed. 1,5-DHN (18.7 mM) and rose Bengal (0.98 mM) were dissolved in 100 ml of TAA and irradiated under direct sunlight conditions (AGR $\geq$ 238 J/cm^2/hr, < 39 % diffuse radiation) for three hours. Isolated yields of up to 69 % were achieved, which represents a significant improvement over artificial laboratory conditions (500 W halogen lamp) with the additional saving of up to 4669.2 kJ of electrical energy.

In comparison, under partial sunlight conditions (AGR = 183 J/cm^2/hr, 55 – 69 % diffuse irradiation), isolated yields of only 33-34 % were achieved over the same time period. Moreover, an experiment conducted on an overcast day (AGR = 130 J/cm^2/hr, > 70 % diffuse irradiation) saw a drop in yield to 26 % after 5 hours of

irradiation. The results indicate that optimal solar conditions (AGR ≥ 238 J/cm^2/hr, < 39 % diffuse radiation) are required to efficiently perform the solar dye sensitized photooxygenation of 1,5-DHN (Table 2.11). Figure 2.13 illustrates the linear relationship between available solar radiation and percent yield of juglone. The results clearly demonstrate that for the dye sensitized photooxygenation of 1,5-DHN high levels of solar radiation are required. Such conditions are only obtained a few days each year in Ireland.

Table 2.11: Laboratory scale dye sensitized solar photooxygenation of 1,5-DHN (Dublin City University).

Exp No	Solvent (100ml)	Time (hr)	Weather conditions	AGR (J/cm^2/hr)	% conversion
39	TAA	3	Direct sun	238	69
40	TAA	3	Partial sun	183	33
41	TAA	3	Partial sun	183	34
42	TAA	5	Overcast	130	26

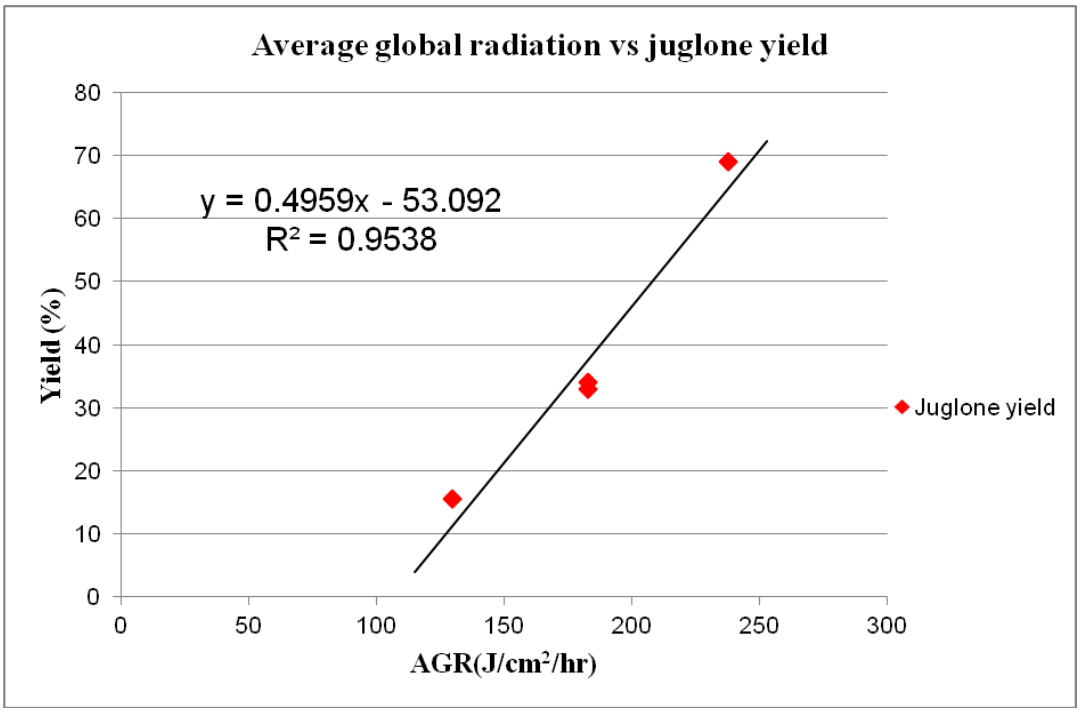

Figure 2.13 Plot of AGR vs juglone yield (Assuming 15.6 % yield after 3 hours for Exp 39).

In addition to experiments conducted under Irish solar conditions, two experiments were performed at the University of Almeria, Spain (latitude 36° 49' 50'' N and longitude 2° 24' 26'' W) in late October which gave isolated yields of 69 % after 2 hours of direct solar irradiation (Table 2.12). Unfortunately, meteorological data was not available for the time period of these two experiments.

Table 2.12: Laboratory scale dye sensitized solar photooxygenation of 1,5-DHN (University of Almeria).

Exp No	Starting material (mM)	Sensitizer (mM)	TAA (ml)	Time (hr)	Weather conditions	% conversion
43	20	0.49	50	2	Direct sun	47
44	10	0.245	100	2	Direct sun	69

The results of both sets of experiments clearly demonstrates that for the dye sensitized photooxygenation of 1,5-DHN to be performed efficiently large quantities of direct sunlight are necessary. At DCU this represents the need for a "sunny day" normally only received a few times a year during the summer months.

2.3.2.2 Dye sensitized solar photooxygenation of α-terpinene

Using the same experimental setup used for the solar dye sensitized synthesis of juglone (Figure 2.12) the solar dye sensitized photooxygenation of α-terpinene was also performed (Table 2.13). α-Terpinene (52 mM) and rose Bengal (0.25 mM) were dissolved in 100 ml of TAA. The solution was then irradiated under solar conditions for 5 hours. Initial solar conditions saw direct radiation (AGR $\geq$ 238 J/cm^2/hr, < 39 % diffuse radiation) for the first hour followed by partial sun conditions (AGR = 183 J/cm^2/hr, 55 – 69 % diffuse irradiation) for the remaining four hours. An isolated yield of 66 % was achieved after 5 hours of irradiation.

A second experiment was performed under direct sunlight conditions. α-Terpinene (260 mM) and rose Bengal (0.25 mM) were dissolved in 100 ml of TAA. The solution was then irradiated under direct solar conditions for 3 hours. An isolated yield of 45 % was achieved. It is important to note that while the concentration of sensitizer was kept constant the concentration of the starting material was very high

(260 mM). A yield of 45 % represents a conversion of 11.7 mmol of α-terpinene to ascaridole in three hours under optimal solar conditions.

Table 2.13: Laboratory scale dye sensitized solar photooxygenation of α-terpinene.

Exp No	Starting material (mM)	Sensitizer (mM)	Time (hr)	Weather conditions	AGR (J/cm^2/hr)	% conversion
45	52	0.25	5	Direct sun (1hr) Partial sun (4hr)	238 183	66
46	260	0.25	3	Direct sun	238	45

The results, similar to that of the solar dye sensitized photooxygenation of 1,5-DHN, confirmed that while the solar dye sensitized photooxygenation of α-terpinene is feasible under Irish solar conditions it cannot be performed efficiently without direct sunlight.

The results from the solar dye sensitized photooxygenations of both 1,5-DHN and α-terpinene confirmed that optimal solar conditions are required for these reactions to be performed efficiently. However, these conditions are present only a few times each year during the summer months at DCU. The next stage of the work was to implement a flat bed reactor which is designed to be more efficient than the Schlenk flask setup. The flat bed reactor allows for the irradiation of up to 4 L of reaction solution compared to the maximum 300 ml with the Schlenk flask. In addition the flat bed reactor was designed to have a short path length (~ 1 cm) to allow for the simultaneous irradiation of the entire reaction mixture. This improved irradiation offers a significant advantage over the Schlenk flask which has a smaller irradiation area as a consequence of its cylindrical shape.

2.3.3 Dye sensitized solar photooxygenations using a 1st generation flatbed reactor

The 1st generation flat bed reactor was designed and constructed by MPI, Mulheim (Demuth) (Figure 2.14). It was constructed of Plexiglas and joined with super glue at the joints. It had the dimensions 97 x 37 x 1.2 cm with an internal working volume of 4 L. It was designed to provide a large transparent surface area (0.359 m^2) with a relatively short internal path length (~1 cm) for irradiation. Air bubbling

was achieved thorough a thin horizontal pipe at the bottom of the reaction vessel. A second clear plastic tube worked through the reaction vessel provided water cooling. The reaction vessel was fitted to a wedge shaped racking system at an angle of 30 °. This was done in order to have an incident irradiation angle of 90 °. However, it was later determined that the correct angel was closer to 38 ° based upon Dublin City University's latitude for the summer months.[20]

Figure 2.14: 1st Generation flatbed reactor showing solvent outlet and inner cooling tubing.

This 1st generation flatbed reactor was developed for applications in synthetic photochemistry and was developed to be chemically inert to alcoholic solvents. Unfortunately, this was not the case when using TAA or IPA (Figure 2.15). The TAA reacted with both the Plexiglas and the superglue during the solar photooxygenation of 1,5-dihydroxynaphthlene. The superglue quickly dissolved and the Plexiglas became brittle and eventually degraded enough to finally collapse under its own weight. Consequently all further flatbed reactors were made of glass.

Figure 2.15: Degradation of Plexiglas after 24 hr in MeOH, EtOH, IPA and TAA.

2.3.4 2nd Generation flatbed reactor

A prototype 2nd generation flatbed reactor was first developed from a small double glazed window in order to determine if it would be suitable for dye sensitized photooxygenations. The small scale (1.3 L) reactor consisted of a double glazed window with two holes drilled in the side in order to both load the reactor and to allow for an air supply (Figure 2.16). The solar dye sensitized photooxygenation of 1,5-DHN was performed in order to determine if the window and the rubber glue used during its construction were stable under reaction conditions (Experiment 47). Briefly, 1,5-DHN (7.8 mM) and rose Bengal (0.075 mM) were dissolved in 1.3 L of TAA. This was then irradiated for 6 hours under partial sun conditions (AGR = 183 J/cm^2/hr, 55 – 69 % diffuse irradiation) resulting in an isolated yield of 16 %. This relatively low yield was attributed to the loss of approximately 300 ml of reaction solution while emptying the reactor. In addition, the concentration of rose Bengal was significantly lower than that of previous solar dye sensitized photooxygenations.

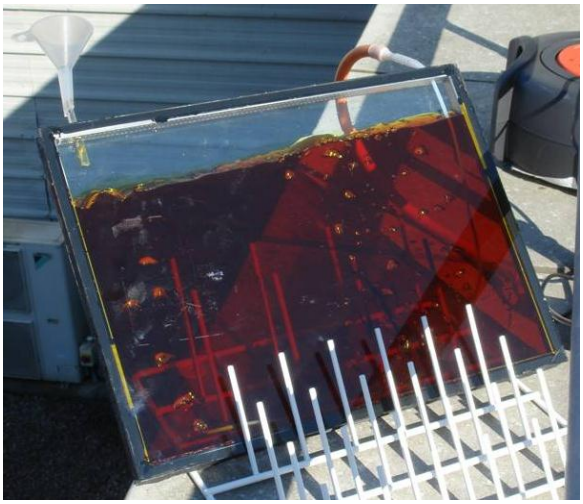

Figure 2.16: Prototype 2nd generation flatbed reactor showing air supply tubing and funnel for loading the reactor.

Despite these issues the prototype reactor had proved to be chemically inert to the reaction conditions. Resulting from this a custom built flat bed reactor was designed, commissioned and manufactured by Viking Glass Wexford. Its design incorporated an air inlet valve for air bubble supply and a solvent outlet valve. This allowed for the easy removal of the reaction mixture. The reactor had the dimensions 98 x 68 x 3.5 cm and a surface area of 0.67 m^2 with an internal working volume of 8 L (Figure 2.17).

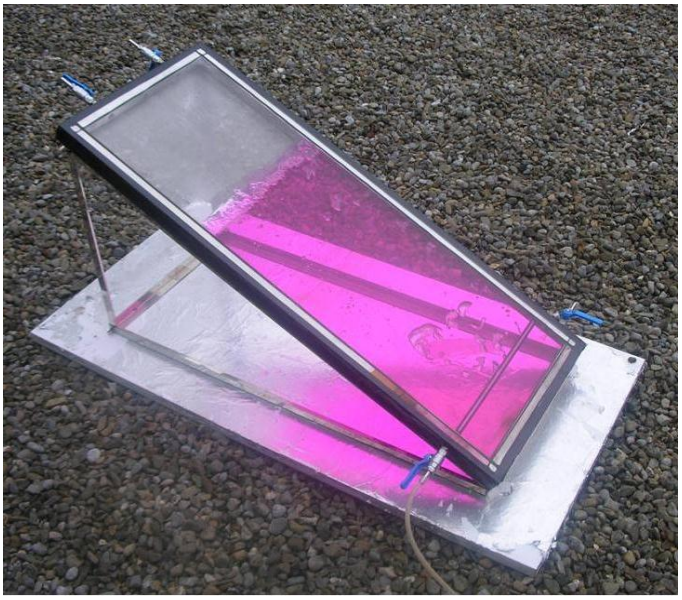

Figure 2.17: 2nd Generation flatbed reactor.

The custom built 2nd generation flatbed reactor was used to successfully synthesize juglone in both IPA and TAA (Experiments 48-49). Percentage conversions of 72 and 84 % were determined (^{1}H NMR, acetone-d_6) respectively after 6 hours of solar radiation under partial cloud conditions (AGR = 190 J/cm^2/hr, 45-54 % diffuse radiation). Under these non optimal Irish solar conditions juglone could be synthesized with yields up to 84 % on a large scale using the flatbed reactor. The increased surface area (0.67 m^2) allowed for more of the reaction solution to be irradiated simultaneously increasing yields, even in non optimal conditions (Table 2.14).

Table 2.14: Solar dye sensitized photooxygenation of 1,5-DHN and β-citronellol using the 2nd generation flat bed reactor.

Exp No	SM	Solvent	Time (hr)	Weather conditions	AGR (J/cm²/hr)	% conversion
48	1,5-DHN	IPA (8L)	6	Partial cloud	190	72
49	1,5-DHN	TAA (8L)	6	Partial cloud	190	85
50	β-citronellol	TAA (5L)	4	Direct sun	238	100

The solar dye sensitized photooxygenation of β-citronellol was also performed using optimal conditions outlined for the synthesis of juglone with the 2nd generation flatbed reactor (Experiment 50). Using TAA and rose Bengal complete conversion of β-citronellol to products was achieved in only 4 hours under direct sunlight conditions.

Although the solar dye sensitized photooxygenations of 1,5-DHN and β-citronellol were performed successfully using the custom built 2nd generation flat bed reactor several issues were identified. Firstly, the air supply tube was too far up from the bottom of the reaction vessel (Figure 2.17). Consequently, only the upper portion of the solution was aerated. This also resulted (juglone synthesis) in the settling of product and sensitizer at the bottom of the vessel. In addition the air bubbles generated by the tube were non uniform and far too big as the diameter of the air outlets were too large. Furthermore, the reactor was placed on the frame from the 1st generation flatbed reactor (30 °) which was not the optimal angle for solar insolation at our latitude during the summer months. Finally, water tubing was to allow for cooling was not incorporated into the design. Consequently, water cooling was applied every 20 minutes in the form of a stream of water over the surface of the reactor. This was both inefficient and hazardous.

2.3.5 3rd Generation flatbed reactor

A 3rd generation flatbed reactor was developed in order to rectify the issues raised during the operation of the 2nd generation flatbed reactor (Figure 2.18). Firstly, the air inlet tube was moved closer to the bottom of the reaction vessel. In addition, the air outlet diameters were decreased generating a fine stream of air bubbles. They

were also faced towards the bottom of the vessel in order to prevent settling of any precipitates and to generate a directional current in the vessel to ensure complete homogeneity of the reaction solution. The angle of the flatbed reactor was also adjusted to 38 ° by constructing a new wedge shaped frame from aluminium box tubing. Finally, a sheet of reflective Mylar® was adhered to the rear surface of the reactor. Reflective Mylar® is a sheet of polyethylene terephthalate (PET) coated with a reflective membrane used in the hydroponics industry. It reflects up to 98 % of all incident light. By adhering this to the back of the reactor we could reflect any unabsorbed light back through the reaction solution increasing light intensity within the reaction solution.

Figure 2.18: 3rd Generation flatbed reactor showing 38 ° aluminium wedge, reflective mylar and lowered air inlet tube.

The third generation flatbed reactor was not utilised for any solar dye sensitized photooxygenations. Although delivered to DCU inadequate solar conditions did not allow for its use before it was shipped to Dr. Michael Oelgemoeller, James Cook University, Townsville, Queensland, Australia for further solar chemical research.

2.3.6 Juglone synthesis using artificial and solar light: comparison of data

Table 2.15 below shows the relevant data collected during the synthesis of juglone using both artificial and solar radiation.

Table 2.15: Solvent, sensitizer, time, radiation, energy, water usage and yield data for the synthesis of juglone.

Exp No	Setup	Solvent	SM (mM)	RB (mM)	Time (hr)	Water (L/min)	Light	Energy (kJ/hr)	Yield / conversion (%)
21	Schlenk	TAA	10	0.25	3	4	500 W	1561.4	65
22	Schlenk	TAA	10	0.25	3	4	500 W	1561.4	62
23	Schlenk	TAA	10	0.25	3	4	500 W	1561.4	60
39	Schlenk	TAA	18.7	0.98	3	4	AGR = 238	5.2	69
40	Schlenk	TAA	18.7	0.98	3	4	AGR = 183	5.2	33
41	Schlenk	TAA	18.7	0.98	3	4	AGR = 183	5.2	34
42	Schlenk	TAA	18.7	0.98	5	4	AGR = 130	5.2	26
44	Schlenk	TAA	10	0.245	3	N/A	Direct sun	N/A	69
48	2^{nd} gen Flat bed	TAA	10	0.25	6	N/A	AGR = 190	72	85
49	2^{nd} gen Flat bed	IPA	10	0.25	6	N/A	AGR = 190	72	72

The results from Table 2.15 demonstrate that juglone can be synthesized successfully using a Schlenk flask apparatus with either artificial (500 W halogen lamp) or solar radiation. However, utilization of solar radiation results in the direct saving of up to 1556.4 kJ/hr of electric energy. This is a significant reduction in electrical energy required and is in compliance with rule 6 of the twelve principles of green chemistry. In addition, superior yields have been achieved (Experiment 39) under optimal Irish solar conditions (AGR $\geq$ 238 J/cm^2/hr, < 39 % diffuse radiation). The use of flat bed reactor technology further improves the efficiency of the synthetic process (Experiments 48 & 49). Under partial cloud conditions (AGR = 190 J/cm^2/hr, 45-54 % diffuse radiation) rates of conversion of up to 85 % were realized using TAA as the reaction solvent. Lower conversion rates (72 %) were achieved using IPA as

solvent. Both of these results are superior than those obtained using a 500 W halogen lamp. They are also superior to those obtained using a Schlenk flask apparatus.

However, despite these encouraging results, the results of experiments 39 to 42 demonstrate how the amount of available solar radiation profoundly affects the outcome of these reactions (Figure 2.13). For the dye sensitized photooxygenation of 1,5-DHN to be performed efficiently, optimal (Irish) solar conditions are required. At DCU this represents a sunny day with no cloud cover. Weather conditions such as these are achieved only a limited number of times a year during the summer months. For this reason the setup of a pilot scale solar chemical plant at DCU would not be viable.

2.3.7 Green issues with dye sensitized solar photooxygenations

The solar dye sensitized photooxygenations of 1,5-dihydroxynaphthalene, β-citronellol and α-terpinene are considered to be "green" synthetic processes as they satisfy the same set of rules outlined for indoor laboratory scale reactions (Section 2.2.3). Solar photooxygenations also have the added advantage of large energy savings compared to the use of the 500 W halogen lamp. The synthetic processes are now more energy efficient with only 5.2 kJ/hr or 72kJ/hr of energy required to supply a stream of air (depending on the pump used). However, despite this large energy saving on an already "green" synthetic process a number of potential issues and hazards were identified.

2.3.7.1 Laboratory scale solar photooxygenations (Schlenk flask)

Laboratory scale solar photooxygenations were performed using the same experimental setup as was used in the laboratory leading to several issues.

- Both water and electricity had to be supplied to the balcony using electrical extension leads and long lengths of water tubing via an open window (safety issue).

- A condenser was fitted to the Schlenk flask to prevent any loss of volatile solvents to the atmosphere. This added a degree of complexity to the experimental setup as water had to be supplied to both the cold finger and the condenser.
- The experimental setup had to be tethered to the balcony in order to stabilize it as sudden gusts of wind could knock it over.
- Solar tracking was impossible due to the tethering of the apparatus.
- Sunlight conditions had a profound effect on the overall result of the experiments.
- Purification using column chromatography was still necessary to remove the sensitizer.

2.3.7.2 Solar photooxygenations using flatbed reactors

Solar photooxygenations were performed using flatbed reactors and showed that the use of this technology greatly improved isolated yields and conversion rates. Despite this several health and safety issues were identified.

- Similar to the laboratory scale solar photooxygenations, both water and electricity had to be supplied to the balcony using electrical extension leads and long length of water tubing via an open window.
- In the case of the 2nd generation flatbed reactor no cooling system was implemented and as a result cold water had to be run over the external surface of the reactor every 20 minutes.
- Large volumes of solvents had to be transported to and from the balcony including the filling and emptying of the flatbed reactors (VOC exposure).
- Work up was also an issue with up to 8 L of solvent to be removed under vacuum post reaction. Without proper instrumentation this is both laborious and time consuming.
- Similar to laboratory scale solar photooxygenations sunlight conditions profoundly affected the final results.
- Purification using column chromatography was still necessary to remove the sensitizer.

2.4 Conclusion

The primary goal of this work was to determine if the dye sensitized photooxygenations of 1,5-dihydroxynaphthalene, α-terpinene and β-citronellol could be performed under Irish solar conditions. The secondary goal of this work was to determine if a small scale pilot plant could be established for the year round production of fine chemicals through these processes.

In order to accomplish these goals, the dye sensitized photooxygenations of the three target compounds were initially performed on a laboratory scale (50-100 ml) under artificial light (500 W halogen lamp) conditions. It was established that the light source, water cooling and purification methods required under these conditions impacted the "greenness" of the process. The photooxygenations were then performed under solar conditions to eliminate the need for the 500 W halogen lamp. Unfortunately, the water cooling and column chromatography could not be replaced as they were necessary for all experiments performed.

Initial results from the solar dye sensitized photooxygenation of 1,5-dihydroxynaphthalene confirmed that it was feasible to synthesize juglone in high yields (up to 84 %) under Irish solar conditions. This was in conjunction with the added saving of up to 1556.4 kJ/hr of electrical energy. Despite these early promising results, it became apparent that both laboratory and large scale reactions were heavily dependent on the amount of solar radiation available. Even during the summer months of May, June and July it required an unusually clear sunny day to achieve these high yields.

In conjunction with this realisation, several other factors were identified that would deter the establishment of a small scale pilot plant for the photochemical production of fine chemicals at DCU These issues fell under three separate headings; water cooling, purification and safety issues.

Water cooling

Water cooling (via a cold finger) was compulsory during all dye sensitized photooxygenations performed under artificial light (500 W halogen lamp) conditions

in the laboratory. This was due to the large quantities of thermal energy generated by the halogen lamp. In addition, flow rate measurements showed that up to 4 L/min or 240 L/hr of water were required to maintain ambient temperatures.

When performing solar photooxygenations (under Irish solar conditions) using the Schlenk flask it was found that water cooling was required, again comsuming up to 4 L/min of water. While utilising flat bed reactor technology it was found that due to the increased surface area of the reactor the reaction mixture quickly began to heat up, especially under optimal solar conditions (AGR $\geq$ 238 J/cm^2/hr, < 39 % diffuse radiation). The addition of the reflective sheet of Mylar on the 2nd generation flat bed reactor further compounded this issue. As water cooling tubing was not incorporated into the design of the custom built flat bed reactors water cooling was applied by running a stream of water over the surface of the reactor every 20 minutes. This would have reduced the rate of water consumption however, if water cooling tubing was incorporated into the design it would use similar quantities of water as the Schlenk flask setup (depending on tubing diameter).

Purification

^{1}H NMR and UV-Vis spectroscopy were used to determine the percent conversion of starting materials into product(s) throughout this work. However, isolation of the final products required purification in the form of column chromatography. This was true even in cases where complete conversion to product(s) was achieved. In order to isolate the pure products the sensitizer had to be removed. Although this was a simple process, column chromatography resulted in large quantities of waste in the form of waste silica gel and solvents (primarily ethyl acetate and cyclohexane).

Safety issues

As mentioned in Section 2.3.7.2 a series of health and safety issues were identified.

If a small scale pilot plant was established at DCU it would have to address each of these issues. In addition to facing south it would have to be designed to incorporate fail safe systems to prevent release of chemicals to the environment. Also any

systems put in place would have to be resistant to adverse weather conditions and/or easily dismantled for storage during the winter months.

In conclusion, the establishment of a multi liter scale pilot plant for the synthesis of fine chemicals through the solar photooxygenations of 1,5-dihydroxynaphthalene, α-terpinene and β-citronellol is not recommended. The overall cost of the initial setup would not justify the operation of the plant during the summer months only. Ireland simply does not receive enough sunlight annually for such a plant to be cost effective. As a result any further research into the area of synthetic photochemistry should concentrate on the concept of microflow photochemistry. Microflow technology could provide consistent and reproducible low cost, low energy consumption radiation conditions for the synthesis of fine chemicals through dye sensitized photooxygenations. Furthermore, if the sensitizers could be immobilised onto a solid support, purification of the reaction mixture would be simplified, eliminating unwanted waste.

2.5 Experimental

2.5.1 Solvents and reagents

All solvents and reagents were purchased from either Sigma-Aldrich or Fluka and were used as received unless otherwise stated.

2.5.2 Spectroscopic methods

UV-Vis spectroscopy

UV-Vis spectra were recorded on a Varian Cary 50 UV-Vis spectrophotometer in reagent grade *iso*-propyl alcohol or *tert*-amyl alcohol.

FT-IR spectroscopy

FT-IR spectra were recorded using KBr disks on a Perkin Elmer system 2000 FT-IR spectrophotometer.

NMR spectroscopy

NMR specta were recorded on a Bruker 400 UltrashieldTM instrument (400 MHz for ^{1}H; 100 MHz for ^{13}C) using the XWin-NMR 2.6 software. Chemical shift values are referred to solvent residual resonances: $CDCl_3$ (^{1}H, 7.26 / ^{13}C, 77.36 ppm), acetone-d_6 (^{1}H, 2.05 / 29.8 and ^{13}C, 206.3 ppm). Chemical shifts (δ) are given in ppm, coupling constant (J) in Hz.

2.5.3 Light intensity measurements

All light intensity measurements were performed using a hand held, data logging lux meter (ATP LX-8890A) and recorded in lux.

2.5.4 Column chromatography

Column chromatography was carried out using Merck silica gel 60 (particle size 0.063-0.200 nm for column chromatography) 70-230 mesh.

2.5.5 Validation of the dye sensitized photooxygenation of 1,5-DHN (Experiments 1-13)

2.5.5.1 Experimental setup

The general experimental setup for the synthesis of juglone can be seen in Figure 2.12.

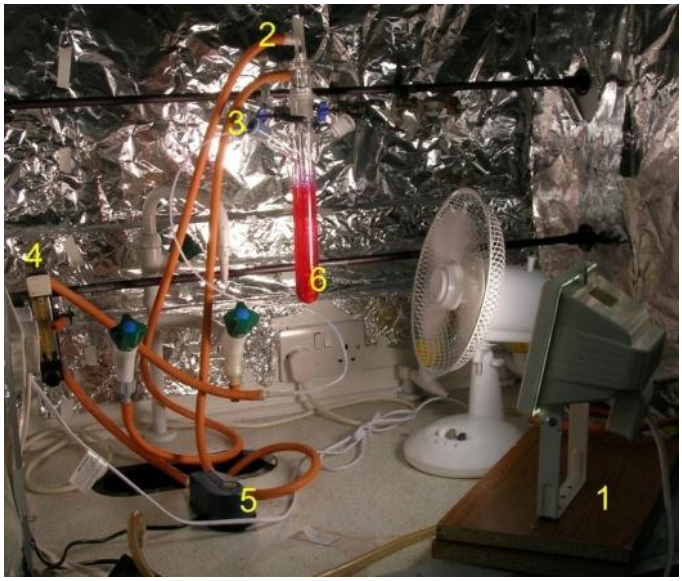

Figure 2.12: Experimental setup for synthesis of juglone. 1) 500 W halogen lamp, 2&3) cold finger showing water inlet and outlet, 4) air flow meter, 5) aquarium pump, 6) Schlenk flask showing HPLC inlet filter.

All reactions were performed in either 100 ml or 50 ml Pyrex Schlenk flasks with constant air bubbling during the irradiation time unless otherwise stated. The air flow to the reaction solution was kept constant throughout all experiments using an air flow meter. In order to minimise the size of the air bubbles entering the reaction solution an HPLC inlet filter was fitted to the end of the air supply tube. Water cooling was applied via a "cold finger". This helped to maintain the reaction solution at an ambient temperature (15-25 °C). During experiments where volatile solvents were used a condenser was fitted to prevent the unwanted loss of solvent. Depending on the experiment in question several light sources were utilised. A 500 W halogen lamp (IQ group) was used predominantly however, while investigating the sensitizer free synthesis of juglone UV light was required. This came from two sources; 1) The Rayonet photochemical chamber reactor (RPR200, Southern New

England) fitted with 16 RPR-3000Å lamps (λ = 300±25 nm) and 2) a medium pressure mercury lamp (400 W, model 3040, Photochemical Reactors Limited). The emission spectra for each of these lamps can be found in the appendix.

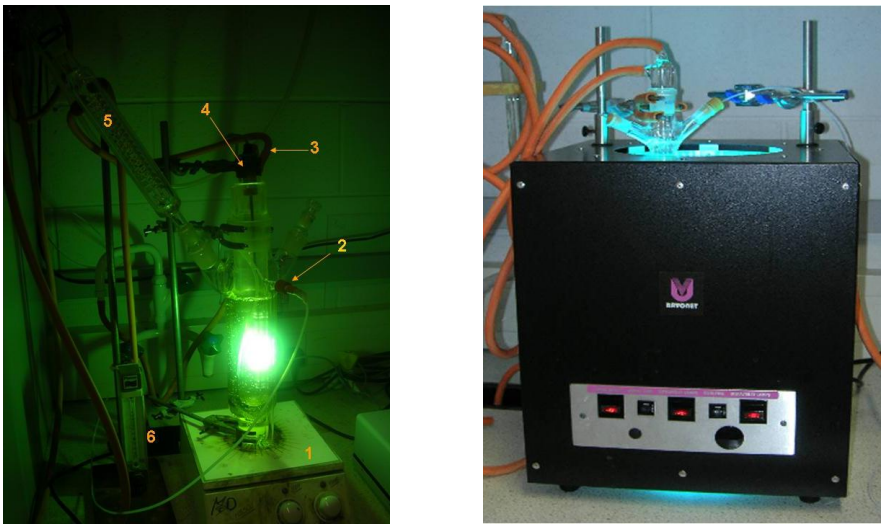

Figure 2.13: A) Medium pressure mercury lamp showing 1) stirring plate, 2) air supply, 3) water inlet, 4) power supply to lamp, 5) condenser and 6) air flow meter. B) Rayonette UV photochemical reactor showing Schlenk flask and cold finger in use.

2.5.5.2 Dark room experiments

General procedure

1,5-Dihydroxynaphthalene (1.44 mg, 0.18 mM) was dissolved in 50 ml of solvent under red light conditions with and without the presence of rose Bengal (12.7 mg, 0.25 mM). The solution was then left to react for 4 – 12 hours in complete darkness with constant air bubbling. Cooling via cold finger was not required as no light source was present. ^{1}H NMR (acetone-d_6) was used to determine percent conversions. ^{1}H NMR showed no evidence for the formation of juglone. Subsequent purification and isolation of juglone was not attempted.

Experiment 1 Dark synthesis with IPA and RB

1,5-DHN (1.44 mg, 0.18 mM) was dissolved in 50 ml of IPA along with rose Bengal (12.7 mg, 0.25 mM). ^{1} H NMR confirmed that no formation of juglone had occurred after 4 hours.

Experiment 2 Dark synthesis with IPA and no sensitizer

1,5-DHN (1.44 mg, 0.18 mM) was dissolved in 50 ml of IPA without rose Bengal. ^{1}H NMR confirmed that no formation of juglone had occurred after 4 hours.

Experiment 3 Dark synthesis with TAA and RB

1,5-DHN (1.44 mg, 0.18 mM) was dissolved in 50 ml of TAA along with rose Bengal (12.7 mg, 0.25 mM). ^{1}H NMR confirmed that no formation of juglone had occurred after 4 hours.

Experiment 4 Dark synthesis with TAA and no sensitizer

1,5-DHN (1.44 mg, 0.18 mM) was dissolved in 50 ml of TAA without rose Bengal. ^{1}H NMR confirmed that no formation of juglone had occurred after 4 hours.

Experiment 5 Dark synthesis with acetone and no sensitizer

1,5-DHN (1.44 mg, 0.18 mM) was dissolved in 50 ml of acetone without rose Bengal. ^{1}H NMR confirmed that no formation of juglone had occurred after 4 hours.

Experiment 6 Dark synthesis with TAA and RB

1,5-DHN (1.44 mg, 0.18 mM) was dissolved in 50 ml of IPA along with rose Bengal (12.7 mg, 0.25 mM). ^{1}H NMR confirmed that no formation of juglone had occurred after 12 hours.

2.5.5.3 Sensitizer free experiments

General procedure

Sublimed or technical grade 1,5-dihydroxynaphthalene (80 mg, 10 mM) was dissolved in 50 ml of TAA using sonication. The solution was then irradiated for 6 hours using either visible or ultra violet (UV) light. ^{1}H NMR (acetone-d_6) was used to determine the rates of conversion to juglone.

Experiment 7 ***Sensitizer free synthesis using sublimed 1,5-DHN (halogen lamp)***

Sublimed 1,5-DHN (80 mg, 10 mM) was dissolved in 50 ml of TAA with sonication. This was then irradiated for 6 hours using a 500 W halogen lamp. ^{1}H NMR (acetone-d_6) confirmed a 14 % conversion to juglone.

Experiment 8 ***Sensitizer free synthesis using technical grade 1,5-DHN (halogen lamp)***

Technical grade 1,5-DHN (80 mg, 10 mM) was dissolved in 50 ml of TAA with sonication. This was then irradiated for 6 hours using a 500 W halogen lamp. ^{1}H NMR (acetone-d_6) confirmed an 8 % conversion to juglone.

Experiment 9 ***Sensitizer free synthesis using technical grade 1,5-DHN (Hg lamp)***

Technical grade 1,5-DHN (80 mg, 10 mM) was dissolved in 50 ml of TAA with sonication. This was then irradiated for 6 hours using a 400 W medium pressure Hg lamp. ^{1}H NMR (acetone-d_6) confirmed a 24 % conversion to juglone.

Experiment 10 ***Sensitizer free synthesis using technical grade 1,5-DHN (Rayonet reactor)***

Technical grade 1,5-DHN (80 mg, 10 mM) was dissolved in 50 ml of TAA with sonication. This was then irradiated for 6 hours using the Rayonet ($\lambda = 300 \pm 25$ nm) reactor. ^{1}H NMR (acetone-d_6) confirmed a 19 % conversion to juglone.

2.5.5.4 Synthesis with nitrogen and helium purging

Experiment 11 ***Synthesis with N_2 purge and N_2 bubbling***

1,5-DHN (80 mg, 10 mM) and rose Bengal (12.7 mg, 0.25 mM) were dissolved in 50 ml of TAA with sonication. This solution was then degassed using N_2 for 160 minutes. The reaction solution was then irradiated for 6 hours using a 500 W halogen lamp. N_2 was bubbled through the reaction solution constantly during the irradiation time. ^{1}H NMR (acetone-d_6) showed a 10 % conversion to juglone.

Experiment 12 Synthesis with He purge and no bubbling

1,5-DHN (10 mM) and rose Bengal (80 mg, 0.25 mM) were dissolved in 50 ml of TAA with sonication. This solution was then degassed with He for 60 minutes. The reaction solution was then irradiated for 6 hours using a 500 W halogen lamp. N_2 or He bubbling was not performed during the 6 hour reaction time. ^{1}H NMR (acetone-d_6) showed a 30 % conversion to juglone.

Experiment 13 Synthesis with He purge and N_2 bubbling

1,5-DHN (10 mM) and rose Bengal (80 mg, 0.25 mM) were dissolved in 50 ml of TAA with sonication. This solution was then degassed with helium for 60 minutes. The reaction solution was then irradiated for 6 hours using a 500 W halogen lamp. N_2 was bubbled through the reaction solution constantly during the irradiation time. ^{1}H NMR (acetone-d_6) showed no evidence for the formation of juglone.

2.5.6 Solvent optimisation for the dye sensitized photooxygenation of 1,5-DHN (Experiments 14-20)

General procedure

1,5-Dihydroxynaphthalene (80 mg, 10 mM) and rose Bengal (12.7 mg, 0.25 mM) were dissolved in 50 ml of solvent with sonication. This was then irradiated for 4 hours (500 W halogen lamp) with constant air bubbling and cooling with a cold finger. ^{1}H NMR (acetone-d_6) was used to determine the final rate of conversion.

Experiment 14 Dye sensitized photooxygenation of 1,5-DHN using methanol

The general procedure was followed using methanol as the solvent. ^{1}H NMR confirmed a 22 % conversion to juglone.

Experiment 15 Dye sensitized photooxygenation of 1,5-DHN using ethanol

The general procedure was followed using ethanol as the solvent. ^{1}H NMR confirmed a 30 % conversion to juglone.

Experiment 16 Dye sensitized photooxygenation of 1,5-DHN using IPA

The general procedure was followed using IPA as the solvent. ^{1}H NMR confirmed a 32 % conversion to juglone.

Experiment 17 Dye sensitized photooxygenation of 1,5-DHN using TAA

The general procedure was followed using TAA as the solvent. ^{1}H NMR confirmed a 39 % conversion to juglone.

Experiment 18 Dye sensitized photooxygenation of 1,5-DHN using acetone

The general procedure was followed using acetone as the solvent. ^{1}H NMR confirmed a 14 % conversion to juglone.

Experiment 19 Dye sensitized photooxygenation of 1,5-DHN using ethyl acetate

The general procedure was followed using ethyl acetate as the solvent. ^{1}H NMR confirmed a 9.5 % conversion to juglone.

Experiment 20 Dye sensitized photooxygenation of 1,5-DHN using water

The general procedure was followed using water as the solvent. ^{1}H NMR confirmed an 11 % conversion to juglone.

2.5.7 Optimised dye sensitized photooxygenation of 1,5-DHN (Experiments 21-23)

General procedure

1,5-Dihydroxynaphthalene (80 mg, 10 mM) and rose Bengal (12.7 mg, 0.25 mM) were dissolved in 50 ml of TAA with sonication. The solutions were irradiated in front of a 500 W halogen lamp (27 cm) for 3 hours with constant air bubbling and cooling via a cold finger. The resulting crude reaction mixture was then evaporated to dryness under vacuum to afford a brown/orange solid. Juglone was isolated as bright orange crystals from this crude solid via column chromatography using silica gel (Merck) and a mixture of 3:1 cyclohexane/ethyl acetate as the mobile phase.

Experiment 21 Optimised dye sensitized photooxygenation of 1,5-DHN (1)

The general procedure was followed. Juglone was isolated as fluffy bright orange crystals in a 65 % yield (56.6 mg).

^{1}H NMR: (400 MHz, Acetone-d_6) δ (ppm) = 7.04 (d, 1H, **H_{quin}**, J^3 = 10.4 Hz); 7.08 (d, 1H, **H_{quin}**, J^3 = 10.4 Hz); 7.33 (d, 1H, **H_{arom}**, J^3 = 8.4 Hz, J^4 = 1.2 Hz); 7.58 (d, 1H, **H_{arom}**, J^3 = 7.6 Hz, J^4 = 1.2 Hz); 7.78 (dd, 1H, **H_{arom}**, J^3 = 7.6 Hz, 8.4 Hz); 11.92 (s, 1H O**H**).

UV-Vis: (MeOH) λ (nm) = 248, 419.

MP: 164-165 º C

Experiment 22 Optimised dye sensitized photooxygenation of 1,5-DHN (2)

The general procedure was followed. Juglone was isolated as fluffy bright orange crystal in a 66 % yield (57.5 mg).

Experiment 23 Optimised dye sensitized photooxygenation of 1,5-DHN (3)

The general procedure was followed. Juglone was isolated as fluffy bright orange crystal in a 60 % yield (52.2 mg).

2.5.8 Dye sensitized photooxygenation of α-terpinene in acetone (Experiments 24-26)

General procedure

The experimental setup was identical to the synthesis of juglone (Section 2.6.1). Sensitizer (0.25 mM) was dissolved in 50 ml of acetone with sonication. This was placed 27 cm from a 500 W halogen lamp with constant air bubbling and cooling via a cold finger. α-Terpinene (1ml, 104 mM) was added and the solution irradiated for 2 hours. The solvent was removed after this time via rotary evaporation to afford a viscous oil. Column chromatography was performed using silica gel (Merck) and a mobile phase of 95:5 cyclohexane/ethyl acetate. This afforded ascaridole as a clear pale yellow oil.

Experiment 24 Dye sensitized photooxygenation of α-terpinene using RB

The general procedure was followed using rose Bengal as sensitizer. Ascaridole was isolated in a 58 % yield (0.5073 g).

Experiment 25 Dye sensitized photooxygenation of α-terpinene using MB

The general procedure was followed using methylene blue as sensitizer. Ascaridole was isolated in a 42 % yield (0.3674 g).

Experiment 26 Dye sensitized photooxygenation of α-terpinene using TPP

The general procedure was followed using tetraphenyl porphyrin as sensitizer. Ascaridole was isolated in a 61 % yield (0.5336 g).

2.5.9 UV-Vis calibration curves

The wavelength of maximum absorbance or λ-max was determined for α-terpinene in reagent grade IPA, TAA and ethanol. These were 265.5, 267 and 266 nm respectively. Three solutions of α-terpinene (0.26 mM) were made up in these solvents and a set of serial dilutions were then performed to provide a set of calibration standards ranging from 0.26 to 0.0163 mM for UV-Vis analysis (Table 2.5). The absorbance of each solution was measured (in triplicate) at the appropriate λ-max using a UV-Vis spectrophotometer. The average absorbance values were then plotted against concentration to generate accurate calibration curves (Figures 2.5-2.7).

2.5.10 Synthesis of TPP and TCPP (Experiments 27 – 28)

Experiment 27 Synthesis of TPP

TPP was synthesized using the Adler method.[21] 1.4 ml (20 mmol) Of freshly distilled pyrrole and 2 ml (20 mmol) of benzaldehyde were dissolved in 100 ml of propionic acid and refluxed (160 °C) for 2 hours. TPP formed as a purple precipitate. The precipitate was collected via vacuum filtration and washed with methanol (3 x 20 ml). TPP was isolated as bright purple crystals in 20 – 25 % yields (0.615-0.768 g)

^{1}H NMR: (400 MHz, $CDCl_3$) δ (ppm) = -2.69 (s, 2H, NH), 7.77 (brs, 12H, *m*Ph & *p*Ph), 8.25 (brs, 8H, *o*Ph), 8.88 (s, 8H, βH). Data in agreement with literature.[21]

UV-Vis: (DCM) λ (nm) = 417, 515, 551, 592, 647

UV-Vis: ($CHCl_3$) λ (nm) = 417, 514, 549, 589, 644

Experiment 28 Synthesis of TCPP

TCPP was synthesized using the Adler method.[21] 3.5 ml (50 mmol) Of freshly distilled pyrrole and 7.5 g (50 mmol) of 4-carboxybenzaldehyde were dissolved in 130 ml of propionic acid and refluxed (160 °C) for 2 hours. TCPP formed as a purple precipitate. The precipitate was collected via vacuum filtration and washed with DCM (3 x 20 ml). The resulting purple solid was then dissolved in an aqueous NaOH solution (1 M). A solution of 0.1 M HCl was then added slowly to re-precipitate the TCPP. The resulting precipitate was collected by vacuum filtration and washed with ice cold water (3 x 20 ml) followed by DCM (2 x 20 ml). TCPP was isolated as dull purple crystals in 25 – 30 % yield (2.4926-2.9652 g).

^{1}H NMR: (400 MHz, DMSO-d_6) δ (ppm) = -2.94 (s, 2H, NH), 8.40 (m, 16H, *m*Ph & *o*Ph), 8.87 (s, 8H, βH), 13.32 (s, 4H, COOH). Data in agreement with literature.[22]

UV-Vis: (Methanol) λ (nm) = 415, 515, 549, 591,646.

UV-Vis: (Ethanol) λ (nm) = 419, 514, 548, 588, 645.

2.5.11 Dye sensitized photooxygenation of α-terpinene in TAA (Experiments 29-31)

General procedure

Sensitizer (0.25 mM) was dissolved in 50 ml of TAA with sonication. This was placed 27 cm from a 500 W halogen lamp with constant air bubbling and cooling via a cold finger. α-Terpinene (1 ml, 104 mM) was added and the solution irradiated for 2 hours. 0.1 ml Samples were taken every 15 minutes and diluted by a factor of 1000. The absorbance was then measured at 267 nm and the percentage conversion calculated based upon previously generated calibration curves.

Experiment 29 Dye sensitized photooxygenation of α-terpinene using RB

The general procedure was followed using rose Bengal as sensitizer. The percentage conversion was calculated to be 97 % after 2 hours.

Experiment 30 Dye sensitized photooxygenation of α-terpinene using MB

The general procedure was followed using methylene blue as sensitizer. The percentage conversion was calculated to be approximately 15 % after 2 hours.

Experiment 31 Dye sensitized photooxygenation of α-terpinene using TCPP

The general procedure was followed using TCPP as sensitizer. Complete conversion was realised after 2 hours.

2.5.12 Dye sensitized photooxygenation of β-citronellol (Experiments 32-38)

General procedure

The experimental setup was identical to the synthesis of juglone (Section 2.6.1). Sensitizer (0.25 mM) was dissolved in 50 ml of solvent with sonication. This was placed 27 cm from a 500 W halogen lamp with constant air bubbling and cooling via a cold finger. 1 ml (104 mM) Of β-citronellol was added and the solution irradiated for 2 hours. The solvent was removed after this time via rotary evaporation and ^{1}H NMR ($CDCl_3$) was used to determine the rate of conversion.

Experiment 32 Dye sensitized photooxygenation of β-citronellol with TAA and RB

The general procedure was followed using rose Bengal as the sensitizer and TAA as the reaction solvent. ^{1}H NMR confirmed a 44 % conversion after 2 hours.

Experiment 33 Dye sensitized photooxygenation of β-citronellol with TAA and MB

The general procedure was followed using methylene blue as the sensitizer and TAA as the reaction solvent. ^{1}H NMR confirmed a 52 % conversion after 2 hours.

Experiment 34 ***Dye sensitized photooxygenation of β-citronellol with acetone and RB***

The general procedure was followed using rose Bengal as the sensitizer and acetone as the reaction solvent. ^{1}H NMR confirmed a 62 % conversion after 2 hours.

Experiment 35 ***Dye sensitized photooxygenation of β-citronellol with acetone and MB***

The general procedure was followed using methylene blue as the sensitizer and acetone as the reaction solvent. ^{1}H NMR confirmed a 90 % conversion after 2 hours.

Experiment 36 ***Dye sensitized photooxygenation of β-citronellol with acetone and TPP***

The general procedure was followed using tetraphenyl porphyrin as the sensitizer and acetone as the reaction solvent. ^{1}H NMR confirmed a 86 % conversion after 2 hours.

Experiment 37 ***Dye sensitized photooxygenation of β-citronellol with acetone and TCPP***

The general procedure was followed using TCPP as the sensitizer and acetone as the reaction solvent. ^{1}H NMR confirmed a 60 % conversion after 2 hours.

Experiment 38 ***Dye sensitized photooxygenation of β-citronellol with TAA and TCPP***

The general procedure was followed using TCPP as the sensitizer and TAA as the reaction solvent. ^{1}H NMR confirmed a 51 % conversion after 2 hours.

2.5.13 Laboratory scale solar dye sensitized photooxygenations (Experiments 39-44)

2.5.13.1 Laboratory scale solar dye sensitized photooxygenation of 1,5-DHN (Irish solar conditions)

General procedure

The experimental setup was identical to the synthesis of juglone (Section 2.6.1). Rose Bengal (0.98 mM) and 1,5-dihydroxynaphthalene (18.7 mM) were dissolved in 100 ml of TAA with sonication. This was placed outdoors under solar radiation for

3 hours with constant air bubbling and cooling via a cold finger. Solar conditions were noted and compared to data collected by MET Eireann for the same time period. This allowed for the direct comparison of the final percent conversion to the average global radiation (AGR) received. The crude reaction solution was dried under vacuum to afford a brown/orange solid. Soxhlet extraction with hexanes or column chromatography (3:1 cyclohexane/ethyl acetate) were performed to isolate juglone as fluffy bright orange crystals.

Experiment 39 Solar dye sensitized photooxygenation of 1,5-DHN (1)

The reaction received direct sun (AGR $\geq$ 238 J/cm^2/hr, <39 % diffuse radiation) during all three hours of the reaction. Column chromatography was preformed to isolate juglone in a 69 % yield (0.2246 g).

Experiment 40 Solar dye sensitized photooxygenation of 1,5-DHN (2)

The reaction received partial sun (AGR $\geq$ 183 J/cm^2/hr, 55-69 % diffuse radiation) during all three hours of the reaction. Soxhlet extraction was performed to isolate juglone in a 33 % yield (0.1075 g).

Experiment 41 Solar dye sensitized photooxygenation of 1,5-DHN (3)

The reaction received partial sun (AGR $\geq$ 183 J/cm^2/hr, 55-69 % diffuse radiation) during all three hours of the reaction. Column chromatography was performed to isolate juglone in a 34 % yield (0.1107 g).

Experiment 42 Solar dye sensitized photooxygenation of 1,5-DHN (4)

The reaction conditions were overcast (AGR $\geq$ 130 J/cm^2/hr, >70 % diffuse radiation) during all three hours of the reaction. Column chromatography was performed to isolate juglone in a 26 % yield (0.0845 g).

2.5.13.2 Laboratory scale solar dye sensitized photooxygenation of 1,5-DHN (Spanish solar conditions)

General procedure

The experimental setup was identical to the synthesis of juglone (Section 2.6.1). Rose Bengal and 1,5-dihydroxynaphthalene were dissolved in 100 ml of TAA with sonication. This was placed outdoors under solar irradiation for 2 hours with constant air bubbling and cooling via a cold finger. Solar conditions were noted. Unfortunately average global radiation could not be calculated as meteorological data for this region could not be obtained. Column chromatography (3:1 cyclohexane/ethyl acetate) was performed to isolate juglone as fluffy bright orange crystals.

Experiment 43 Solar dye sensitized photooxygenation of 1,5-DHN (1)

Rose Bengal (0.49 mM) and 1,5-DHN (20 mM) were dissolved in 100 ml of TAA with sonication. This was then irradiated under direct sunlight conditions for 2 hours. The reaction solvent was removed under vacuum and the crude solid purified via column chromatography. Juglone was isolated in a 47 % yield (0.1639 g).

Experiment 44 Solar dye sensitized photooxygenation of 1,5-DHN (2)

Rose Bengal (0.245 mM) and 1,5-DHN (10 mM) were dissolved in 100 ml of TAA with sonication. This was then irradiated under direct sunlight conditions for 2 hours. The reaction solvent was removed under vacuum and the crude solid purified via column chromatography. Juglone was isolated in a 69 % yield (0.1204 g).

2.5.13.3 Laboratory scale solar dye sensitized photooxygenation of α-terpinene (Irish solar conditions)

Experiment 45 Solar dye sensitized photooxygenation of α-terpinene (1)

Rose Bengal (0.25 mM) and α-terpinene (52 mM) were dissolved in 100 ml of TAA with sonication. The solution was then irradiated for 5 hours under direct (1hr, AGR $\geq$238 J/cm^2/hr, < 39 % diffuse radiation) and partial (4hr, 183 J/cm^2/hr, 55-69 % diffuse radiation) sun conditions with constant air bubbling and cooling via cold finger. The reaction solvent was removed under vacuum and the crude oil was

purified via column chromatography (95:5 cyclohexane/ethyl acetate). Ascaridole was isolated in a 66 % yield (0.5774 g)

Experiment 46 Solar dye sensitized photooxygenation of α-terpinene (2)

Rose Bengal (0.25 mM) and α-terpinene (260 mM) were dissolved in 100 ml of TAA with sonication. The solution was then irradiated for 3 hours under direct sun conditions (AGR ≥ 238 J/cm^2/hr, < 39 % diffuse light) with constant air bubbling and cooling via cold finger. The reaction solvent was removed under vacuum and the crude oil was purified via column chromatography (95:5 cyclohexane/ethyl acetate). Ascaridole was isolated in a 45 % yield (1.9681 g).

2.5.14 Solar dye sensitized photooxygenations using a 2nd generation flat bed reactor

2.5.14.1 Solar dye sensitized photooxygenations using a prototype 2nd generation flat bed reactor

Experiment 47 Solar dye sensitized photooxygenation of 1,5-DHN

1,5-Dihydroxynaphthalene (7.8 mM) and rose Bengal (0.075 mM) were dissolved in 1.3 L of TAA with sonication. This was then transferred to the prototype flatbed reactor and irradiated for 6 hours under partial sun conditions (AGR = 183 J/cm^2/hr, 55-69 % diffuse light). The solvent was removed under vacuum and column chromatography using a mixture of 3:1 cyclohexane/ethyl acetate as the mobile phase was performed. Juglone was isolated in a 16 % yield as bright orange crystals (0.2823 g).

2.5.14.2 Solar dye sensitized photooxygenations using a custom built 2nd generation flat bed reactor

Experiment 48 Solar dye sensitized photooxygenation of 1,5-DHN in TAA

Rose Bengal (0.25 mM) and 1,5-dihydroxynaphthalene (10 mM) were dissolved in 8L of TAA with sonication and transferred into the 2nd generation flatbed reactor. This was irradiated for 6 hours under partial cloud (AGR = 190, 40-54 % diffuse radiation) conditions with constant air bubbling. Cooling was applied hourly by a stream of cold water on the external surface of the reactor. Solar conditions were

noted and compared to MET Eireann data for the same time period. ^{1}H NMR (acetone-d_6) showed an 85 % conversion to juglone.

Experiment 49 Solar dye sensitized photooxygenation of 1,5-DHN in IPA

Rose Bengal (0.25 mM) and 1,5-dihydroxynaphthalene (10 mM) were dissolved in 8L of IPA with sonication and transferred into the 2nd generation flatbed reactor. This was irradiated for 6 hours under partial cloud (AGR = 190, 40-54 % diffuse radiation) conditions with constant air bubbling. Cooling was applied hourly by a stream of cold water on the external surface of the reactor. Solar conditions were noted and compared to MET Eireann data for the same time period. ^{1}H NMR (acetone-d_6) showed a 72 % conversion to juglone.

Experiment 50 Solar dye sensitized photooxygenation of β-citronellol in TAA

β-Citronellol (40 mM) and rose Bengal (0.2 mM) were dissolved in 5 L of TAA with sonication. This was then transferred to the 2nd generation flatbed reactor and irradiated for 6 hours under direct sun conditions (AGR $\geq$ 238 J/cm^2/hr, < 39 % diffuse radiation). Samples (2 ml) were taken every hour for ^{1}H NMR analysis. ^{1}H NMR showed complete conversion of β-citronellol to its corresponding hydroperoxides in only 4 hours.

2.6 References

(1) Anastas, P. T.; Kirchhoff, M. M. *Acc. Chem. Res.* **2002**, *35*, 686-694.

(2) Jin, H.; Liu, H.; Zhang, Q.; Wu, Y. *J. Org. Chem.* **2005**, *70*, 4240-4247.

(3) Suzuki, M.; Ohtake, H.; Kameya, Y.; Hamanaka, N.; Noyori, R. *J. Org. Chem.* **1989**, *54*, 5292-5302.

(4) Valente, P.; Avery, T. D.; Taylor, D. K.; Tiekink, E. R. T. *J. Org. Chem.* **2009**, *74*, 274-282.

(5) Duchstein, H.; Wurm, G. *Arch Pharm* **1984**, 809-812.

(6) Murtinho, D.; Pineiro, M.; Pereira, M.M. *J.Chem.Soc., Perkin Trans 2*. **2000**, 2441.

(7) Luiz, M.; Soltermann, A. T. *Can. J. Chem.* **1996**, *74*, 49-54.

(8) Hurst, J. R.; McDonald, J. D.; Schuster, G. B. *J. Am. Chem. Soc.* **1982**, *104*, 2065-2067.

(9) Hurst, J. R.; Schuster, G. B. *J. Am. Chem. Soc.* **1983**, *105*, 5756-5760.

(10) Long, C. A.; Kearns, D. R. *J. Am. Chem. Soc.* **1975**, *97*, 2018-2020.

(11) Schweitzer, C.; Schmidt, R. *Chem. Rev.* **2003**, *103*, 1685-1758.

(12) Schmidt, R. *J. Am. Chem. Soc.* **1989**, *111*, 6983-6987.

(13) Brautbar, N.; Williams II, J. *Int. J. Hyg. Environ. Health* **2002**, *205*, 479-491.

(14) Alfonsi, K.; Colberg, J.; Dunn, P. J.; Fevig, T.; Jennings, S.; Johnson, T. A.; Kleine, H. P.; Knight, C.; Nagy, M. A.; Perry, D. A.; Stefaniak, M. *Green Chem.* **2008**, *10*, 31-36.

(15) Clennan, E. L.; Noe, L. J.; Wen, T.; Szneler, E. *J. Org. Chem.* **1989**, *54*, 3581-3584.

(16) Rodgers, M. A. J. *J. Am. Chem. Soc.* **1983**, *105*, 6201-6205.

(17) Studer, S. L.; Brewer, W. E.; Martinez, M. L.; Chou, P. T. *J. Am. Chem. Soc.* **1989**, *111*, 7643-7644.

(18) Young, R. H.; Brewer, D.; Keller, R. A. *J. Am. Chem. Soc.* **1973**, *95*, 375-379.

(19) Fuke, K.; Ueda, M.; Itoh, M. *J. Am. Chem. Soc.* **1983**, *105*, 1091-1096.

(20) Anonymous.; *www. http://energyworksus.com/solar_installation_position.html*.

(21) Molaei, H.; Dehghani, H. *Inorg. Chim. Acta* **2012**, *384*, 133-136.

(22) Gianferrara, T.; Bergamo, A.; Bratsos, I.; Milani, B.; Spagnul, C.; Sava, G.; Alessio, E. *J. Med. Chem.* **2010**, *53*, 4678-4690.

Chapter 3:

Heterogeneous dye sensitized photooxygenations:

Immobilisation of sensitizers onto Merrifeld resins.

3.1 Introduction

Dye sensitized photooxygenations are most commonly performed under homogenous conditions resulting in the need for purification of the crude reaction mixture to remove the sensitizer. Although this method is robust and the sensitizer can be removed easily the requirement for column chromatography (the use of large quantities of solvents and silica gel) means the synthetic process as a whole suffers with regards to environmental impact (1^{st} and 5^{th} rules of twelve principle of green chemistry).[1] Despite using catalytic amounts of sensitizer (9^{th} rule of the twelve principles of green chemistry) [1] large volumes of waste are still generated as a direct result of column chromatography. In addition to this, the sensitizer is not generally isolated during column chromatography and is discarded.

Immobilisation of the sensitiser onto Merrifield resin beads may provide a solution to these issues by eliminating the need for column chromatography. In the case of dye sensitized photooxygenations the sensitizer can be covalently bound to Merrifield resin beads. As a result, removal of the sensitizer from the crude reaction solution can then be achieved by simple gravity filtration or centrifugation. This elimination of column chromatography creates a more environmentally friendly synthetic process. Furthermore, the sensitizer can be easily recycled and used multiple times if desired.

First reported in 1963 by R.B. Merrifield, Merrifield resin beads were designed as solid supports for the synthesis of peptides.[2-5] Designed to be porous and chemically inert, Merrifield resin beads are a copolymer of polystyrene and 4-chloromethyl polystyrene with varying degrees of crosslinking with divinylbenzene (DVB) (Figure 3.1). Larger amounts of DVB increase the rigidity and mechanical strength of the beads. The amount of chloromethyl groups (linkers) can also be controlled during the polymer synthesis. Today these beads are commercially available with a wide range of bead sizes, degree of crosslinking and amount of linker present.

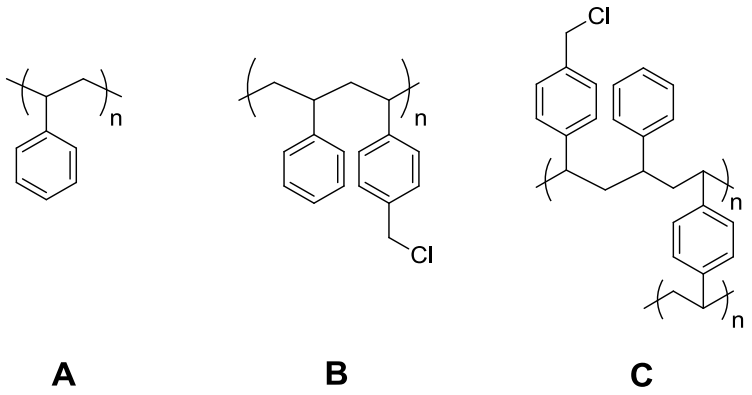

Figure 3.1: A) Polystyrene, B) Copolymer showing polystyrene and 4-chloromethyl polystyrene, C) Crosslinked Merrifield resin.

Immobilisation of a sensitizer to a solid support is known to reduce the singlet oxygen quantum yield (Φ^1O_2) of the sensitizer. Rose Bengal has a quantum yield of 0.76 in methanol.[6, 7] However, when bound to Merrifield resin beads this quantum yield of singlet oxygen decreases to 0.43.[8-10] thereby reducing the rate of a heterogeneous photooxygenation in comparison to homogenous based systems. The dye sensitized photooxygenation of α-terpinene to ascaridole was chosen as the model reaction to test the photosensitizing efficacy of the sensitizer/Merrifield resin beads since this reaction gave the fastest rate of conversion of the three dye sensitized photooxygenations discussed in Chapter 2. TCPP, and RB were covalently immobilized onto the Merrifield resin beads (RB covalently immobilised onto Merrifield resin beads is available commercially under the trade name Sensitox®.) since these sensitisers gave excellent results as outlined in Chapter 2. Results from the literature have shown that the incorporation of either zinc or palladium into the centre of porphyrins significantly increases the quantum yields of singlet oxygen and consequently, for this reason, TCPPZn was also synthesized and investigated.

3.2 Results and discussion

3.2.1 Control experiments

In order to determine if unfunctionalised Merrifield resin beads could catalyze (or affect) the dye sensitized photooxygenation of α-terpinene to ascaridole three control experiments were performed (Experiments 51-53). Two solutions of α-terpinene (104 mM) in 50 ml of IPA were allowed to react for 8 hours in the presence of 500 mg of unfunctionalised Merrifield resin beads with constant air bubbling. One of the reaction mixtures was irradiated using a 500 W halogen lamp and the other was placed in complete darkness for 8 hours. In addition, a third experiment was devised in order to determine if α-terpinene, similar to 1,5-DHN, could self sensitize to yield ascaridole. The resulting crude solutions were analysed by UV-Vis spectroscopy (265.5 nm) after 8 hours. The results are shown below in Table 3.1.

Table 3.1: Control experiments for the dye sensitized photooxygenation of α-terpinene using Merrifield resin beads.

Exp No	Light	MR (mg)	Air	Time (hr)	% Conversion
51	No	500	Yes	8	No Reaction
52	Yes	500	Yes	8	16
53	Yes	0	Yes	8	11

Experiment 51 shows that under dark room conditions no conversion of α-terpinene to ascaridole occurs. However, in Experiment 52 a 16 % conversion of α-terpinene to ascaridole was found after 8 hours of irradiation. The observed conversion was due to the self sensitization of α-terpinene to ascaridole as confirmed by Experiment 53 which gave an 11 % conversion after 8 hours of irradiation. The results of the control experiments demonstrate how unfunctionalised Merrifield resin beads may have a slight positive effect on the dye sensitized photooxygenation of α-terpinene.

3.2.2 Covalent functionalisation of Merrifield resin beads with TCPP and characterisation

Merrifield resin beads (200-400 mesh, 4.5 mmol Cl/g) were covalently functionalised with TCPP using a modified method described by Merrifield (Scheme 3.1, Experiment 54).[2]

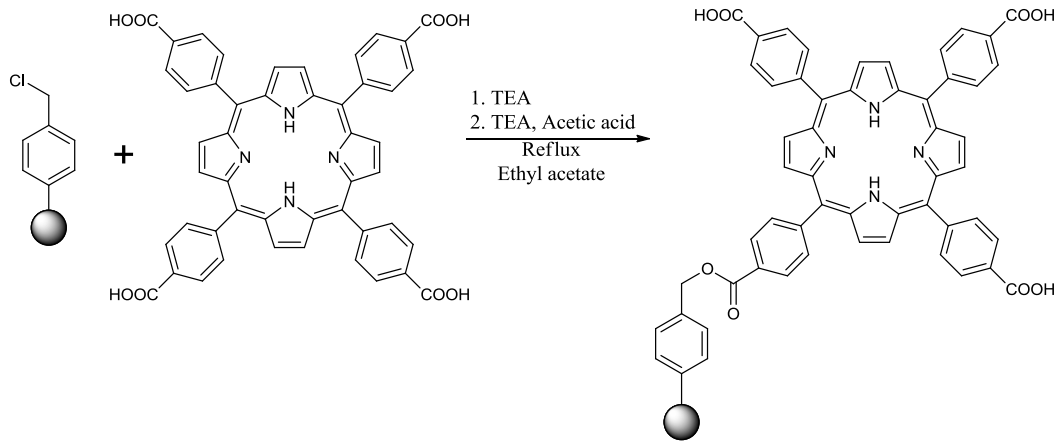

Scheme 3.1: Covalent functionalisation of Merrifield resin beads with TCPP.

Successful immobilisation of TCPP onto the Merrifield resin beads was followed by soxhlet extraction using methanol (48 hours) in order to remove any free sensitizer from the beads. The resulting TCPP Merrifield resin (TCPP-MR) beads were analysed by FT-IR and diffuse reflectance UV-Vis spectroscopy.

Diffuse reflectance UV-Vis spectra (KBr disk) were obtained for both TCPP and TCPP-MR. The TCPP spectrum clearly shows the Soret band at 428 nm and the four Q-bands at 529,573,618 and 680 nm (Figure 3.2). Comparison of this with the TCPP-MR spectrum shows that TCPP is present (Figure 3.3). UV-Vis spectroscopic analysis of methanol washings, form the soxhlet extraction of TCPP-MR beads, showed no presence of TCPP. Therefore, any signal recorded during the diffuse reflectance UV-Vis spectrum of the TCPP-MR beads is due to covalently immobilised TCPP. The Soret band for TCPP-MR can be seen at 422 nm and the Q-bands at 519, 553, 593 and 649 nm.

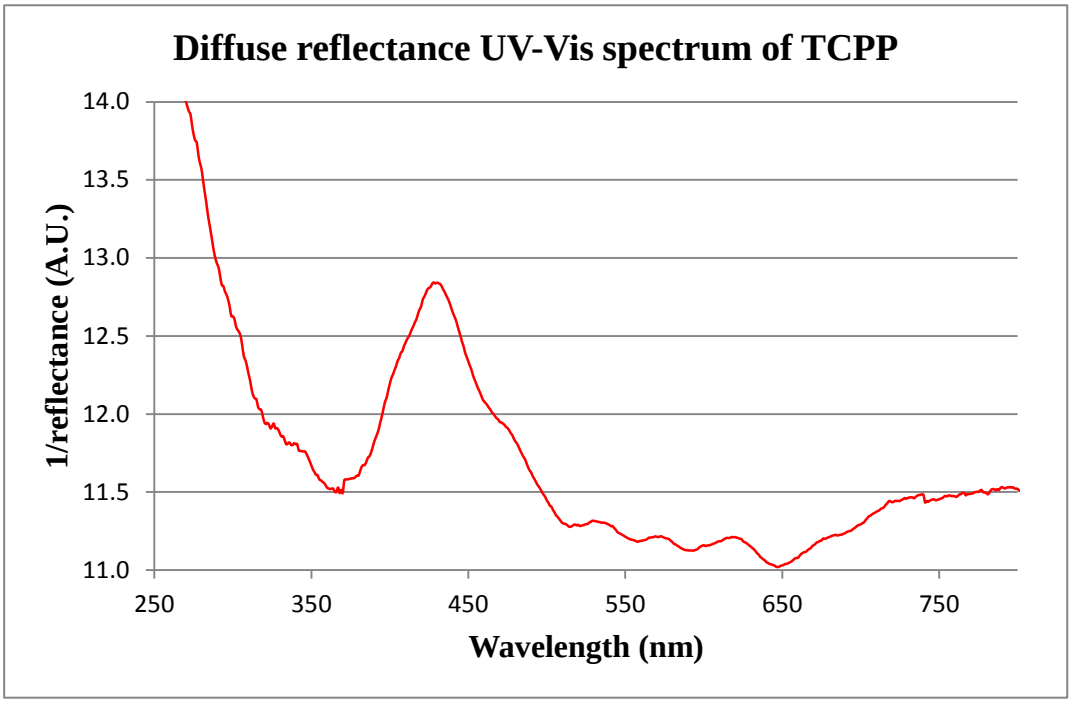

Figure 3.2: The diffuse reflectance UV-Vis spectrum of TCPP.

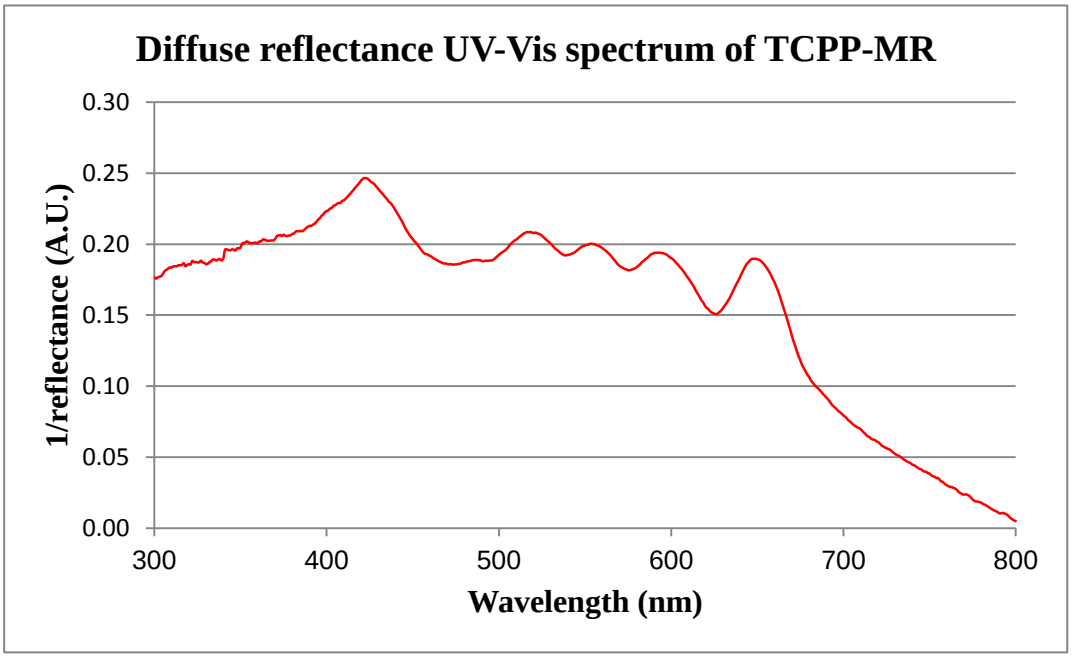

Figure 3.3: The diffuse reflectance UV-Vis spectrum of TCPP-MR.

FT-IR spectroscopy also confirmed that successful covalent attachment of TCPP onto Merrifield resin beads was achieved. Comparison of the two FT-IR spectra of MR and TCPP-MR shows the disappearance of the absorbance peak at 675 cm^{-1} (Figure 3.4). This absorbance peak is due to alkyl halide (C-Cl) stretching vibrations of MR. The disappearance of this peak in the TCPP-MR spectrum indicates that TCPP is covalently bound to the Merrifield resin. Further evidence of covalent binding of TCPP to the resin is also found at 1720 cm^{-1} in the TCPP-MR spectrum. A similar peak is found at 1700 cm^{-1} in the TCPP spectrum which corresponds to the C=O stretching vibration of the carboxylic acid groups.[11] This shift of ~20 cm^{-1} is due to the overlap of the carbonyl C=O stretch of the carboxylic acid group with the carbonyl C=O stretch of the newly formed ester linkage.

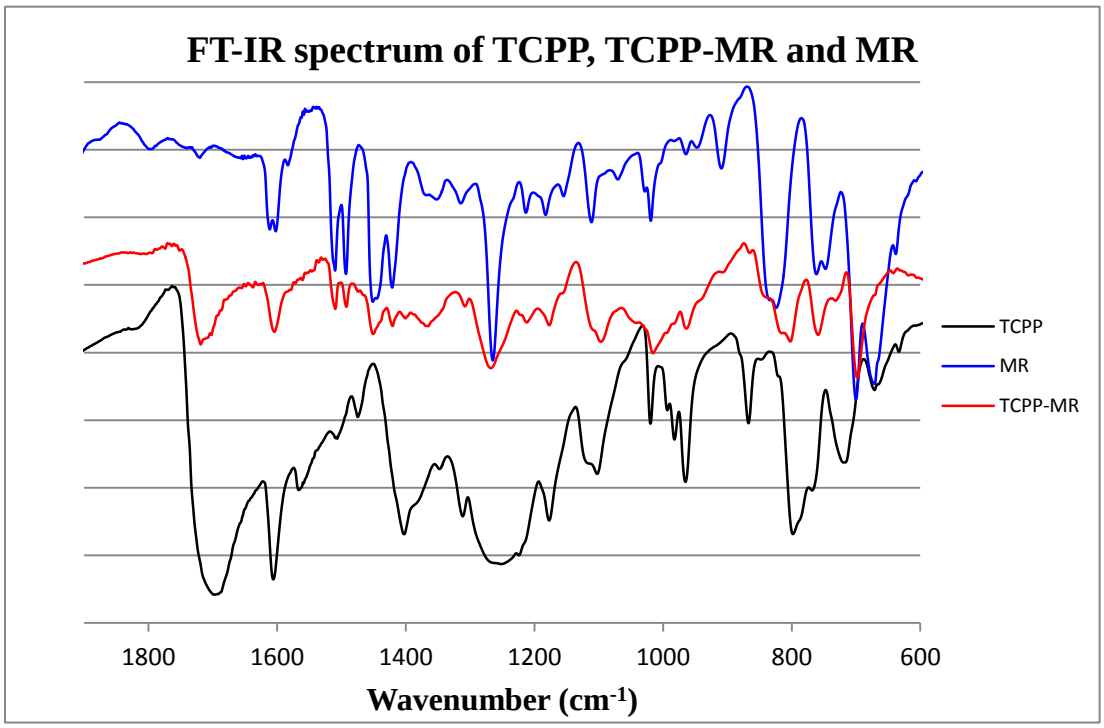

Figure 3.4: FT-IR spectra of TCPP, TCPP-MR and MR.

3.2.3 Dye sensitized photooxygenation of α-terpinene using TCPP-MR beads

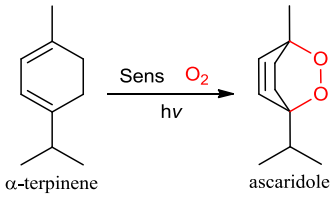

Scheme 3.2: Dye sensitized photooxygenation of α-terpinene to ascaridole.

3.2.3.1 Dye sensitized photooxygenation of α-terpinene using TCPP-MR beads in IPA

The dye sensitized photooxygenation of α-terpinene using TCPP-MR beads was performed using the optimised conditions outlined for the synthesis of juglone (Section 2.2.1.5). Four separate experiments were set up. Solutions of α-terpinene (104 mM) in 50 ml of IPA were irradiated (500 W halogen lamp) with constant air bubbling and cooling via a cold finger for 6 hours with varying amounts of TCPP-MR (25-200 mg). The percent conversion was monitored hourly by UV-Vis spectroscopy (Figure 3.5).

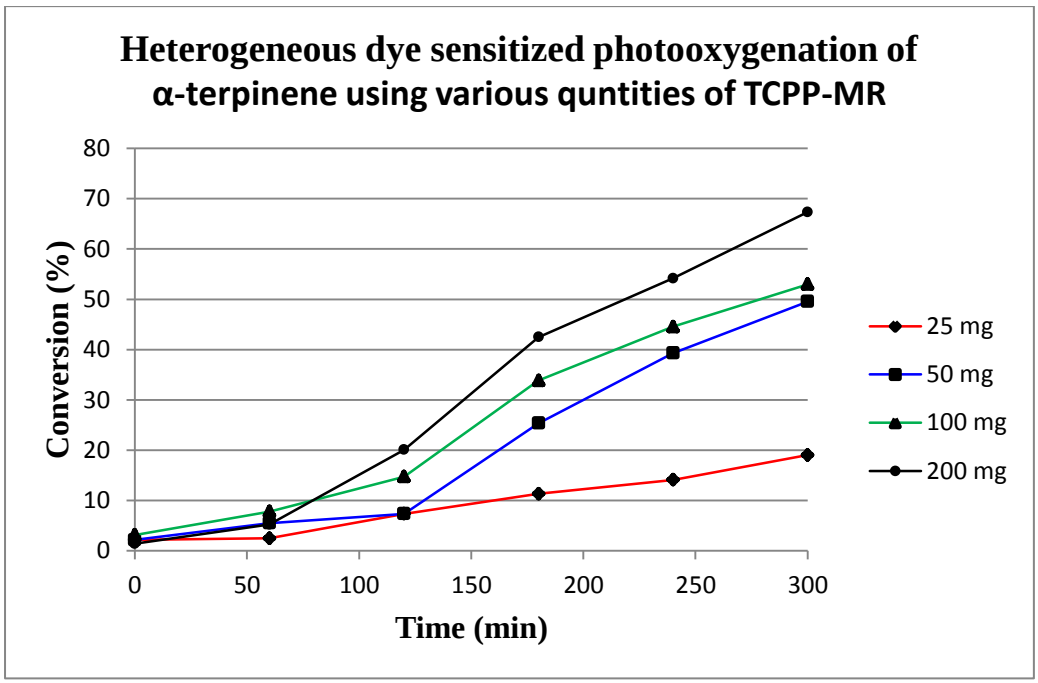

Figure 3.5: Heterogeneous dye sensitized photooxygenation of α-terpinene in IPA using varying amounts of TCPP-MR.

The results clearly demonstrate that TCPP-MR can be utilized for the dye sensitized photooxygenation of α-terpinene to ascaridole. As expected, the rate of the reaction is slower compared to conventional homogenous solutions. Under homogenous conditions complete conversion to ascaridole can be achieved in 2 hours (Section 2.2.2.1). However, by increasing the quantity of TCPP-MR, the rate of conversion can also be increased (Figure 3.5). Conversions of up to 67 % were achieved in 6 hours using 200 mg of TCPP-MR. Extended reaction times (8 hrs) showed complete conversion to ascaridole using 200 mg of TCPP-MR. In addition, a further reaction was performed using 500 mg of TCPP-MR as the sensitizer (Exp 59). Using this quantity of TCPP-MR beads afforded complete conversion to ascaridole in only 6 hours (Table 3.2).

Table 3.2: The dye sensitized photooxygenation of α-terpinene in IPA using varying amounts of TCPP-MR.

Exp No	MR used (mg)	Time (hr)	Absorbance (265.5 nm)	% Conversion
55	25	6	0.6365	19
56	50	6	0.4117	49
57	100	6	0.3843	53
58	200	6	0.2693	67
59	500	6	0.0043	100

These results were significant. Complete conversion of α-terpinene to ascaridole provided us with a unique situation. Column chromatography was not required to purify the product. Simple gravity filtration or centrifugation was used to remove the TCPP-MR from the reaction solution. The pure product could be obtained by simple rotary evaporation to remove the reaction solvent. This represented significant reductions in both waste generation compared to traditional homogenous syntheses and a significant time saving since chromatography was avoided.

The recyclability of the TCPP-MR beads was also investigated (Experiments 60 a-e). A fresh 200 mg sample of TCPP-MR beads was used for the heterogeneous dye sensitized photooxygenation of α-terpinene to ascaridole and the rate of conversion

monitored hourly by UV-Vis spectroscopy (265.5 nm, Figure 3.6). After 8 hours of irradiation a final conversion of 93 % was achieved. The TCPP-MR beads were separated from the reaction solution by centrifugation and then washed with IPA. These beads were then recycled, under the same reaction conditions, four times and the rates of conversion are shown in Table 3.3.

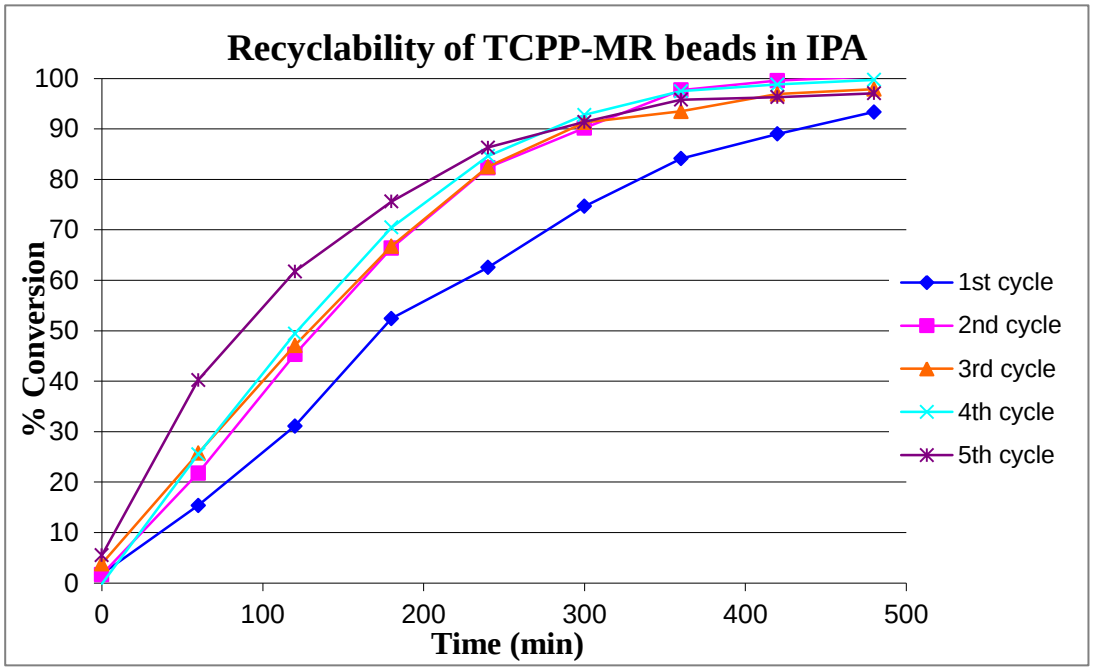

Figure 3.6: Conversion rates of TCPP-MR (200 mg) in IPA over five cycles.

Table 3.3: Recyclability of TCPP-MR beads (200 mg) in IPA.

Exp No	Cycle	Absorbance (265.5 nm)	% Conversion
60a	1	0.1403	93
60b	2	0.0045	100
60c	3	0.0245	98
60d	4	0.0099	99
60e	5	0.0312	97

Experiments 60 a-e demonstrate clearly that TCPP-MR beads can be recycled up to at least 5 times without loss of efficacy. Interestingly, the rate of conversion increased from the 1st to the 2nd cycle. This can be attributed to two separate factors;

1) swelling of the TCPP-MR beads and 2) physical degradation of the TCPP-MR beads into smaller particles.

1) Merrifield resin bead swelling

Merrifield resin beads are designed to be porous allowing reaction media to diffuse through them. This rate of diffusion is optimal when the beads are fully swollen in a solvent. This swelling can take up to two hours depending on the solvent. Experiment 60a shows that the rate of conversion after two hours was only 31 % during the 1st cycle. However, The conversion is significantly higher in subsequent reactions (45-61 %). This lower rate of conversion was due to bead swelling. During the first 2 hours the beads had not yet swollen fully and the rate of conversion was significantly lower due to lack of diffusion of the reaction media through the beads. Therefore, new TCPP-MR beads should be "swollen" in the reaction solvent for two hours prior to their use in heterogeneous dye sensitized photooxygenations. It is important to note that the TCPP-MR beads were not dried out between repeat reaction cycles. They were washed and stored in IPA.

2) Physical degradation of Merrifield resin beads

In addition to the swelling of the Merrifield resins, physical degradation of the TCPP-MR beads may also help to explain the increase in conversion rates. It should be noted that the reactive oxygen species generated by the covalently bound sensitizer may interact with the polymer backbone and result in further degradation or fragmentation of the crosslinked polymer. This fragmentation of the beads creates a greater surface area and ultimately allows for a greater rate of diffusion of the reaction media through the beads. Scanning electron microscopy (SEM) images (Figure 3.7) clearly shows the extent of fragmentation and helps to explain the increasing rate of conversion over the 5 cycles.

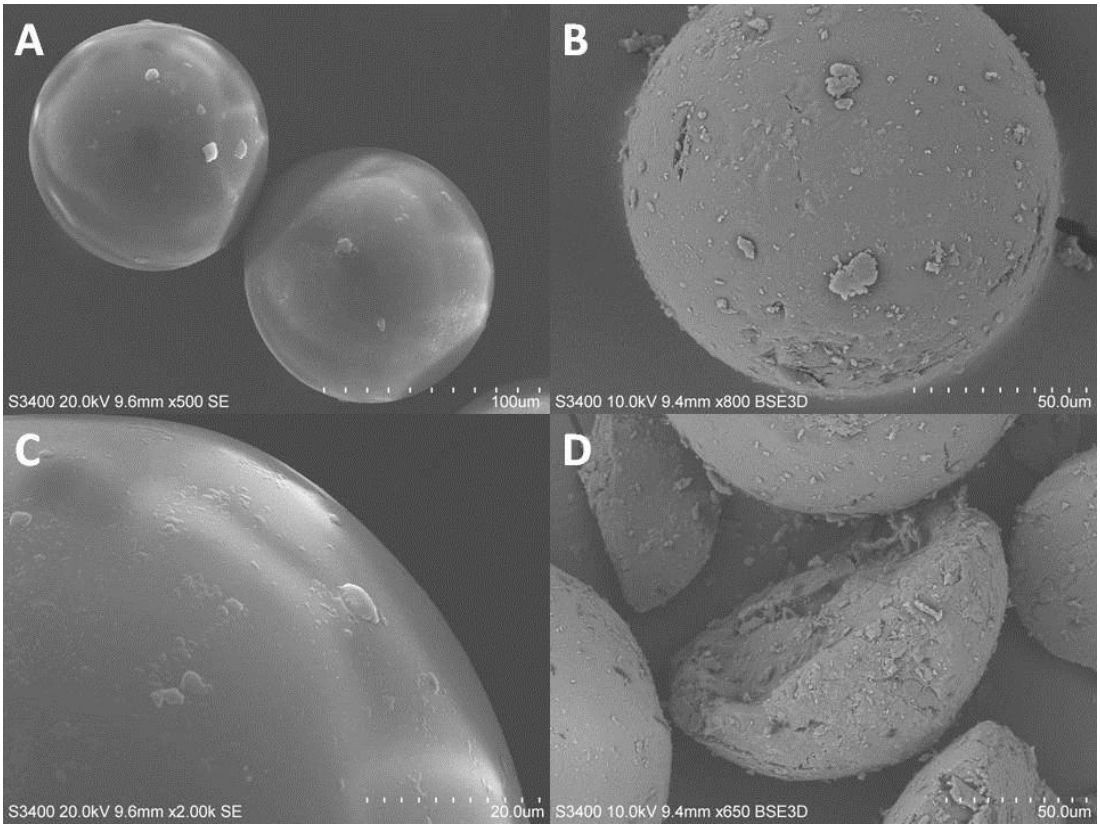

Figure 3.7: SEM images showing fresh TCPP-MR beads (A & C) and the physical degradation and fragmentation of the TCPP-MR beads (B & D).

3.2.3.2 Dye sensitized photooxygenation of α-terpinene using TCPP-MR beads in TAA

The dye sensitized photooxygenation of α-terpinene to ascaridole was also performed in TAA using 500 mg of TCPP-MR (Exp 61). The quantity of TCPP-MR was increased to 500 mg in order to reduce the reaction time from 8 hours. The percentage conversion was monitored hourly using UV-Vis spectroscopy. Interestingly, the final rate of conversion was < 20 % after 8 hours of irradiation. This is a significant decrease in the rate of conversion of α-terpinene and may be attributed to the lack of swelling of the TCPP-MR beads in TAA. If no swelling occurred, the reaction would not proceed as the reaction media would be unable to diffuse through the beads. The degree of swelling of Merrifield resin beads was determined using several green solvents listed on Pfizer's preferred solvent list (Experiment 62a-f).

A series of unfunctionalised Merrifield resin beads were placed into 5 ml syringes and their volumes were noted. Next a 5 ml aliquot of solvent was added to each and left for 2 hours. The final volumes of the beads were noted in the syringes and the percentage increase in volumes calculated (Table 3.4).

Table 3.4: Merrifield resin bead swelling tests in various solvents.

Exp No	Solvent (5 ml)	MR (mg)	Initial Volume (ml)	Final Volume (ml)	% volume increase
62a	TAA	500	0.40	0.45	12.5
62b	IPA	500	0.40	0.60	50
62c	Ethanol	500	0.45	0.60	33
62d	Methanol	500	0.40	0.60	50
62e	Acetone	500	0.40	1.20	200
62f	Ethyl acetate	500	0.40	1.50	275

The Merrifield resin swelling tests confirmed that TAA did not swell the Merrifield resins to the same extent as IPA. The amount of swelling of the Merrifield resin beads was four times greater in IPA than TAA. This result may explain the poor rate of conversion of α-terpinene to ascaridole using TCPP-MR beads in TAA.

3.2.4 Synthesis of TCPPZn (Experiment 63)

TCPPZn was synthesized based upon a procedure by Granados-Oliveros *et al* (Scheme 3.3).[12] TCPP (520 mg, 0.66 mmol) was dissolved in 140 ml of DMF with sonication. Anhydrous $ZnCl_2$ (500 mg, 3.64 mmol) was then added and the solution was allowed to stir under reflux for 2 hours. DMF was removed via distillation and H_2O added to precipitate TCPPZn. This was filtered and washed with H_2O and DCM. The crude solid was then dissolved in a 0.1 M NaOH solution and re-precipitated using 1 M HCl. The resulting precipitate was isolated via centrifugation and washed with water to yield TCPPZn as a dark purple solid in quantitative yields. UV-Vis (Figure 3.8) and ^{1}H NMR spectroscopy confirmed that the TCPPZn was pure.

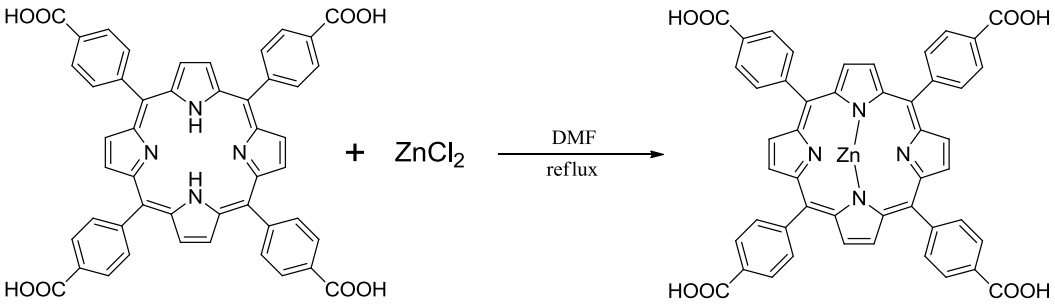

Scheme 3.3: Synthesis of TCPPZn.

Figure 3.8 shows clearly the Soret bands for TCPP and TCPPZn at 416 and 424 nm with a bathochromic shift of 8 nm. Also shown are the four Q-bands of TCPP and the two Q-bands of TCPPZn(II).

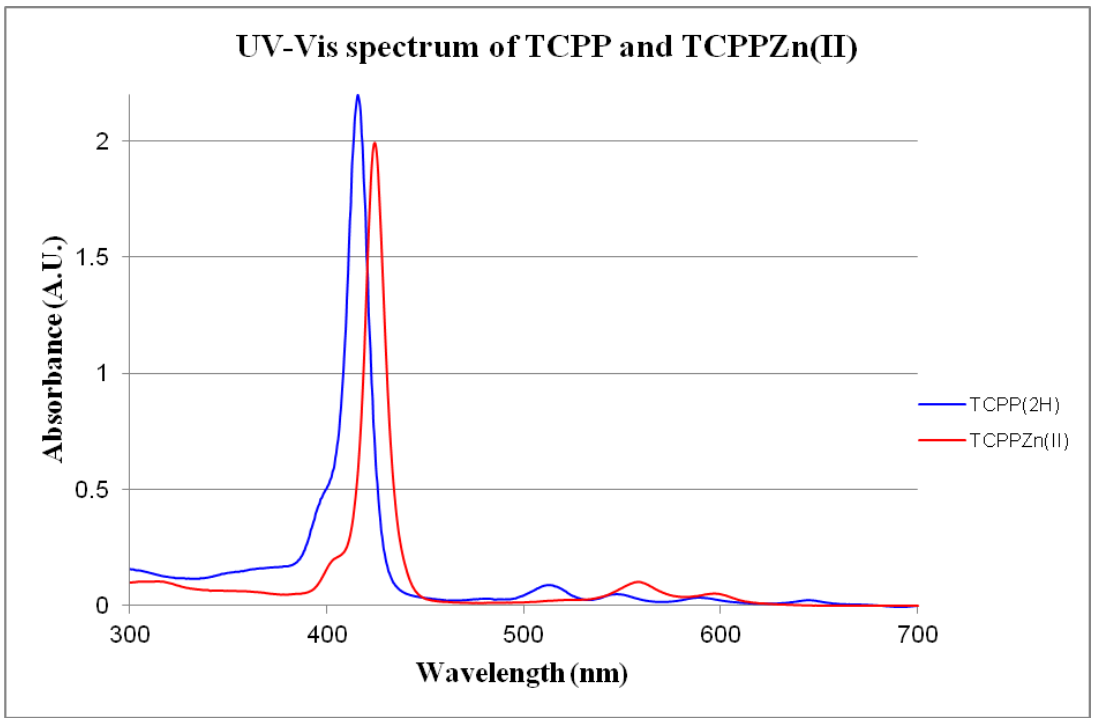

Figure 3.8: UV-Vis spectra of TCPP and TCPPZn(II) in methanol.

3.2.5 Covalent functionalisation of Merrifield resins with TCPPZn(II) (Experiment 64)

TCPPZn was covalently immobilized onto Merrifield resins based upon a modified procedure by Merrifield (Scheme 3.4).[2] Briefly, 800 mg Merrifield resin beads (200-400 mesh, 1% DVB, 4.5 mmol Cl/g) were placed in 30 ml of ethyl acetate. To this TCPPZn (0.75 mmol) and 0.5 ml of triethylamine (TEA) were added. This mixture

was then refluxed for 12 – 14 hours. After this period of time 0.6 ml of acetic acid was added along with a further 2 ml of TEA in 10 ml of ethyl acetate. This was allowed to reflux for a further 4 hours. The Merrifield resin beads were filtered and washed with 50 ml portions of ethyl acetate, ethanol, water and methanol. They were then soxhlet extracted with methanol for 48 hrs to remove any free sensitizer. UV-Vis spectroscopy was used to confirm that washings contained no free sensitizer after 48 hours. The beads were air dried overnight.

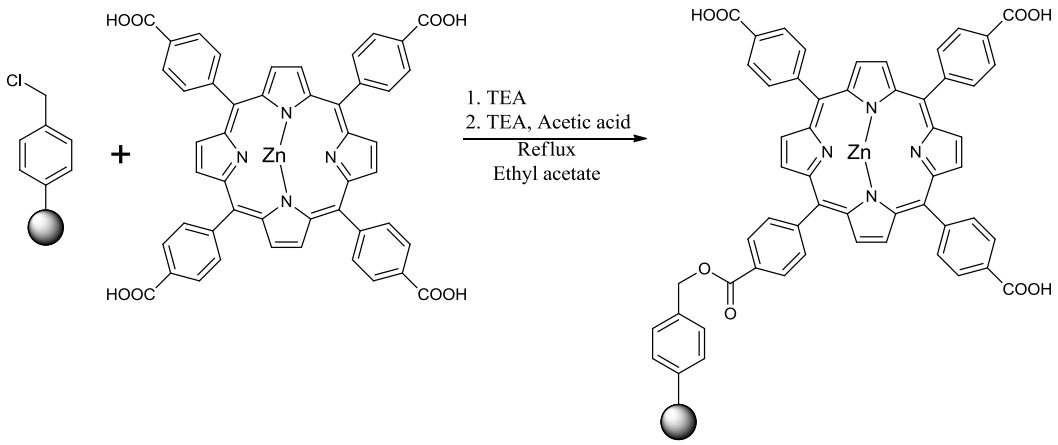

Scheme 3.4: Covalent functionalisation of Merrifield resin beads with TCPPZn.

3.2.6 Dye sensitized photooxygenation of α-terpinene using TCPPZn-MR beads (Experiments 65-67)

Using the optimised conditions outlined for the synthesis of juglone (Section 2.2.1.5) the dye sensitized photooxygenation of α-terpinene to ascaridole was performed using TCPPZn-MR in both IPA and TAA. Percentage conversions were monitored hourly using UV-Vis spectroscopy. Table 3.5 shows these results.

Table 3.5: The heterogeneous dye sensitized photooxygenation of α-terpinene using TCPPZn-MR in IPA and TAA.

Exp No	Solvent	TCPPZn-MR (mg)	Time (hr)	Absorbance	% Conversion
65	IPA	200	8	0.4008	51
66	IPA	200	8	0.3988	51
67	TAA	200	6	0.6985	16

Merrifield resin beads were covalently functionalised with TCPPZn as the incorporation of zinc into the centre of a porphyrin molecule increases the quantum yield of singlet oxygen. It was proposed that the use of TCPPZn instead of TCPP would provide superior rates of conversion. However, this was not the case as the results of experiments 64 and 65 (repeat) clearly demonstrate. Conversion rates of only 51 % were obtained after 8 hours of irradiation using TCPPZn-MR beads (200 mg) in IPA. Furthermore, the use of TCPPZn-MR showed only a 16 % conversion after 6 hours in TAA. Although these are relatively low conversion rates the results are in agreement with Section 3.2.3.2. TAA is an unsuitable solvent for the heterogeneous dye sensitized photooxygenation of alpha terpinene when using Merrifield resin beads as solid supports.

3.2.7 Characterisation of TCPPZn-MR beads

To understand the reasons for the poor performance of the TCPPZn-MR beads further characterisation of the beads were carried out. Diffuse reflectance UV-Vis spectroscopy was used to characterize both TCPPZn and TCPPZn-MR to confirm if covalent immobilization of TCPPZn onto the Merrifield resin beads was successful (Figure 3.9). The spectrum of TCPPZn shows clearly the Soret band at 432 nm and the two Q-bands at 562 and 506 nm respectively. The disappearance of two Q-bands going from TCPP to TCPPZn is proof that chelation of zinc to the porphyrin centre had occurred.

In contrast, the spectrum of the TCPPZn-MR showed a soret band at 430 nm and four Q bands at 521,561,613 and 666 nm. The reappearance of these two Q-bands is evidence that zinc was removed from the centre of the porphyrin during the immobilization process. The TCPPZn-MR beads therefore should provide similar yields to TCPP-MR as no metal centre was present. The results (Section 3.2.6) however show that this is not the case. The final rates of conversion decrease by approximately 50 % compared to TCPP-MR beads in Section 3.2.3.1.

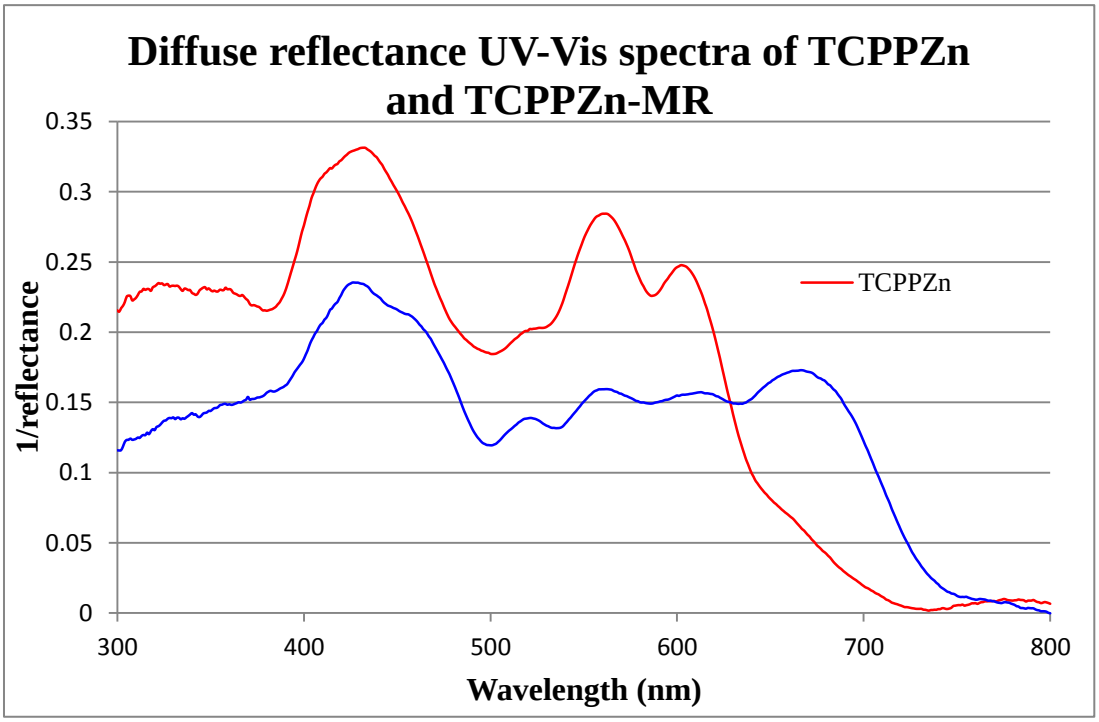

Figure 3.9: Diffuse reflectance UV-Vis spectra of TCPPZn and TCPPZn-MR in KBr disk.

FT-IR spectroscopy (KBr disk) was also used to characterize TCPPZn, TCPPZn-MR and unfunctionalised Merrifield resins in order to determine if immobilization of TCPPZn onto Merrifield resin beads was successful. Figure 3.10 confirms that TCPP-Zn has been covalently immobilised onto the Merrifield resin beads. Similar to TCPP, TCPPZn is also covalently immobilised through an ester bridge. The FT-IR of TCPPZn-MR shows two distinct peaks at 1741 and 1719 cm^{-1}. These two peaks represent the carbonyl stretching of the newly formed ester bridge and the carbonyl stretch of the carboxylic acid on the porphyrin. The peak at 675 cm^{-1} in the Merrifield resin spectrum represents the alkyl halide (C-Cl) stretching of the chloromethyl groups. Comparison with the TCPPZn-MR spectrum shows that this peak is also present. This result would indicate that complete immobilisation of TCPPZn onto MR had not taken place since there were still unreacted chloromethyl groups available on the Merrifield resin beads. This could explain why conversion rates of α-terpinene to ascaridole were significantly lower than that of TCPP-MR. The degree of loading of TCPP onto the Merrifield resin beads was higher than that of TCPPZn.

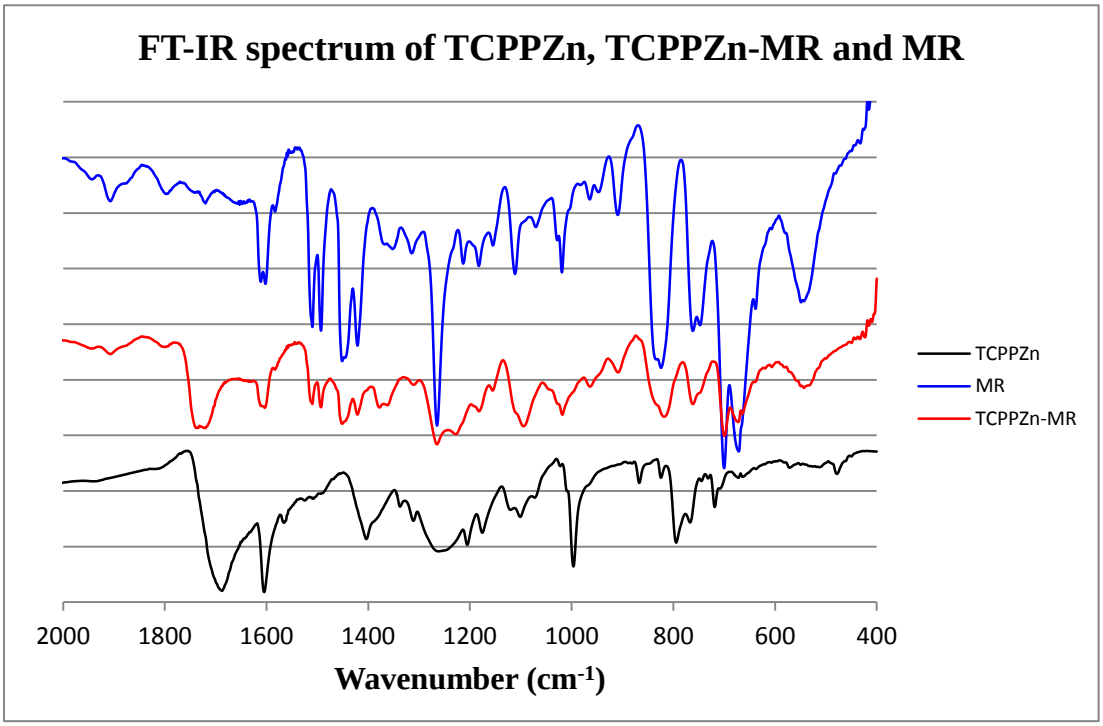

Figure 3.10: FT-IR spectra of TCPPZn, TCPPZn-MR and MR in KBr disk.

3.2.8 Covalent functionalisation of Merrifield resin beads with rose Bengal (RB-MR) and characterisation

Rose Bengal covalently immobilized onto Merrifield resin beads is commercially available under the trade name Sensitox® and is used as a polymer supported sensitizer for heterogeneous dye sensitized photooxygenations. Despite the commercial availability, rose Bengal functionalized Merrifield resin beads (RB-MR) were synthesized (Scheme 3.5, Experiment 68) as follows. Rose Bengal (2g, 2.1 mmol) was dissolved in 60 ml of DMF along with 2 g of Merrifield resin beads (200-400 mesh, ~4.5 mmol of Cl/gram, 1 % DVB) and refluxed overnight. The resulting functionalized Merrifield resin beads were then filtered and washed with methanol. Soxhlet extraction with methanol was then employed until the washings ran clear. UV-Vis analysis showed that no rose Bengal was present in the washings.

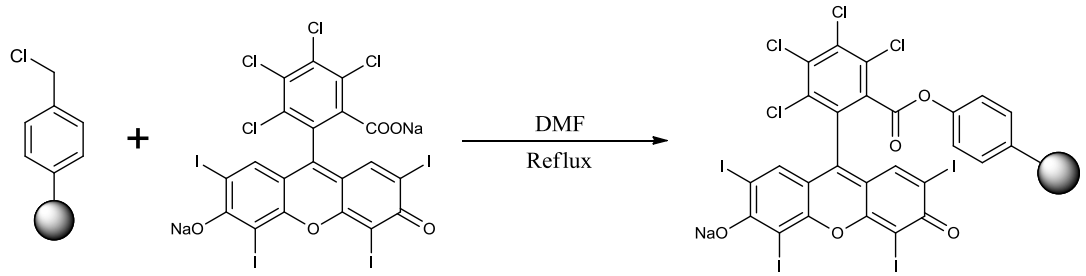

Scheme 3.5: Functionalisation of Merrifield resin beads with rose Bengal.

Figure 3.11 shows that rose Bengal has been covalently bound to the Merrifield resin beads. The absorbance peak at 675 cm^{-1} in the spectrum of the Merrifield resin (due to C-Cl stretching vibrations) is absent in the RB-MR spectrum indicating that complete covalent coupling through this alkyl halide had taken place. Similar to the covalent immobilisation of TCPP an ester bridge is formed. Evidence of this can be seen in the form of a sharp absorbance peak at 1703 cm^{-1}.

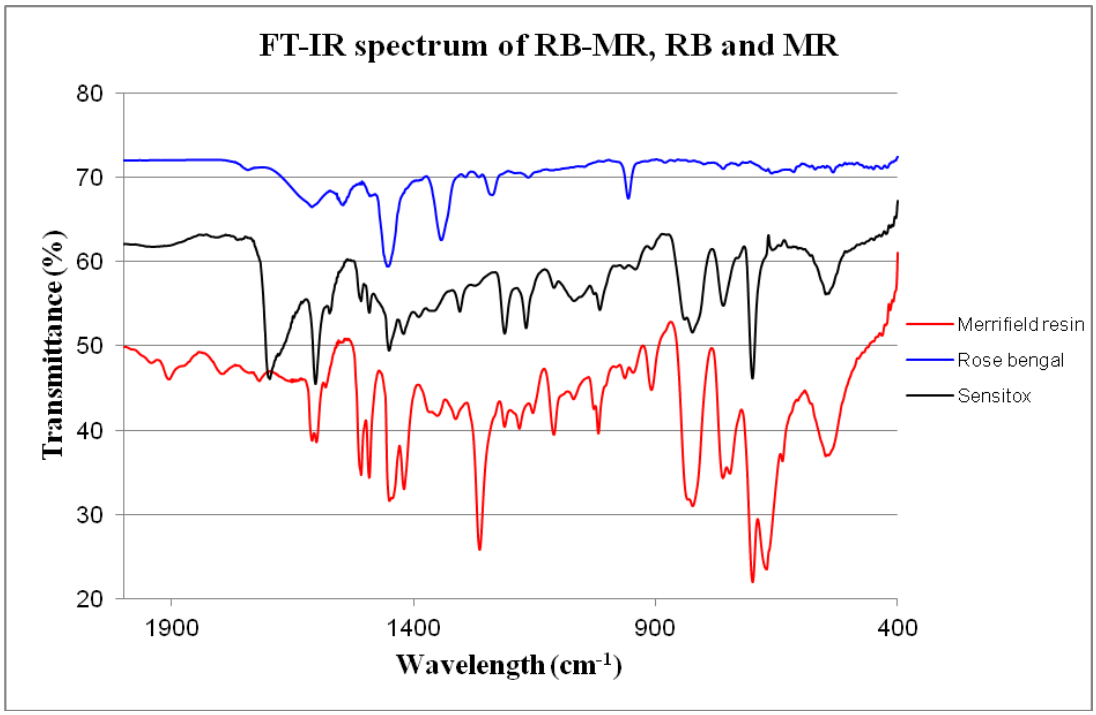

Figure 3.11: FT-IR spectra of RB, RB-MR and MR in KBr disks.

Figure 3.12 shows the diffuse reflectance UV-Vis spectrum of the RB-MR beads. A strong absorbance at 548 nm indicates the presence of rose Bengal in the RB-MR beads. UV-Vis analysis of the methanol washings from Soxhlet extraction of RB-

MR beads showed no evidence of rose Bengal. Therefore any absorbance recorded in the diffuse reflectance UV-Vis is due to immobilised rose Bengal.

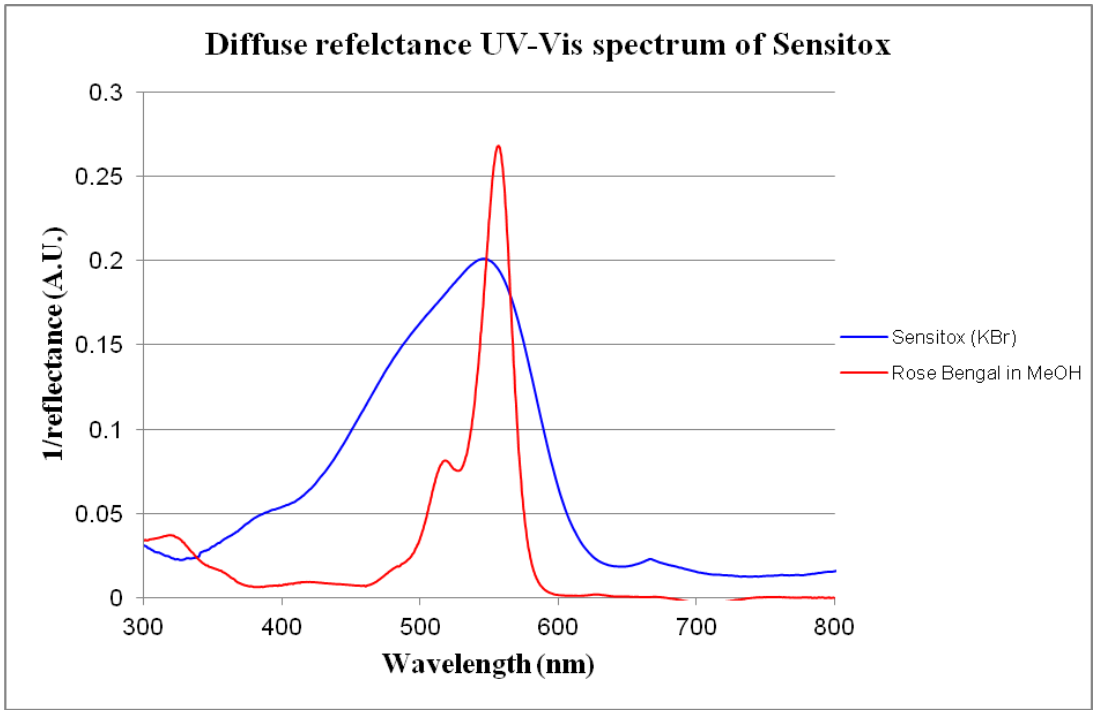

Figure 3.12: Diffuse reflectance UV-Vis spectrum of RB-MR also showing RB in methanol.

3.2.10 Dye sensitized photooxygenation of α-terpinene using RB-MR beads (Experiments 69a-d)

The heterogeneous dye sensitized photooxygenation of α-terpinene using RB-MR beads was performed. 200 mg Of RB-MR beads were dispersed in 50 ml of IPA and placed in front of a 500 W halogen lamp (27 cm) with constant air bubbling. 1 ml (5.2 mmol) Of α-terpinene was then added and the reaction mixture irradiated for 8 hours. UV-Vis spectroscopy showed percent conversions up to 32 % after 8 hours (Table 3.6).

Table 3.6: Heterogeneous dye sensitized photooxygenation of α-terpinene using RB-MR.

Exp No	Solvent	Sensitox (mg)	Cycle	Conversion (%)
69a	IPA	200	1	23
69b	IPA	200	2	27
69c	IPA	200	3	32
69d	IPA	200	4	28

The results shown in Table 3.6 show that low conversions of ascaridole were obtained after 8 hours of irradiation. In comparison, 200 mg of TCPP-MR beads achieved complete conversion during the same time period indicating that TCPP-MR is a superior sensitizer for the synthesis of ascaridole. This result is in agreement with homogenous dye sensitized photooxygenations performed in Section 2.2.2.1.

3.3 Conclusion

The results obtained in this chapter have demonstrated that the covalent immobilization of TCPP and RB onto commercially available Merrifield resin beads was achieved. The immobilization of TCPPZn however, was not deemed successful as the zinc centre was removed from the porphyrin during the immobilization process and the percent loading of the sensitiser onto the resin was lower than that with TCPP.

In addition to the covalent immobilization of TCPP and RB onto Merrifield resin beads the results have shown that these beads can then be used for the heterogeneous dye sensitized photooxygenation of α-terpinene to ascaridole.

Using 500 mg of the TCPP-MR beads complete conversion of α-terpinene to ascaridole can be achieved in only 6 hours of irradiation in IPA. Purification of the reaction mixture only required centrifugation to remove TCPP-MR, eliminating chromatography. The recyclability of these beads was also demonstrated showing no loss of efficacy over 5 cycles in IPA. Interestingly the rate of conversion actually increased with use due to bead swelling and physical degradation. The synthesis of ascaridole was also performed using TAA as solvent. This provided final rates of conversion < 20 % after 8 hours of irradiation demonstrating that TAA was not a suitable solvent when using Merrifield resin beads as solid supports. Swelling tests in various green solvents confirmed this to be true.

Using 200 mg of the RB-MR beads percent conversions of up to 32 % were achieved in 8 hours of irradiation time in IPA. These results show that while the dye sensitized photooxygenation of α-terpinene using RB-MR beads is possible, the yields are significantly lower than that of TCPP-MR. It is clear that covalent immobilisation of TCPP onto Merrifield resin beads provides a superior polymer supported sensitizer for heterogeneous dye sensitized photooxygenations.

According to the 1st rule of the twelve principle of green chemistry it is "*better to prevent waste than to treat or clean up waste after it is formed".* It is also important according to the 5th rule that *"the use of auxiliary substances (e.g. solvents,*

separation agents, etc) should be made unnecessary wherever possible and, innocuous when used". Finally the 7th rule states that *"a raw material of feedstock should be renewable rather than depleting wherever technically and economically practicable"*. The use of TCPP covalently bound to Merrifield resin beads achieves all three of these principles.

By covalently immobilizing TCPP onto Merrifield resin beads we have eradicated the need for column chromatography to remove the sensitizer from the crude reaction mixture. Removal of the sensitizer from the reaction solution is now achieved via simple gravity filtration or centrifugation without the need for additional solvents or silica gel. This achievement satisfies both the 1st and 5th rule of the twelve principles of green chemistry. In addition to satisfying these two rules we have also addressed the 7th rule. Although TCPP is not a renewable resource we can now recycle the TCPP-MR beads several times without loss of efficacy.

3.4 Experimental

3.4.1 Spectroscopic methods

FT-IR spectroscopy

FT-IR spectra were recorded using KBr disks on a Perkin Elmer system 2000 FT-IR spectrophotometer.

Diffuse reflectance UV-Vis spectroscopy

Diffuse reflectance UV-Vis spectra were recorded using KBr disks on a Jasco V-670 UV/Vis/NIR spectrophotometer.

3.4.2 Experimental setup

3.4.2.1 Immobilization of TCPP, TCPPZn and RB onto Merrifield resin beads

Covalent immobilization of TCPP, TCPPZn and RB onto Merrifield resin beads was performed in a 100 ml round bottom flask equipped with a magnetic stirrer and refluxed for 12 – 14 hours. Crude TCPP-MR, TCPPZn-MR and RB-MR beads were soxhlet extracted with methanol for 48 hrs to remove any free sensitizer.

3.4.2.2 Heterogeneous dye sensitized photooxygenation of α-terpinene

The experimental setup was similar to that of juglone synthesis (Section 2.2.1.5). All reactions were performed in 50 ml Pyrex Schlenk flasks with constant air bubbling during the irradiation time unless otherwise stated. The amount of air supplied to the reaction solution was controlled using an air flow meter. To minimise the size of the air bubbles present a HPLC solvent inlet filter (SUPELCO) was also attached to the air supply tube. Water cooling was utilised via a "cold finger". This helped to maintain the reaction solution at an ambient temperature. A 500 W halogen lamp (IQ group) was used in all experiments. TCPP or TCPPZn, covalently immobilised onto Merrifield resin beads were used as sensitizers in all experiments unless otherwise stated.

3.4.3 Control experiments (Experiments 51-53)

General procedure for control experiments

1 ml (5.2 mmol) Of α-terpinene was dissolved in 50 ml of IPA and was allowed to react for 8 hours with constant air bubbling. UV-Vis spectroscopy was used to determine the final rate of conversion after 8 hours.

Experiment 51 ***Photooxygenation of α-terpinene with 500 mg Merrifield resin beads and no light source***

500 mg of unfunctionalised Merrifield resin beads were placed into the reaction solution and allowed to react for 8 hours in the dark. UV-Vis spectroscopy confirmed that no reaction had occurred after 8 hours.

Experiment 52 ***Photooxygenation of α-terpinene with 500 mg Merrifield resin beads and 500 W halogen lamp***

500 mg of unfunctionalised Merrifield resin beads were placed into the reaction solution and irradiated for 8 hours (500 W halogen lamp). UV-Vis spectroscopy confirmed a 16 % conversion after 8 hours.

Experiment 53 ***Self sensitized photooxygenation of α-terpinene***

No Merrifield resin beads were added to the reaction solution. This was then irradiated for 8 hours. UV-Vis spectroscopy confirmed an 11 % conversion after 8 hours.

3.4.4 Covalent functionalisation of Merrifield resin beads with TCPP (Experiment 54)

TCPP was covalently immobilized onto Merrifield resin beads based upon a modified procedure by Merrifield.[2] A 100 ml round bottomed flask equipped with a stirring bar was charged with 800 mg Merrifield resin beads (200-400 mesh, 1% DVB, 4.5 mmol Cl/g) along with 30 ml of ethyl acetate. To this TCPP (0.75 mmol) and 0.5 ml of triethylamine (TEA) were added. This was then refluxed for 12 – 14 hours. After this period of time 0.6 ml of acetic acid was added along with a further 2 ml of TEA in 10 ml of ethyl acetate. This was allowed to reflux for a further 4 hours. After reflux the Merrifield resin beads were filtered and washed with 50 ml

portions of ethyl acetate, ethanol, water and methanol. The beads were then washed via Soxhlet extraction over a 48 hour period using methanol to remove any free TCPP. UV-Vis spectroscopy confirmed that washings after 48 hours contained no sensitizer. The beads were air dried overnight.

3.4.5 Dye sensitized photooxygenation of α-terpinene using TCPP-MR beads in IPA (Experiments 55-58)

General procedure

TCPP-MR beads were placed into a 50 ml Pyrex Schlenk flask along with 50 ml of IPA. This was placed in front of a 500 W halogen lamp (27 cm) and irradiated for 6 hours with constant air bubbling. At time zero 1 ml (5.2 mmol) of α-terpinene was added. 0.1 ml Samples were removed hourly starting at time zero for the duration of the experiment. These were subsequently diluted by a factor of 1000 and UV-Vis spectroscopic analysis (265.5 nm) was performed. Conversion rates were calculated based upon these absorbance measurements.

Experiment 55 ***Dye sensitized photooxygenation of α-terpinene using 25 mg of TCPP-MR beads***

25 mg of TCPP-MR beads were used as sensitizer. UV-Vis spectroscopy showed a 19 % conversion after 6 hours.

Experiment 56 ***Dye sensitized photooxygenation of α-terpinene using 50 mg of TCPP-MR beads***

50 mg of TCPP-MR beads were used as sensitizer. UV-Vis spectroscopy showed a 49 % conversion after 6 hours.

Experiment 57 ***Dye sensitized photooxygenation of α-terpinene using 100 mg of TCPP-MR beads***

100 mg of TCPP-MR beads were used as sensitizer. UV-Vis spectroscopy showed a 53 % conversion after 6 hours.

Experiment 58 ***Dye sensitized photooxygenation of α-terpinene using 200 mg of TCPP-MR beads***

200 mg of TCPP-MR beads were used as sensitizer. UV-Vis spectroscopy showed a 67 % conversion after 6 hours.

Experiment 59 ***Dye sensitized photooxygenation of α-terpinene using 500 mg of TCPP-MR beads***

500 mg of TCPP-MR beads were used as sensitizer. UV-Vis spectroscopy showed complete conversion after 6 hours.

3.4.6 Recyclability of TCPP-MR beads (Experiments 60a-e)

General procedure

TCPP-MR beads were placed into a 50 ml pyrex Schlenk flask along with 50 ml of IPA. This was placed in front of a 500 W halogen lamp (27 cm) and irradiated for 8 hours with constant air bubbling. At time zero 1 ml (5.2 mmol) of α-terpinene was added. 0.1 ml Samples were removed hourly starting at time zero for the duration of the experiment. These were subsequently diluted by a factor of 1000 and UV-Vis spectroscopic analysis (265.5 nm) was performed. Conversion rates were calculated based upon these absorbance measurements.

Experiment 60a ***Dye sensitized photooxygenation of α-terpinene using 200 mg of TCPP-MR beads in IPA***

200 mg of TCPP-MR beads were used as sensitizer. UV-Vis spectroscopy showed an 83 % conversion after 8 hours.

Experiment 60b ***Dye sensitized photooxygenation of α-terpinene using 200 mg of TCPP-MR beads in IPA***

200 mg of TCPP-MR beads from experiment 55 were used as sensitizer. UV-Vis spectroscopy showed a 100 % conversion after 8 hours.

Experiment 60c ***Dye sensitized photooxygenation of α-terpinene using 200 mg of TCPP-MR beads in IPA***

200 mg of TCPP-MR beads from experiment 56 were used as sensitizer. UV-Vis spectroscopy showed a 98 % conversion after 8 hours.

Experiment 60d ***Dye sensitized photooxygenation of α-terpinene using 200 mg of TCPP-MR beads in IPA***

200 mg of TCPP-MR beads from experiment 57 were used as sensitizer. UV-Vis spectroscopy showed a 99 % conversion after 8 hours.

Experiment 60e ***Dye sensitized photooxygenation of α-terpinene using 200 mg of TCPP-MR beads in IPA***

200 mg of TCPP-MR beads from experiment 58 were used as sensitizer. UV-Vis spectroscopy showed a 97 % conversion after 8 hours.

3.4.7 Dye sensitized photooxygenation of α-terpinene using 500 mg of TCPP-MR beads in TAA

General procedure

TCPP-MR beads were placed into a 50 ml Pyrex Schlenk flask along with 50 ml of TAA. This was placed in front of a 500 W halogen lamp (27 cm) and irradiated for 8 hours with constant air bubbling. At time zero 1 ml (5.2 mmol) of α-terpinene was added. 0.1 ml Samples were removed hourly starting at time zero for the duration of the experiment. These were subsequently diluted by a factor of 1000 and UV-Vis spectroscopic analysis (267 nm) was performed.

Experiment 61 ***Dye sensitized photooxygenation of α-terpinene using 500 mg of TCPP-MR beads in TAA***

The general procedure was followed using 500 mg of TCPP-MR beads. UV-Vis spectroscopy showed < 20 % conversion after 8 hours.

3.4.8 Merrifield resin swelling tests

Experiment 62 (a-f)

Six separate 5 ml syringes were taken and the ends sealed using a gas flame. The plunger was then removed and 500 mg of unmodified Merrifield resin beads were added. The samples were shaken slightly to ensure that all the beads had settled to the bottom of the syringe and the initial volume of beads was recorded. 5 ml of solvent was added and the plunger replaced. The syringes were then shaken for 2 minutes. After this the syringes were left to settle for 2 hours and the final volume of

beads in each syringe was recorded. The percent increase in volume was then calculated for each solvent.

3.4.9 Synthesis of TCPPZn (Experiment 63)

TCPPZn was synthesized based upon a procedure by Grandos *et al* (Scheme 3.3).[12] TCPP (520 mg, 0.66 mmol) was dissolved in 140 ml of DMF with sonication. Anhydrous $ZnCl_2$ (500 mg, 3.64 mmol) was then added and the solution was allowed to stir under reflux for 2 hours. DMF was removed via distillation and H_2O added to precipitate TCPPZn. This was filtered and washed with H_2O (30 ml x 3) and DCM (20 ml x 1). The crude solid was then dissolved in a 0.1 M NaOH solution and re-precipitated using 1 M HCl. The resulting precipitate was isolated via centrifugation and washed with water to yield TCPPZn as a dark purple solid in quantitative yields. ^{1}H NMR (DMSO-d_6) showed that the product was pure. The peak at – 2.94 due to the highly deshielded pyrrole hydrogens was not present indicating that zinc had chelated to the center of the porphyrin ring. There was also a slight upfield shift with regards ^{1}H NMR signals due to the remainder of the presenet hydrogen atoms. UV-Vis spectroscopy (Figure 3.8) further confirmed the purity of the product with the disappearance of two of the previous four Q-bands.

^{1}H NMR: (400 MHZ, DMSO-d_6) δ (ppm) = 8.36 (m, 16H, *m*Ph & *o*Ph), 8.79 (s, 8H, βH), 13.24 (brs, 4H, COOH). Data in agreement with literature.

UV-Vis: (methanol) λ (nm) = 424, 557, 597

3.4.10 Covalent functionalisation of Merrifield resin beads with TCPPZn (Experiment 64)

TCPPZn was covalently immobilized onto Merrifield resin beads based upon a modified procedure by Merrifield.[2] A 100 ml round bottomed flask equipped with a stirring bar was charged with 800 mg Merrifield resin (200-400 mesh, 1% DVB, 4.5 mmol Cl/g) along with 30 ml of ethyl acetate. To this TCPPzn (0.75 mmol) and 0.5 ml of triethylamine (TEA) were added. This was then refluxed for 12 – 14 hours. After this period of time 0.6 ml of acetic acid was added along with a further 2 ml of TEA in 10 ml of ethyl acetate. This was allowed to reflux for a further 4 hours.

After reflux the Merrifield resin beads were filtered and washed with 50 ml portions of ethyl acetate, ethanol, water and methanol. The beads were then washed via Soxhlet extraction over a 48 hour period using methanol to remove any free TCPP-Zn. UV-Vis spectroscopy was used to confirm that washings contained no free sensitizer after 48 hours. The beads were air dried overnight.

3.4.11 Dye sensitized photooxygenation of α-terpinene using 200 mg TCPPZn-MR in IPA and TAA

General procedure

The general procedure for the synthesis of ascaridole using TCPPZn-MR beads was identical to the procedure using TCPP-MR beads (Section 3.4.6).

Experiment 65 Dye sensitized photooxygenation of α-terpinene in IPA

200 mg of TCPPZn-MR beads were used as sensitizer. UV-Vis spectroscopy showed a 51 % conversion after 8 hours.

Experiment 66 Dye sensitized photooxygenation of α-terpinene in IPA

200 mg of TCPPZn-MR beads were used as sensitizer. UV-Vis spectroscopy showed a 51 % conversion after 8 hours.

Experiment 67 Dye sensitized photooxygenation of α-terpinene in TAA

200 mg of TCPPZn-MR beads were used as sensitizer. UV-Vis spectroscopy showed a 16 % conversion after 6 hours.

3.4.12 Covalent functionalisation of Merrifield resin beads with RB (Experiment 68)

RB was covalently immobilized onto Merrifield resin beads based upon a modified procedure by Merrifield.[2] A 100 ml round bottomed flask equipped with a stirring bar was charged with 2 g Merrifield resin (200-400 mesh, 1% DVB, 4.5 mmol Cl/g) along with 60 ml of DMF. To this RB (2 g, 2.1 mmol) was added. This was then refluxed for 12 – 14 hours. After reflux the RB-MR beads were filtered and washed with 30 ml portions of methanol (x3). The beads were then washed via Soxhlet extraction over a 48 hour period using methanol to remove any free RB. UV-Vis

spectroscopy was used to confirm that washings contained no free sensitizer after 48 hours. The beads were air dried overnight.

3.4.13 Dye sensitized photooxygenation of α-terpinene using 200 mg of RB-MR beads (Experiments 69a-d)

General procedure

The general procedure for the dye sensitized photooxygenation of α-terpinene using RB-MR beads was identical to the procedure using TCPP-MR beads (Section 3.4.6).

Experiment 69a Dye sensitized photooxygenation of α-terpinene using 200 mg of RB-MR beads in IPA

The general procedure was followed. UV-Vis spectroscopy showed a percent conversion of 23 % after 8 hours of irradiation.

Experiment 69b Dye sensitized photooxygenation of α-terpinene using 200 mg of RB-MR beads in IPA

The general procedure was followed. UV-Vis spectroscopy showed a percent conversion of 27 % after 8 hours of irradiation.

Experiment 69c Dye sensitized photooxygenation of α-terpinene using 200 mg of RB-MR beads in IPA

The general procedure was followed. UV-Vis spectroscopy showed a percent conversion of 32 % after 8 hours of irradiation.

Experiment 69d Dye sensitized photooxygenation of α-terpinene using 200 mg of RB-MR beads in IPA

The general procedure was followed. UV-Vis spectroscopy showed a percent conversion of 28 % after 8 hours of irradiation.

3.5 References

(1) Anastas, P. T.; Kirchhoff, M. M. *Acc. Chem. Res.* **2002**, *35*, 686-694.

(2) Merrifield, R. B. *J. Am. Chem. Soc.* **1963**, *85*, 2149-2154.

(3) Merrifield, R. B. *J. Am. Chem. Soc.* **1964**, *86*, 304-305.

(4) Merrifield, R. B. *Biochemistry* **1964**, *3*, 1385-1389.

(5) Merrifield, R. B. *J. Org. Chem.* **1964**, *29*, 3100-3102.

(6) Lambert, C. R.; Kochevar, I. E. *J. Am. Chem. Soc.* **1996**, *118*, 3297-3298.

(7) Lamberts, J. J. M.; Schumacher, D. R.; Neckers, D. C. *J. Am. Chem. Soc.* **1984**, *106*, 5879-5883.

(8) Schaap, A. P.; Thayer, A. L.; Blossey, E. C.; Neckers, D. C. *J. Am. Chem. Soc.* **1975**, *97*, 3741-3745.

(9) Paczkowski, J.; Neckers, D. C. *Macromolecules* **1985**, *18*, 1245-1253.

(10) Nowakowska, M.; Kępczyński, M.; Dabrowska, M. *Macromolecular Chemistry and Physics* **2001**, *202*, 1679-1688.

(11) Wan, J.; Wang, H.; Wu, Z.; Shun, Y. C.; Zheng, X.; Phillips, D. L. *Phys. Chem. Chem. Phys.* **2011**, *13*, 10183-10190.

(12) Granados-Oliveros, G.; Páez-Mozo, E. A.; Martínez Ortega, F.; Piccinato, M.; Silva, F. N.; Guedes, C. L. B.; Di Mauro, E.; Costa, M. F. d.; Ota, A. T. *Journal of Molecular Catalysis A: Chemical* **2011**, *339*, 79-85.

Chapter 4:

Heterogensous dye sensitized photooxygenation of α-terpinene: Immobilisation of TCPP and TCPPZn onto silica nano particles.

4.1 Introduction

The rapid development of functionalised monodisperse silica nano particles over the past few years has resulted in a growing interest in the application of these particles in nanomedicine. Research into their applications in this area is primarily due to their large surface area to volume ratio, their facile and reproducible manufacture and their capacity for doping and/or functionalisation.

As a result of these advantages silica nano particles have been used as biomarkers in cell imaging, [1-3] as drug delivery systems[4], biosensors[5,6] and even used as solid supported catalysts for the epoxidation of alkenes and hydroxylation of alkanes. [7]

The utilisation of silica nano particles as potential solid supports for heterogeneous dye sensitized photooxygenations offers three distinct key advantages. Firstly, the particles are white in colour. Consequently, they do not absorb light in the visible region and will not compete with the sensitizer. Secondly, the particles will be significantly smaller than the Merrifield resin beads described in Chapter 3. Due to their small size (~200 nm) these particles have significantly larger surface areas and it will also be possible to use silica particles in conjunction with the newly developed photochemical microflow reactor (Chapter 5). Thirdly, the sensitizer functionalised silica nano particles can also be removed from crude reaction mixtures by centrifugation, thus will eliminating the need for column chromatography.

Silica nano particles are in general synthesized by the ammonia catalyzed hydrolysis and condensation of alkyl silicates and water in low molecular weight alcohols. This method is commonly known as the Stöber method and has been subject to much investigation since it was first reported in 1968.[8] The Stöber method provides a facile and reproducible method for the synthesis of spherical, monodisperse silica nano particles (SNPs) from tetraethyl orthosilicate (TEOS). It also represents a "one-pot" synthesis that avoids the use of potentially toxic organic solvents and surfactants.[9] It is widely accepted that the formation of these silica nano particles can be represented by the following three equations:

$$\equiv Si\text{-}OR + H_2O \rightarrow \equiv Si\text{-}OH + ROH \text{ (hydrolysis)}$$

$$\equiv Si\text{-}OR + HO\text{-}Si\equiv \rightarrow \equiv Si\text{-}O\text{-}Si\equiv + ROH \text{ (alcohol condensation)}$$

$$\equiv Si\text{-}OH + HO\text{-}Si\equiv \rightarrow \equiv Si\text{-}O\text{-}Si\equiv + H_2O \text{ (water condensation)}$$

Scheme 4.1: Stöber synthesis of silica nano particles.

The formation of silica nano particles can be divided into two main stages: nucleation and growth.

Nucleation involves the formation of the initial primary silica particles via hydrolysis of TEOS followed by complex condensation reactions of the hydrolysed products. The growth stage involves the increase in diameter of the particles via Ostwald ripening, aggregation and further addition of low molecular weight hydrolysed products through condensation reactions.

During the nucleation process condensation reactions occur between hydrolysed products in such a fashion as to maximize the amount of Si-O-Si bonds while minimizing the amount of hydroxyl groups. Thus polymeric rings are quickly formed to which further monomers add to generated 3-dimensional particles. These particles then undergo internal condensation to form compact particles confining any remaining hydroxyl groups to the surface. These primary particles can then enter the growth stage and act as nuclei for further growth. This growth can occur via Ostwald ripening, aggregation and by addition of further monomers via condensation reactions. Growth effectively stops when the solubility of the largest and smallest particles differs by a few parts per million (ppm).

The final product(s) of the hydrolysis and condensation reactions are pH dependant. Below pH 7 the product(s) tend to be silicon based polymers that eventually extend to form 3-dimensional (3D) gels. Above pH 7 the product(s) tend to be monodisperse silica nano particles.

Below pH 7:

In any given solution of silicate species the most acidic silanol groups will be found on the most highly condensed species and these are the most likely of the silanol groups to become deprotonated. As a result further condensation occurs primarily between the more highly condensed species and the less condensed neutral species. For this reason the rate of dimerisation is low but once dimers are formed they react readily with monomers to form tetramers. Cyclisation occurs rapidly at this point due to the proximity of chain ends. Internal condensation occurs to form primary particles. Polymerisation occurs by addition of lower molecular weight species to these more highly condensed primary particles and cyclic polymers. Continued growth of the polymer network to form a gel occurs by further condensation reactions, Ostwald ripening and aggregation.

Above pH 7:

Initial polymerization occurs via the same mechanisms as below pH 7. However, because the condensed species are more likely to be ionized above pH 7 growth occurs primarily by addition of monomers to more highly condensed species. Aggregation tends not to occur due to mutual repulsion between the ionized hydrolyzed species. Compact particles 1-2 nm in size develop within several minutes and due to the increased solubility of SiO_2 above pH 7 growth occurs via Oswald ripening. This leads to the growth of silica nano particles rather than gel formation.

Based upon extensive research five main factors have been identified as having an influence on the size and morphology of the final silica nano particles. These are namely: i) TEOS concentration, ii) ammonia concentration, iii) water concentration, iv) alcohol used and v) reaction temperature.[10] By changing each of these factors the overall size and morphology of silica nano particles can be controlled.

i) TEOS concentration

Rao *et al* have reported that the concentration of TEOS can either reduce or increase the final size of the SNPs depending on the concentration of water within the

reaction solution.[11] During syntheses, where there was a low concentration of water, particle size increased with increasing TEOS concentration and vice versa in solutions of high water concentration. These results can be explained by the findings of Chen *et al*. [12] Chen and co-worker describe the initial hydrolysis of TEOS to be first order with respect to TEOS.

Nozawa *et al* have shown in a series of experiments, where all conditions were kept constant except that rate of the addition of TEOS, that at greater addition rates of TEOS produces smaller particles.[13]

ii) Water and ammonia concentration

High concentrations of water and ammonia have both been reported to produce smaller particles. Hydrolysis reactions are normally very slow reactions and as such ammonia is used to catalyze the hydrolysis of TEOS. In situations with high concentrations of water the hydrolysis reaction occurs faster and secondary nucleation occurs causing the formation of smaller primary particles. The same holds true with ammonia concentration. Higher concentrations speed up the rate of hydrolysis causing secondary nucleation. Aelion *et al* have reported that the rate of hydrolysis is affected most notably by the concentration of ammonia and that solvent and temperature affects are secondary to this.[14]

iii) Effect of alcohol used

The effect of alcohols used as reaction solvent on the final size and morphology of silica nano particles has been well documented in the literature. Particle diameters of 30 – 800 nm have been reported using low molecular weight alcohols such as methanol, ethanol, propanol and butanol.[15] The use of MeOH to produce < 100 nm silica nano particles is also well documented. However, the particles often suffer from aggregation leading to larger particles.[16] In addition, use of longer chain alcohols such as n-butanol often results in the formation of polydisperse nano particles.[17] In general, increasing alcohol molecular weight results in larger silica nano particles however, ethanol or propanol should be used to avoid aggregation and polydispersity issues.

iv) Temperature

Rahman *et al* have reported the reduction in particle size of silica particles from 92.3 nm down to 32.6 nm by increasing the reaction temperature from 45 – 65 °C during the synthesis of SNPs via a modified Stöber method.[18] This result however, is in conflict with the generally accepted concept that particle growth increases with increasing temperature. As the temperature increases so too does the solubility of the primary silica particles increasing the rate of Ostwald ripening and the final size of the SNPs.

4.2 Results and discussion

4.2.1 "One pot" synthesis of TCPP and TCPPZn SNPs

A "one pot" synthesis of TCPP and TCPPZn SNPs was devised based upon the Stöber method (Scheme 4.2).[8] The sensitizer was dissolved in dry ethanol along with TEOS prior to addition of ammonia. Consequently, upon addition of the ammonia the sensitizer would be physically encapsulated into the SNPs during their formation.

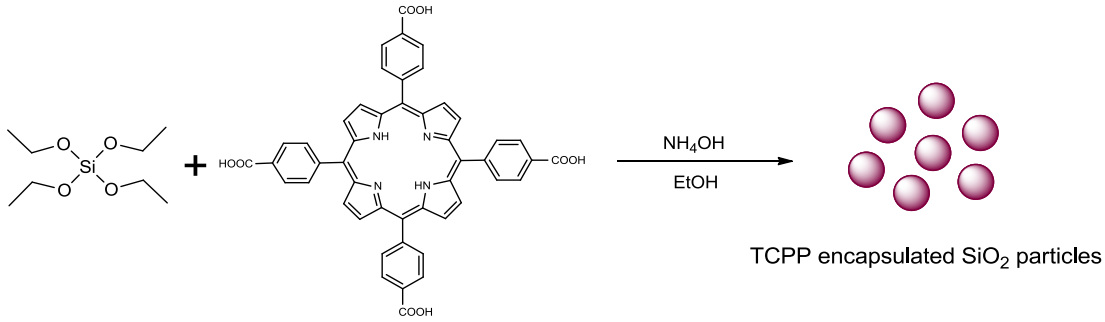

Scheme 4.2 "One pot" synthesis of TCPP SNPs.

4.2.1.1 "One pot" synthesis of TCPP SNPs (Experiment 70)

TEOS (1.5 ml, 6.72 mmol) was dissolved in 50 ml of dry ethanol along with TCPP (15 mg, 0.019 mmol) with the aid of sonication. To this mixture 4 ml of 25 % ammonia was added rapidly and the solution was stirred at room temperature for 90 minutes. At this time the reaction solution was centrifuged at 9,000 rpm for 3 minutes and the supernatant removed. The resulting TCPP encapsulated SNPs were re-dispersed in dry ethanol and centrifuged at 9,000 rpm for 3 minutes to remove any remaining TEOS, ammonia and sensitizer from the surface of the SNPs. The process was repeated until UV-Vis spectroscopy confirmed that the ethanol washings contained no free sensitizer. The resulting TCPP SNPs were pale purple in colour and were dried under vacuum at 40 °C overnight.

The FT-IR spectrum of "one pot" TCPP SNPs shows characteristic absorbance peaks due to Si-O-Si symmetric stretching, asymmetric stretching and bridge rocking vibrations at 1090, 800 and 475 cm^{-1} respectively (Figure 4.1).[19,20,21] The broad absorbance between 3700 and 2700 cm^{-1} may be attributed to Si-OH stretching

vibrations of surface silanol groups. The weak absorption peaks between 2989 and 2852 cm^{-1} are due to C-H stretching vibrations. This is attributed to un-hydrolysed TEOS (ethoxy groups) present on the surface of the SNPs. Interestingly, there is no absorbance peak at ~ 1600 cm^{-1} which would indicate the presence of TCPP. Comparison with the FT-IR spectrum of unfunctionalised SNPs shows that there is no evidence to suggest TCPP functionalisation has occurred. A possible reason for this may be due to minute amounts of TCPP being encapsulated within the silica matrix. As a result FT-IR spectroscopy cannot distinguish TCPP from the bulk silica matrix. In addition to encapsulation, chemisorption of TCPP to the surface of the SNPs may also have occurred. However, the amount of TCPP present would still remain very low in comparison to the bulk silica matrix.

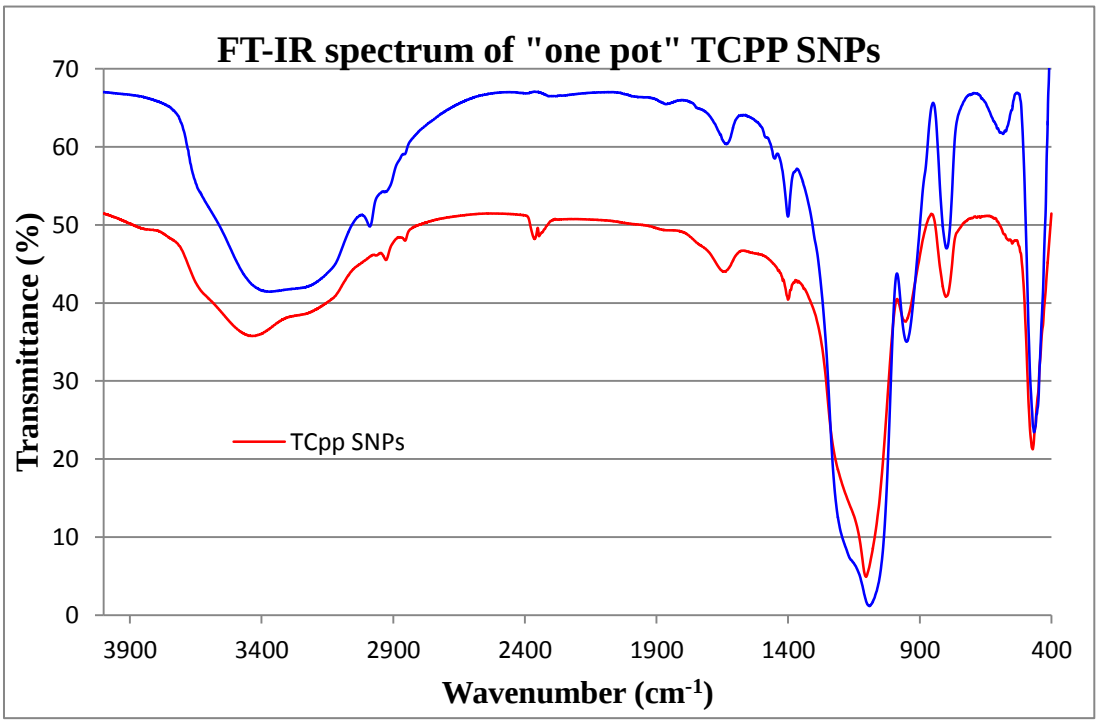

Figure 4.1: FT-IR spectrum of "One pot" TCPP SNPs.

The diffuse reflectance UV-Vis spectrum of the "one pot" TCPP SNPs helps to bolster this explanation (Figure 4.2).

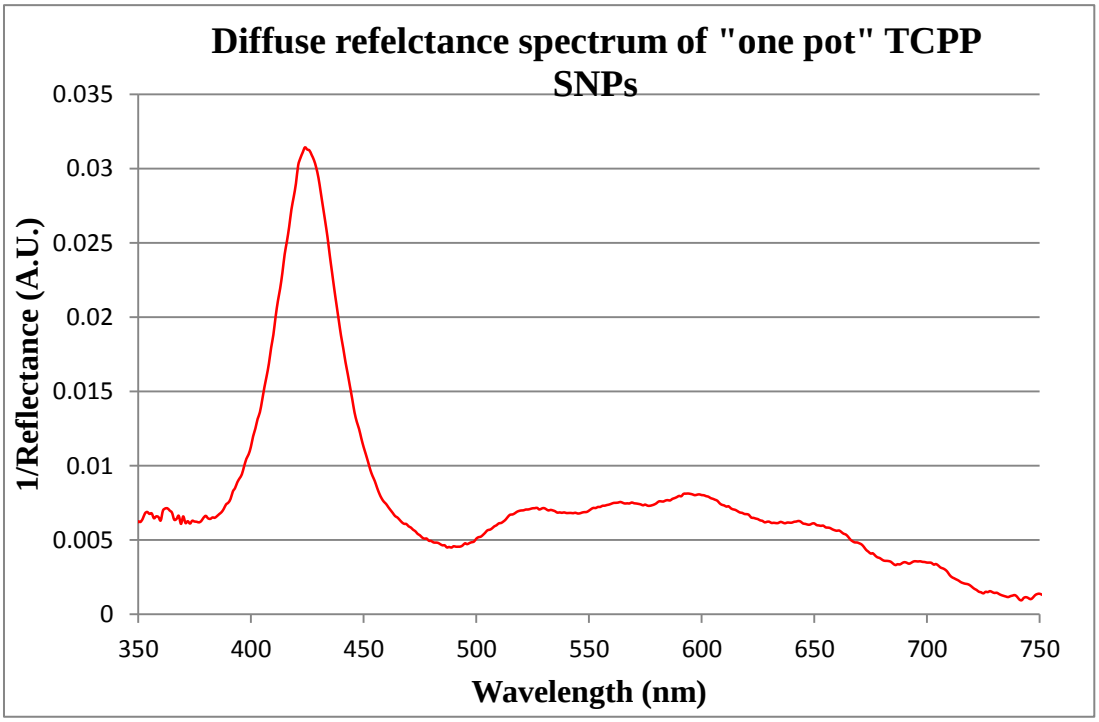

Figure 4.2: Diffuse reflectance UV-Vis spectrum of "one pot" TCPP SNPs.

The diffuse reflectance UV-Vis spectrum confirms that TCPP is present either encapsulated within or present on the surface of the SNPs. UV-Vis spectroscopic analysis of ethanol washings from the "one pot" TCPP SNPs confirmed that no TCPP was present. This indicated that any TCPP encapsulated within the SNPs or present on the surface must be physically or chemically bound to the SNPs. However, the intensity of the spectrum is quite weak suggesting a minimal amount of TCPP present. This is in agreement with the results obtained from FT-IR analysis of the SNPs. The diffuse reflectance UV-Vis spectrum shows the TCPP Soret band at 425 nm and the four Q-bands at 525, 565, 596 and 650 nm.

Dynamic Light Scattering (DLS) measurements were not performed to identify the mean diameter of the "one pot" TCPP SNPs as they could not be dispersed (with sonication) in ethanol after drying overnight.

4.2.1.2 Heterogeneous dye sensitized photooxygenation of α-terpinene using "one pot" TCPP SNPs (Experiment 71)

The results of Chapter 3 (dye sensitized photooxygenations using Merrifield resins as solid supports) have shown that when a sensitizer is covalently bound to the surface of a solid support the singlet oxygen quantum yields decrease, sometimes significantly resulting in reduced reaction rates. Consequently, due to its relatively fast rate of reaction, the dye sensitized photooxygenation of α-terpinene was chosen as a test reaction (Scheme 4.3).

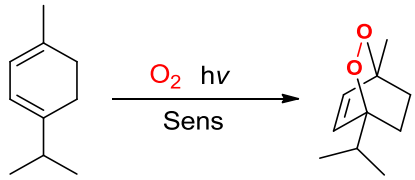

Scheme 4.3: Dye sensitized photooxygenation of α-terpinene to ascaridole.

The heterogeneous dye sensitized photooxygenation of α-terpinene was performed using 200 mg of the "one pot" TCPP SNPs. The procedure was the same as that for the synthesis of ascaridole using TCPP-MR beads (Section 3.2.3.1). 200 mg Of the TCPP SNPs were placed in 50 ml of IPA. Dispersion of the SNPs was attempted via sonication. However, the SNPs could not be fully dispersed in IPA resulting in the 'clumping' of SNPs. This was similar to dispersion tests in EtOH in Section 4.2.1.1. Despite incomplete dispersion of the SNPs the reaction mixture was then placed in front of a 500 W halogen lamp (27 cm distance) with constant air bubbling. At time zero 1 ml (5.2 mmol) of α-terpinene was added and the reaction mixture was irradiated for 8 hours. UV-Vis spectroscopy confirmed a percent conversion of 20% after 8 hours. This result indicated that the "one pot" TCPP SNPs were ineffective solid support sensitizers for dye sensitized photooxygenations. In comparison, control experiments (Section 3.2.1) have shown that α-terpinene can self sensitize to give percent conversions of up to 11 % in 8 hours. This low percent conversion (20 %) may be due to minimal amounts of TCPP encapsulated within or chemisorbed onto the surface of the SNPs. However, the low yield may indicate that any TCPP that is present is encapsulated within the SNPs. During the formation of the SNPs

TEOS undergoes complex hydrolysis and condensation reactions to produce highly packed silica nano particles. If TCPP was encapsulated into this matrix then the system may suffer the same problems as "un-swollen" Merrifield resin beads. The reaction media may not be able to diffuse through the silica particles and as a result little if any conversion to products is observed.

Interestingly, ^{1}H NMR showed that of the product that was formed, 87 % of was in fact *p*-cymene (Figure 4.3).

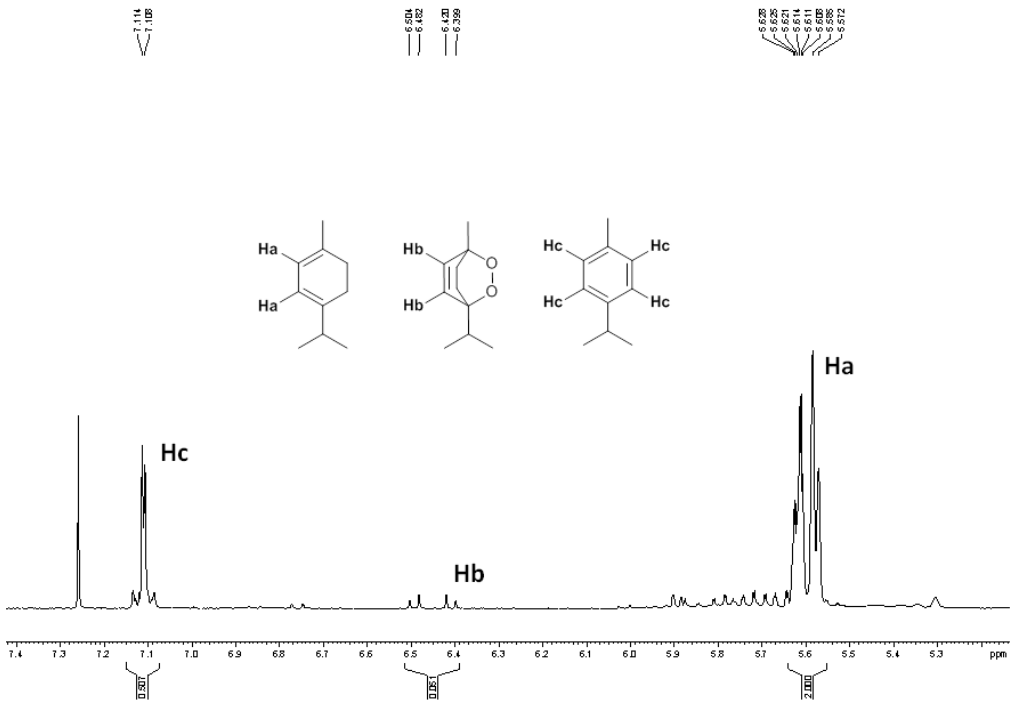

Figure 4.3: ^{1}H NMR ($CDCl_3$) showing up to 87 % of product formed was p-cymene.

This large amount of *p*-cymene may have been due to the formation of super oxide anions. The production of these anions is due to the fact that silica is a known semiconducting material. Upon excitation the sensitizer is capable of an electron transfer to the conduction band of the silica matrix. This then transfers the electron to molecular oxygen adsorbed to the semiconducting surface generating superoxide radical anions and sensitizer radical cations (Figure 4.4).

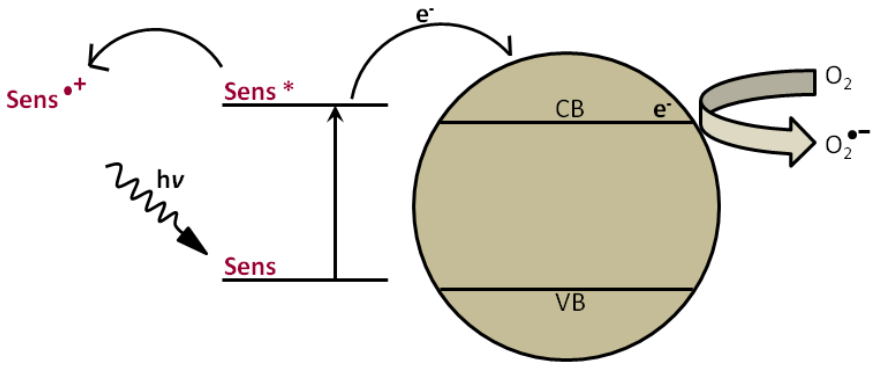

Figure 4.4: Dye sensitized generation of superoxide radical anions.

These superoxide radical anions are then capable of reacting with α-terpinene to generate *p*-cymene in large quantities relative to ascaridole (Scheme 4.4).

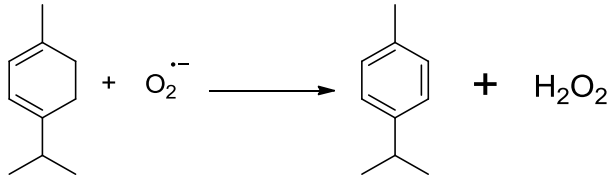

Scheme 4.4: Reaction of α-terpinene with superoxide radical anion to generate p-cymene.

p-Cymene shows a broad but weak absorbance peak in the same region of the UV-Vis spectrum as α-terpinene. These large quantities of *p*-cymene produced by superoxide radical anions may result in false negative results from UV-Vis spectroscopic analysis. In order to determine if this was the case a series of solutions in IPA were prepared starting with 104 mM α-terpinene (100 %). This was consistent with initial concentrations of α-terpinene during dye sensitized photooxygenations. Dilution solutions were then prepared at 10 % increments. The absorbance of each solution was obtained (265.5 nm) and the "percent conversion" determined (Table 4.1).

Table 4.1: Affect of increased quantities of p-cymene on UV-Vis spectroscopic analysis.

	Sample A			Sample B	
AT (%)	**Absorbance**	**% Conversion**	**AT/PC (%)**	**Absorbance**	**% Conversion**
100	0.825	0	100/0	0.83	0
90	0.759	6.8	90/10	0.754	6.2
80	0.663	18.2	80/20	0.647	16.8
70	0.585	28	70/30	0.599	26.2
60	0.503	38.2	60/40	0.515	36.7
50	0.417	48.9	50/50	0.434	46.8
40	0.337	58.9	40/60	0.362	55.8
30	0.248	70	30/70	0.285	65.4
20	0.177	78.9	20/80	0.206	75.2
10	0.085	90.3	10/90	0.136	84
N/A	N/A	N/A	0/100	0.048	95

AT = α-terpinene, PC = *p*-cymene.

The results from Table 4.1 demonstrate that while *p*-cymene shows a weak absorbance in the same region of the UV-Vis spectrum as α-terpinene, increased quantities present due to superoxide radical anion formation do not affect UV-Vis spectroscopic analysis significantly. Table 4.1 shows how in a situation where complete conversion of α-terpinene to *p*-cymene was achieved, UV-Vis spectroscopic analysis would only deviate by ~5 %. Despite the increased formation of *p*-cymene relative to ascaridole the overall percent conversions remain low and as such UV-Vis spectroscopic analysis remains a valid method for percent conversion determination. In addition, UV-Vis spectroscopy can be use as a visual aid to determine if large quantities of *p*-cymene are produced. Figure 4.5 demonstrates the appearance of a shoulder peak at 273 nm corresponding to *p*-cymene. This peak becomes distinguishable from that of α-terpinene at concentrations > 30 %.

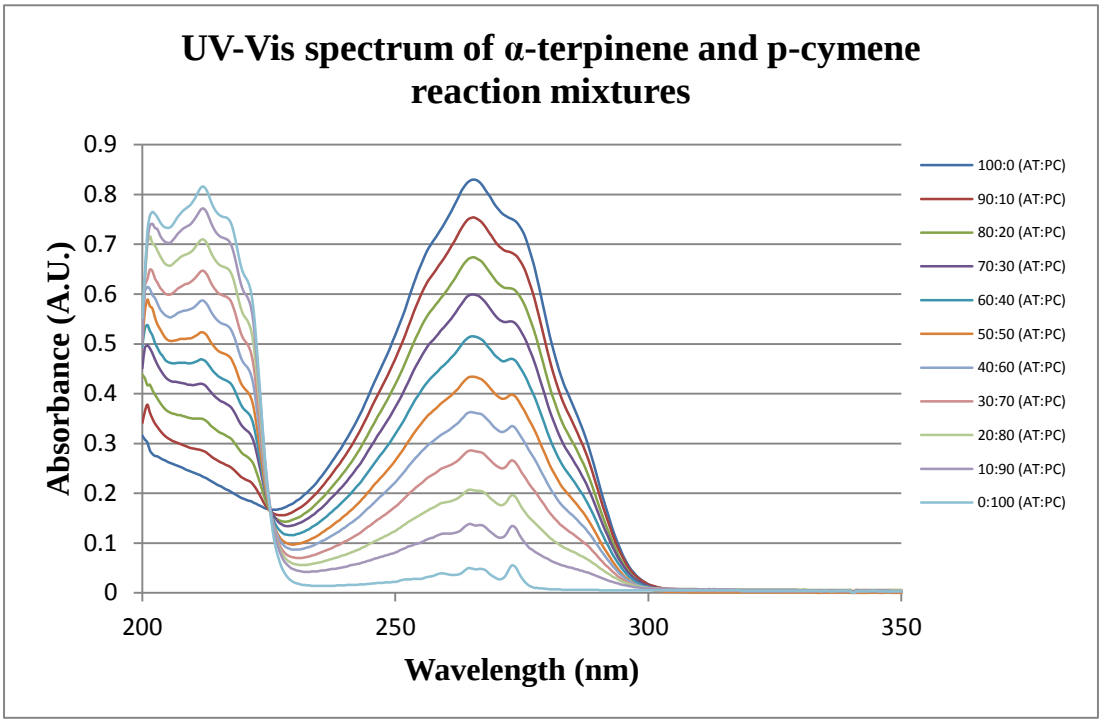

Figure 4.5: UV-Vis spectrum of α-terpinene showing 10 % increments of p-cymene.

4.2.1.3 "One pot" synthesis of TCPPZn SNPs (Experiment 72)

The synthetic procedure was identical to the synthesis of "one pot" TCPP SNPs (Section 4.2.1.1) except 15 mg (0.0176 mmol) of TCPPZn was used. The resulting TCPPZn SNPs were pale green in colour.

Similar to the FT-IR spectrum of "one pot" TCPP SNPs the FT-IR spectrum of "one pot" TCPPZn shows characteristic absorbance peaks at 1070, 806 and 475 cm^{-1} due to Si-O-Si symmetric stretching, asymmetric stretching and bridge rocking vibrations (Figure 4.6). Si-OH stretching and C-H stretching vibrational peaks are also visible between 3700-2700 and 2985-2855 cm^{-1}. Interestingly, the FT-IR spectrum of "one pot" TCPPZn SNPs also shows no evidence of the presence of TCPPZn. This again may be due to minute quantities of TCPPZn being present.

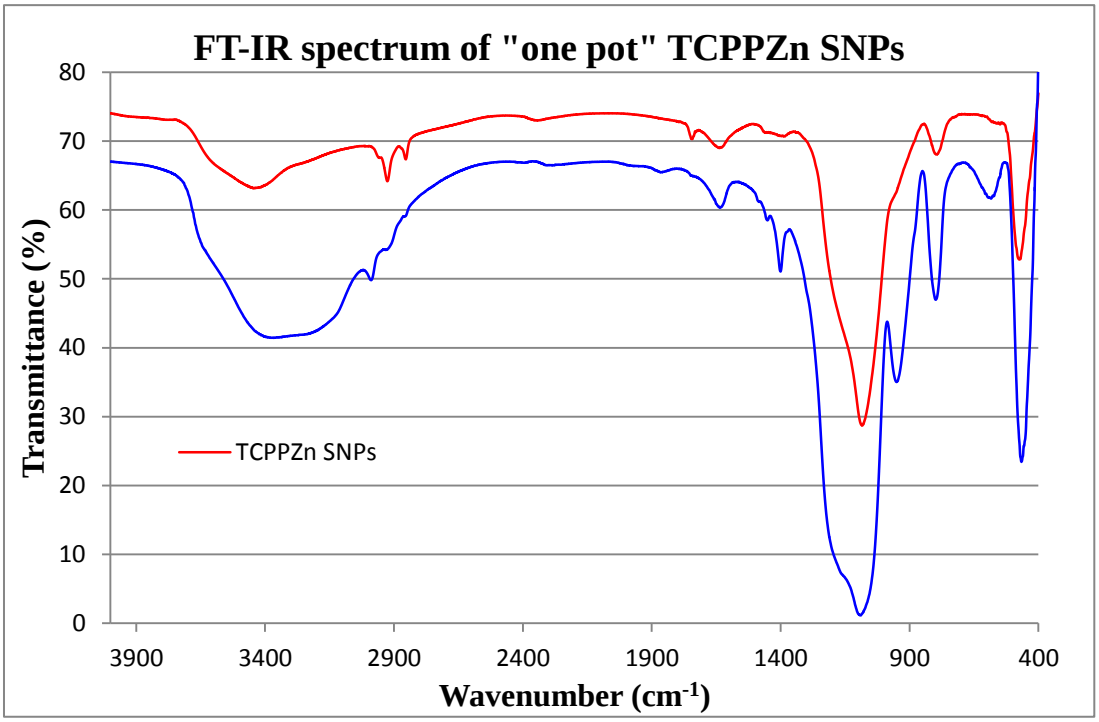

Figure 4.6: FT-IR spectrum of "One pot" TCPPZn SNPs.

In contrast, the diffuse reflectance UV-Vis spectrum shows that TCPPZn is present either encapsulated within or chemisorbed onto the surface of the SNPs (Figure 4.7).

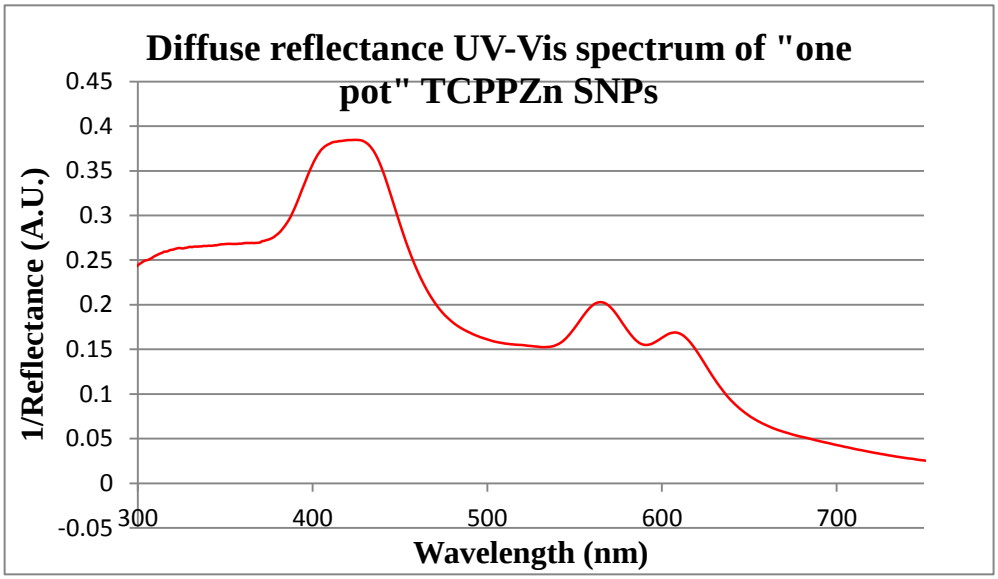

Figure 4.7: Diffuse reflectance UV-Vis spectrum of "one pot" TCPPZn SNPs.

UV-Vis spectroscopic analysis of ethanol washings from TCPPZn SNPs confirmed that no TCPPZn was present in the ethanol washings indicating that any TCPPZn present must be physically or chemically bound to the SNPs. The diffuse reflectance UV-Vis spectrum shows the TCPPZn Soret band at 421 nm and two Q-bands at 565 and 607 nm.

Additionally, dynamic light scattering (DLS) measurements were performed in ethanol. These measurements showed the SNPs to be polydisperse with very large average diameters of up to ~2000 and 5500 nm (Figure 4.8).

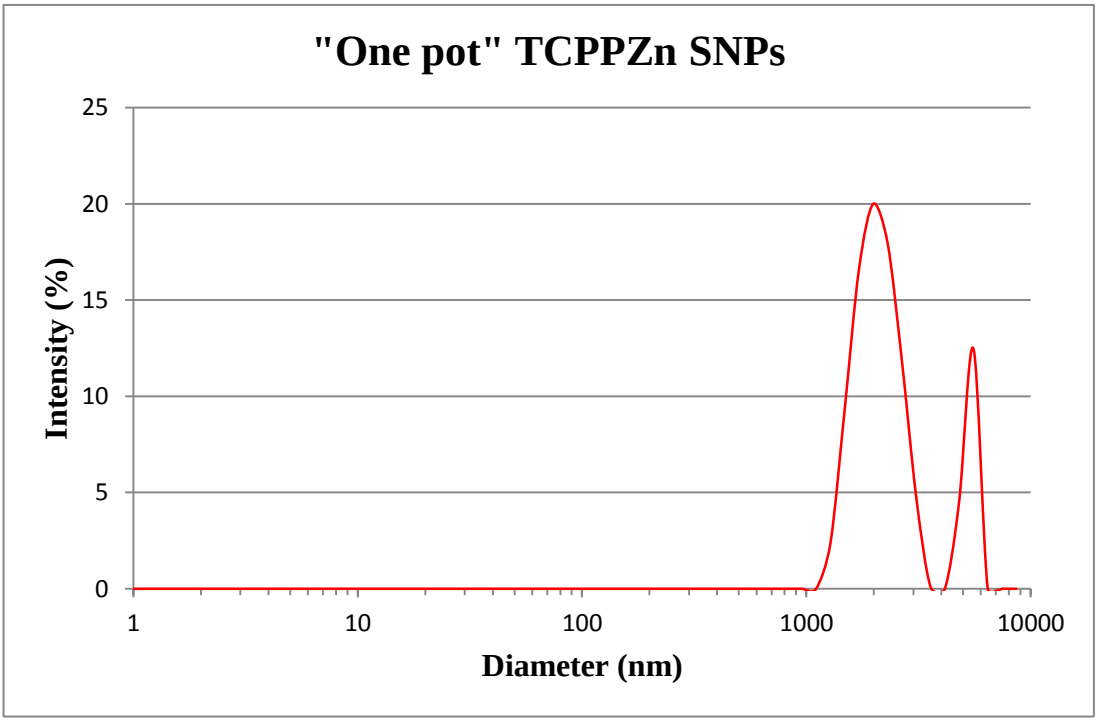

Figure 4.8: DLS measurements of "one pot" TCPPZn SNPs.

4.2.1.4 Heterogeneous dye sensitized photooxygenation of α-terpinene using "one pot" TCPPZn SNPs (Experiment 73)

The heterogeneous dye sensitized photooxygenation of α-terpinene was performed using 200 mg of "one pot" TCPPZn SNPs. The procedure was the same as that for the synthesis of ascaridole using TCPP-MR beads (Section 3.2.3.1). 200 mg of the TCPPZn SNPs were dispersed in 50 ml of IPA with sonication. This mixture was then placed in front of a 500 W halogen lamp (27 cm distance) with constant air

bubbling and cooling via a cold finger. At time zero 1 ml (5.2 mmol) of α-terpinene was added and the reaction mixture was irradiated for 8 hours. UV-Vis spectroscopy confirmed a percent conversion of 29% after 8 hours. Similar to TCPP SNPs, ^{1}H NMR showed that up to 83 % of the product formed was *p*-cymene. This increase in overall yield and quantity of *p*-cymene produced was expected due to the chelation of zinc to the porphyrin centre. The metal centre of the porphyrin efficiently transfers electrons to the semi conducting silica particles which in turn generate superoxide anions. These then react with α-terpinene to generate *p*-cymene. Another reason for the increased quantity of product formed may lie in the fact that the TCPPZn SNPs could be dispersed in IPA unlike the TCPP SNPs.

Although the TCPPZn SNPs provided a superior yield to that of TCPP SNPs the results show that they are still ineffective solid support sensitizers for dye sensitized photooxygenations. Similar to TCPP SNPs this may be due to the inability of the reaction media to diffuse through the silica matrix.

Covalent immobilisation of sensitizers onto the surface of the SNPs may help to overcome this issue. Synthesis of bare silica nano particles and subsequent surface functionalisation with TCPP will allow for interaction between TCPP and the reaction media. In addition, the incorporation of alkyl chain "spacers" may further help to increase this interaction and improve the rate of conversion of α-terpinene to ascaridole.

4.2.2 Synthesis of unfunctionalised silica nano particles

Silica nano particles were synthesized based upon the Stöber method (Scheme 4.5).[8] SNPs were initially synthesized under three separate sets of experimental conditions in order to determine the most reproducible and robust method for SNP production. The concentrations of TEOS, ammonia, ethanol and water were kept constant throughout the three sets of experiments. Physical conditions such as temperature and synthesis under constant sonication were employed. In addition, the average diameter of the SNPs was controlled by reaction time. Samples were taken at set

times and DLS measurements were performed to determine the average diameter with respect to time of reaction.

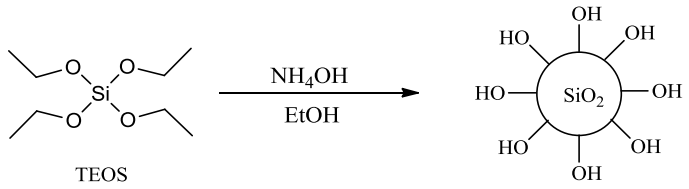

Scheme 4.5: Stöber synthesis of silica nano particles.

4.2.2.1 Room temperature synthesis of silica nano particles (Experiment 74)

TEOS (1.5 ml, 6.72 mmol) was dissolved in 50 ml of dry ethanol and placed under an argon atmosphere. This solution was then stirred vigorously and 4 ml of 25 % ammonia was added rapidly. Samples (1 ml) were taken at 30, 60, 120, 240 and 300 minutes. DLS measurements were performed (in triplicate) in order to determine the average diameter (by intensity) of the SNPs at these times (Figure 4.9). The results show, that as expected, the diameter of the silica particles increased with time as aggregation of smaller particles and Ostwald ripening processes occurred. At 30 minutes the average diameter of the particles was 212.9 nm with a polydispersity index of between 0.009 and 0.060. This increased steadily up to an average diameter of 331.6 nm at 240 minutes. Interestingly, there is a significant decrease in diameter size between 240 and 300 minutes (Figure 4.10). At 300 minutes the mean particle diameter was 288.2 nm. This could be a possible result of internal condensation of both Si-OR and Si-OH groups within the silica particles causing a reduction in overall size of the particles.

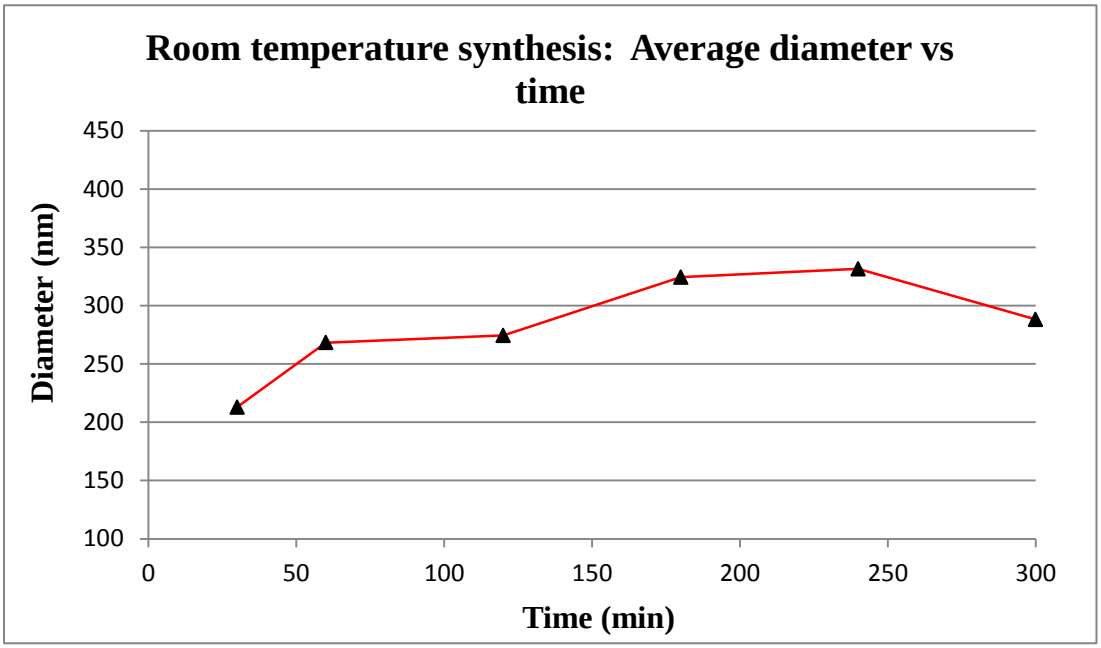

Figure 4.9: Room temperature synthesis of SNPs. Average diameter vs time.

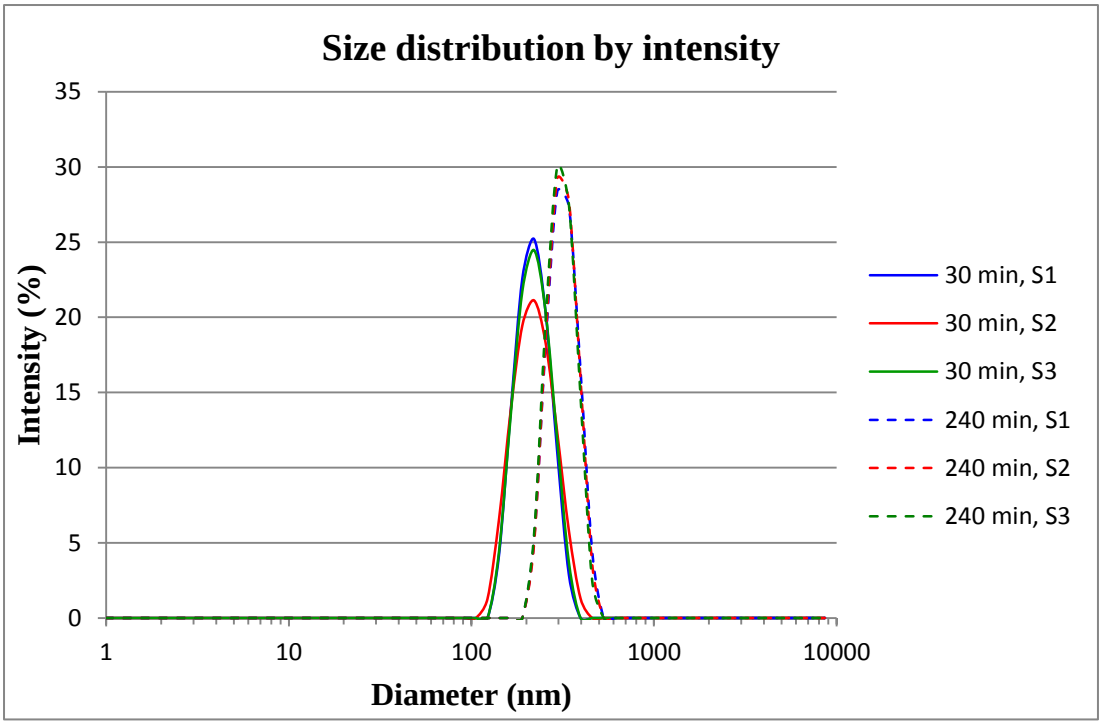

Figure 4.10: DLS measurements of SNPs synthesized at room temperature at 30 and 240 minutes.

In order to increase the overall surface area available for functionalisation the synthesis of smaller particles was attempted. Reduction of the reaction temperature to 0 °C was adopted to reduce the rate of Ostwald ripening resulting in slower particle growth.

4.2.2.2 Zero degrees Celsius synthesis of silica nano particles (Experiment 75)

The synthesis of silica nano particles at 0 °C was performed in an identical manner as to the synthesis at room temperature. The temperature was reduced to 0 °C using an ice bath. Sampling and DLS measurements were also performed at the times indicated for room temperature experiments. DLS measurements showed that the diameters of silica nano particles synthesized at 0 °C were initially smaller than the particles synthesized at room temperature. After 30 minutes the average diameter was measured at 141.6 nm. Interestingly, after approximately 90 minutes the mean diameter of these particles increased dramatically before rapidly decreasing in a similar manner to those synthesized at room temperature (Figure 4.11). The average diameter of the particles at 300 minutes was 204.3 nm (Figure 4.12). The rapid decrease in particle size could also be a result of internal condensation of both Si-OR and Si-OH groups within the silica particles. The rapid particle growth may be attributed to agglomeration of smaller particles. As the temperature decreases the rate of growth should also decrease as Ostwald ripening processes slow down as a result of lower solubility of the silica particles. However, as a result of this lower solubility more of the particles are forced out of solution and agglomeration of these particles occurs resulting in rapid particle growth.

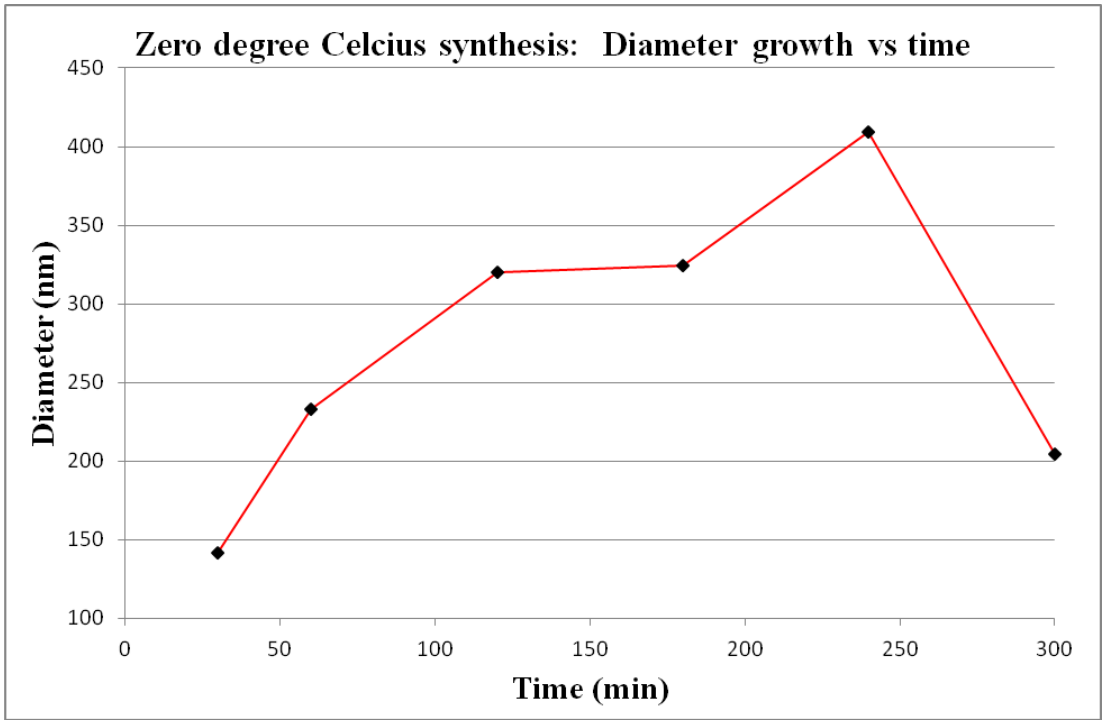

Figure 4.11: Synthesis of SNPs at 0 °C. Diameter growth vs time.

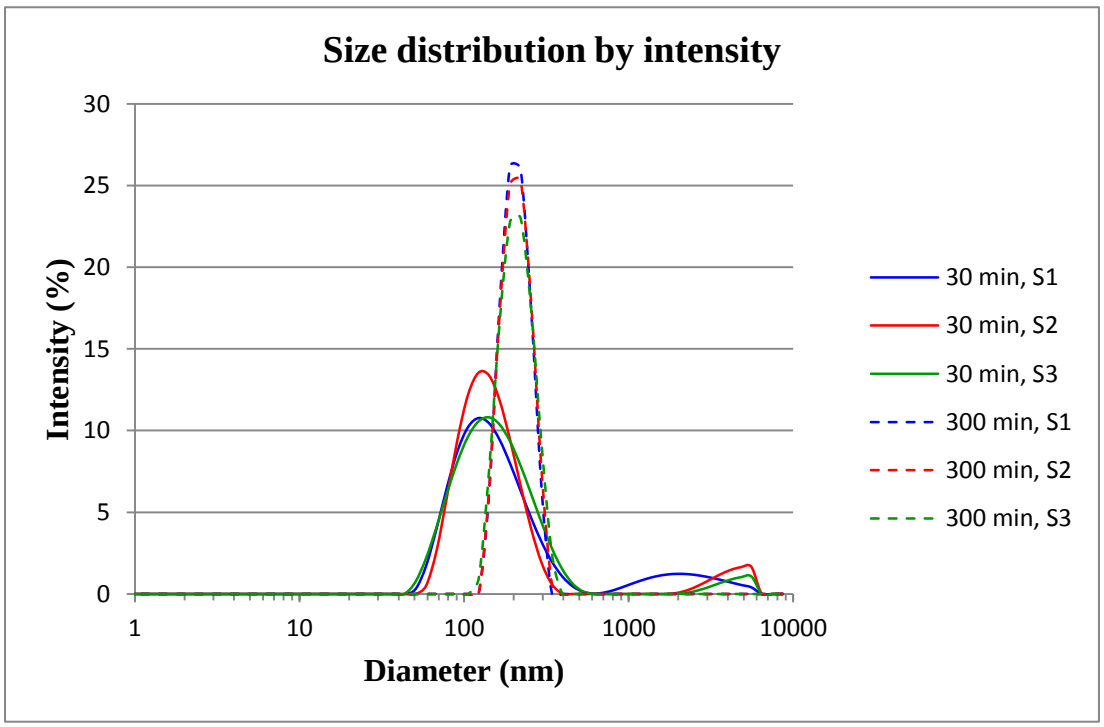

Figure 4.12: Synthesis of SNPs at 0 °C. DLS measurements at 30 and 300 minutes.

In order to prevent this agglomeration the experiment was repeated again at room temperature under constant sonication. Sonication was applied in order to prevent particle growth via agglomeration resulting in a more uniform rate of growth.

4.2.2.3 Room temperature synthesis under constant sonication (Experiment 76)

The synthesis of silica nano particles was performed under constant sonication at room temperature using a Branson 3510 sonicator. The temperature was increased back to room temperature to increase the rate of particle growth via Ostwald ripening processes. Sonication of the reaction was employed to reduce particle growth via agglomeration. DLS measurements at the times indicated for the previous two syntheses showed that the rate of particle growth was much more uniform under these reaction conditions (Figure 4.13). Initial DLS measurements at 30 minutes show a mean diameter of 185.1 nm. With time this diameter grows uniformly to an average of 242.9 nm after 300 minutes (Figure 4.14). In contrast to the previous two syntheses there was no apparent decrease in the final diameter of the silica nano particles.

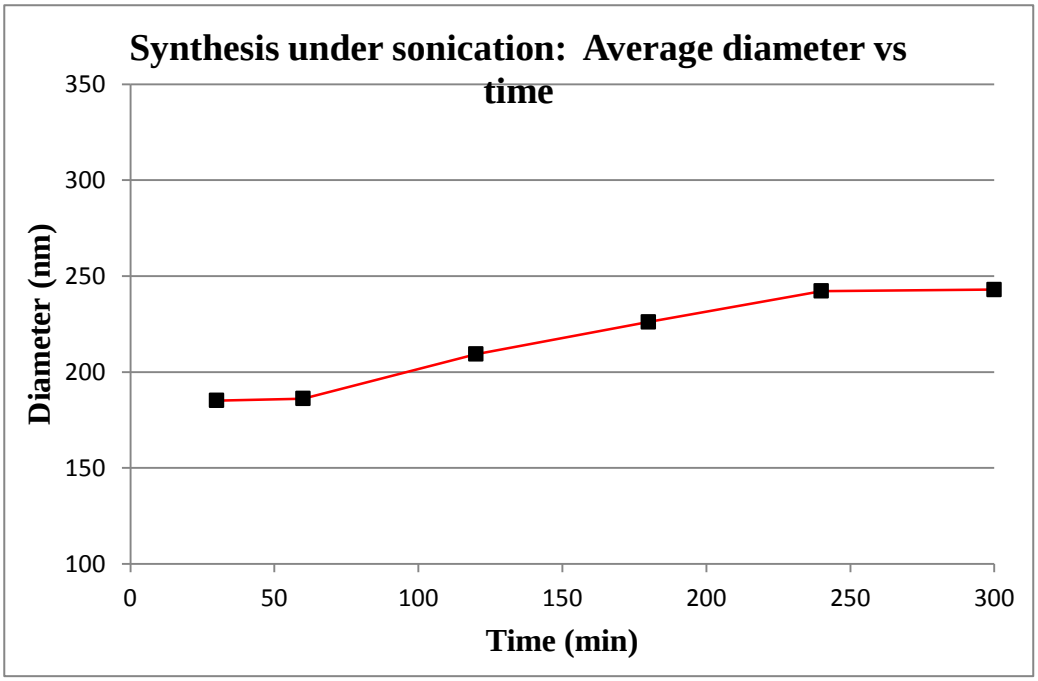

Figure 4.13: Synthesis of SNPs under constant sonication. Average diameter vs time.

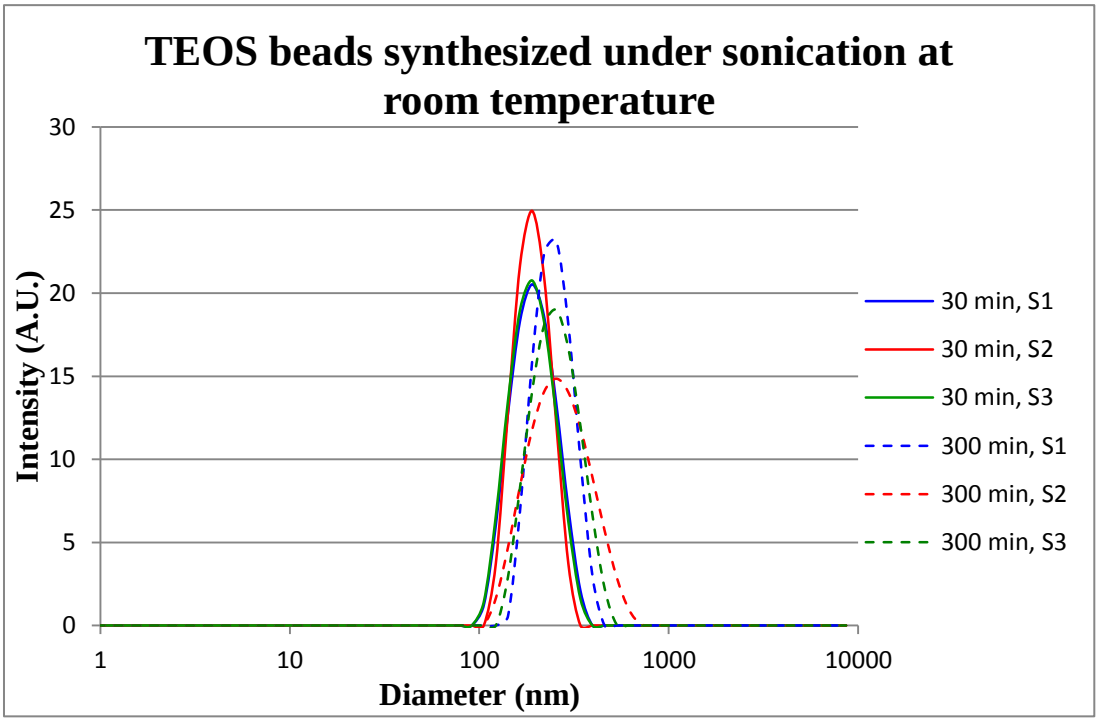

Figure 4.14: DLS measurements of SNPs synthesized at room temperature under constant sonication at 30 and 300 minutes.

The results (Figure 4.13) clearly demonstrate that synthesis of SNPs at room temperature under constant sonication provides the most uniform rate of particle growth. Consequently, all further SNPs were synthesized using this method. In order to synthesize SNPs with a diameter of approximately 200 nm all further reactions were stopped after 90 minutes. This was done by immediate centrifugation at 9,000 rpm for 3 minutes with subsequent removal of the supernatant. The particles were then re-dispersed in dry ethanol under sonication and the process repeated 3 times.

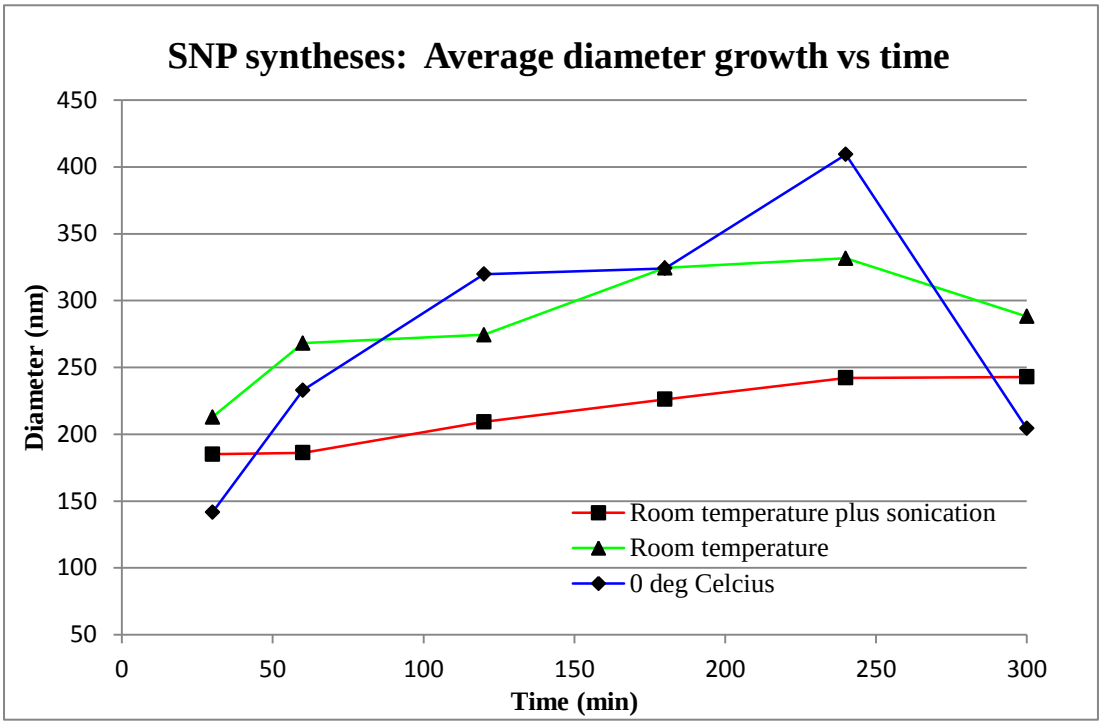

Figure 4.15: Average diameters of SNPs over time synthesized under three sets of experimental conditions.

4.2.2.4 Reproducibility of SNP diameter (Experiment 77 a-e)

In order to demonstrate the reproducibility of the synthesis of SNPs at room temperature under constant sonication the process was repeated five times. Briefly, TEOS (1.5 ml, 6.72 mmol) was dissolved in 50 ml of dry ethanol and placed under an argon atmosphere. This solution was then placed under constant sonication and 4 ml of 25 % ammonia was added rapidly. After 90 minutes the solution was centrifuged at 9,000 rpm for 3 minutes. The supernatant was discarded and the SNPs were re-dispersed in dry ethanol using sonication. This process was repeated three times to wash the SNPs and remove any traces of ammonia. DLS measurements in dry ethanol of the five experiments are tabulated in Table 4.2.

Table 4.2: Reproducibility of SNP diameter.

Exp No	Mean diameter (nm)	PDI
73a	222.4	0.002-0.046
73b	216.33	0.055-0.116
73c	219.7	0.011-0.028
73d	222.4	0.004-0.051
73e	208.8	0.009-0.034

Figure 4.16 clearly demonstrates that monodisperse silica nano particles with average diameters of 208-222 nm can be easily and quickly produced by the above adopted synthetic method. Scanning Electron Microscopy (SEM) images of the SNPs were also obtained and help to show visually the monodispersity of the SNPs synthesized by this method (Figures 4.17 and 4.18).

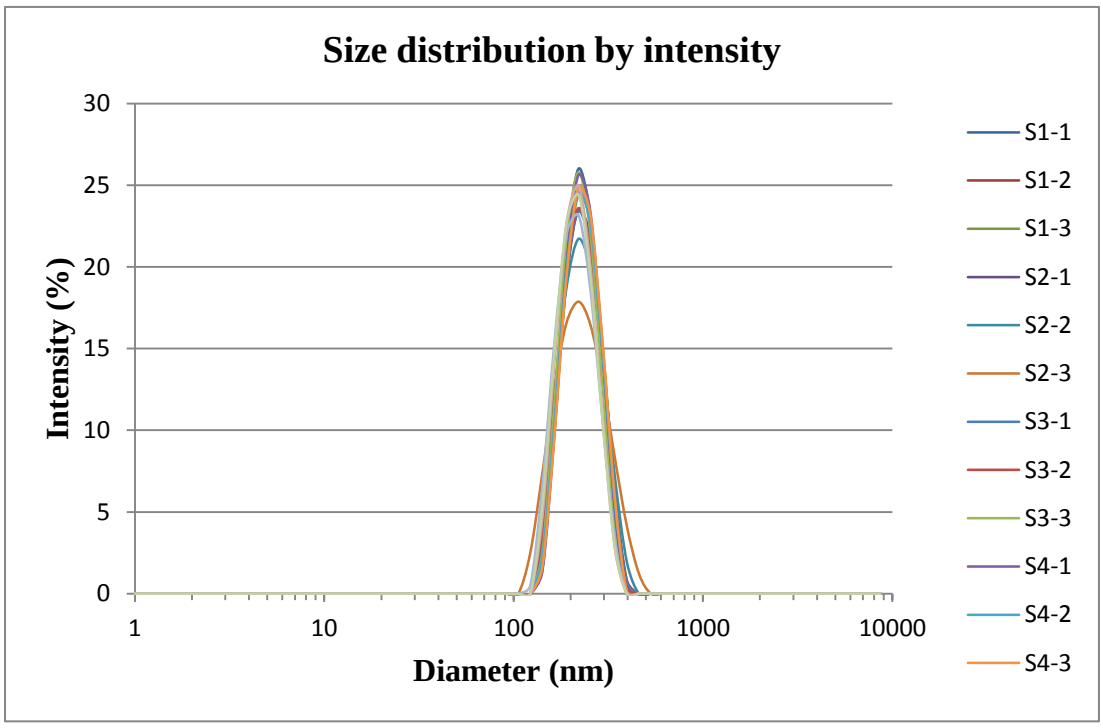

Figure 4.16: DLS measurements (in triplicate) of experiments 71a to 71e.

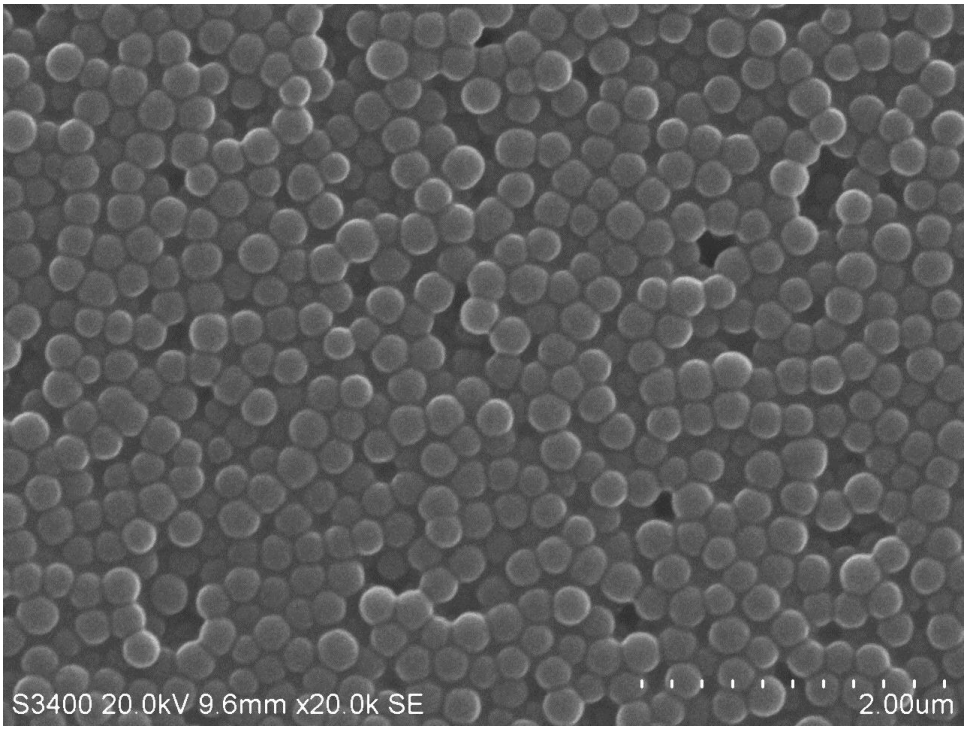

Figure 4.17: SEM image of SNPs synthesized at room temperature under constant sonication.

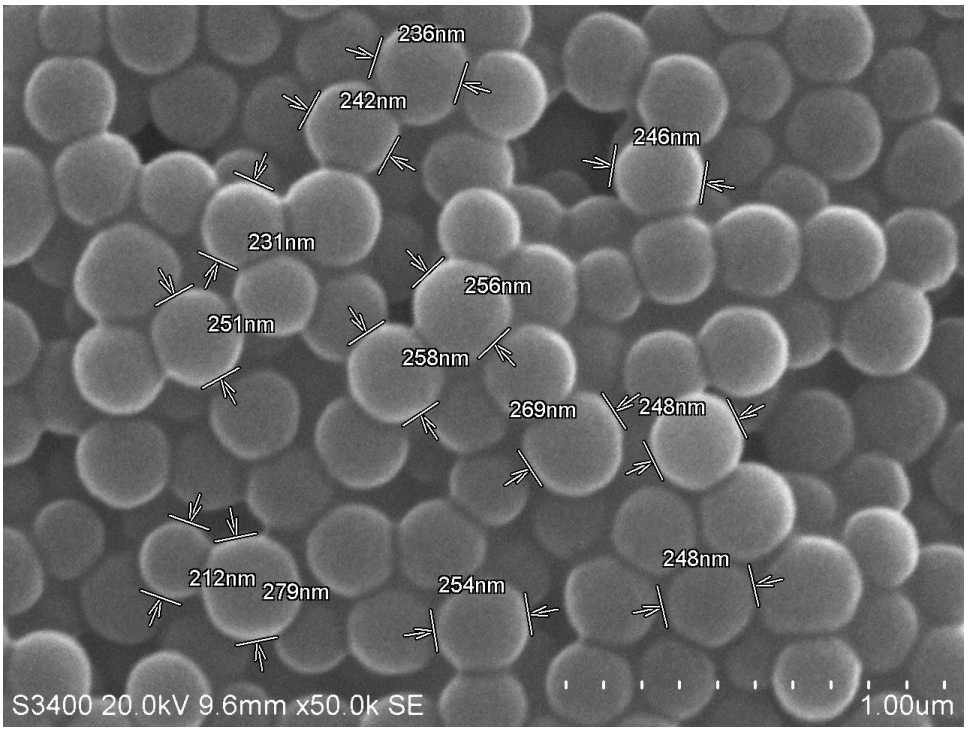

Figure 4.18: SEM image of SNPs synthesized at room temperature under constant sonication, also shown are the diameters (nm) of several SNPs.

4.2.3 Surface functionalisation of SNPs

4.2.3.1 Synthesis of TCPP-APTES SNPs

Surface functionalisation of SNPs with APTES (Experiment 78)

Silica nano particles synthesized at room temperature under constant sonication were functionalized with 3-aminopropyltriethoxy silane (APTES) under base catalysed conditions (Scheme 4.6).

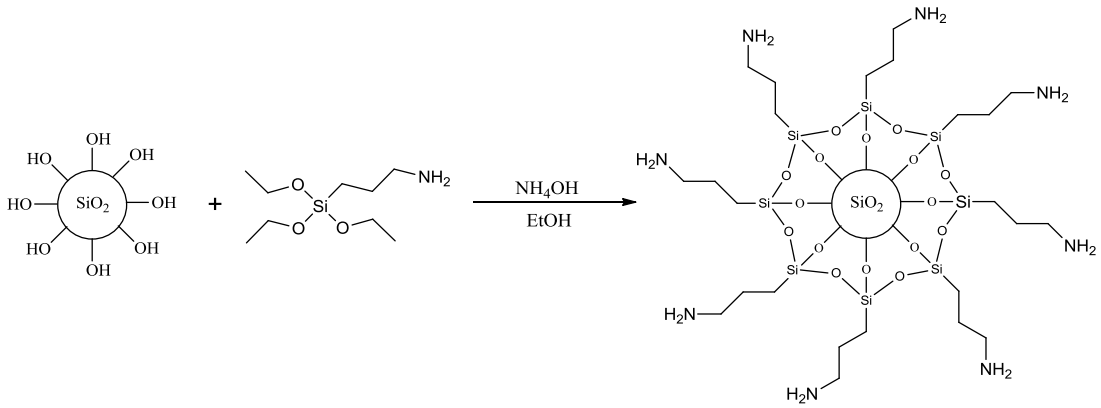

Scheme 4.6: Base catalysed functionalisation of SNPs with APTES.

The bare silica particles were dispersed in 50 ml of dry ethanol and placed under a N_2 atmosphere. To this mixture APTES (100 μL, 0.43 mmol) was added followed by rapid addition of 4 ml of 25 % ammonia. The solution was then left to stir overnight. The resulting APTES-SNPs were separated by centrifugation and washed three times in dry ethanol. They were then re-dispersed and stored in dry ethanol.

Covalent linking of TCPP to APTES-SNPs (Experiment 79)

APTES-SNPs were further functionalized by covalent attachment of TCPP to the surface which was achieved using peptide coupling chemistry, generating an amide linkage (Scheme 4.7). TCPP (100 mg, 0.126 mmol) was dissolved in 5 ml dry DMF and placed under a N_2 atmosphere and cooled to 0 °C using an ice bath. This mixture was then stirred for 20 minutes. Next, 1-ethyl-3-(3-dimethylaminopropyl)-carbodiimide hydrochloride (EDC, 96 mg, 0.504 mmol) was added in 1 ml of dry DMF and the solution allowed to stir for a further 15 minutes. N-hydroxysuccinimide (NHS, 57 mg, 0.504 mmol) was then added and the solution

allowed to stir for 1 hour. Finally, the APTES SNPs were added in 5 ml of dry DMF and the solution allowed to stir at room temperature overnight.

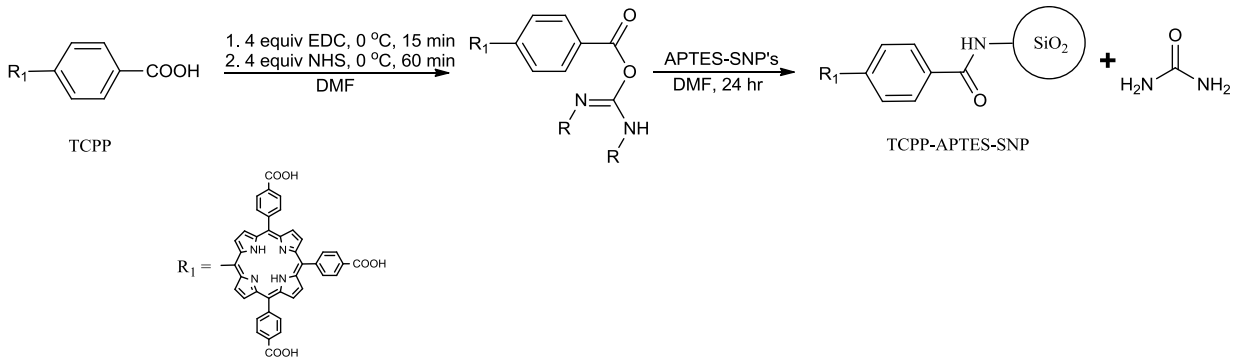

Scheme 4.7: EDC/NHS coupling of TCPP to APTES-SNPs.

The resulting TCPP-APTES-SNPs were then analysed by FT-IR (Figure 4.19) and diffuse reflectance UV-Vis spectroscopy (Figure 4.20).

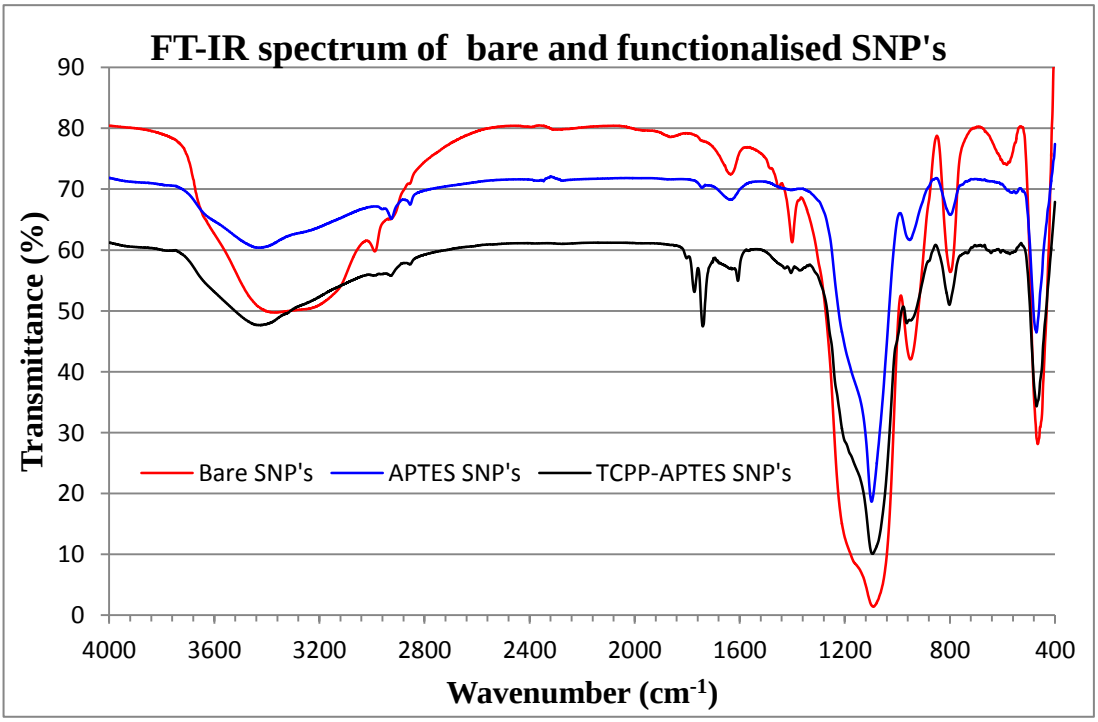

Figure 4.19: FT-IR spectra of bare SNPs, APTES-SNPs and TCPP-APTES-SNPs.

The FTIR spectrum of the TCPP-APTES SNPs shows the characteristic absorbance peaks at 1090, 790 and 475 cm^{-1} due to Si-O-Si symmetric stretching, asymmetric

stretching and bridge rocking vibrations. These can also be seen in the FT-IR spectra of APTES SNPs and unfunctionalised SNPs. The broad absorbance peak seen at 600 cm^{-1} in the spectrum of the bare SNPs is attributed to cyclic tetrameric siloxane species still present in the silica matrix.[22] Weak absorbance peaks between 2865 and 2933 cm^{-1} in all three spectra are due to C-H stretching vibrations and indicate that some un-hydrolysed TEOS remains on the surface of the SNPs. A strong absorbance peak between 3700 and 2700 cm^{-1} is due to the Si-OH stretching of the silanol groups on the surface of the SNPs. The intensity of this absorbance peak decreases in the spectra of the functionalised SNPs. This effect is due to the replacement of a significant portion of the surface silanol groups with primary amines and amide bridge functionalities. However, in the FT-IR spectrum of APTES-SNPs two sharp absorbance peaks between 3500 and 3300 cm^{-1}, characteristic of primary amines are not seen due to masking by remaining surface silanol groups. The absorbance peaks at 1608, 1745 and 1775 cm^{-1} in the TCPP-APTES SNPs spectrum can be attributed to phenyl ring deformation of TCPP, C=O stretching of TCPP and C=O stretching of the secondary amide bridge respectively. The presence of these peaks proves that covalent linkage of TCPP to the APTES SNPs was successful. The presence of these absorbance peaks also suggests that there is significantly more TCPP present compared to the "one pot" TCPP SNPs.

The diffuse reflectance UV-Vis spectrum of TCPP-APTES SNPs (Figure 4.20) confirms that TCPP is present on the surface of the SNPs. UV-Vis spectroscopic analysis of ethanol washings from the TCPP-APTES SNPs confirmed that no TCPP was present in these washings, indicating that any TCPP present must be chemically bound to the surface of the SNPs. The diffuse reflectance UV-Vis spectrum shows the TCPP Soret band at 438 nm and the four Q-bands at 521, 555, 593 and 648 nm.

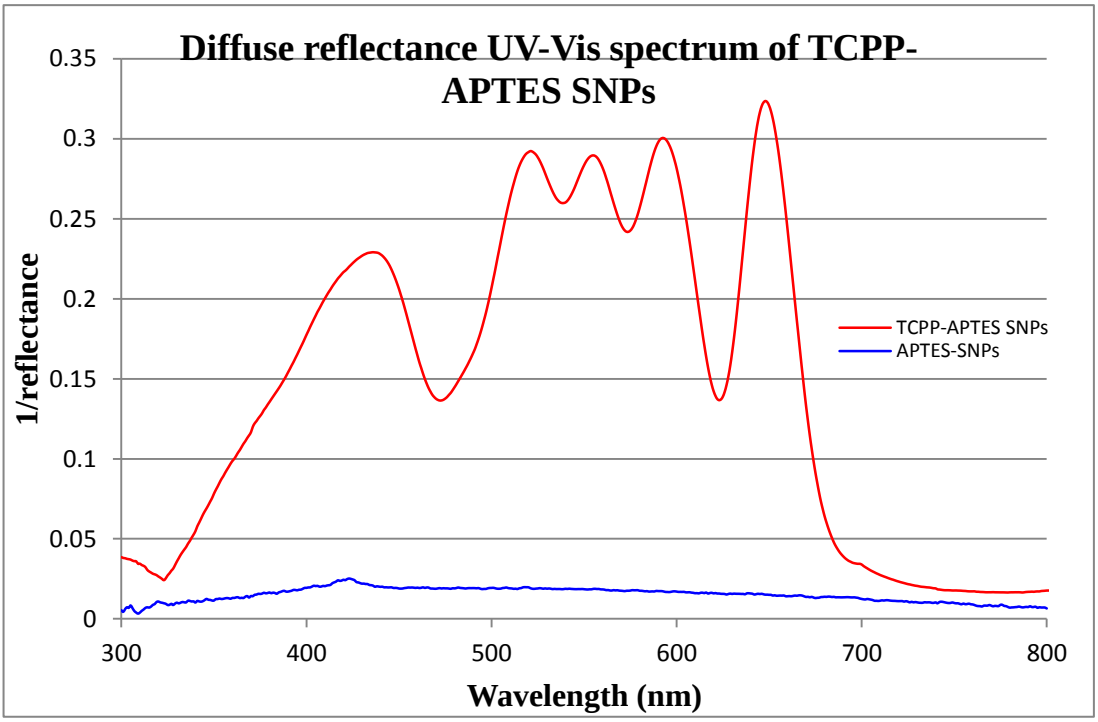

Figure 4.20: Diffuse reflectance UV-Vis spectrum of TCPP-APTES SNPs.

4.2.3.2 Heterogeneous dye sensitized photooxygenation of α-terpinene using TCPP-APTES SNPs (Experiment 80)

The heterogeneous dye sensitized photooxygenation of α-terpinene was performed in 50 ml of IPA with 200 mg of TCPP-APTES SNPs. The solution was irradiated using a 500 W halogen lamp (27 cm distance) with constant air bubbling and cooling via cold finger for 8 hours. Samples (0.1 ml) were taken hourly and analysed by UV-Vis spectroscopy (λ-max 265.5 nm). The percent conversion of α-terpinene to products was determined using the calibration curves previously developed in Section 2.2.2. ^{1}H NMR analysis was employed to determine the ratio of *p*-cymene to ascaridole (Table 4.3).

Table 4.3: Difference in percentage conversion determined by UV-Vis and ^{1}H NMR spectroscopy.

Exp No	Conversion (%)	^{1}H NMR data	
		***p*-cymene (%)**	**Ascaridole (%)**
80a	54	2	98
80b	45	11	89
80c	N/A	18	82

UV-Vis spectroscopic analysis showed that a percent conversion of up to 54 % could be achieved in 8 hours of irradiation. This conversion was a notable increase over that of "one pot" TCPP SNPs, indicating that immobilisation of the sensitizer onto the surface of the silica particles allowed for more interaction of the sensitizer with the reaction media. Interestingly, ascaridole was produced almost exclusively during the first cycle (80a) indicating the production of singlet oxygen. However, subsequent cycles show the formation of increasing quantities of *p*-cymene. This observation could be explained by photo bleaching of the sensitizer which would significantly reduce the amount of singlet oxygen produced and consequently, ascaridole. Electron transfer processes however, may still occur as shown in Figure 4.4. Such processes would allow for the formation of superoxide radical anions and favour the formation of *p*-cymene. These results are in agreement with observations by Ribeiro *et al*. [23]

4.2.3.3 Synthesis of TCPP-Hex-APTES SNPs

Previous syntheses saw the incorporation and immobilisation of TCPP both into and onto the surface of silica nano particles. It is possible that the close proximity of the TCPP to the SNPs resulted in the generation of superoxide anions and the formation of *p*-cymene. By placing the porphyrin further away from the SNPs the production of superoxide anions and *p*-cymene maybe reduced. To test this hypothesis functionalised SNPs with a 6-aminohexanoic acid spacer were synthesized.

Surface functionalisation of SNPs with APTES

Bare silica nano particles were functionalized with APTES as described in Section 4.2.3.1.

N-Boc protection of 6-aminohexanoic acid (Experiment 81)

6-Aminohexanoic acid (656 mg, 5 mmol) was dissolved in 70 ml of a dioxane / H_2O solution (v/v 2:1) and chilled to 0 °C using an ice bath. To this was added 5 ml of a 1M NaOH solution followed by di-*tert*-butyl dicarbonate (1.2 g, 5.5 mmol). The resulting reaction mixture was allowed to stir for 3 hours. The N- Boc protected 6-aminohexanoic acid was isolated in quantitative yields (Scheme 4.8). ^{1}H NMR results were in agreement with results from the literature.[24-26]

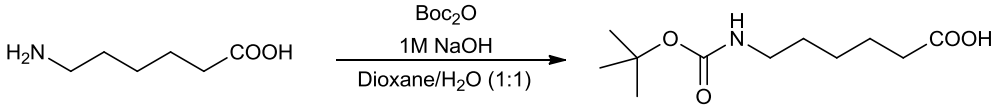

Scheme 4.8: N-BOC protection of 6-aminohexanoic acid.

EDC/NHS coupling of N- Boc protected 6-aminohexanoic acid to APTES SNPs (Experiment 82)

APTES-SNPs were then functionalized with N-BOC protected 6-aminohexanoic acid using EDC/NHS coupling chemistry (Scheme 4.9). The resulting N-Boc protected Hex-APTES SNPs were isolated via centrifugation and washed with DMF and ethanol. The N-Boc protected Hex-APTES SNPs were light brown in colour and were stored in dry ethanol until further use.

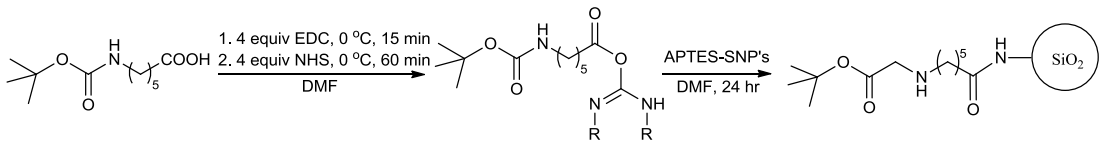

Scheme 4.9: EDC/NHS coupling of N- Boc 6-aminohexanoic acid to APTES SNPs.

Deprotection of N- Boc 6-aminohexanoic acid APTES SNPs (Experiment 83)

N-Boc 6-aminohexanoic acid APTES SNPs were de-protected using a solution of 4 M HCl in dioxane (Scheme 4.10). The resulting de-protected particles were

separated via centrifugation and washed three times with H_2O. The SNPs were then re-dispersed in 40 ml of a 0.5 M solution of $NaHCO_3$ and allowed to stir overnight. Again, these were collected by centrifugation and washed three times with water before being re-dispersed in dry DMF.

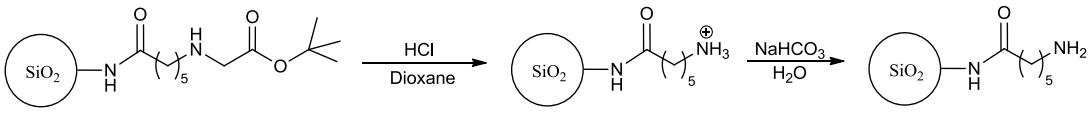

Scheme 4.10: Deprotection of N- Boc protected 6-aminohexanoic acid APTES SNPs.

EDC/NHS coupling of TCPP to 6-aminohexanoic acid APTES SNPs (Experiment 84)

TCPP was covalently bound to 6-aminohexanoic acid APTES SNPs using EDC/NHS coupling chemistry (Scheme 4.11). The resulting TCPP-Hex-APTES SNPs were separated by centrifugation and washed with DMF and ethanol before being stored in dry ethanol until further use. The TCPP-Hex-APTES SNPs were purple in colour.

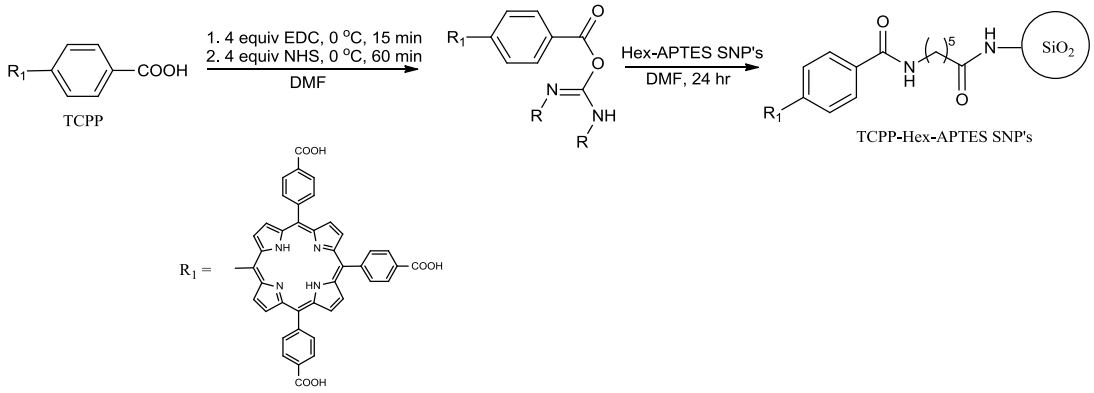

Scheme 4.10: EDC/NHS coupling of TCPP to 6-aminohexanoic acid APTES SNPs.

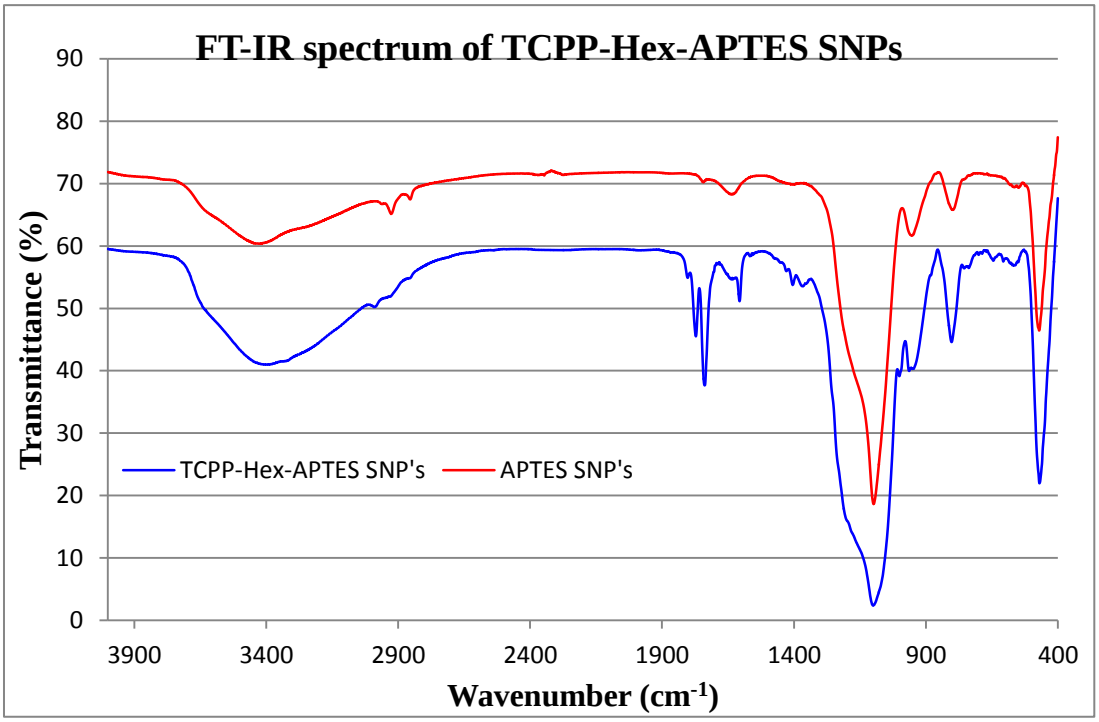

Figure 4.21: FT-IR spectrum of TCPP-Hex-APTES SNPs.

Similar to Figure 4.19 the absorption bands at ~ 1100, 806 and 470 cm^{-1} represent Si-O-Si asymmetric stretching, symmetric stretching and bridge rocking vibrations. In addition the broad absorption band between 3700 and 2700 cm^{-1} is representative of the hydroxyl groups present on the surface of the particles in the form of silanol groups and carboxylic acid groups of TCPP. The appearance of weak absorption peaks in the region of 2860 – 2997 cm^{-1} are attributed to C-H stretching vibrations of the alkyl chain due to APTES and 6-aminohexanoic acid. The peaks at 1607, 1741 and 1773 cm^{-1} may be attributed to C=O stretching of the porphyrin carboxy group and C=O stretching of the amide bridge. The presence of the two C=O stretching vibrational modes indicate that TCPP is covalently bound to the surface of the SNPs through an amide linkage.

The diffuse reflectance UV-Vis spectrum confirms that TCPP is present on the surface of the SNPs (Figure 4.22).

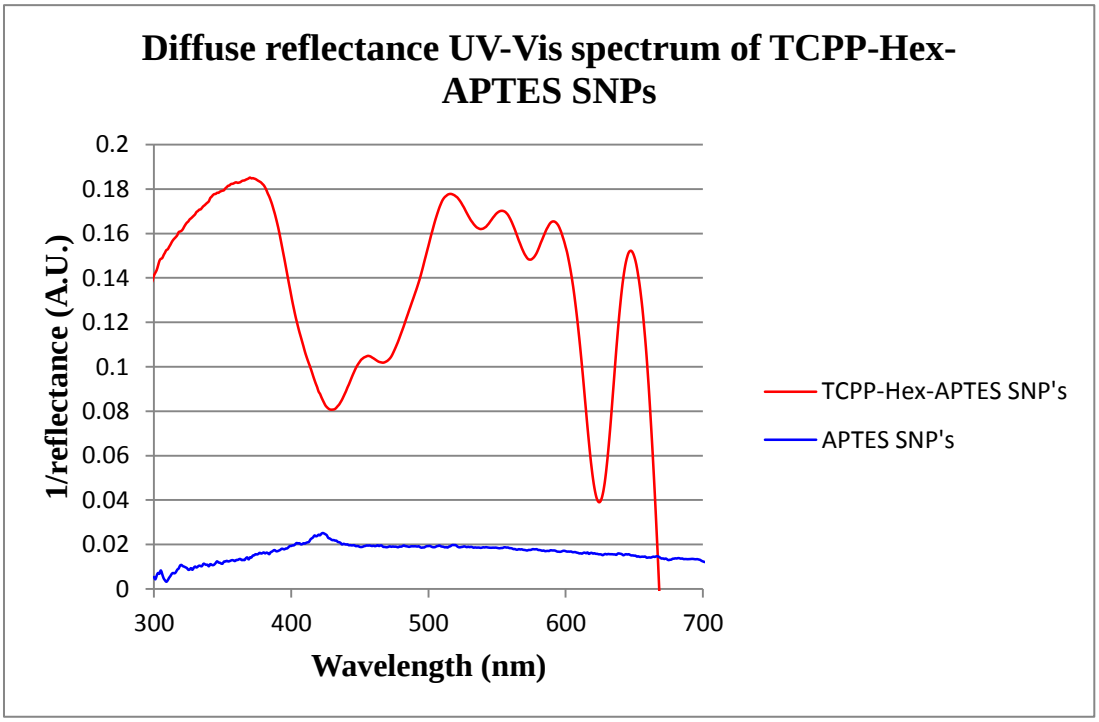

Figure 4.22: Diffuse reflectance UV-Vis spectrum of TCPP-Hex-APTES SNPs.

4.2.3.4 Heterogeneous dye sensitized photooxygenation of α-terpinene using TCPP-Hex-APTES SNPs (Experiment 85)

The heterogeneous dye sensitized photooxygenation of α-terpinene using TCPP-Hex-APTES SNPs was performed using the same method as described for TCPP-APTES SNPs (Section 4.2.4.1). Percent conversions were determined by UV-Vis spectroscopy. ^{1}H NMR was used to determine *p*-cymene to ascaridole ratios.

Table 4.4: Heterogeneous dye sensitized photooxygenation of α-terpinene using TCPP-Hex-APTES SNPs.

Exp No	% Conversion (UV-Vis)	^{1}H NMR Data	
		p-cymene (%)	Ascaridole (%)
85a	37	0	100
85b	20	44	56
85c	N/A	42	58

Table 4.4 shows that initial percent conversions to product(s) are lower than that of the TCPP-APTES SNPs. This was an unexpected result as it was believed that increasing the distance of the porphyrin from the SNPs would increase percent conversions to ascaridole. However, similar to TCPP-APTES SNPs the overall conversion of α-terpinene to products decreases with each cycle. In addition, the quantity of *p*-cymene increases significantly. These results suggest that with each cycle more non Type II processes are occurring and increasing the amount of *p*-cymene formed thus making our hypothesis invalid. One possible reason for this may be the ability of the extended alkyl chain to fold back upon itself and allow contact of the sensitizer with the silica surface, thereby increasing the rate of electron transfer from the sensitizer to the silica particle conduction band (Figure 4.23).

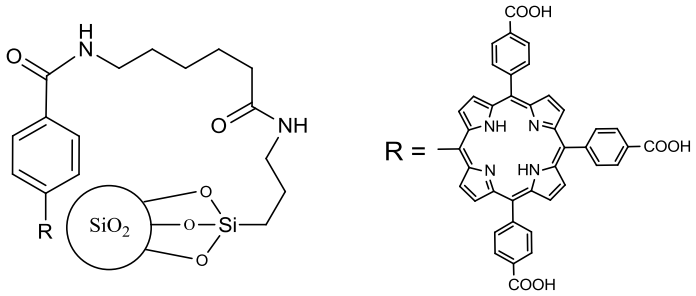

Figure 4.23: Representation of bending of alkyl chain to allow interaction of TCPP with the surface of the SNPs.

4.3 Conclusion

The results have shown that the physical encapsulation of TCPP and TCPPZn into SNPs was realised. Furthermore, the covalent immobilisation of TCPP onto the surface of monodisperse SNPs was achieved using peptide coupling chemistry.

TCPP and TCPPZn encapsulated SNPs were characterised and tested as solid support sensitizers for the heterogeneous dye sensitized photooxygenation of α-terpinene. Characterisation showed that only minute quantities of sensitizer were present in the SNPs. In addition, due to the tightly packed nature of the silica particles this minute amount of sensitizer was not readily accessible by the reaction media. Consequently, total percent conversion of only 20 and 29 % were achieved for TCPP and TCPPZn SNPs respectively after 8 hours irradiation. Unfortunately, these results show that sensitizer encapsulated "one pot" SNPs were not effective solid support sensitizers for the heterogeneous dye sensitized photooxygenation of α-terpinene. However, ^{1}H NMR of the reaction products showed that 61 and 83 % of the product formed was *p*-cymene for TCPP and TCPPZn SNPs respectively. It was proposed that due to the encapsulation of the sensitizers that superoxide radical anions were produced due to electron transfer from the sensitizer to the silica. This resulted in the direct formation of *p*-cymene, which was a significant result, as the direct production of *p*-cymene from α-terpinene has not yet been reported with such high selectivity.

The reproducible synthesis of unfunctionalised SNPs was realised with average diameters of ~200 nm. Functionalisation of these SNPs with APTES then allowed for the covalent immobilisation of TCPP onto the surface via peptide coupling chemistry. Characterisation of TCPP-APTES SNPs showed that covalent attachment of TCPP to the surface was successful. As the sensitizer was now immobilised onto the surface of the SNPs it could interact more readily with the reaction media during heterogeneous dye sensitized photooxygenations. These modified silica particles resulted in percent conversions of up to 54 %. However, despite this encouraging yield subsequent recycles of the TCPP-APTES SNPs showed an overall percent conversion drop due to photo bleaching of the sensitizer.

This was also the case with TCPP-Hex-APTES SNPs. Similar to the sensitizer encapsulated "one pot" SNPs the heterogeneous dye sensitized photooxygenation of α-terpinene using TCPP-APTES SNPs saw increased *p*-cymene production. However, only up to 18 % *p*-cymene was produced. This lower rate of *p*-cymene production has been attributed to the APTES linker between the sensitizer and the silica surface, which may have slowed the rate of electron transfer to the silica surface. In comparison, TCPP-Hex-APTES SNPs yielded up to 44 % *p*-cymene. This result maybe explained by the ability of the extended alkyl chain to fold back upon itself, allowing for contact of the sensitizer with the silica surface resulting in an increased rate of electron transfer to the silica conduction band.

The low to moderate percent conversions obtained from the heterogeneous dye sensitized photooxygenation of α-terpinene using SNP solid support sensitizers has demonstrated that such sensitizers are not effective enough to offer a green alternative to traditional homogeneous systems. However, the unexpected and interesting high levels of *p*-cymene production indicate that further investigation into semi-conductor supported sensitizers should be further explored. Covalent immobilisation of TCPP onto semi-conductors such as titanium dioxide (TiO_2) or iron oxide (Fe_3O_4) should be investigated. In addition chelation of several metal ions to the centre of the porphyrin should also be investigated so as to increase the rate of ISC.

4.4 Experimental

4.4.1 "One pot" TCPP and TCPPZn SNPs

4.4.1.1 "One pot" synthesis of TCPP and TCPPZn SNPs (Experiments 70 & 72)

General procedure

TEOS (1.5 ml, 6.72 mmol) was dissolved in 50 ml of dry ethanol along with TCPP or TCPPZn (15 mg) with the aid of sonication. To this 4 ml of 25 % ammonia was added and the solution was stirred at room temperature for 90 minutes. At this time the reaction solution was centrifuged at 9,000 rpm for 3 minutes and the supernatant removed. The resulting porphyrin encapsulated SNPs were re-dispersed in dry ethanol via sonication and re-centrifuged at 9,000 rpm for 3 minutes. This was to ensure that all free porphyrin, TEOS and ammonia were removed from the surface of the SNPs. The process was repeated until UV-Vis spectroscopy confirmed that there was no porphyrin present in the supernatant. The resulting sensitizer encapsulated SNPs were dried under vacuum overnight at 40 °C. The SNPs were then analysed by FT-IR, diffuse reflectance UV-Vis spectroscopy and DLS measurements. See Figures 4.1, 4.2, and 4.6 to 4.8.

Experiment 70 "One pot" synthesis of TCPP SNPs

DLS measurements of the TCPP SNPs were not performed as the SNPs could not be dispersed in dry ethanol. The SNPs were light purple in colour.

Experiment 72 "One pot" synthesis of TCPPZn SNPs

DLS measurements of the TCPPZn SNPs were performed in dry ethanol. The SNPs were large with an average diameter of ~1950 nm. The TCPPZn SNPs were light green in colour.

4.4.1.2 Heterogeneous dye sensitized photooxygenation of α-terpinene using "one pot" TCPP and TCPPZn SNPs (Experiment 71 & 73)

General procedure

200 mg of sensitizer encapsulated SNPs were dispersed in 50 ml of IPA via sonication. The mixture was then placed in front of a 500 W halogen lamp (27 cm) with constant air bubbling and cooling via a cold finger. α-terpinene (1 ml, 5.2 mmol) was added and the solution irradiated for 8 hours. 0.1 ml Samples were taken at 60 minutes intervals for UV-Vis analysis. Samples were prepared by centrifugation at 9,000 rpm for 3 minutes. The supernatant was removed and 10 μL was dissolved in 10 ml of reagent grade IPA (dilution factor of 1000). This was then analysed at 265.5 nm and the rate of conversion was determined base upon calibrations curves described in Section 2.2.2.

The SNPs were recovered by centrifugation (9,000 rpm, 3 minutes). The crude supernatant was reduced under vacuum to afford a clear yellow oil. This was weighted and ^{1}H NMR was used to determine the percentage conversion of α-terpinene to products. The SNPs were re-dispersed in reagent grade ethanol via sonication and re-centrifuged at 9,000 rpm for 3 minutes. This process was repeated twice to ensure that the SNPs were free from un-reacted reagents and products. The SNPs were then stored in dry ethanol until further use.

The supernatant was also analysed by UV-Vis spectroscopy to ensure no leaching of TCPP from the SNPs had occurred.

Experiment 71 Dye sensitized photooxygenation using TCPP SNPs

UV-Vis spectroscopy showed a final conversion of 20 % after 8 hours. ^{1}H NMR ($CDCl_3$) showed a *p*-cymene to ascaridole ratio of 87:13 after 8 hours.

Experiment 73 Dye sensitized photooxygenation using TCPPZn SNPs

UV-Vis spectroscopy showed an overall percent conversion of 29 % after 8 hours. ^{1}H NMR ($CDCl_3$) showed a *p*-cymene to ascaridole ratio of 83:17 after 8 hours.

4.4.1.3 UV-Vis studies of α-terpinene and *p*-cymene

General procedure

104 -10.4 mM solutions of α-terpinene were prepared in IPA (5 ml) with increments of 10 %. Similarly, solutions of α-terpinene and *p*-cymene were also prepared in the range of 104-10.4 mM in IPA (5 ml). Table 4.3 below illustrates the volumes of solvent and reagents used. These were the analysed between 350 and 200 nm. The combined absorbance for α-terpinene and *p*-cymene was determined at 265.5 nm for each sample and the "percent conversion" determined based upon the calibration curve of Section 2.2.2.

Table 4.3: Volumes and concentration of reagents for UV-Vis analysis.

Sample A		**Sample B**			
AT (ml)	**Concentration (mM)**	**AT/PC (ml)**		**Concentration (mM)**	
0.1	104	0.1	0.0	104	0
0.09	93.6	0.09	0.081	93.6	10.4
0.08	83.2	0.08	0.162	83.2	20.8
0.07	72.8	0.07	0.243	72.8	31.2
0.06	62.4	0.06	0.324	62.4	41.6
0.05	52	0.05	0.405	52	52
0.04	41.6	0.04	0.486	41.6	62.4
0.03	31.2	0.03	0.567	31.2	72.8
0.02	20.8	0.02	0.648	20.8	83.2
0.01	10.4	0.01	0.729	10.4	93.6
N/A	N/A	N/A	0.8110	0	100

AT = α-terpinene, PC = *p*-cymene.

4.4.2 Synthesis of unfunctionalised SNPs

4.4.2.1 Synthesis at room temperature using a modified Stöber method (Experiment 74)

Silica nano particles were synthesized by a modified Stöber method.[8] TEOS (1.5 ml, 6.72 mmol) was dissolved in 50 ml of dry ethanol in a 100 ml round bottomed flask equipped with a stirring bar and placed under N_2 atmosphere. To this 4 ml of a 25% ammonia solution was quickly added and the solution stirred for 5 hours. Samples were taken at 30, 60, 120, 180, 240 and 300 minutes to monitor the rate of growth of the silica nano particles by DLS measurements. Samples were prepared for DLS measurements by immediate centrifugation at 9,000 rpm for 3 minutes. The supernatant was removed and the SNPs were re-dispersed in dry ethanol via sonication. This process was repeated twice to ensure all remaining ammonia was removed from the surface of the SNPs. DLS measurements were performed in dry ethanol and in triplicate (Figures 4.9 and 4.10).

4.4.2.2 Synthesis at zero degrees Celsius using a modified Stöber method (Experiment 75)

Synthesis of silica nano particles at zero degrees Celsius was performed in an ice bath equipped with a temperature probe. The synthesis was identical to the procedure followed for the synthesis of silica particles at room temperature (Section 4.4.2.1) including sampling times and DLS measurements (Figures 4.11 and 4.12).

4.4.2.3 Synthesis at room temperature using a Branson 3510 sonicator (Experiment 76)

Silica nano particles were synthesized using the procedure for the synthesis of silica particles at room temperature (Section 4.4.2.1). However, one modification was made to the synthesis. Namely the stirring bar was removed from the 100 ml round bottomed flask and the reaction solution was sonicated using a Branson 3510 sonicator throughout the synthesis. Sampling times and DLS measurements were also preformed as per room temperature synthesis (Figures 4.13 and 4.14).

4.4.2.4 Reproducibility of SNP synthesis (Experiment 76 a-e)

All subsequent silica nano particles were synthesized via the modified room temperature Stöber method under constant sonication. TEOS (1.5 ml, 6.72 mmol) was dissolved in 50 ml of dry ethanol in a 100 ml round bottomed flask and placed under N_2 atmosphere. To this 4 ml of a 25% ammonia solution was quickly added and the solution sonicated for 90 minutes. At this point the reaction was stopped by centrifugation at 9,000 rpm for 3 minutes. The supernatant was removed and the resulting white SNPs were re-dispersed in ethanol via sonication. This process was repeated twice to ensure all remaining ammonia was removed from the surface of the SNPs. The SNPs were stored in dry ethanol until further use. DLS measurements were performed in dry ethanol (Figure 4.16).

4.4.3 Functionalisation of SNPs

4.4.3.1 Surface functionalisation of SNPs with APTES (Experiment 78)

Bare SNPs were surface functionalized with APTES under base catalysed conditions. Bare SNPs were dispersed in 50 ml of dry ethanol and placed under N_2 atmosphere. To this APTES (100 μL, 0.43 mmol) was added followed by quick addition of 4 ml of 25 % ammonia. The solution was then allowed to stir overnight. The resulting APTES functionalized SNPs were isolated via centrifugation at 9,000 rpm for 3 minutes. The supernatant was discarded and the SNPs were re-dispersed in ethanol. This procedure was repeated three times to remove all free ammonia and APTES from the surface of the SNPs. The APTES functionalized SNPs were stored in dry ethanol until further use.

4.4.3.2 EDC/NHS coupling of TCPP to APTES functionalized SNPs (Experiment 79)

340 mg (0.43 mmol) of TCPP was dissolved in 5 ml of dry DMF and placed into a 25 ml 2-neck round bottomed flask. This was then placed under argon atmosphere and placed into an ice bath. The solution was stirred for 20 minutes. Four equivalents (1.72 mmol, 328 mg) of EDC was added in 4 ml dry DMF and the solution stirred for a further 15 minutes. Four equivalents (1.72 mmol, 200 mg) of

NHS in 2 ml dry DMF was then added and the solution was stirred for a further 60 minutes. The APTES functionalized silica nano particles were then added in 5 ml dry DMF and the solution allowed to stir at room temperature for 24 hours. The resulting TCPP-APTES coupled SNPs were collected by centrifugation. The SNPs were re-dispersed in ethanol and centrifuged again to remove any free porphyrin on the surface of the particles. This process was repeated until UV-Vis analysis of the supernatant confirmed the absence of TCPP. Diffuse reflectance UV-Vis and FTIR spectroscopic analysis confirmed the presence of TCPP on the surface of the SNPs (Figures 4.19 and 4.20).

4.4.2.3 N-Boc protection of 6-aminohexanoic acid (Experiment 81)

6-Aminohexanoic acid (656 mg, 5 mmol) was dissolved in 70 ml of a dioxane / H_2O solution (v/v 2:1) and chilled to 0 °C using an ice bath. To this was added 5 ml of a 1M NaOH (5 mmol) solution followed by di-*tert*-butyl dicarbonate (1.2 g, 5.5 mmol). The resulting reaction solution was allowed to stir for 3 hours. The crude mixture was reduced under vacuum and the resulting aqueous layer was extracted with 40 ml of EtOAc. The remaining aqueous layer was then acidified to pH 1 with 1M HCl and extracted with 40 ml EtOAc three times. The organic layers were combined, dried over $MgSO_4$ and filtered. The EtOAc was then removed under vacuum to afford a colourless oil in quantitative yield (1.150 g, ~5 mmol). This slowly crystallized overnight.

^{1}H NMR: (400 MHz, $CDCl_3$) δ (ppm) = 11.13 (brs, 1H, -COO**H**), 4.72 (brs, 1H, -N**H**), 3.10-2.94 (m, 2H, -NH-C**H_2**-), 2.28 (t, 2H, -C**H_2**-COOH, ^{3}J = 7.44 Hz), 1.49-1.24 (m, 15H, -CH_2-**(**C**H_2**$)_3$-CH_2-, **(**C**H_3**$)_3$**-C-O-). Data in agreement with literature.[26]

4.4.2.4 EDC/NHS coupling of N-Boc protected 6-aminohexanoic acid to APTES functionalized SNPs (Experiment 82)

100 mg (0.43 mmol) of N-Boc protected 6-aminohexanoic acid was dissolved in 5 ml of dry DMF and placed into a 25 ml 2-neck round bottomed flask. This was then placed under N_2 atmosphere and placed into an ice bath. The solution was stirred for

20 minutes. One equivalent (0.43 mmol, 82 mg) of EDC in 4 ml dry DMF was added and the solution stirred for a further 15 minutes. One equivalent (0.43 mmol, 50 mg) of NHS in 2 ml dry DMF was then added and the solution was stirred for a further 60 minutes. The APTES functionalized silica nano particles (dispersed in 2 ml of dry DMF) were then added and the solution allowed to stir at room temperature for 24 hours. The resulting modified SNPs were collected by centrifugation (9,000 rpm for 3 minutes). The SNPs were re-dispersed in ethanol via sonication and centrifuged again to remove any remaining reagents on the surface of the particles. This process was repeated 3 times. The clean functionalized SNPs were then stored in dry ethanol until further use.

4.4.2.5 Deprotection of N-Boc 6-aminohexanoic acid functionalized SNPs (Experiment 83)

The N-Boc protected 6-aminohexanoic acid APTES SNPs were dispersed in a 5 ml aliquot of 4 M HCl in dioxane. This was left to stir overnight and the resulting deprotected particles were separated via centrifugation (9,000 rpm, 3 minutes). The supernatant was discarded and the functionalized SNPs were re-dispersed in Mili-Q water. The functionalized SNPs were centrifuged again (9,000 rpm, 3 minutes) and the supernatant discarded. Next the functionalized SNPs were dispersed in 40 ml of a 0.5 M solution of $NaHCO_3$ and allowed to stir overnight. The functionalized SNPs were collected by centrifugation (9,000 rpm, 3 minutes) and washed three times with water before being re-dispersed in dry DMF.

4.4.2.6 EDC/NHS coupling of TCPP to 6-aminohexanoic acid functionalized APTES SNPs (Experiment 84)

TCPP (100 mg, 0.126 mmol) was dissolved in 5 ml of dry DMF, placed under N_2 atmosphere and chilled to 0 °C using an ice bath. Four equivalents of EDC (96 mg, 0.504 mmol) was then added and the solution was stirred for 15 minutes. Four equivalents of NHS (57 mg, 0.504 mmol) was then added and the solution was allowed to stir for a further 60 minutes followed by the addition of the 6-aminohexanoic acid APTES SNPs in 5 ml of dry DMF. This was then allowed to stir at room temperature overnight. The resulting TCPP-Hex-APTES SNPs were

separated by centrifugation (9,000 rpm, 3 minutes) and the supernatant discarded. The functionalized SNPs were re-dispersed in DMF via sonication and centrifuged (9,000 rpm, 3 minutes) to remove any free TCPP and other reagents. This process was repeated until UV-Vis spectroscopy confirmed that no TCPP was present in the supernatant. FTIR (KBr) and diffuse reflectance UV-Vis (KBr) spectroscopic analysis confirmed the presence of TCPP on the surface of the SNPs (Figures 4.21 and 4.22). The TCPP-Hex-APTES SNPs were stored in dry ethanol until further use.

4.4.2.7 Dye sensitized photooxygenation of α-terpinene using TCPP-APTES SNPs (Experiment 80 a-c)

General procedure:

200 mg of TCPP-APTES SNPs were dispersed in 50 ml of IPA via sonication. This was then placed in front of a 500 W halogen lamp (27 cm) with constant air bubbling and cooling via a cold finger. α-Terpinene (1 ml, 5.2 mmol) was added and the solution irradiated for 8 hours. 0.1 ml Samples were taken every 60 minutes for UV-Vis analysis. Samples were prepared by centrifugation at 9,000 rpm for 3 minutes. The supernatant was removed and 10 μL was dissolved in 10 ml of reagent grade IPA (dilution factor of 1000). This was then analysed at 265.5 nm and the rate of conversion was determined base upon calibrations curves described in Section 2.2.2.1 (Figure 2.6).

The SNPs were recovered by centrifugation (9,000 rpm, 3 minutes). The crude supernatant was reduced under vacuum to afford a clear yellow oil. This was weighted and ^{1}H NMR was used to determine the percent conversion of α-terpinene to products. The SNPs were re-dispersed in reagent grade ethanol via sonication and re-centrifuged at 9,000 rpm for 3 minutes. This process was repeated twice to ensure that the SNPs were free from any α-terpinene. The SNPs were then stored in dry ethanol until further use.

The supernatant was also analysed by UV-Vis spectroscopy to ensure no leaching of TCPP from the SNPs had occurred.

Experiment 80a Synthesis of ascaridole using TCPP-APTES SNPs

UV-Vis spectroscopy showed a 54 % conversion to products after 8 hours of irradiation. ^{1}H NMR ($CDCl_3$) showed a *p*-cymene to ascaridole ratio of 1.5:98.5.

Experiment 80b Synthesis of ascaridole using TCPP-APTES SNPs

UV-Vis spectroscopy showed a 45 % conversion to products after 8 hours of irradiation. ^{1}H NMR ($CDCl_3$) showed a *p*-cymene to ascaridole ratio of 11:89.

Experiment 80c Synthesis of ascaridole using TCPP-APTES SNPs

Determination of the percentage conversion to products was not performed by UV-Vis spectroscopy. ^{1}H NMR ($CDCl_3$) showed a *p*-cymene to ascaridole ratio of 18:82.

4.4.4.2 Dye sensitized photooxygenation of α-terpinene using TCPP-Hex-APTES SNPs (Experiment 85 a-c)

General procedure

The general procedure was identical to that of the photooxygenation of α-terpinene using TCPP-APTES SNPs (Section 4.4.4.1).

Experiment 85a Synthesis of ascaridole using TCPP-Hex-APTES SNPs

UV-Vis spectroscopy showed a 37 % conversion to products after 8 hours of irradiation. ^{1}H NMR ($CDCl_3$) showed a *p*-cymene to ascaridole ratio of 0:100.

Experiment 85b Synthesis of ascaridole using TCPP-Hex-APTES SNPs

UV-Vis spectroscopy showed a 20 % conversion to products after 8 hours of irradiation. ^{1}H NMR ($CDCl_3$) showed a *p*-cymene to ascaridole ratio of 44:56.

Experiment 85c Synthesis of ascaridole using TCPP-Hex-APTES SNPs

Determination of the percentage conversion to products was not performed by UV-Vis spectroscopy. ^{1}H NMR ($CDCl_3$) showed a *p*-cymene to ascaridole ratio of 42:58

4.5 References

(1) Ye, Z.; Tan, M.; Wang, G.; Yuan, J. *Anal. Chem.* **2004**, *76*, 513-518.

(2) Yi, D. K.; Selvan, S. T.; Lee, S. S.; Papaefthymiou, G. C.; Kundaliya, D.; Ying, J. Y. *J. Am. Chem. Soc.* **2005**, *127*, 4990-4991.

(3) Bottini, M.; Cerignoli, F.; Mills, D. M.; D'Annibale, F.; Leone, M.; Rosato, N.; Magrini, A.; Pellecchia, M.; Bergamaschi, A.; Mustelin, T. *J. Am. Chem. Soc.* **2007**, *129*, 7814-7823.

(4) Slowing, I.; Trewyn, B. G.; Lin, V. S. Y. *J. Am. Chem. Soc.* **2006**, *128*, 14792-14793.

(5) Qhobosheane, M.; Santra, S.; Zhang, P.; Tan, W. *Analyst* **2001**, *126*, 1274-1278.

(6) Grant, S. A.; Weilbaecher, C.; Lichlyter, D. *Sensors Actuators B: Chem.* **2007**, *121*, 482-489.

(7) Battioni, P.; Bartoli, J. F.; Mansuy, D.; Byun, Y. S.; Traylor, T. G. *J. Chem. Soc. , Chem. Commun.* **1992**, *15*, 1051-1053.

(8) Stöber, W.; Fink, A.; Bohn, E. *J. Colloid Interface Sci.* **1968**, *26*, 62-69.

(9) Rossi, L. M.; Shi, L.; Quina, F. H.; Rosenzweig, Z. *Langmuir* **2005**, *21*, 4277-4280.

(10) Bogush, G. H.; Zukoski IV, C. F. *J. Colloid Interface Sci.* **1991**, *142*, 1-18.

(11) Rao, K. S.; El-Hami, K.; Kodaki, T.; Matsushige, K.; Makino, K. *J. Colloid Interface Sci.* **2005**, *289*, 125-131.

(12) Chen, S.; Dong, P.; Yang, G.; Yang, J. *Ind Eng Chem Res* **1996**, *35*, 4487-4493.

(13) Nozawa, K.; Gailhanou, H.; Raison, L.; Panizza, P.; Ushiki, H.; Sellier, E.; Delville, J. P.; Delville, M. H. *Langmuir* **2005**, *21*, 1516-1523.

(14) Aelion, R.; Loebel, A.; Eirich, F. *J. Am. Chem. Soc.* **1950**, *72*, 5705-5712.

(15) Yoo, J. W.; Yun, D. S.; Kim, H. K. *J. Nanosci. Nanotechnol.* **2006**, *6*, 3343-3346.

(16) Marini, M.; Pourabbas, B.; Pilati, F.; Fabbri, P. *Colloids Surf. Physicochem. Eng. Aspects* **2008**, *317*, 473-481.

(17) Yun, D. S.; Kim, H. J. *Bull. Korean Chem. Soc.* **2005**, *26*, 1927-1928.

(18) Rahman, I. A.; Vejayakumaran, P.; Sipaut, C. S.; Ismail, J.; Bakar, M. A.; Adnan, R.; Chee, C. K. *Colloids Surf. Physicochem. Eng. Aspects* **2007**, *294*, 102-110.

(19) Freris, I.; Cristofori, D.; Riello, P.; Benedetti, A. *J. Colloid Interface Sci.* **2009**, *331*, 351-355.

(20) Innocenzi, P.; Falcaro, P.; Grosso, D.; Babonneau, F. *J Phys Chem B* **2003**, *107*, 4711-4717.

(21) Bartholome, C.; Beyou, E.; Bourgeat-Lami, E.; Chaumont, P.; Lefebvre, F.; Zydowicz, N. *Macromolecules* **2005**, *38*, 1099-1106.

(22) Yoshino, H.; Kamiya, K.; Nasu, H. *J. Non Cryst. Solids* **1990**, *126*, 68-78.

(23) Ribeiro, S. M.; Serra, A. C.; Rocha Gonsalves, A. M. d. *Journal of Molecular Catalysis A: Chemical* **2010**, *326*, 121-127.

(24) Biraboneye, A. C.; Madonna, S.; Laras, Y.; Krantic, S.; Maher, P.; Kraus, J. *J. Med. Chem.* **2009**, *52*, 4358-4369.

(25) Moriguchi, N.; Tsugaru, T.; Amiya, S. *J. Mol. Struct.* **2001**, *562*, 205-213.

(26) Quelever, G.; Kachidian, P.; Melon, C.; Garino, C.; Laras, Y.; Pietrancosta, N.; Sheha, M.; Louis Kraus, J. *Org. Biomol. Chem.* **2005**, *3*, 2450-2457.

Chapter 5

Design and implementation of a novel photochemical microflow bubble reactor for dye sensitized photooxygenations.

5.1 Introduction

Flow chemistry has been well established within the chemical industry for decades for high throughput production of chemicals. However, increasing interest in miniaturization across all sectors of technology in the past few years has led to the development of microflow chemistry. In general, standard microflow systems consist of two or more feed pumps that pump reaction mixtures into a single capillary tube where the reagents then mix and react to form products (Figure 5.1). The coiled capillary has a definite length and internal diameter which allows for the calculation of total volume. By measuring the flow rate (usually ml/min) the residence time can be calculated based upon the following equation:

Residence time (min) = volume (ml) / flow rate (ml/min).

By changing the flow rate the residence time can be easily adjusted. In addition to this feature the temperature of the coiled capillary tube can also be easily controlled via temperature control software. Other advancements such as microwave assisted synthesis and real time in process monitoring by ATR FTIR spectroscopy in capillary tubes have also been reported in the literature. [1-3]

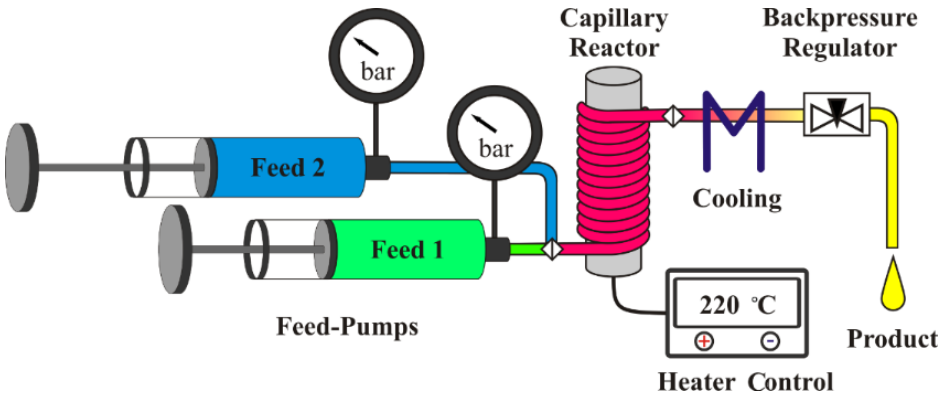

Figure 5.1: Standard microflow chemistry system.

Microflow chemistry has several distinct key advantages over traditional batch type syntheses which include:

- Reduced energy usage / operating costs
- Unlimited scalability (high throughput chemistry, continuous process, numbering up)
- Fast and efficient mixing of chemicals
- Superior heat and mass transfer
- Superior safety (reduced reaction volumes, containment of hazardous chemicals and intermediates)
- Space saving
- Robust and reproducible chemistry
- Real time, integrated analysis
- Significantly reduced reaction times.

However, despite these advantages standard microflow systems, as depicted in Figure 5.1 are not designed for photochemical applications as they do not incorporate light sources. Recently, the Nolan group, in Collaboration with Professor Michael Oelgemoeller of James Cook University Australia, have reported the design and implementation of a dual capillary photochemical microreactor for the sensitized photoaddition of isopropyl alcohol to furanones (Scheme 5.1)[4] where 4,4-dimethoxybenzophenone (DMBP) was utilised as the sensitizer.

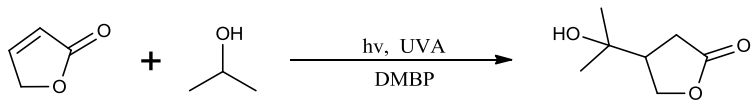

Scheme 5.1: Sensitized photoaddition of IPA to furanone.

The results of this work demonstrated that sensitized photochemical reactions could be performed efficiently utilising such systems. Space time yield (STY) results showed that the dual capillary microreactor provided comparable to superior results compared to the traditional batch system (Rayonet reactor –Schlenck flask)). Additionally, significant electrical energy savings were realised as the microreactor utilised only one low energy UVA lamp compared to the 16 UVA lamps of the Rayonet reactor. Figure 5.2 shows the dual capillary system.

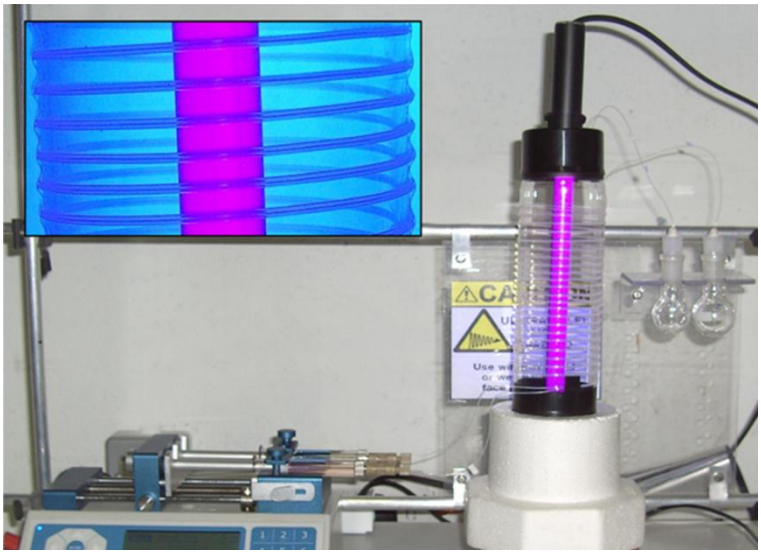

Figure 5.2: Dual capillary photochemical microreactor.

In addition to this work, a new parallel photochemical microreactor has also been developed by the above groups and was recently reported.[5] This new reactor allows for up to ten reaction solutions to be irradiated simultaneously. This process commonly known as "numbering up" significantly increased the quantity of product formed per unit time while keeping the electrical energy demand of the system to a minimum. Other work reported by the Nolan/Oelgemoeller groups has focused upon the sensitized photoaddition of IPA to furanones and acetone-sensitized photodecarboxylation reactions involving phthalimides in both Dwell devices and photochemical UV-LED microchips.[6,7] Comparison of these two types of photochemical reactors has shown that the newly developed dual capillary and parallel capillary microreactors provide equivalent to superior results than traditional batch reactors and microchip set-ups.[8]

Despite these advantages these photochemical systems do not allow for dye sensitized photooxygenations to be performed efficiently as they do not incorporate an oxygen (air) inlet. However, a new large scale bubble reactor was developed at DCU by the Nolan group that works for dye sensitized photooxygenations however its only short coming is that it does not function as a flow reactor but as a single 'bulk' reactor (Figure 5.3).[9]

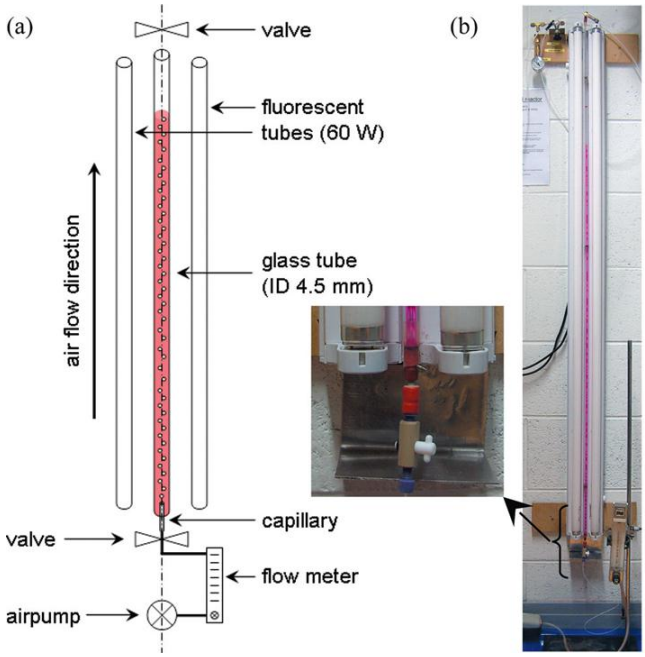

Figure 5.3: Novel bubble reactor for dye sensitized photooxygenations.

The bubble reactor consisted of a glass tube (ID 4.5 mm) placed between two standard fluorescent lamps. The tube could then be filled with a reaction mixture and irradiated under constant air bubbling. It was found that the amount of air supplied, the size of the air inlet capillary and the shape of the resulting bubbles formed, profoundly affected the rate of conversion to products (Figure 5.4).

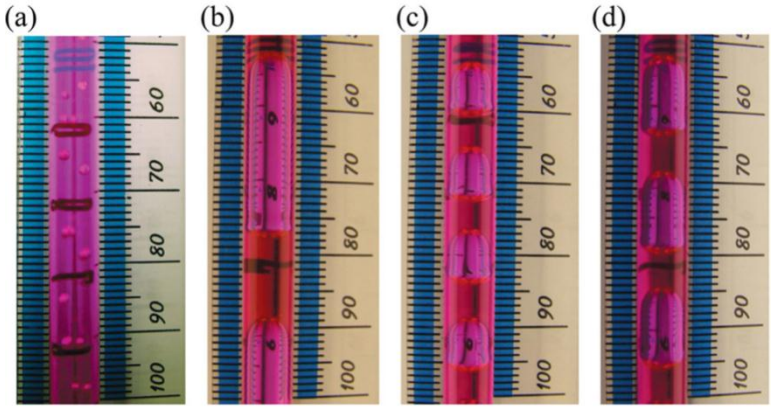

Figure 5.4: Bubble flow and shape in a) IPA/H_2O (9:1) with 100 µm capillary, b) MeOH/H_2O (9:1) with 500 µm capillary,c) IPA/H_2O (9:1) with 500 µm capillary,d) TAA/H_2O (9:1) with 500 µm capillary.

The formation of air “slugs” between sections of solvent greatly increased the rate of conversion to products. This increase in rate can be attributed to the formation of a thin layer of solvent between the air bubble and the glass wall of the reaction tube which allowed for increased light penetration and mass transfer. However, despite these significant advancements the bubble reactor still remains a batch type system. The reaction tube had to be evacuated after each irradiation and cleaned. In order to improve further upon this type of bubble reactor we describe the development of a cost effective, low energy consuming continuous microflow system with the incorporation of an air inlet for dye sensitized photooxygenations.

5.2 Development of photochemical microflow reactor

A photochemical microflow reactor was developed to incorporate both a light source and an air inlet for dye sensitized photooxygenations. The reactor consisted of 10 meters of PTFE tubing with an internal diameter of 0.8 mm coiled around a clear Pyrex tube with a diameter of 65 mm. This gave an internal volume of 5 ml. An 8 W fluorescent lamp was placed through the centre of the Pyrex tube. Two types of fluorescent tubes were used. A "cool white" fluorescent tube with a wide emission spectrum between 400-700 nm and a 419 nm fluorescent tube with an emission spectrum centred at 419 nm (Appendix C). Utilisation of an 8 W fluorescent lamp provided two distinct advantages over previously used light sources (500 W halogen lamp). Firstly, the energy demand of the 8 W fluorescent lamp is significantly lower than that of the 500 W halogen lamp. Secondly, the fluorescent lamps generated very little thermal energy and as a result a low energy consuming electric fan was fitted to the base of the microflow system to provide cooling via an induced air flow (Figure 5.5), completely eliminating water as coolant.

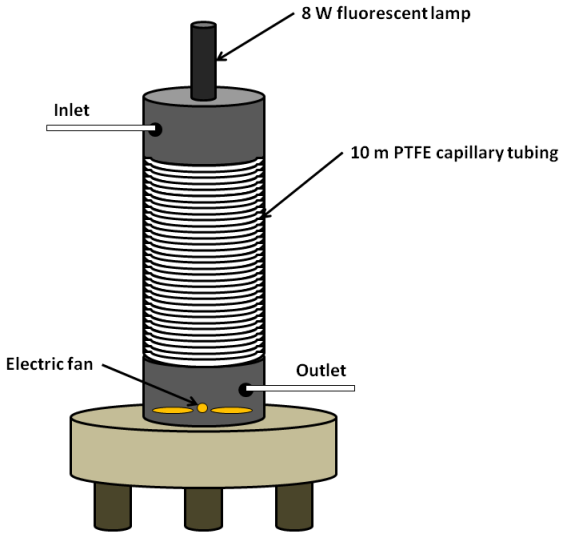

Figure 5.5: Modified microflow system to incorporate light source and cooling mechanism.

A peristaltic pump was attached to the outlet of the coiled PTFE capillary tubing to generate a flow current via suction. Based upon the rotation speed of the pump the flow rate of the reaction media through the coiled capillary tubing could be

controlled. A T-junction modified with a 5 cm section of a gas chromatography column with an internal diameter of 100 µm was fitted to the inlet of the microflow system (Figure 5.6). Similar to the bubble reactor this introduced a constant and controllable flow of air bubbles into the system.

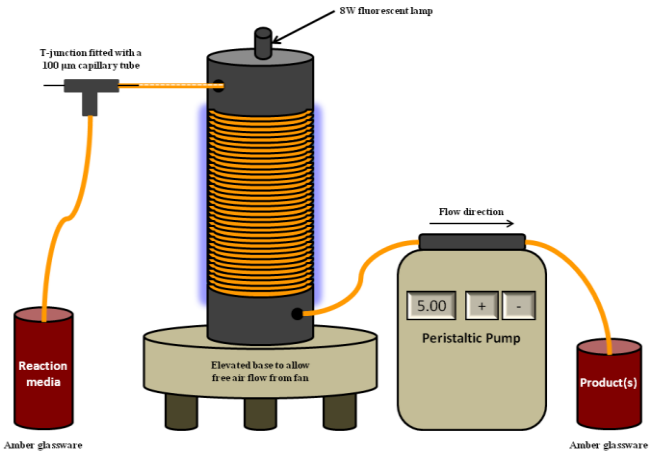

Figure 5.6: Modified microflow system to incorporate light source, air inlet and cooling mechanism.

To further improve the efficiency of the microflow system a reflective sheet of Mylar® was fitted around the coiled capillary tower (Figure 5.7). This sheet of Mylar® is capable of reflecting up to 98 % of visible light preventing the escape of the majority of light to the surroundings.

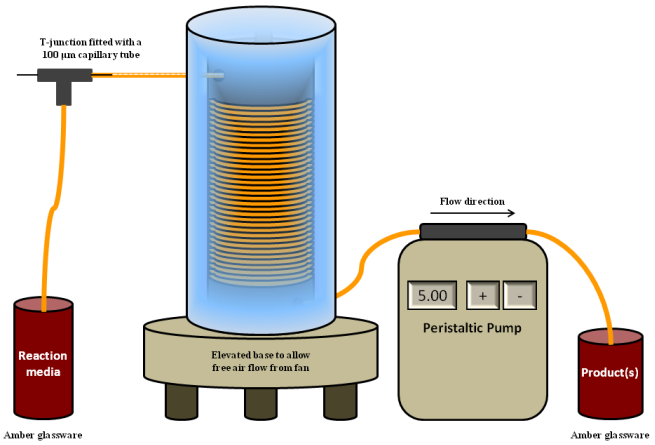

Figure 5.7: Modified microflow system to incorporate light source, air inlet, cooling mechanism and reflective Mylar® sheet.

The incorporation of a low energy demanding light source and air inlet into a microflow system should allow for the creation of ‘bubbles’, as occurs in the bubble reactor, allowing for dye sensitized photo-oxidations to occur. However, unlike the bubble reactor, this new reactor set-up will function under flow conditions.

5.3 Results and discussion

5.3.1 Microflow and Schlenk flask data

All relevant data for the apparatus used during the dye sensitized photooxygenations of 1,5-DHN, β-citronellol and α-terpinene are shown in Appendix D.

5.3.2 Flow rate optimisation

The flow rate of the photochemical microflow system was controlled using a peristaltic pump via a flow rate gauge. However, the units of this gauge were arbitrary. For this reason no direct correlation could be made between the gauge rate and flow rate in ml/min. Consequently the flow rate was determined manually and the units of the rate gauge noted and calibrated accordingly. The incorporation of the air inlet allowed for the entry of air into the capillary tubing (forming air slugs Fig. 5) prior to irradiation. However, entry of air into the capillary tubing changed the flow rate in comparison to solvent only flow rates. Therefore, air and solvent flow rates were determined manually and the total flow rate was calculated based on the following equation.

$$\text{Total flow rate (ml/min)} = \text{air flow rate} + \text{solvent flow rate}$$

It is noteworthy to mention that the flow rate also greatly affected the quantity of air that entered the capillary tubing. For this reason the flow rate was first optimised for air slug uniformity. It was found that air slug uniformity could be maintained between total flow rates of 0.316 and 0.746 ml/min. This represented an air slug size of 0.8 mm in length. The total, air and solvent flow rates at these speeds were determined manually and are illustrated in Table 5.1.

Table 5.1: Total flow rates showing air and solvent flow rates.

Gauge rate (A.U.)	Total flow rate (ml/min)	Air flow rate (ml/min)	Solvent flow rate (ml/min)
5.00	0.312	0.220	0.096
10.00	0.746	0.300	0.446
15.00	1.028	0.383	0.645
20.00	1.268	0.450	0.818

Outside of these flow rates air slug uniformity could not be sufficiently maintained. Beyond a total flow rate of 0.746 ml/min decreasing quantities of air entered the system, which resulted in large sections of reaction media between air slugs and percent conversions decrease noticeably. Adverse to this, if the flow rate is too low, large quantities of air enter the capillary tube resulting in large air slugs between reaction media. Under these conditions complete conversion to product(s) is often achieved however; the flow rate of reaction solvent is minimal. Figure 5.8 illustrates these processes.

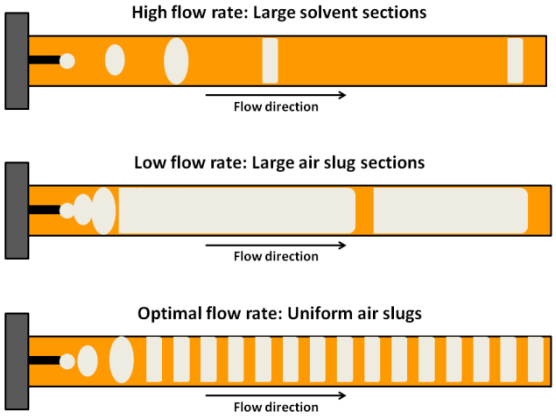

Figure 5.8: Effect of flow rate on air slug uniformity.

5.3.3 Control experiments using the photochemical microflow system

5.3.3.1 Sensitizer free experiments

Before the dye sensitized photooxygenations of 1,5-DHN, β-citronellol and α-terpinene were investigated using the newly developed photochemical microflow system a series of sensitizer free experiments were performed using the "cool white" and 419 nm fluorescent lamps as the light source (Scheme 5.1). The solutions were

pumped through the photochemical microflow system at a flow rate of 0.316 ml/min. This was the slowest flow rate at which air slug uniformity could be maintained and corresponded to a residence time of 15.82 minutes.

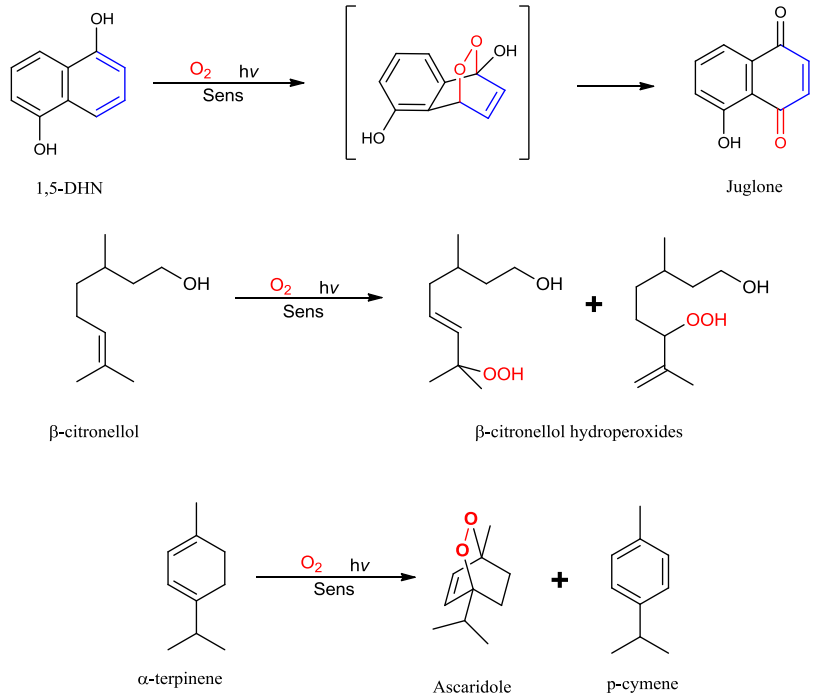

Scheme 5.2: Dye sensitized photooxygenation of 1,5-DHN, β-citronellol and α-terpinene.

The results demonstrated that, in contrast to sensitizer free experiments in Section 2.2.1.1 self sensitization of 1,5-DHN and β-citronellol had not occurred. This was due to the fact that the absorption spectra of both starting materials had no overlap with the emission spectra of the lamps (Appendix C). However, UV-Vis and ^{1}H NMR spectroscopy showed that relatively low percent conversions of between 25 and 31 % were achieved in the case of α-terpinene (Table 5.2).

Table 5.2: Sensitizer free experiments.

Exp No	Starting material	Residence time (min)	Lamp	% Conversion
86	1,5-DHN (10 mM)	15.82	419 nm	0
87	β-citronellol (26 mM)	15.82	419 nm	0
88	α-terpinene (26 mM)	15.82	419 nm	31
89	1,5-DHN (10 mM)	15.82	Cool white	0
90	β-citronellol (26 mM)	15.82	Cool white	0
91	α-terpinene (26 mM)	15.82	Cool white	25

Interestingly, ^{1}H NMR showed a significant increase in the ratio of *p*-cymene to ascaridole. This *p*-cymene to ascaridole ratio increased to 36:64 for the 419 nm fluorescent lamp and up to 47:53 for the "cool white" fluorescent lamp. These results indicated that in the absence of a sensitizer a non singlet oxygen reaction pathway was being followed.

5.3.3.2 Dye sensitized photooxygenations without air inlet

In order to determine the increased efficiency of the photochemical microflow reactor due to the incorporation of a 100 μm air inlet the dye sensitized photooxygenation of 1,5-DHN, β-citronellol and α-terpinene were performed without the inlet (Table 5.3). The experiments were performed using IPA pre saturated with air as solvent and TCPP as the sensitizer. The flow rate was set at 0.316 ml/min. The 419 nm lamp was used with TCPP as sensitzer. ^{1}H NMR and UV-Vis spectroscopy were used to determine percent conversions.

Table 5.3: Dye sensitized photooxygenations without air inlet.

Exp No	Starting material	Residence time (min)	% Conversion
92	1,5-DHN (10 mM)	15.82	28
93	β-citronellol (26 mM)	15.82	15
94	α-terpinene (26 mM)	15.82	49

The results demonstrate that while the dye sensitized photooxygenations of 1,5-DHN and β-citronellol are possible using the photochemical microflow system without an air inlet the percent conversions are low. This would suggest that the quantity of

dissolved oxygen in the reaction solvent is not sufficient to allow for complete conversion to products. Interestingly, a percent conversion of 49 percent was determined for the dye sensitized photooxygenation of α-terpinene. However, ^{1}H NMR spectroscopy showed a *p*-cymene to ascaridole ratio of 31:69. The results indicate that for dye sensitized photooxygenations to be performed efficiently using the photochemical microflow system an air inlet is essential.

5.3.4 Dye sensitized photooxygenation of 1,5-DHN using the photochemical microflow system

The dye sensitized photooxygenation of 1,5-DHN was performed using the newly developed photochemical microflow system. Stock solutions (0.25 mM, 100 ml) of RB, MB and TCPP were prepared using IPA and TAA with sonication and stored in the dark. Then solutions of 1,5-DHN (10 mM) were prepared, in a dark room (red light), using each of the stock sensitizer solutions (0.25 mM) in 5 ml volumetric flasks. These solutions were then covered entirely with foil and sonicated for 10 minutes to ensure complete solubilisation of the starting material. The solutions were then pumped through the microflow system under slug flow conditions at a total flow rate of 0.316 ml/min which corresponded to a residence time of 15.82 minutes. The crude samples were collected in 10 ml round bottom flasks made of amber glass to prevent further photochemical reactions due to external light sources. The solvent was removed under vacuum and ^{1}H NMR was used to determine the percent conversion to juglone (Table 5.4). The "cool white" fluorescent lamp was used with RB and MB. The 419 nm fluorescent lamp was used with TCPP. The results are shown in Table 5.4.

Table 5.4: Results for the dye sensitized photooxygenation of 1,5-DHN (10 mM) using the microflow system.

Exp No	1,5-DHN (mM)	Sensitizer (0.25mM)	Solvent	Residence time (min)	% Conversion
95a	10	RB	IPA	15.82	51[a]
95b	10	MB	IPA	15.82	19[a]
95c	10	TCPP	IPA	15.82	100[b]
96a	10	RB	TAA	15.82	49[a]
96b	10	MB	TAA	15.82	5[a]
96c	10	TCPP	TAA	15.82	100[b]

[a] "Cool white" fluorescent lamp, [b] 419 nm fluorescent lamp

The results obtained from these experiments demonstrate that TCPP when used with the 419 nm fluorescent lamp is a superior sensitizer for the dye sensitized photooxygenation of 1,5-DHN. Complete conversion to juglone was achieved with a residence time of only 15.82 minutes. It should be noted that the efficacy of MB decreases dramatically to as low as 5 % when using TAA as reaction solvent. This was attributed to two separate issues. Firstly, MB photo bleaches in the presence of TAA as noted in Section 2.2.2.1. This significantly reduces the formation of singlet oxygen. Secondly, comparison of the emission spectrum of the "cool white" fluorescent lamp with the absorption spectrum of MB shows that there is insufficient overlap of the two spectra. Figure 5.9 demonstrates that only one of MB's two absorption peaks overlaps partially with the emission spectrum of the "cool white" fluorescent lamp. This dramatically decreases the absorption of available light and also significantly reduces the production of singlet oxygen. In contrast, Figure 5.10 shows the sufficient overlap of the "cool white" fluorescent lamp with the absorption spectrum of RB.

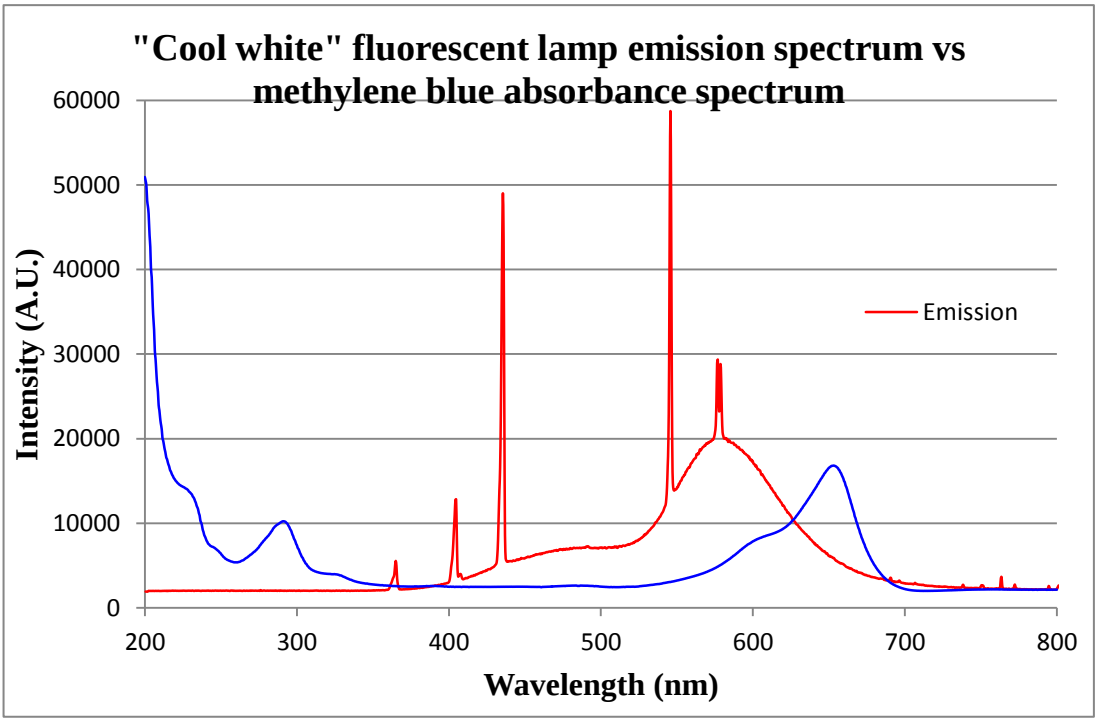

Figure 5.9 Emission spectrum of "cool white" fluorescent lamp vs. absorbance spectrum of methylene blue.

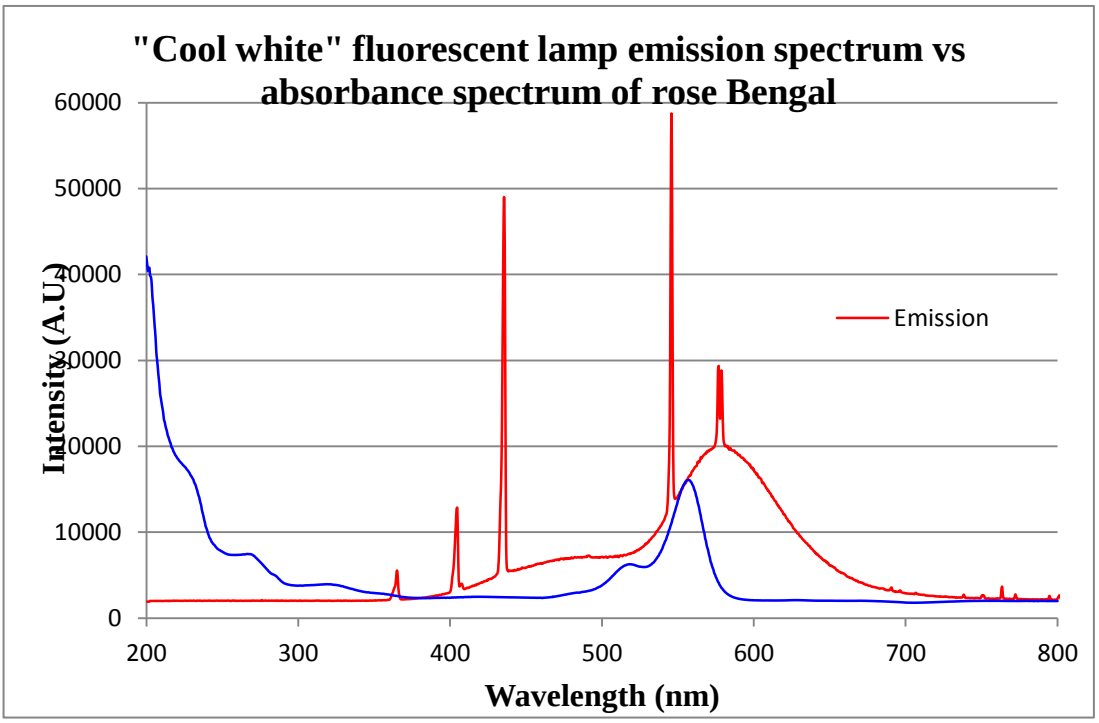

Figure 5.10: Emission spectrum of "cool white" fluorescent lamp vs. absorbance spectrum of rose Bengal.

An 8 W fluorescent lamp, with an emission spectrum centred at 419 nm, was chosen to irradiate solutions containing TCPP. This was done as there was no sufficient overlap between the absorption spectrum of TCPP with the emission spectrum of either the "cool white" lamp or the standard fluorescent lamp (Appendix C). Figure 5.11 shows the overlap of the 419 nm fluorescent lamp emission spectrum with the absorbance spectrum of TCPP. The significant overlap of the 419 nm fluorescent lamp emission spectrum with the Soret band (417 nm) and second Q band (546 nm) of TCPP explains the superior percent conversion of 1,5-DHN to juglone. The emission and absorption spectra for all sensitizers and lamps utilised in this thesis are shown in Appendix C.

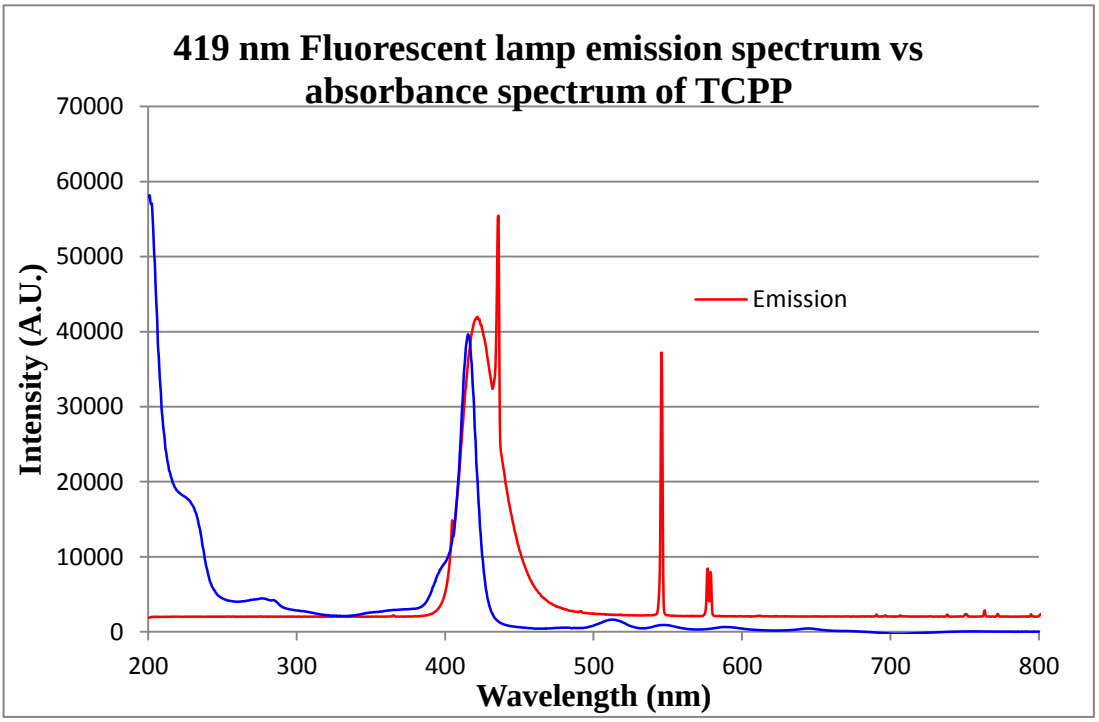

Figure 5.11: Emission spectrum of "cool white" fluorescent lamp vs. absorbance spectrum of TCPP.

The results shown in Table 5.4 have also demonstrated that TAA provides superior percent conversions to juglone compared to IPA when using TCPP as the sensitizer. However, due to increased solubility, RB provides slightly better percent conversions in IPA. It should be noted that the initial concentration of 1,5-DHN (10 mM) used was identical to that of the batch scale experiments (Section 2.2.1.5). ^{1}H

NMR spectroscopy showed that complete conversion was achieved using both IPA and TAA as reaction solvent with TCPP and the 419 nm fluorescent lamp. These experiments were then repeated at a higher concentration of 1,5-DHN (20 mM) and the results are shown in Table 5.5.

Table 5.5: Results for the dye sensitized photooxygenation of 1,5-DHN (20 mM) using the microflow system.

Exp No	1,5-DHN (mM)	Sensitizer (0.25mM)	Solvent	Residence time (min)	% Conversion
97a	20	RB	IPA	15.82	30[a]
97b	20	MB	IPA	15.82	6[a]
97c	20	TCPP	IPA	15.82	**89**[b]
98a	20	RB	TAA	15.82	21[a]
98b	20	MB	TAA	15.82	5[a]
98c	20	TCPP	TAA	15.82	**100**[b]

[a] "Cool white" fluorescent lamp, [b] 419 nm fluorescent lamp

The results are in agreement with those shown in Table 5.4. RB and MB show significantly inferior percent conversions to juglone compared to TCPP. A percent conversion of 89 % was achieved in IPA using TCPP. In comparison, complete or 100% conversion to juglone was realised using TAA as the reaction solvent with TCPP as photosensitizer.

The determination of a space time yield (STY) for a reaction requires that less than 100% conversion occurs. Since a 20 mM solution of 1,5-DHN in both IPA and TAA represents a saturated solution, then it is not possible to use an increased concentration to obtain conversions below 100%. To determine a space time yield for the TCPP sensitised reactions in IPA and TAA, it was necessary to increase the total flow rate of the system, thereby reducing the residence time. It was found that a flow rate of 1.268 ml/min could prevent the complete conversion of 1,5-DHN to juglone. Air and solvent flow rates were determined to be of 0.450 and 0.818 ml/min respectively. This flow rate lay outside of the optimal flow band and resulted in non uniform air slugs. Despite this issue, percent conversions of up to 77 % were realised (Experiment 99) allowing for a STY to be calculated (Section 5.3.7).

In order to compare the results obtained using the microflow system to that of previous batch scale (Schlenk flask) results the energy efficiencies for each reaction platforms were determined. These results were calculated based upon millimoles of product formed per lamp power and millimoles of product formed per irradiated area. The formulae for these calculations are given below:

$$\text{Product per lamp power (mmol.W}^{-1}\text{.hr}^{-1}\text{)} = \frac{\text{Product (mmol)}}{\text{Lamp power (W) X Residence time (hr)}}$$

$$\text{Product per irradiated area (mmol.W}^{-1}\text{.hr}^{-1}\text{.cm}^{-2}\text{)} = \frac{\text{Product (mmol)}}{\text{Lamp power (W) X Residence time (hr) X Irradiated area (cm}^{2}\text{)}}$$

Figures 5.12 and 5.13 show that in the case of the dye sensitized photooxygenation of 1,5-DHN to juglone using IPA and TAA with TCPP the photochemical microflow system was significantly more energy efficient than batch (Schlenk flask) conditions using a 500 W halogen lamp. Comparison of Experiments 22 and 99 show that the microflow system is ~590 times more efficient with regards to product formed per lamp power (mmol.W^{-1}.hr^{-1}).

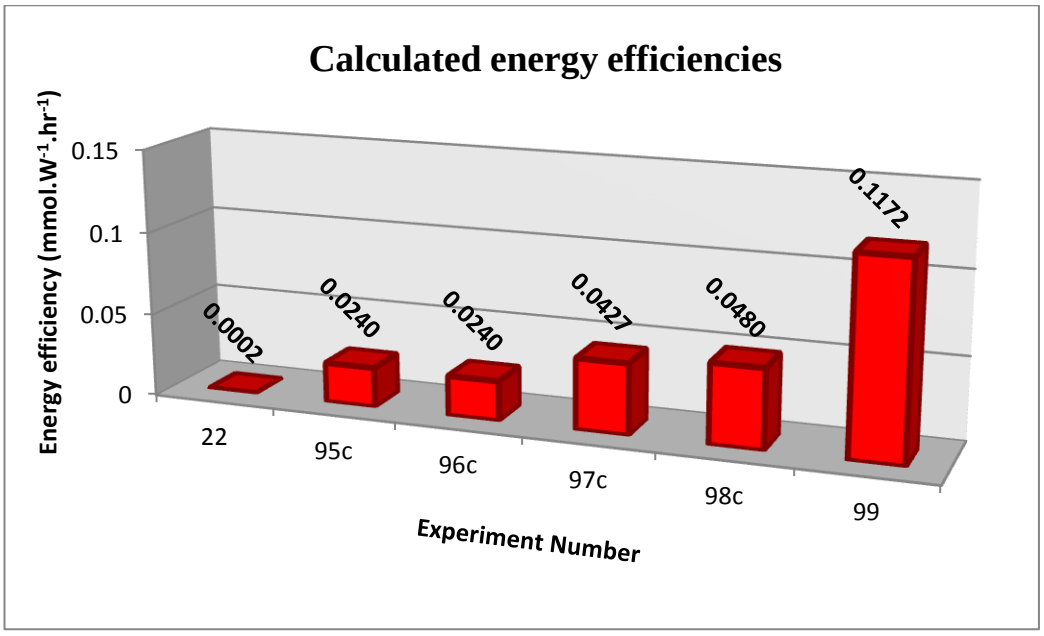

Figure 5.12: Product formed per lamp power (mmol.W^{-1}.hr^{-1})

Energy efficiency calculations also showed that the microflow system was 180 times more efficient with regards to product formed per irradiated area (mmol/W^{-1}.hr^{-1}.cm^{-2}). It is noteworthy to mention that the initial reaction solution of 1,5-DHN and sensitizer in either IPA or TAA is dark brown in colour. Consequently, light penetration, when using the Schlenk flask apparatus is relatively low. This results in photochemical reactions only occurring close to the wall of the reaction vessel. In contrast the capillary tube of the microflow system has an internal diameter of 400 µm. This allows for complete irradiation of the reaction mixture simultaneously resulting in significantly greater energy efficiencies with regards to product formed per lamp power and irradiated area. Energy efficiencies for all dye sensitized photooxygenations performed within this Chapter are shown in Appendix E.

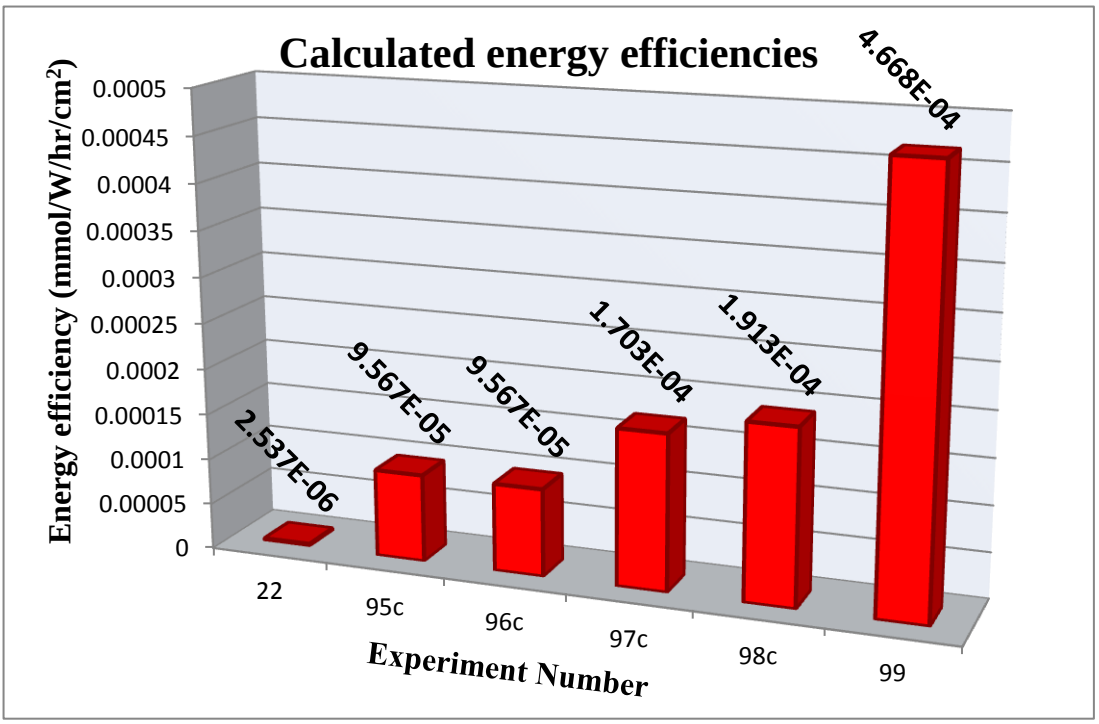

Figure 5.13: Product formed per irradiated area (mmol.W^{-1}.hr^{-1}.cm^{-2}).

In addition to being substantially more energy efficient in comparison to previous syntheses using the Schlenk flask setup, the microflow system also eliminated the requirement for water cooling. This was a direct saving of up to 4 L/min of water compared to both indoor and solar Schlenk flask systems. This was a significant improvement with regards to environmental impact and the twelve principles of

green chemistry. Energy efficiency calculations were not performed for solar dye sensitized photooxygenations as no electrical lamps were utilised.

5.3.5 Dye sensitized photooxygenation of β-citronellol using the photochemical microflow system

The dye sensitized photooxygenation of β-citronellol was performed using the photochemical microflow system using the dye sensitized photooxygenation of 1,5-DHN (Section 5.3.4). In Section 5.3.4 complete conversion of solutions of 1,5-DHN (20 mM) were realised using the microflow system. Therefore, initial solutions (25 mM) of β-citronellol were prepared in 5 ml volumetric flasks using stock solutions of sensitizers (0.25 mM) in IPA and TAA. These were prepared under dark room conditions. The solutions were then pumped through the photochemical microflow system (0.316 ml/min, slug flow conditions) and collected in 10 ml amber round bottom flasks. The solvent was removed under vacuum and ^{1}H NMR used to confirm the percent conversion to products (Table 5.6).

Table 5.6 Dye sensitized photooxygenation of β-citronellol (26 mM) using the microflow system.

Exp No	β-citronellol (mM)	Sensitizer (0.25mM)	Solvent	Residence time (min)	% Conversion
100a	26	RB	IPA	15.82	83[a]
100b	26	MB	IPA	15.82	45[a]
100c	26	TCPP	IPA	15.82	100[b]
101a	26	RB	TAA	15.82	100[a]
101b	26	MB	TAA	15.82	58[a]
101c	26	TCPP	TAA	15.82	100[b]

[a] "Cool white" fluorescent lamp, [b] 419 nm fluorescent lamp

Similar to the synthesis of juglone, the combination of the 419 nm fluorescent lamp and TCPP provided superior percent conversions compared to the "cool white" lamp with MB as sensitizer. Complete conversion of β-citronellol to products was achieved in both IPA and TAA using TCPP as the sensitizer. In addition, complete conversion was also realised in TAA using RB and the "cool white" fluorescent

lamp. To determine STYs, the concentration of β-citronellol was increased to 52 mM and the experiments were repeated (Table 5.7).

Table 5.7: Dye sensitized photooxygenation of β-citronellol (52 mM) using the microflow system.

Exp No	β-citronellol (mM)	Sensitizer (0.25mM)	Solvent	Residence time (min)	% Conversion
102a	52	RB	IPA	15.82	77[a]
102b	52	MB	IPA	15.82	49[a]
102c	52	TCPP	IPA	15.82	74[b]
103a	52	RB	TAA	15.82	63[a]
103b	52	MB	TAA	15.82	29[a]
103c	52	TCPP	TAA	15.82	84[b]

[a] "Cool white" fluorescent lamp, [b] 419 nm fluorescent lamp

The results of Table 5.7 show that the combination of the 419 nm fluorescent lamp, TCPP and TAA provides the highest percent conversion to products, while MB showed superior results in IPA compared to TAA, as was found previously (Sections 2.2.2.1 and 5.3.4). RB also showed slightly better percent conversions in IPA due to increased solubility. This is in agreement with the results of Section 5.3.4.

Energy efficiency calculations were then performed for the dye sensitized photooxygenation of β-citronellol using the microflow and batch scale (Schlenk flask) systems. The results of Figure 5.14 show the dye sensitized photooxygenation of β-citronellol, using the photochemical microflow system, is significantly more energy efficient than the batch (Schlenk flask) systems.

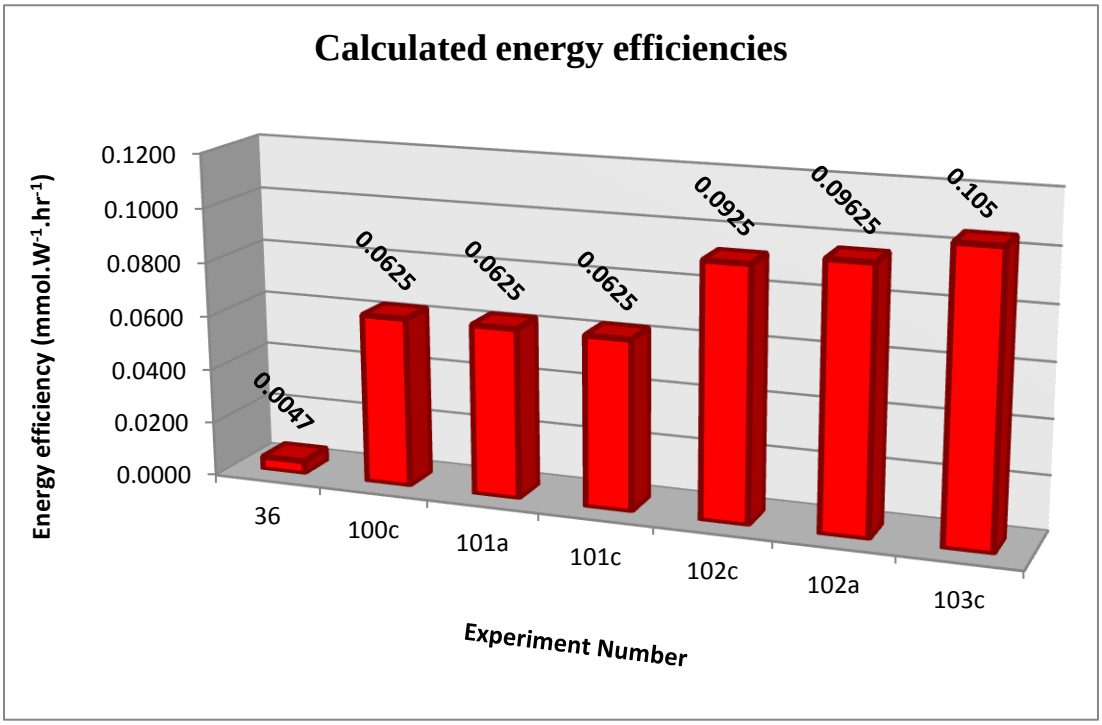

Figure 5.14: Product formed per lamp power (mmol.W^{-1}.hr^{-1})

The photochemical microflow system is > 22 times more energy efficient than the Schlenk flask setup with regards to product formed per lamp power. The results of Figure 5.15 show that the photochemical microflow system is > 7 times more efficient that the Schlenk flask setup with regards to product formed per irradiated area.

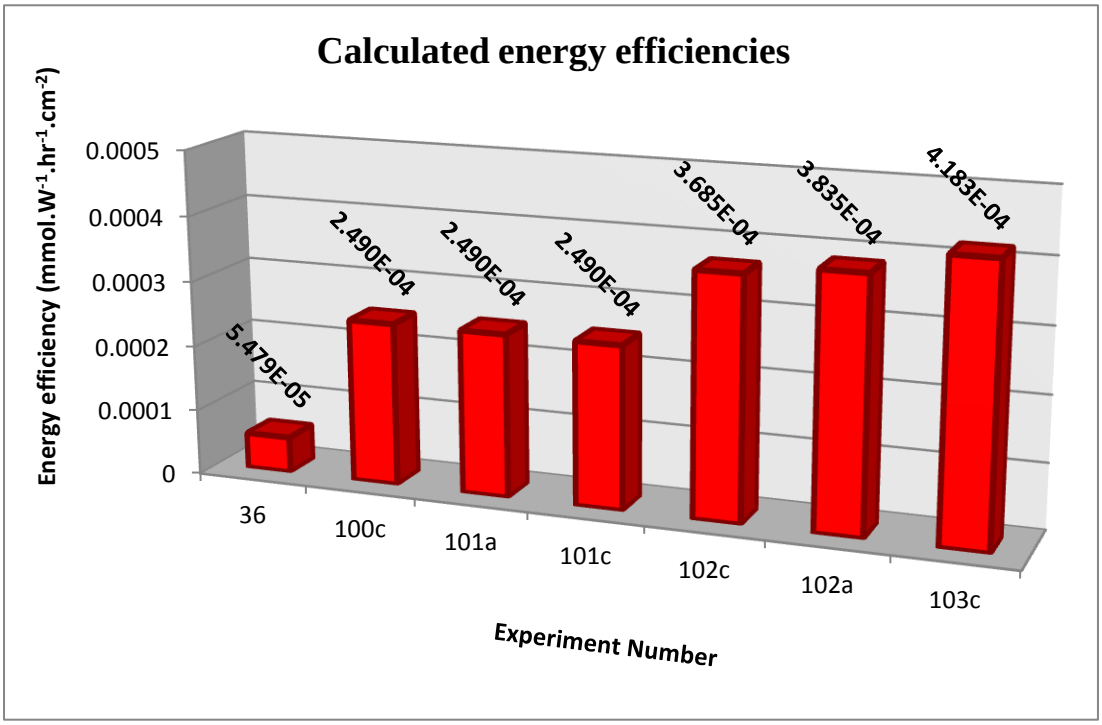

Figure 5.15: Product formed per irradiated area (mmol.W^{-1}.hr^{-1}.cm^{-2}).

Energy efficiency calculations were not performed for solar photooxygenations of β-citronellol as no lamps were used.

5.3.6 Dye sensitized photooxygenation of α-terpinene using the photochemical microflow system

The photochemical microflow system was also used for the dye sensitized photooxygenation of α-terpinene (Table 5.8). All samples (two separate concentrations 26 and 52 mM) were made up in a dark room using the sensitizer (0.25 mM) stock solutions in IPA. The solutions were then pumped through the photochemical microflow system (0.316 ml/min) and collected in 10 ml amber round bottom flasks. UV-Vis spectroscopy was used to determine the percent conversion to products and ^{1}H NMR was used to determine the ratio of *p*-cymene to ascaridole in the crude product.

Table 5.8: Dye sensitized photooxygenation of α-terpinene(26 & 52 mM) using the microflow system.

Exp No	α-terpinene (mM)	Sensitizer (0.25mM)	Solvent	Residence time (min)	% Conversion (UV-Vis)	^{1}H NMR (*p*-cymene / ascaridole)
104a	26	RB	IPA	15.82	100	6:94[a]
104b	26	MB	IPA	15.82	100	2:98[a]
104c	26	TCPP	IPA	15.82	100	12:88[b]
105a	52	RB	IPA	15.82	88	5:95[a]
105b	52	MB	IPA	15.82	75	3:97[a]
105c	52	TCPP	IPA	15.82	86	12:88[b]

[a] "Cool white" fluorescent lamp, [b] 419 nm fluorescent lamp

Similar to the dye sensitized photooxygenation of β-citronellol using the microflow system, complete conversion of solutions (26 mM) of α-terpinene were achieved using RB, MB and TCPP in IPA. At a concentration of 52 mM, percent conversions of 88, 75 and 86 % were achieved using RB, MB and TCPP respectively. These results were in agreement with the Schlenk flask experiments in Section 2.2.2.1. Interestingly, ^{1}H NMR has shown that there is a greater selectivity of *p*-cymene in the crude product when TCPP is used as the sensitizer. Up to 12 % of the product formed is *p*-cymene. These results suggest that Type I and III photooxygenations may also be occurring when using TCPP as sensitizer.

Energy efficiency calculations were performed in order to compare the dye sensitized photooxygenation of α-terpinene using both the photochemical microflow and batch scale (Schlenk flask) systems based upon product formed per lamp power and irradiated area (Figures 5.16 and 5.17).

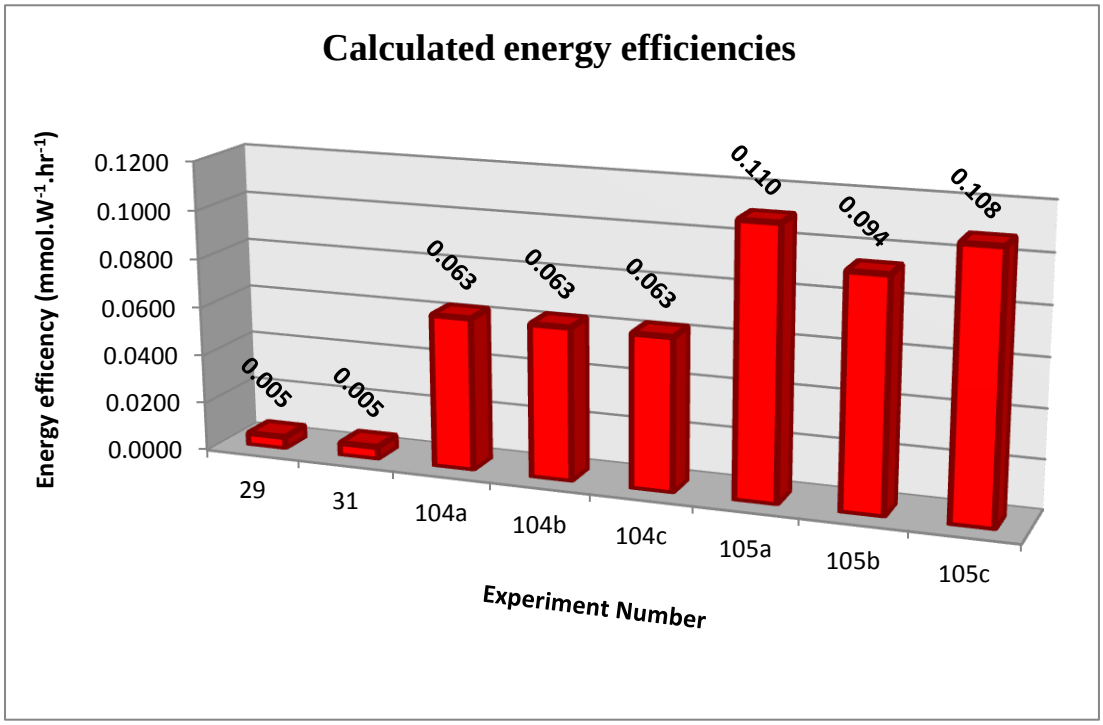

Figure 5.16: Product formed per lamp power (mmol.W^{-1}.hr^{-1}).

The results of Figure 5.16 show that similar to the dye sensitized photooxygenation of 1,5-DHN and β-citronellol, the dye sensitized photooxygenation of α-terpinene is also significantly more energy efficient using the microflow system. The microflow system is ~ 20 times more energy efficient than the Schlenk flask system with regards to product formed per lamp power. Figure 5.17 demonstrates further that the microflow system is ~ 7 times more efficient than the Schlenk flask system with regards to product formed per irradiated area.

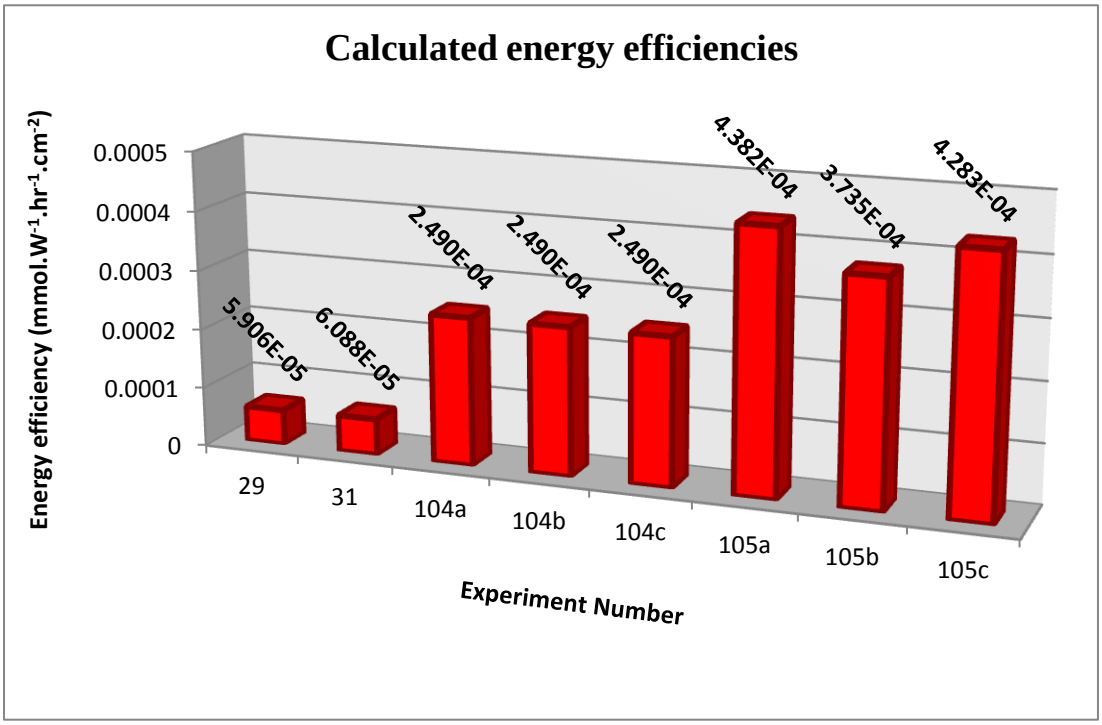

Figure 5.17: Product formed per irradiated area (mmol.W^{-1}.hr^{-1}.cm^{-2}).

5.3.7 Space-time-yield calculations

In addition to energy efficiency calculations the Schlenk flask and photochemical microflow systems were further evaluated using space time yield (STY) calculations. These calculations are dependent on both reactor geometry and rates of conversion and were determined using the following equation.

$$STY = N / (Vr \times t)$$

Where N is the number of moles of product(s) formed within the reactor volume Vr and t is the residence time in minutes.

STYs were calculated for all dye sensitized photooxygenations of 1,5-DHN, β-citronellol and α-terpinene (Appendix E). As the calculations are dependent on the reactor geometry and do not include energy efficiencies, STYs were also calculated for all photooxygenations performed under solar conditions including photooxygenations performed using flat bead reactor technology.

5.3.7.1 Dye sensitized photooxygenation of 1,5-DHN

Figure 5.18 depicts the results of STY calculations for the dye sensitized photooxygenation of 1,5-DHN using the Schlenk flask and flat bed batch reactors along with the microflow system.

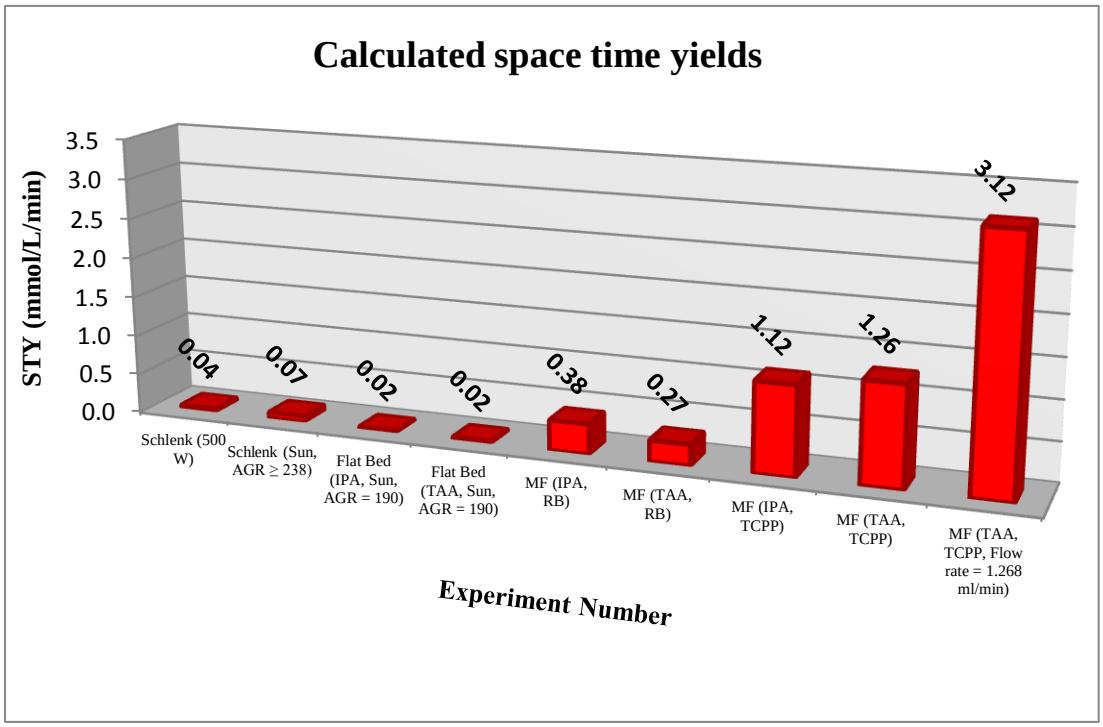

Figure 5.18: Calculated space time yields for the dye sensitized photooxygenation of 1,5-DHN.

Figure 5.18 clearly demonstrates that the dye sensitized photooxygenation of 1,5-DHN using the microflow system is significantly more efficient than that of the Schlenk flask or flat bed reactors. The microflow system is up to 53 times more efficient than the 2nd generation flat bed reactor and 17 times more efficient than the solar Schlenk flask syntheses. Furthermore, despite utilising the sun as the source of irradiation, the flat bed and Schlenk flask reactors are still inefficient systems since they require water cooling. Water cooling results in up to 4 L/min of water being wasted. Over a 6 hour reaction period this equals 240 L of water! Although the microflow system requires electrical energy to run the peristaltic pump, the fluorescent lamp and the electric fan the energy usage (117.72 kJ/hr) is negligible

compared to the water lost during solar syntheses. In fact the flat bed reactor setup actually uses up to 62 % (72 kJ/hr) of this energy to supply air to the system.

5.3.7.2 Dye sensitized photooxygenation of β-citronellol

Figure 5.19 depicts the results of STY calculations for the dye sensitized photooxygenation of β-citronellol using the Schlenk flask and flat bed reactor batch reactors along with the microflow system.

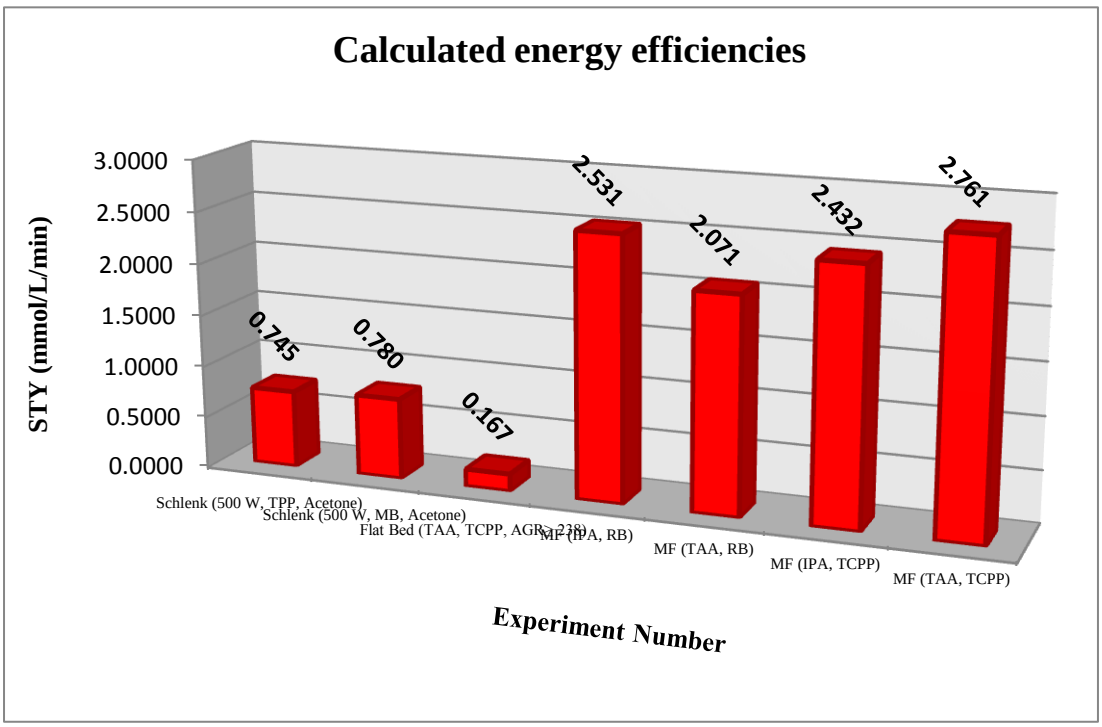

Figure 5.19: Calculated space time yields for the dye sensitized photooxygenation of β-citronellol.

The results again show that the microflow system is significantly more efficient than either the Schlenk flask or flat bed systems. The microflow system is up to 3.5 times more efficient than the Schlenk flask system (Experiment 36).

5.3.7.3 Dye sensitized photooxygenation of α-terpinene

Figure 5.20 depicts the results of STY calculations for the dye sensitized photooxygenation of α-terpinene. Similar to the STY calculations for 1,5-DHN and β-citronellol the dye sensitized photooxygenation of α-terpinene using the microflow

system is significantly more efficient than the traditional Schlenk flask setup. The microflow system is > 3 times more efficient than the Schlenk flask setup.

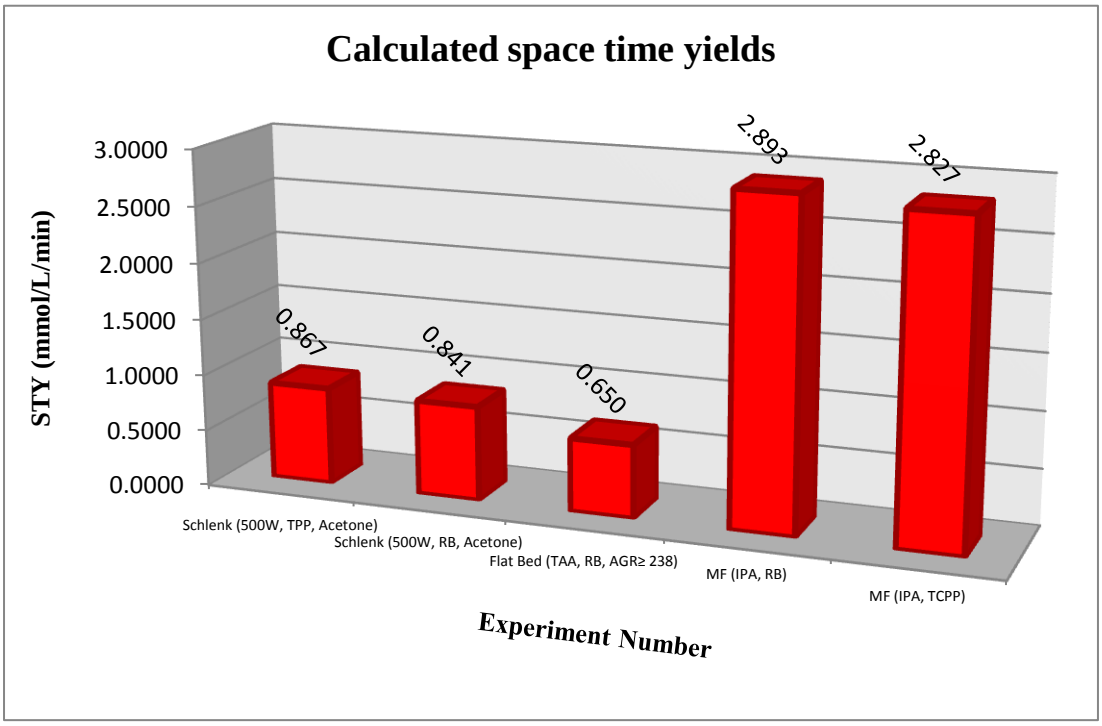

Figure 5.20: Calculated space time yields for the dye sensitized photooxygenation of α-terpinene.

5.4 Conclusion

The design and implementation of a novel low cost, low energy demanding photochemical microflow reactor has been described for the homogeneous dye sensitized photooxygenation of 1,5-DHN, α-terpinene and β-citronellol.

The photochemical microflow system was designed based upon established coiled capillary microflow systems. PTFE tubing (10 m) with an internal diameter of 0.8 mm and volume of 5 ml was used as the capillary tubing. The relatively small internal diameter of the PTFE tubing provided a unique situation where the light source need only be powerful enough to penetrate 0.8 mm of reaction media. Consequently, an 8 W fluorescent lamp was utilised. This had a direct saving of up to 1527 kJ/hr of electrical energy compared to the 500 W halogen lamp. Additionally, the utilisation of an 8 W fluorescent lamp dramatically reduced the amount of thermal energy generated. Consequently, water cooling was completely eliminated and cooling was achieved by a small low energy electric fan.

Incorporation of an air source was also found to be essential for dye sensitized photooxygenations to be performed efficiently in a microflow system. However, flow rate optimisations demonstrated that air slug uniformity could only be maintained between 0.312 and 0.746 ml/min. Outside of these values the photochemical microflow system is still a viable system however optimal percent conversions and reaction times are not achieved.

The percent conversions achieved in this work demonstrate that the photochemical microflow system could be used to efficiently perform the dye sensitized photooxygenations of 1,5-DHN, α-terpinene and β-citronellol. STYs and energy efficiency calculations demonstrated that in all cases, the microflow system was significantly more energy efficient than Schlenk flask and the solar flat bed reactors. In the case of the dye sensitized photooxygenation of 1,5-DHN the microflow system was almost 600 times more efficient than the Schlenk flask and the 500 W halogen lamp with regards to product formed per lamp power ($mmol.W^{-1}.hr^{-1}$). It

was also ~180 times more efficient with regards to product formed per irradiated area ($mmol.W^{-1}.hr^{-1}.cm^{-2}$).

It is noteworthy to mention that despite the significant advantages of the photochemical microflow system it still suffers from one issue that negatively affects the environmental impact of the system. All experiments described within this chapter were homogeneous in nature. Column chromatography is still required to purify the crude reaction mixture post irradiation. However, the utilisation of nano structured solid support sensitizers may provide an answer to this issue.

5.5 Experimental

5.5.1 Sensitizer stock solutions

All sensitizer stock solutions (0.25 mM) were prepared in reagent grade IPA and TAA in 100 ml volumetric flasks and stored in the dark. The quantities of sensitizer required to prepare each of these stock solutions is illustrated in Table 5.9.

Table 5.9: Quantities of sensitizers required to make 0.25 mM solution in 100 ml volumetric flask.

Sensitizer	Solution concentration (mM)	Quantity (mg)
RB	0.25	25
MB	0.25	7.86
TCPP	0.25	19.44

5.5.2 Dye sensitized photooxygenations using the photochemical microflow system

All solutions were made up in a dark room using sensitizer stock solutions (0.25 mM) and then wrapped in foil to insure no light reached the reaction media. Dye sensitized photooxygenations were performed using the newly developed photochemical microflow system with a flow rate of 0.312 ml/min unless otherwise stated. The crude product was collected in 10 ml amber round bottom flasks and the solvent removed under vacuum. ^{1}H NMR (acetone-d_6 and $CDCl_3$) and UV-Vis spectroscopy were used to determine percent conversions to product(s). Samples were also taken of the initial reaction media to ensure no conversion to products occurred due to external light sources. The light source utilised was dependent on the sensitizer. The 419 nm lamp was used in conjunction with TCPP and the "cool white" lamp in conjunction with RB and MB.

5.5.3 Control experiments

5.5.3.1 Sensitizer free experiments (Experiments 86-91)

General procedure

Solutions of 1,5-DHN (10 mM), β-citronellol (26 mM) and α-terpinene (26 mM) were prepared using reagent grade IPA in a dark room without any sensitizer. These were then pumped through the photochemical microflow system at a flow rate of 0.312 ml/min (Corresponding gauge rate of 5.00) and collected in 10 ml amber round bottom flasks. Both the 419 nm and "cool white" fluorescent lamps were utilised as the light source. The percent conversion to products was determined by ^{1}H NMR (acetone-d_6 and $CDCl_3$) and UV-Vis spectroscopy.

Sensitizer free photooxygenation of 1,5-DHN, 419 nm lamp (experiment 86)

^{1}H NMR (acetone-d_6) confirmed no conversion to products had occurred.

Sensitizer free photooxygenation of β-citronellol, 419 nm lamp (experiment 87)

^{1}H NMR ($CDCl_3$) confirmed no conversion to products had occurred.

Sensitizer free photooxygenation of α-terpinene, 419 nm lamp (experiment 88)

UV-Vis spectroscopy confirmed a percent conversion of 31 %. ^{1}H NMR ($CDCl_3$) showed a *p*-cymene to ascaridole ratio of 36:64

Sensitizer free photooxygenation of 1,5-DHN, "cool white" lamp (experiment 89)

^{1}H NMR (acetone-d_6) confirmed no conversion to products had occurred.

Sensitizer free photooxygenation of β-citronellol, "cool white" (experiment 90)

^{1}H NMR ($CDCl_3$) confirmed no conversion to products had occurred.

Sensitizer free photooxygenation of α-terpinene, "cool white" (experiment 91)

UV-Vis spectroscopy confirmed a percent conversion of 25 %. ^{1}H NMR ($CDCl_3$) showed *p*-cymene to ascaridole ratio of 47:53.

5.5.3.2 Dye sensitized photooxygenations without an air inlet (Experiments 92-94)

General procedure

Solutions of 1,5-DHN (10 mM), β-citronellol (26 mM) and α-terpinene (26 mM) were prepared using the TCPP stock solution (0.25 mM) in a dark room. These were then bubbled with air for 30 minutes. Next the solutions were pumped through the photochemical microflow system at a flow rate of 0.312 ml/min (Gauge rate = 5.00) using either the 419 nm or "cool white" fluorescent lamps and collected in 10 ml amber round bottom flasks. The percent conversion to products was determined by ^{1}H NMR (acetone-d_6 and $CDCl_3$) and UV-Vis spectroscopy.

Dye sensitized photooxygenation of 1,5-DHN without air inlet (Experiment 92)

^{1}H NMR (acetone-d_6) confirmed a percent conversion of 28 %.

Dye sensitized photooxygenation of β-citronellol without air inlet (Experiment 93)

^{1}H NMR ($CDCl_3$) confirmed a percent conversion of 15 %.

Dye sensitized photooxygenation of α-terpinene without air inlet (Experiment 94)

UV-Vis spectroscopy confirmed a percent conversion of 15 %. ^{1}H NMR ($CDCl_3$) confirmed a *p*-cymene to ascaridole ratio of 31:69.

5.5.4 Dye sensitized photooxygenations using the photochemical microflow reactor

5.5.4.1 Dye sensitized photooxygenation of 1,5-DHN

General procedure

Solutions of 1,5-DHN (10 and 20 mM) were made up in 5 ml volumetric flasks using the sensitizer stock solutions (0.25 mM) in a dark room. These were covered in foil and pumped through the microflow system at a flow rate of 0.312 ml/min. The crude product was collected in a 10 ml amber round bottom flask and the solvent removed under vacuum. ^{1}H NMR (acetone-d_6) was used to determine the percent conversion to juglone.

Dye sensitized photooxygenation of 1,5-DHN in IPA (Experiments 95a-c)

Solutions of 1,5-DHN (10 mM) were prepared using stock solutions (0.25 mM) of RB, MB and TCPP in IPA. ^{1}H NMR (acetone-d_6) showed percent conversions of 51, 19 and 100 % respectively.

Dye sensitized photooxygenation of 1,5-DHN in TAA (Experiments 96a-c)

Solutions of 1,5-DHN (10 mM) were prepared using stock solutions (0.25 mM) of RB, MB and TCPP in TAA. ^{1}H NMR (acetone-d_6) showed percent conversions of 49, 5 and 100 % respectively.

Dye sensitized photooxygenation of 1,5-DHN in IPA (Experiments 97a-c)

Solutions of 1,5-DHN (20 mM) were prepared using stock solutions (0.25 mM) of RB, MB and TCPP in IPA. ^{1}H NMR (acetone-d_6) showed percent conversions of 30, 6 and 89 % respectively.

Dye sensitized photooxygenation of 1,5-DHN in IPA (Experiments 98a-c)

Solutions of 1,5-DHN (20 mM) were prepared using stock solutions (0.25 mM) of RB, MB and TCPP in TAA. ^{1}H NMR (acetone-d_6) showed percent conversions of 29, 5 and 100 % respectively.

Dye sensitized photooxygenation of 1,5-DHN in TAA (Experiment 99)

A solution of 1,5-DHN (20 mM) was made up in a 5 ml volumetric flask using the TCPP stock solution in TAA (0.25 mM). This was then covered in foil and pumped through the microflow system at a flow rate of 1.268 ml/min. The crude product was collected in a 10 ml amber round bottom flask and the solvent removed under vacuum. ^{1}H NMR (acetone-d_6) showed a 77 % conversion to juglone.

5.5.4.2 Dye sensitized photooxygenation of β-citronellol

General procedure

Solutions of β-citronellol (26 and 52 mM) were made up in 5 ml volumetric flasks using the sensitizer stock solutions (0.25 mM) in a dark room. These were covered in foil and pumped through the microflow system at a flow rate of 0.312 ml/min

(Gauge rate = 5.00). The crude product was collected in a 10 ml amber round bottom flask and the solvent removed under vacuum. ^{1}H NMR (acetone-d_6) was used to determine the percent conversion to products.

Dye sensitized photooxygenation of β-citronellol in IPA (Experiments 100a-c)

Solutions of β-citronellol (26 mM) were prepared using stock solutions (0.25 mM) of RB, MB and TCPP in IPA. ^{1}H NMR ($CDCl_3$) showed percent conversions of 83, 45 and 100 % respectively.

Dye sensitized photooxygenation of β-citronellol in TAA (Experiments 101a-c)

Solutions of β-citronellol (26 mM) were prepared using stock solutions (0.25 mM) of RB, MB and TCPP in TAA. ^{1}H NMR ($CDCl_3$) showed percent conversions of 100, 58 and 100 % respectively.

Dye sensitized photooxygenation of β-citronellol in IPA (Experiments 102a-c)

Solutions of β-citronellol (52 mM) were prepared using stock solutions (0.25 mM) of RB, MB and TCPP in IPA. ^{1}H NMR ($CDCl_3$) showed percent conversions of 77, 49 and 74 % respectively.

Dye sensitized photooxygenation of β-citronellol in TAA (Experiments 103a-c)

Solutions of β-citronellol (52 mM) were prepared using stock solutions (0.25 mM) of RB, MB and TCPP in TAA. ^{1}H NMR ($CDCl_3$) showed percent conversions of 63, 29 and 84 % respectively.

5.5.4.3 Dye sensitized photooxygenation of α-terpinene

General procedure

Solutions of α-terpinene (26 and 52 mM) were made up in 5 ml volumetric flasks using the sensitizer stock solutions (0.25 mM) in a dark room. These were covered in foil and pumped through the microflow system at a flow rate of 0.312 ml/min (Gauge rate = 5.00). The crude product was collected in a 10 ml amber round bottom flask and the solvent removed under vacuum. UV-Vis spectroscopy was

used to determine percent conversion to product(s) based upon calibration curves generated in Section 2.2.2.1.

Dye sensitized photooxygenation of α-terpinene in IPA (Experiments 104a-c)

Solutions of α-terpinene (26 mM) were prepared using stock solutions (0.25 mM) of RB, MB and TCPP in IPA. UV-Vis spectroscopy showed complete conversion to products for all three experiments.

Dye sensitized photooxygenation of α-terpinene in IPA (Experiments 105a-c)

Solutions of α-terpinene (52 mM) were prepared using stock solutions (0.25 mM) of RB, MB and TCPP in IPA. UV-Vis spectroscopy showed percent conversions of 88, 75 and 86 % respectively.

5.6 References

(1) Wegner, J.; Ceylan, S.; Kirschning, A. *Chem. Commun.* **2011**, *47*, 4583-4592.

(2) He, P.; Haswell, S. J.; Fletcher, P. D. I. *Applied Catalysis A: General* **2004**, *274*, 111-114.

(3) Comer, E.; Organ, M. G. *Chemistry: A European Journal* **2005**, *11*, 7223-7227.

(4) Yavorskyy, A.; Shvydkiv, O.; Nolan, K.; Hoffmann, N.; Oelgemöller, M. *Tetrahedron Lett.* **2011**, *52*, 278-280.

(5) Yavorskyy, A.; Shvydkiv, O.; Hoffmann, N.; Nolan, K.; Oelgemoeller, M. *Org. Lett.* **2012**, 14, 4342-4345.

(6) Shvydkiv, O.; Yavorskyy, A.; Nolan, K.; Youssef, A.; Riguet, E.; Hoffmann, N.; Oelgemoller, M. *Photochem. Photobiol. Sci.* **2010**, *9*, 1601-1603.

(7) Shvydkiv, O.; Gallagher, S.; Nolan, K.; Oelgemoeller, M. *Org. Lett.* **2010**, *12*, 5170-5173.

(8) Shvydkiv, O.; Yavorskyy, A.; Tan, S. B.; Nolan, K.; Hoffmann, N.; Youssef, A.; Oelgemoller, M. *Photochem. Photobiol. Sci.* **2011**, *10*, 1399-1404.

(9) Yavorskyy, A.; Shvydkiv, O.; Limburg, C.; Nolan, K.; Delaure, Y. M. C.; Oelgemoller, M. *Green Chem.* **2012**, *14*, 888-892.

Chapter 6

Heterogeneous dye sensitized photooxygenations utilizing a novel photochemical microflow bubble reactor.

6.1 Introduction

6.1.1 Silica nano particles

Silica nano particles; their synthesis and applications were previously described in Section 4.1. These modified particles will be used with the photochemical microflow system to perform the heterogeneous dye sensitized photooxygenations of 1,5-DHN, β-citronellol and α-terpinene. Furthermore, superparamagnetic iron oxide (Fe_3O_4) nano particles will also be used for this purpose. These functionalised iron oxide nano particles are ideal solid supports as they can be removed from the reaction mixture via an external magnet.

6.1.2 Iron oxide nano particles

Iron oxide nano particles are a class of superparamagnetic metal oxide nano particles typically in the range of 1 – 200 nm. They are generally formed from ferromagnetic elements such as iron, cobalt or nickel. In recent years superparamagnetic iron oxide nano particles have found a variety of applications in areas such as magnetic fluids[1], solid supported catalysts[2,3], biotechnology and biomedicine[4], magnetic resonance imaging (MRI)[5,6], and data storage.[7] Research into the applications of iron oxide nano particles is attributed to three key advantages. These are namely: i) high surface area to volume ratio, ii) superparamagnetism and iii) facile functionalisation of the surface.

6.1.2.1 Synthesis

Similar to the ammonia catalysed synthesis of silica nano particles the synthesis of superparamagnetic iron oxide nano particles involves two stages, nucleation and growth. As the concentration of the solutes (typically Fe(II) and Fe(III) salts in base) reaches supersaturation a sudden short burst of nucleation occurs resulting in the formation of primary particles or nuclei with a rapid decrease in solute concentration, which is then followed by a slow growth process by diffusion of the remaining solute onto the surface of the growing nuclei. In order to produce monodisperse nano particles these two stages should be separated. i.e. there should be no nucleation during the growth stage. The nucleation stage should be relatively

short lived, followed by an initially fast but progressively slower growth stage (the rate of growth of the particles slows due to a decreasing surface area to volume ratio). The nucleation stage determines the final number of particles and this does not change during the growth stage. The final size of the particles depends on the solute concentration and their solubility. As soon as the concentration of the solute decreases back down to its solubility level the particle growth stops and this process can be illustrated by the La Mer diagram (Figure 6.1).

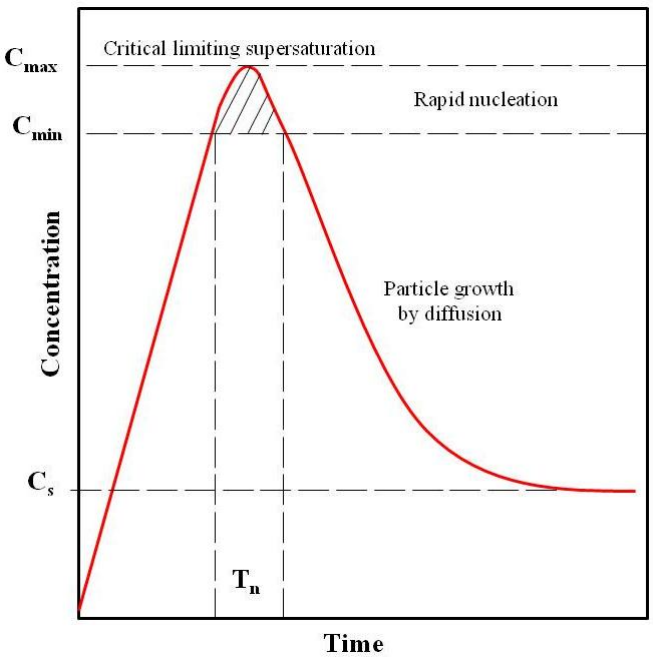

Figure: 6.1: The La Mer diagram.

There are several methods for the synthesis of superparamagnetic iron oxide nano particles including co-precipitation, thermal decomposition, microemulsion synthesis, hydrothermal synthesis and electrochemical synthesis. However, co-precipitation, thermal decomposition and microemulsion assisted synthesis are the most common methods employed and will be discussed further.

Co-precipitation

The co-precipitation technique is probably the most convenient and efficient method of superparamagnetic iron oxide nano particle synthesis. Magnetic iron oxides, magnetite and maghmite (Fe_3O_4 and γFe_2O_3) can be prepared by the mixing of

stoichiometric amounts (1:2) of aqueous solutions of iron(II) and iron(III) salts under alkaline conditions. The reaction is generally performed at room temperature however, elevated temperatures have been reported in the literature. Sodium hydroxide and ammonia are the most commonly used bases with pH values of greater than 10 required for the reaction to proceed. The co-precipitation method also affords very high yields of magnetite and has a short reaction time (minutes) in comparison to other techniques. The formation of magnetite (Fe_3O_4) can be represented by the following equation.

$$Fe^{2+} + 2Fe^{3+} + 8OH^- \rightarrow Fe_3O_4 + 4H_2O$$

Magnetite however, is not stable under ambient conditions, being readily oxidised to maghmite (γFe_2O_3) in air. Magnetite is also sensitive to acidic media. In addition, co-precipitation methods also suffer from poor size distribution, morphology and reproducibility of results. Factors such as types of iron salts used, ratio of iron salts used, pH and reaction temperature all have an effect on the particle size and morphology. The issue of reproducibility can be attributed to uncontrolled aggregation of particles in solution. In order to produce monodisperse superparamagnetic nano particles with a low size distribution the use of organic chelating agents such as oleic acid have been reported. These organic ions chelate to the surface of particles after nucleation. This effectively prevents aggregation and the production of particles up to microns in size. It is important to note that these chelated ions do not prevent growth of the particles by Ostwald ripening processes.

Thermal decomposition

Thermal decomposition is a high temperature method for the synthesis of monodisperse magnetic nano particles from organometallic compounds in organic solvents containing stabilizing surfactants. The organometallic precursors used are primarily metal acetylacetonates with the formula $[M(acac)_n]$ where M = Fe, Mn, Co, Ni.[8] However, the literature also reports the use of metal carbonyls and metal cupferronates.[8,9] Fatty acids, oleic acid and hexadecylamine are often used as the stabilizing surfactants. Oleic acid in particular prevents agglomeration of the iron

oxide nano particles by chelating to the surface of the newly formed particles. The long alkyl chains then physically prevent other iron oxide particles from coming close enough to agglomerate.

Thermal decomposition methods show two main disadvantages over co-precipitation methods. Firstly, the synthesis is often more complicated compared to co-precipitation methods with elevated temperature (>300 °C) required to decompose the organometallic precursors. The reaction temperature can also affect the size and morphology of the resulting iron oxide particles. Secondly, the use of surfactants is also required and the ratio of surfactant to organometallic precursors can also affect size and morphology. Secondly, the reaction times can often be much longer than that of the co-precipitation methods.

Despite these disadvantages thermal decomposition shows two distinct advantages over co-precipitation methods; size distribution and morphology. The size distribution of particles produced by thermal decomposition is much narrower than that of co-precipitation methods. The morphology is also more uniform which is of great concern for nano particles in biomedical applications such as magnetic resonance imaging.

Sun *et al* reported the synthesis of 4 – 8 nm Fe_3O_4 MNPs via the thermal decomposition of $[Fe(acac)_3]$ in the presence of 1,2-hexadecanediol, oleic acid and oleylamine in phenol ether.[10, 11]

Microemulsion synthesis

Microemulsions are clear, stable, isotropic liquid mixtures of at least two immiscible liquids. In order to make the two liquids miscible a surfactant is used. The two basic types of microemulsions are direct (oil dispersed in water, o/w) and reversed (water dispersed in oil, w/o). The aqueous phase may contain salt(s) and/or other ingredients, and the "oil" may actually be a complex mixture of different hydrocarbons and olefins. In w/o microemulsions the aqueous phase is dispersed as micro-droplets within the oil or hydrocarbon phase. The micro-droplets are surrounded by a monolayer of surfactant molecules allowing them to disperse within

the hydrocarbon phase. These droplets are typically in the region of 50 nm in diameter. If two identical w/o microemulsions are mixed the micro-droplets will continuously collide, coalesce and break apart again. This will result in a mixing of the compounds that are contained within the micro-droplets which can allow for a chemical reaction. In this sense we can think of the droplets as nano reactors for nano particles.

Liu *et al* have reported the synthesis of magnetite nano particles using a water-in-oil microemuslion at ambient temperatures.[12] Using Fe(II) and Fe(III) iron chlorides Liu *et al* have developed a microemulsion where sodium hydroxide dissolved in water served as the aqueous phase, toluene as the oil phase, sodium dodecyle benzene sulphonate (DBS) as the surfactant and ethanol and the co-surfactant. Under these conditions magnetite nano particles with an average diameter of 10 nm were synthesized.

Despite the advantage of ambient temperatures and facile recovery of the magnetite nano particles, microemulsions do have two significant disadvantages compared to that of co-precipitation and thermal decomposition methods. Firstly, microemulsion methods in general provide low yields of nano particles. In addition, considerable amounts of solvents are required during the synthesis compared to other methods. Secondly, preparation of the microemulsions can be complicated and often time consuming. Slight differences within the ratios of the iron precursors, aqueous and hydrocarbon phases and the surfactants can have a large effect on the size and shape of the resulting magnetite nano particles.[13]

Table 6.1 summarises the advantages and disadvantages for each of the discussed methods of iron oxide magnetic nano particles synthesis.[14]

Table 6.1: Advantages and disadvantages of the three main methods for superparamagnetic iron oxide nano particle synthesis.

Synthetic Method	Synthesis	Reaction Temp (°C)	Reaction Time	Solvent	Surface Capping	Size Distribution	Shape Control	Yield
Co-precipitation	Simple, ambient conditions	20-100	Minutes	Aqueous	Required	Relatively narrow	Not good	High
Thermal Decomposition	Complicated, inert atmosphere	100-340	Minutes-days	Organic	Required	Very Narrow	Very Good	High
Microemulsion	Complicated, ambient conditions	20-50	Minutes-hours	Aqueous + organic	Required	Relatively narrow	Good	Low

6.1.3 Superparamagnetism

As superparamagnetism is a unique property of suitably small iron oxide nano particles (<128 nm) it will be discussed further here.

6.1.3.1 Ferromagnetism

Ferromagnetism is the basic method in which a compound forms a permanent magnet or is attracted to a magnetic field. Today there are several accepted types of magnetism but ferromagnetism is by far the strongest and the only type to be detectible in everyday life.

In non-magnetic compounds permanent magnetic dipoles tend to line up anti parallel in order to cancel each other out. In ferromagnetic compounds however, the opposite is true. Ferromagnetism arises from the spontaneous lining up of permanent dipoles parallel to each other within a compound. These magnetic dipoles arise from the movement of pairs of electrons within their atomic/molecular orbitals. Ferromagnetism is normally seen in materials that have partially filled outer valence shells. According to the Pauli Exclusion Principle two electrons cannot occupy the same orbitals if they have the same spin. However, under certain conditions, when the orbitals of unpaired outer valence electrons from adjacent atoms overlap, the distribution of their electric charge in space is further apart when the electrons have parallel spins than when they have opposite spins. This reduces

the electrostatic energy of the electrons. In simple terms, the electrons align their spins in order to repel each other. This repulsion moves them further apart and is more energetically favourable than if the electrons were spin paired and closer together.

It is noteworthy to mention that this aligning of magnetic moments does not mean a ferromagnetic compound is magnetic itself. Although in ferromagnetic compounds permanent dipoles do line up they do so in sections known as domains. Throughout the bulk of the material these dipoles line up opposite to each other resulting in an overall zero magnetic moment.

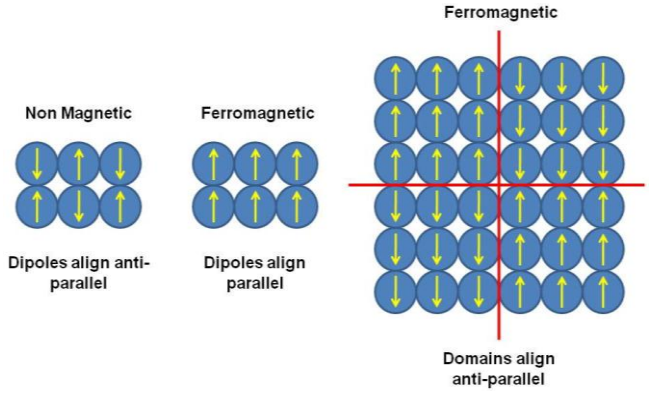

Figure 6.2: Lining up of magnetic moments parallel and anti parallel in ferromagnetic and non magnetic compounds. Also shown in red are the domain walls.

In order to induce permanent magnetism a ferromagnetic compound must be placed within a strong magnetic field. Once in the magnetic field the domains line up parallel to generate one strong magnetic moment. It is known for some materials that the domains remain in this position even when the external magnetic field is removed. This ability of some materials to remember this "magnetic history" is called hysteresis. In most cases only a certain percentage of domains will remain in this configuration and is known as remanence.

6.1.3.2 Paramagnetism

Paramagnetism is a magnetic phenomenon similar to ferromagnetism. Like ferromagnetism, paramagnetism is the aligning or permanent dipole moments

parallel to each other. However unlike ferromagnetism which occurs spontaneously in domains, paramagnetism occurs only when the material is subjected to an external magnetic field. Once the external magnetic field is removed thermal processes randomize the dipole moments resulting in an overall zero magnetic moment.

Paramagnetic materials, similar to ferromagnetic materials have a positive response to external magnetic fields. i.e. they are drawn to them. However, the material reacts as a whole to the magnetic field. For this reason only a small fraction of the dipole moments align with the field producing only a slight effect, unnoticeable in everyday life.

6.1.3.3 Superparamagnetism

Superparamagnetism is a phenomenon found in, but not exclusive to, suitably small iron oxide nano particles. As most iron oxide nano particles are made from ferromagnetic iron it is understandable to assume they would behave in a similar fashion. This is not the case. The dipole moments within a ferromagnetic compound such as iron spontaneously arrange themselves parallel to each other within domains. Once placed in an external magnetic field the domains align parallel to each other and the material becomes magnetically susceptible. Depending on the material used these domains have a minimum size associated with them. For iron oxide this is about 128 nm. Below this size an iron oxide nano particle consists of a single magnetic domain acting like a giant magnetic moment with a rapid response to external magnetic fields. The iron oxide nano particle is now superparamagnetic and can be considered to be a hybrid of ferromagnetism (large magnetic susceptibility) and paramagnetism (no domains).

It is important to note that although iron oxide nano particles (<128 nm) have large magnetic moments they are not magnetic. In a paramagnetic compound the magnetic dipoles randomize due to thermal process resulting in zero net magnetic moment which occurs in magnetic nano particles. However, magnetic nano particles are in a single domain state so all of the dipoles are aligned parallel. In order to have zero net magnetization all of these dipoles must flip simultaneously which results in

the nano particle having two isoenergetic orientations anti-parallel to each other. At room temperature these flips occur rapidly and no net magnetic moment is detectible. Interestingly at sufficiently low temperatures this rapid flipping of dipole moments can be prevented resulting in a measurable net magnetic moment.

6.1.4 Photochemical microflow system utilising silica and iron oxide nano structured solid supports

Based upon experimental results of Section 5.3 the heterogeneous dye sensitized photooxygenation of 1,5-DHN, β-citronellol and α-terpinene was performed in the photochemical microflow reactor using TCPP functionalised silica and iron oxide nano particles.

6.2 Results and discussion

6.2.1 Heterogeneous dye sensitized photooxygenations using the photochemical microflow system and TCPP-APTES SNPs

TCPP-APTES SNPs (synthesized in Section 4.2.3.1) were used as solid support sensitizers for the heterogeneous dye sensitized photooxygenations of 1,5-DHN, β-citronellol and α-terpinene. A stock solution of TCPP-APTES SNPs (4 mg/ml) was prepared in IPA. Solutions of starting materials were prepared in 5 ml volumetric flasks using this functionalised SNP stock solution in a dark room. The solutions were then covered in foil to prevent any photochemical reactions due to external light sources. These solutions were then pumped though the photochemical microflow system at a total flow rate of 0.312 ml/min corresponding to a residence time of 15.82 minutes. The crude reaction mixture was collected in amber Eppendorf vials and the functionalised SNPs were separated from the reaction media by centrifugation at 9,000 rpm for 5 minutes. The supernatant was removed and UV-Vis and/or ^{1}H NMR spectroscopy were used to determine percent conversions to products.

6.2.1.1 Heterogeneous dye sensitized photooxygenation of 1,5-DHN

Scheme 6.1: Heterogeneous dye sensitized photooxygenation of 1,5-DHN.

10 and 20 mM solutions of 1,5-DHN were prepared in 5 ml volumetric flasks in a dark room using the stock solution of functionalised SNPs in IPA. The solution was then covered in foil and pumped through the microflow system. ^{1}H NMR confirmed percent conversions of 16 and 7 %. As expected the TCPP-APTES SNPs showed a loss in efficacy compared to homogeneous experiments performed in Chapter 5. However, sensitizer free experiments also performed in Chapter 5 showed that in the

case of 1,5-DHN no self sensitization occurs when using the photochemical microflow reactor, with the 419 nm lamp, proving that any product formed during the reaction was due to the sensitizing ability of the TCPP-APTES SNPs.

Table 6.2: Heterogeneous dye sensitized photooxygenation of 1,5-DHN.

Exp No	Starting material (mM)	Residence time (min)	Flow rate (ml/min)	% Conversion
106	10	15.82	0.312	16
107	20	15.82	0.312	7

6.2.1.2 Heterogeneous dye sensitized photooxygenation of β-citronellol

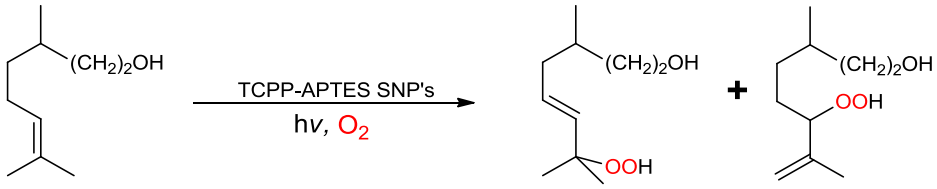

Scheme 6.2: Heterogeneous dye sensitized photooxygenation of β-citronellol.

26 and 52 mM solutions of β-citronellol were prepared in 5 ml volumetric flasks in a dark room using the stock solution of functionalised SNPs in IPA. The solutions were then covered in foil and pumped through the microflow system at a flow rate of 0.312 ml/min. ^{1}H NMR confirmed percent conversions of 23 and 16 % (Table 6.3). Again, these were relatively low results when compared to homogeneous experiments performed in Chapter 5. However, similar to 1,5-DHN, sensitizer free experiments show that β-citronellol does not self sensitize to products in the photochemical microflow reactor demonstrating that the products formed were due to the sensitizing ability of the TCPP-APTES SNPs.

Table 6.3: Heterogeneous dye sensitized photooxygenation of β-citronellol.

Exp No	Starting material (mM)	Residence time (min)	Flow rate (ml/min)	Conversion (%)
108	26	15.82	0.312	23
109	52	15.82	0.312	16

6.2.1.3 Heterogeneous dye sensitized photooxygenation of α-terpinene

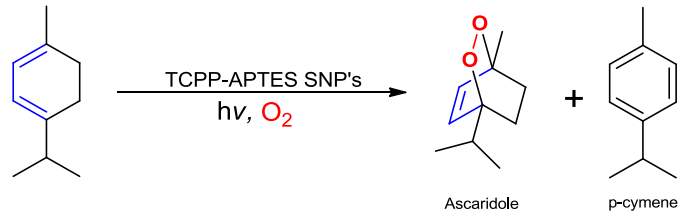

Scheme 6.3: Heterogeneous dye sensitized photooxygenation of α-terpinene.

26 and 52 mM Solutions of α-terpinene were prepared in 5 ml volumetric flasks in a dark room using the stock solution of functionalised SNPs in IPA. The solutions were then covered in foil and pumped through the microflow system at a flow rate of 0.312 ml/min. UV-Vis spectroscopic analysis confirmed percent conversion of 97 and 48 % respectively. ^{1}H NMR confirmed *p*-cymene to ascaridole ratios of 12:88 and 4:96 respectively, (Table 6.4) which are in agreement with results of Section 5.3.6. Utilisation of TCPP as sensitizer increases the quantity of *p*-cymene produced. These percent conversions were significantly higher than that of either 1,5-DHN or β-citronellol reactions. It should be noted that in Section 5.3.3.1 percent conversions of up to 31 % were achieved during sensitizer free photooxygenations of α-terpinene using the 419 nm fluorescent lamp, not all conversion is due to the SNPs.

Table 6.4: Heterogeneous dye sensitized photooxygenation of α-terpinene.

Exp No	Starting material (mM)	Residence time (min)	Conversion (%)	*p*-cymene/Ascaridole (%)
110	26	15.82	97	12:88
111	52	15.82	48	4:96

6.2.1.4 Energy efficiency and STY calculations for the heterogeneous dye sensitized photooxygenations of 1,5-DHN, β-citronellol and α-terpinene

Energy efficiencies and STYs were calculated for all heterogeneous dye sensitized photooxygenations using TCPP-APTES SNPs in the photochemical microflow system. These results were compared to the optimum results obtained from the homogeneous dye sensitized photooxygenations performed in Schlenk flasks. The results can be seen in Figures 6.3 to 6.5. Table 6.5 illustrates the experimental conditions for each of the experiments.

Table 6.5: Experimental conditions for heterogeneous dye sensitized photooxygenations and optimised homogeneous dye sensitized photooxygenations.

Exp No	Setup	SM (mmol)	Conversion (%)	Solvent (ml)	Sensitizer	Lamp (W)	Time (hr)
22	Schlenk	0.5	65	50	RB	500	3
36	Schlenk	5.2	90	50	TPP	500	2
31	Schlenk	5.2	100	50	MB	500	2
106	MF	0.05	16	5	TCPP-SNP	8	0.26
107	MF	0.10	7	5	TCPP-SNP	8	0.26
108	MF	0.13	27	5	TCPP-SNP	8	0.26
109	MF	0.26	16	5	TCPP-SNP	8	0.26
110	MF	0.13	97	5	TCPP-SNP	8	0.26
111	MF	0.26	48	5	TCPP-SNP	8	0.26

The results in Table 6.5 demonstrate that the TCPP-APTES SNPs were not as efficient as homogenous dye sensitized systems detailed in Chapter 5. However, despite this loss of efficacy the TCPP-APTES SNPs, when used in conjunction with the photochemical microflow reactor provided superior energy efficiencies compared to the optimised Schenck flask setups.

Figure 6.3 demonstrates that the heterogeneous dye sensitized photooxygenations of 1,5-DHN, β-citronellol and α-terpinene are significantly more energy efficient than

that of results obtained from optimised homogeneous Schlenk flask syntheses with respect to product formed per lamp power (mmol.W^{-1}.hr^{-1}). The results show that the heterogeneous dye sensitized photooxygenations are 19, 6.25 and 12.89 times more energy efficient than optimised homogeneous Schlenk flask syntheses.

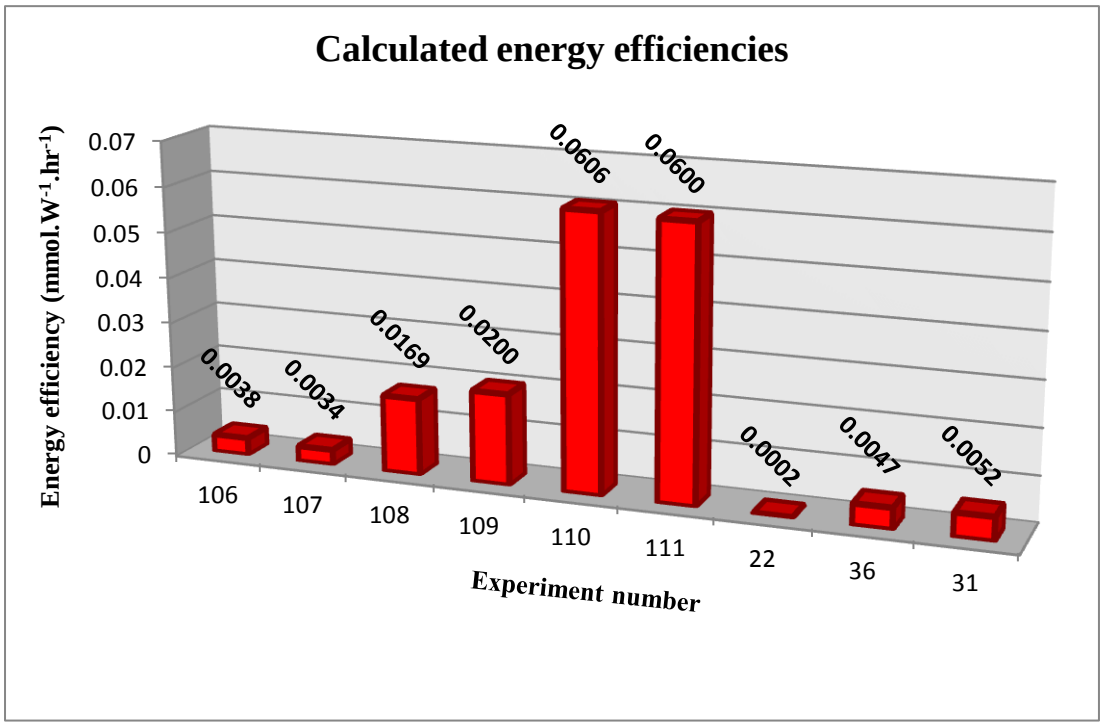

Figure 6.3: Product formed per lamp power (mmol.W^{-1}.hr^{-1}).

Figure 6.4 shows the results of the heterogeneous dye sensitized photooxygenations of 1,5-DHN, β-citronellol and α-terpinene. These reactions are more energy efficient than the homogeneous dye sensitized photooxygenations performed in the Schlenk flasks with respect to product formed per irradiated area (mmol.W^{-1}.hr^{-1}.cm^{-2}). The heterogeneous dye sensitized photooxygenations are 6.03, 1.66 and 3.96 times more energy efficient than the optimised homogeneous Schlenk flask syntheses.

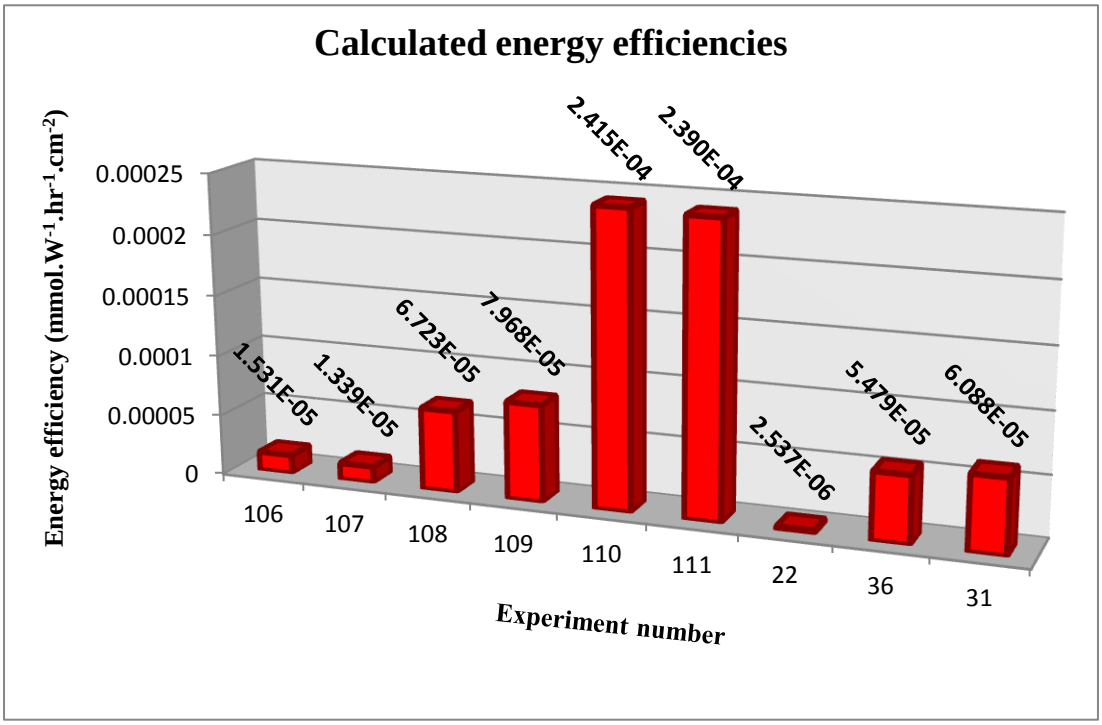

Figure 6.4: Product formed per irradiated area (mmol.W^{-1}.hr^{-1}.cm^{-2}).

STYs were also calculated for the heterogeneous dye sensitized photooxygenations of 1,5-DHN, β-citronellol and α-terpinene and were compared to the ,results obtained from traditional (Schlenk flask) optimised homogeneous syntheses (Figure 6.5). The results illustrate that the heterogeneous dye sensitized photooxygenations of 1,5-DHN and α-terpinene provided superior STYs compared to traditional (Schlenk flask) dye sensitized photooxygenations. In the case of α-terpinene, a percent conversion of 97 % was achieved in 15.82 minutes. These results provide a unique and advantageous situation where the TCPP-APTES SNPs could be retrieved from the reaction mixture via centrifugation and could then be easily recycled resulting in the elimination of column chromatography and associated chemical waste.

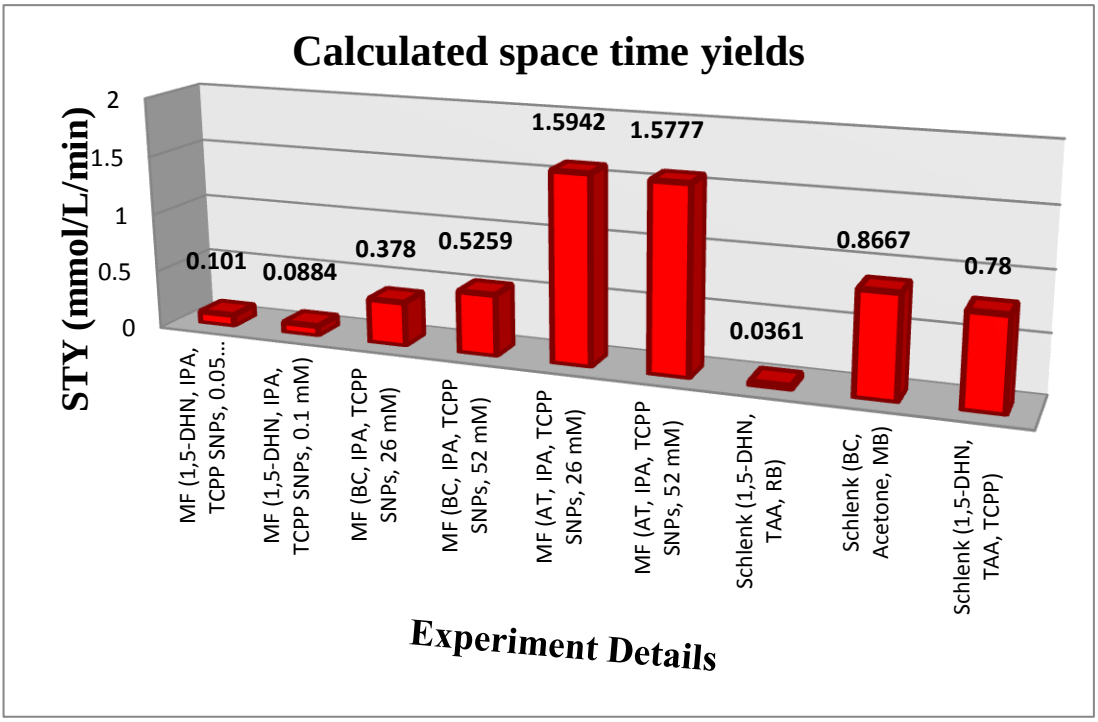

Figure 6.5 Calculated space time yields for the heterogeneous dye sensitized photooxygenations and optimised homogeneous photooxygenations of 1,5-DHN, β-citronellol and α-terpinene.

6.2.2 Synthesis, functionalisation and characterisation of iron oxide magnetic nano particles

6.2.2.1 Synthesis of APTES functionalised iron oxide magnetic nano particles

APTES functionalised iron oxide nano particles (APTES MNPs) with an average diameter of 20 nm were supplied by the research group of Dr. Dermot Brougham. These were supplied as a dispersion of nano particles in MilliQ water (~3.5 mg/ml). These silica coated iron oxide magnetic nano particles were synthesized using a modified thermal decomposition procedure first reported by Pinna *et al* and is described in detail in Section 6.4.2. Dynamic light scattering measurements performed show that the APTES MNPs have diameters below 100 nm with an average diameter of ~20 nm (Figure 6.4). Field emission scanning electron microscopy (FeSEM) images were also obtained in order to illustrate visually the size and dispersity of the APTES MNPs (Figure 6.6).

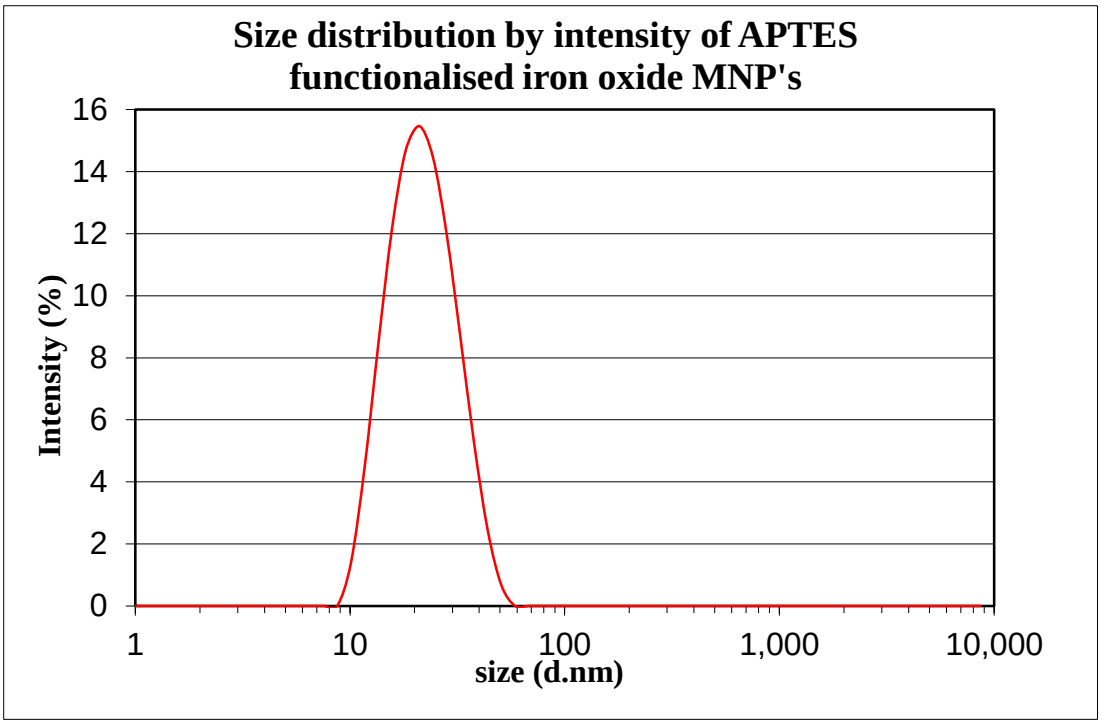

Figure 6.6: DLS measurements of APTES functionalised MNPs.

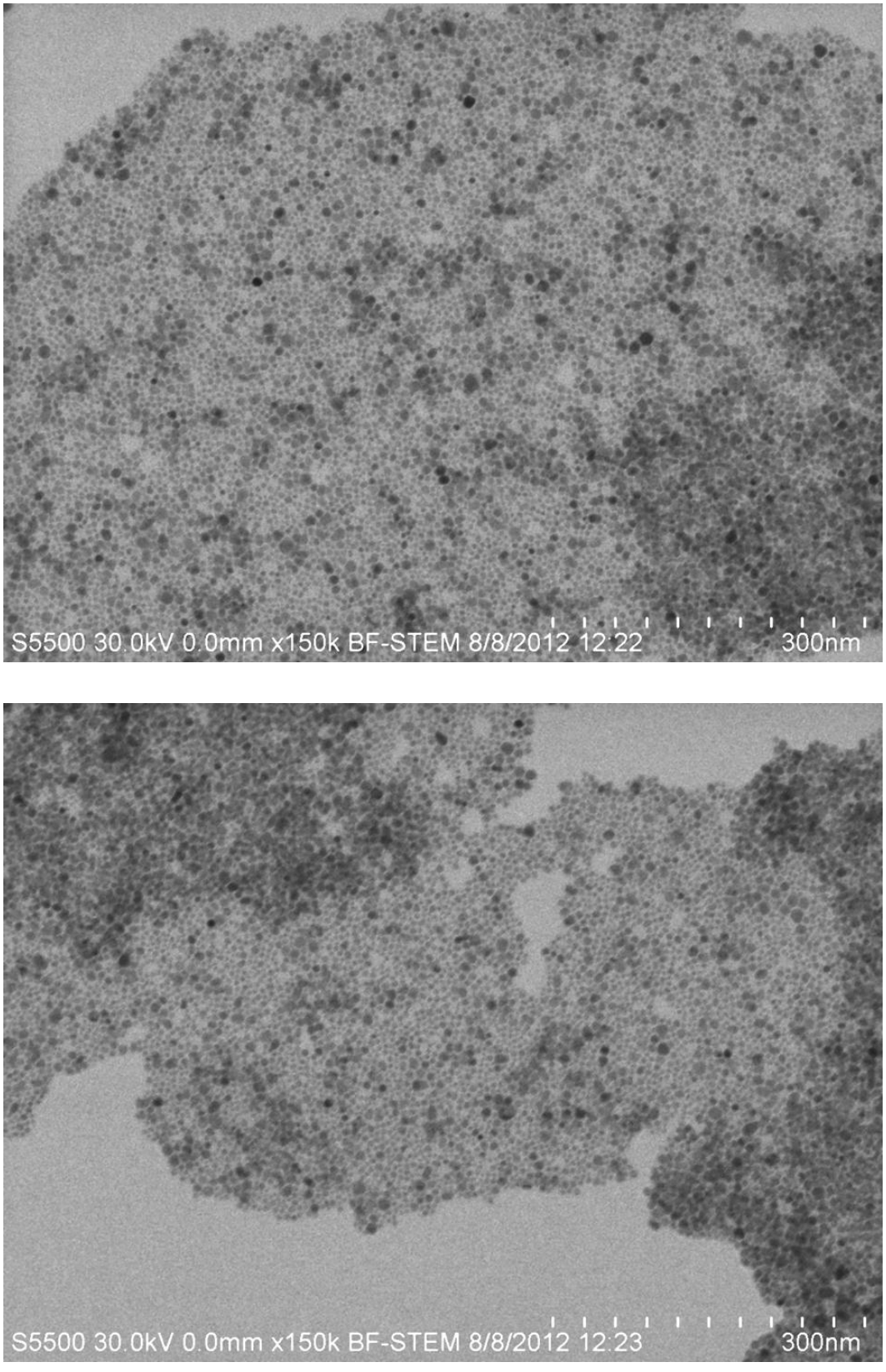

Figure 6.7: FeSEM images of APTES functionalised MNPs.

6.2.2.2 Functionalisation of APTES-MNPs with TCPP

APTES MNPs were functionalised with TCPP using EDC/NHS coupling chemistry (Experiment 112). This was similar to the functionalisation of APTES-SNPs described in Section 4.2.3.1.

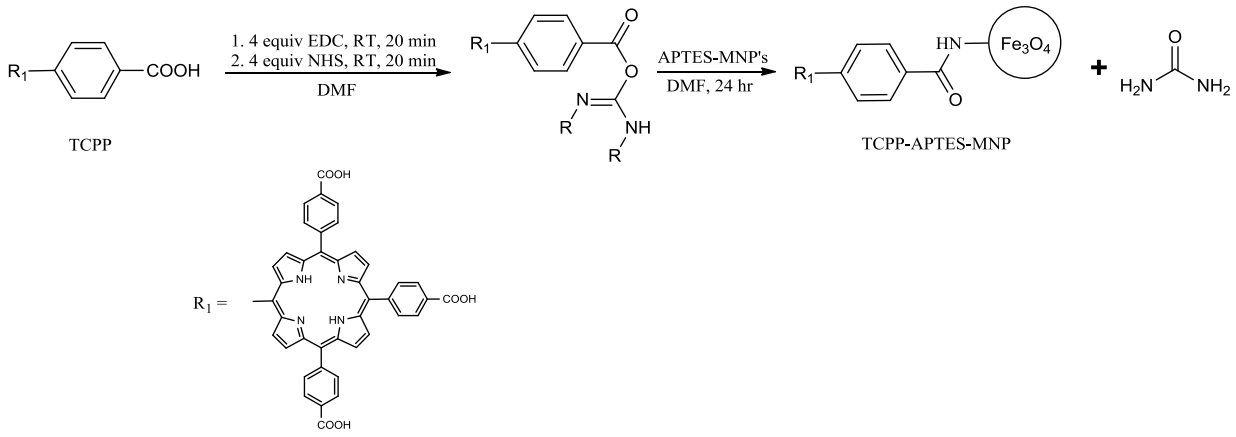

Scheme 6.4: EDC/NHS coupling of TCPP to APTES-MNPs.

Briefly, 10 mg of TCPP (0.0126 mmol) was dissolved in 4 ml of dry DMF. To this 4 equivalents of EDC (9.6 mg, 0.05 mmol) were added. The solution was allowed to stir for 20 minutes followed by the addition of 4 equivalents of NHS (5.8 mg, 0.05 mmol). The solution was allowed to stir for a further 20 minutes before the addition of 1 ml of the supplied APTES MNP solution. This was left to stir overnight and the resulting TCPP-APTES MNPs were separated by centrifugation at 14,680 rpm for 10 minutes. These particles were then re-dispersed in ethanol and re-centrifuged at 14,680 rpm for 5 minutes. This process was repeated 5 times to remove all free TCPP from the functionalised MNPs. UV-Vis spectroscopy of the final washings confirmed that no TCPP was present. FT-IR spectroscopy (KBr) confirmed that covalent immobilisation of TCPP onto the APTES functionalised MNPs was successful. Figure 6.8 depicts the Fe-O stretching vibration of the iron oxide nano particles at 591 cm^{-1}. In addition the absorbance peak at 1118 cm^{-1} corresponds to the Si-O-Si symmetric stretching vibration, confirming the presence of a silicate shell around the MNPs. The strong absorbance peak at 1631 cm^{-1} is due to the N-H bending of the primary amine of the APTES, further indication of the presence of a

shell of APTES around the MNPs. The two absorbance peaks normally seen for primary amines between 3300 and 3500 cm^{-1} are masked by the presence of a large –OH peak due to –OH peaks still present on the surface of the MNPs. C-H stretching vibrations due to APTES are also observed between 2950 and 2850 cm^{-1}.

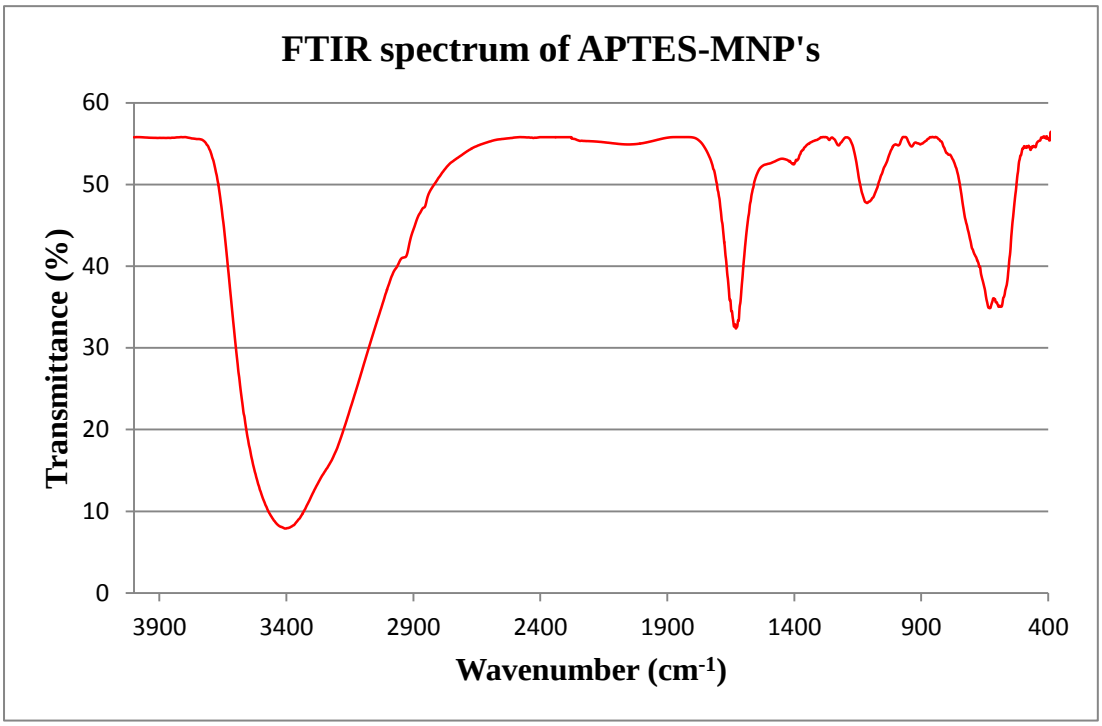

Figure 6.8: FTIR spectrum of APTES-MNPs in KBr disk.

Figure 6.9 shows the FTIR spectrum of the TCPP-APTES MNPs. It confirms that the covalent immobilisation of TCPP onto the APTES MNPs was successful. Strong absorbance peaks at 1741 and 1772 cm^{-1} correspond to the C=O stretching vibrations of the –COOH group of the TCPP and the newly formed amide bridge. The absorbance peak at 1631 cm^{-1} corresponding to N-H bending seen in Figure 6.6 is still present. However, the intensity of the peak has decreased as many of these groups have now been converted to amide bridges. The strong absorbance peak at 3449 cm^{-1} is characteristic of carboxylic acid –OH groups further confirming the presence of TCPP.

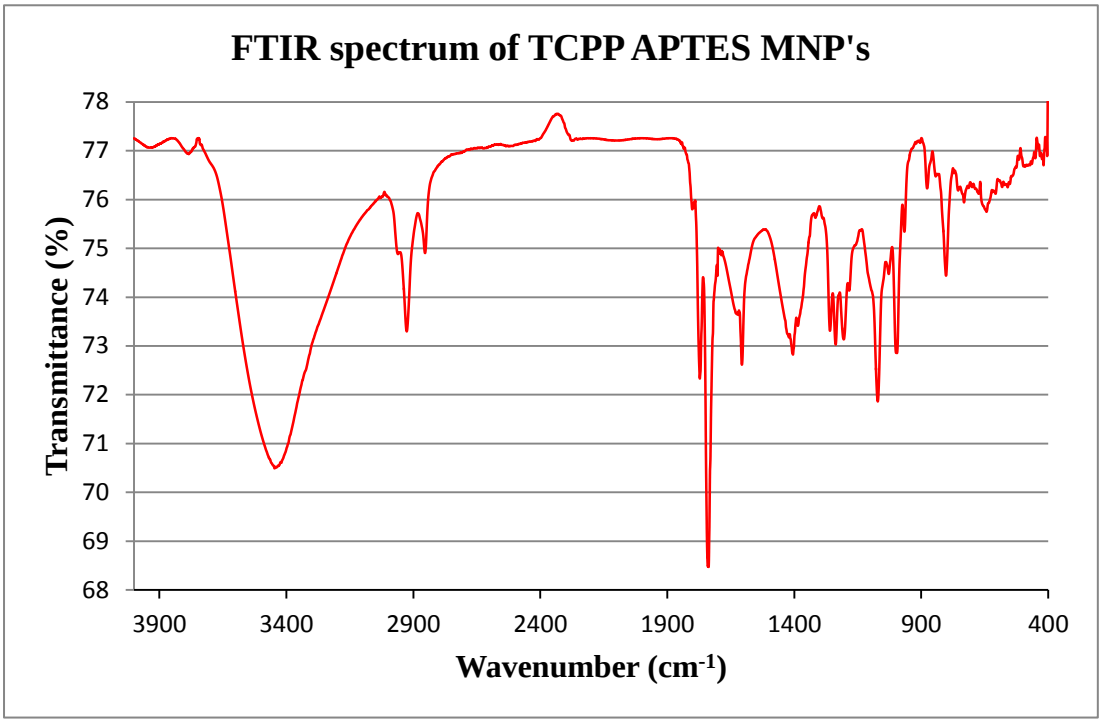

Figure 6.9: FTIR spectrum of TCPP APTES MNPs in KBr disk.

Diffuse reflectance UV-Vis spectroscopy was also employed to determine if the covalent immobilisation of TCPP onto APTES MPN's was successful. Figure 6.10 shows the diffuse reflectance UV-Vis spectra of both APTES and TCPP APTES MNPs. It shows the Soret band (430 nm) and the four Q bands (520, 558, 549 and 649 nm) of TCPP indicating that the immobilisation of TCPP onto the APTES MNPs was successful.

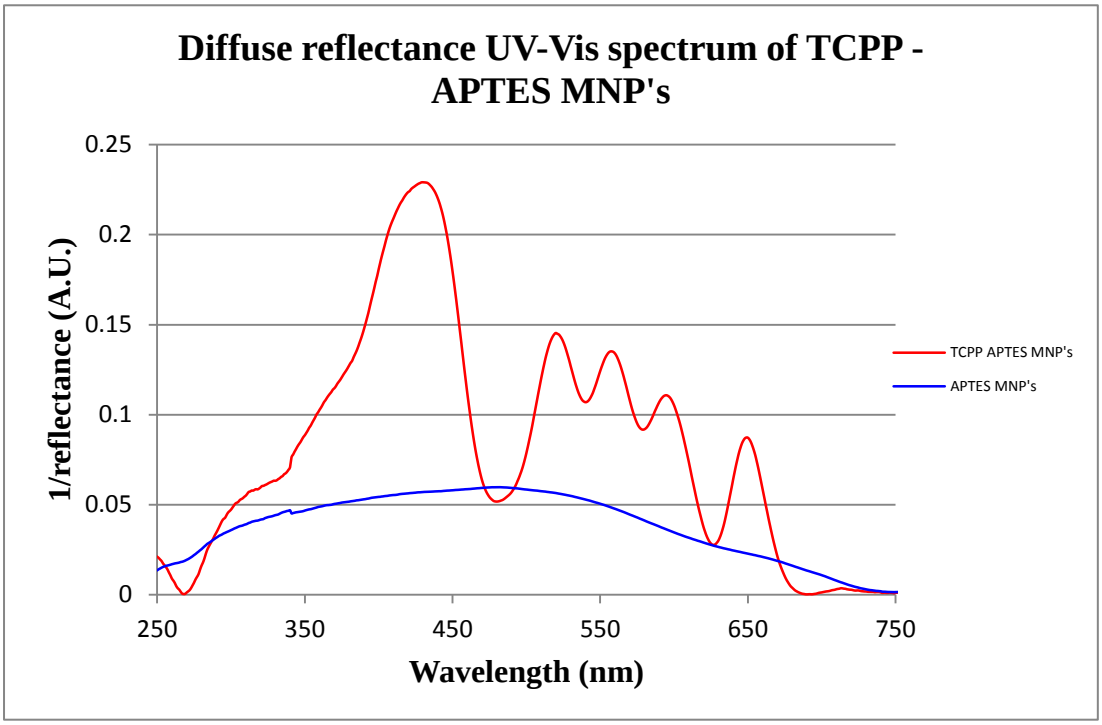

Figure 6.10: Diffuse reflectance UV-Vis spectra of TCPP and APTES MNPs.

In addition to FT-IR and diffuse reflectance UV-Vis spectroscopy FeSEM images of the TCPP-APTES MNPs were also obtained (Figure 6.11). These images show that the MNPs are embedded within an organic matrix. It appears that there is a polymeric film surrounding the APTES MNPs. When dispersed in solution the TCPP-APTES MNPs appears as a clear purple liquid. However, when placed into a sufficiently strong magnetic field (≥ 0.7 Tesla) or centrifuged at an appropriate speed these particles agglomerate and form a deep purple coloured film at the edge of the glass vial.

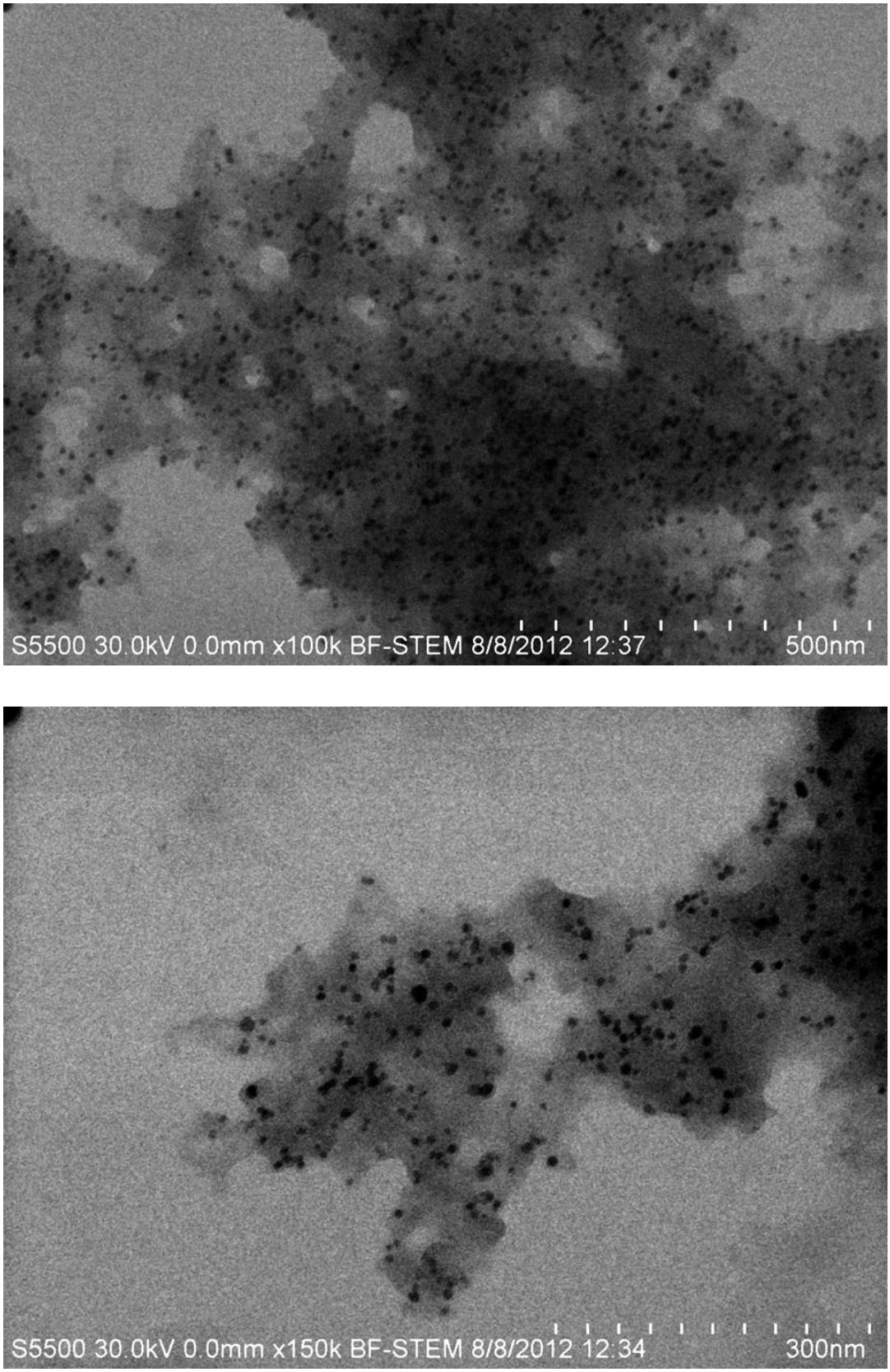

Figure 6.11: FeSEM images of TCPP functionalised MNPs.

6.2.3 Heterogeneous dye sensitized photooxygenations using the photochemical microflow system and TCPP-APTES MNPs

The heterogeneous dye sensitized photooxygenations of 1,5-DHN, β-citronellol and α-terpinene were performed utilizing TCPP-APTES MNPs with the photochemical microflow reactor. A stock solution of TCPP-APTES MNPs (~2 mg/ml) was prepared in IPA. Solutions of starting materials were prepared in 5 ml volumetric flasks using this functionalised MNP stock solution in a dark room. These solutions were then covered in foil and pumped though the photochemical microflow system (0.312 ml/min) and collected in amber Eppendorf vials. The functionalised MNPs were separated from the reaction media by centrifugation at 14,680 rpm for 5 minutes. The supernatant was removed and UV-Vis and ^{1}H NMR spectroscopy were used to determine percent conversions. Although the TCPP-APTES MNP' can be separated from the reaction mixture using an external magnetic field, centrifugation was utilized as it was a faster process. In general, separation of the MNPs by magnetic field often took in excess of 60 minutes using a neodymium permanent magnet with a magnetic field strength of approximately 0.7 tesla.

6.2.3.1 Heterogeneous dye sensitized photooxygenation of 1,5-DHN

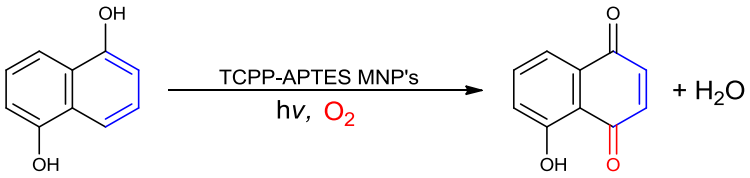

Scheme 6.5: Heterogeneous dye sensitized photooxygenation of 1,5-DHN.

10 and 20 mM solutions of 1,5-DHN were prepared in 5 ml volumetric flasks in a dark room using the stock solution of functionalised MNPs in IPA. The solutions were then covered in foil and pumped through the microflow system at a flow rate of 0.312 ml/min ^{1}H NMR (acetone d_6) confirmed percent conversions of 21 and 9 %.

Table 6.6: Heterogeneous dye sensitized photooxygenation of 1,5-DHN.

Exp No	Starting material (mM)	Residence time (min)	Flow rate (ml/min)	% Conversion
113	10	15.82	0.312	21
114	20	15.82	0.312	9

6.2.3.2 Heterogeneous dye sensitized photooxygenation of β-citronellol

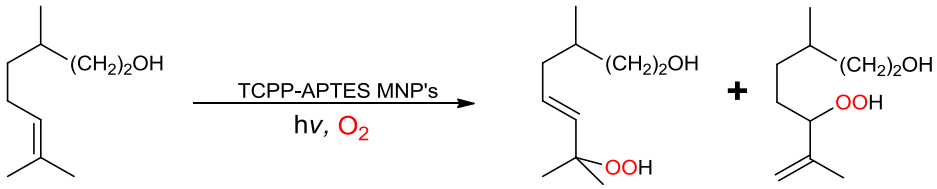

Scheme 6.6: Heterogeneous dye sensitized photooxygenation of β-citronellol.

26 and 52 mM solutions of β-citronellol were prepared in 5 ml volumetric flasks in a dark room using the stock solution of functionalised MNPs in IPA. The solutions were then covered in foil and pumped through the microflow system at a flow rate of 0.312 ml/min. ^{1}H NMR confirmed percent conversions of 11 and ~5 % (Table 6.7).

Table 6.7: Heterogeneous dye sensitized photooxygenation of β-citronellol.

Exp No	Starting material (mM)	Residence time (min)	Flow rate (ml/min)	Conversion (%)
115	26	15.82	0.312	11
116	52	15.82	0.312	~5

6.2.3.3 Heterogeneous dye sensitized photooxygenation of α-terpinene

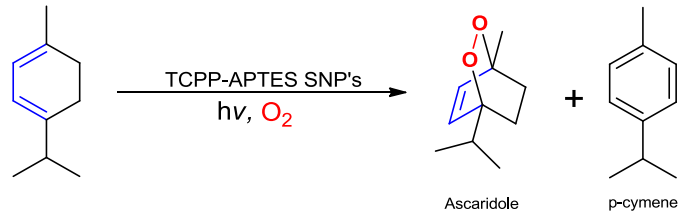

Scheme 6.7: Heterogeneous dye sensitized photooxygenation of α-terpinene.

26 and 52 mM solutions of α-terpinene were prepared in 5 ml volumetric flasks in a dark room using the stock solution of functionalised MNPs in IPA. The solutions were then covered in foil and pumped through the microflow system at a flow rate of 0.312 ml/min. UV-Vis spectroscopic analysis confirmed percent conversions of 40 and 32 % (Table 6.8). ^{1}H NMR confirmed *p*-cymene to ascaridole ratios of 19:81 and 10:90 respectively.

Table 6.8: Heterogeneous dye sensitized photooxygenation of α-terpinene.

Exp No	Starting material (mM)	Conversion (%)	*p*-cymene/Ascaridole (%)
117	26	40	19:81
118	52	32	10:90

These were significantly higher percent conversions than that of either 1,5-DHN or β-citronellol. However, the results of Section 5.3.3.1 have shown that in the case of α-terpinene non Type II processes occur under non sensitized conditions may contribute to these increased percent conversions.

6.2.3.4 Energy efficiency and STY calculations for the heterogeneous dye sensitized photooxygenations of 1,5-DHN, β-citronellol and α-terpinene

Energy efficiencies and STYs were calculated for all heterogeneous dye sensitized photooxygenations using TCPP-APTES MNPs in the photochemical microflow system. The results are illustrated in Figures 6.12 to 6.14. Table 6.9 illustrates the experimental conditions for each of the experiments performed.

Table 69: Experimental conditions for heterogeneous dye sensitized photooxygenations and optimised homogeneous dye sensitized photooxygenations.

Exp No	Setup	SM (mmol)	Conversion (%)	Solvent (ml)	Sensitizer	Lamp (W)	Time (hr)
22	Schlenk	0.5	65	50	RB	500	3
36	Schlenk	5.2	90	50	TPP	500	2
31	Schlenk	5.2	100	50	MB	500	2
113	MF	0.05	21	5	TCPP-MNP	8	0.26
114	MF	0.10	9	5	TCPP-MNP	8	0.26
115	MF	0.13	4	5	TCPP-MNP	8	0.26
116	MF	0.26	5	5	TCPP-MNP	8	0.26
117	MF	0.13	40	5	TCPP-MNP	8	0.26
118	MF	0.26	32	5	TCPP-MNP	8	0.26

Figure 6.12 demonstrates that the heterogeneous dye sensitized photooxygenations of 1,5-DHN, β-citronellol and α-terpinene using the photochemical microflow system are significantly more energy efficient than that of optimised homogeneous Schlenk flask syntheses. The results show that the heterogeneous dye sensitized photooxygenations are 25, 1.5 and 7.7 times more energy efficient than optimised homogeneous Schlenk flask syntheses with respect to product formed per lamp power ($mmol.W^{-1}.hr^{-1}$).

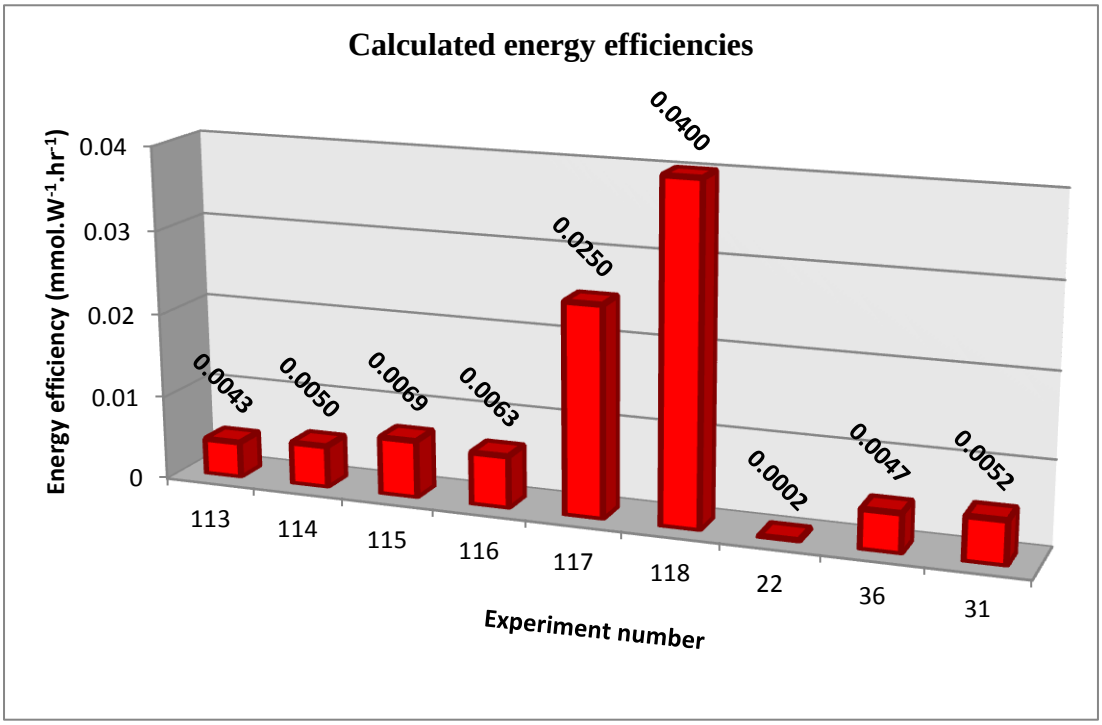

Figure 6.12: Product formed per lamp power (mmol.W^{-1}.hr^{-1}).

Similar to Figure 6.12 the results of Figure 6.13 show that the heterogeneous dye sensitized photooxygenations of 1,5-DHN and α-terpinene are more energy efficient than homogeneous dye sensitized photooxygenations performed in Schlenk flasks with respect to product formed per irradiated area (mmol.W^{-1}.hr^{-1}.cm^{-2}). The heterogeneous dye sensitized photooxygenations are 7.9 and 2.6 times more energy efficient than optimised homogeneous syntheses.

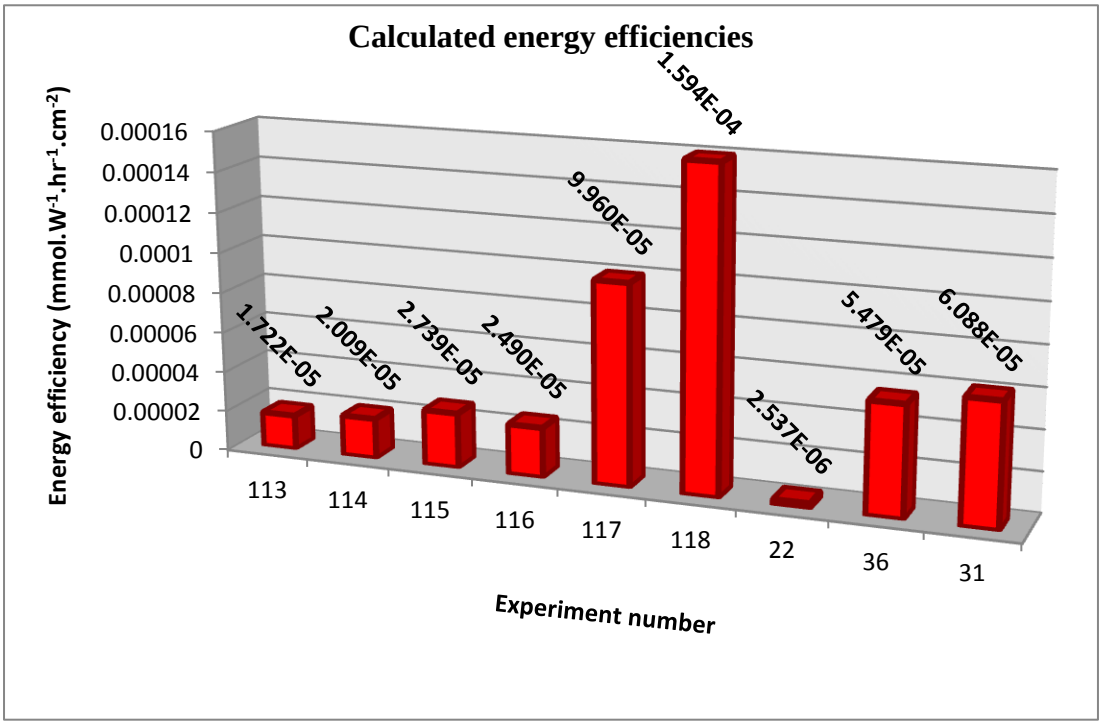

Figure 6.13: Product formed per irradiated area (mmol.W^{-1}.hr^{-1}.cm^{-2}).

Similar to TCPP-APTES SNPs, calculated space time yields for TCPP-APTES MNPs are superior to traditional batch scale (Schlenk flask) systems in the case of the photooxygenations of 1,5-DHN and α-terpinene (Figure 6.14). The photooxygenation of β-citronellol did not show superior results. Reasons for superior STYs for the photooxygenation of 1,5-DHN and α-terpinene were discussed in Section 6.2.1.4.

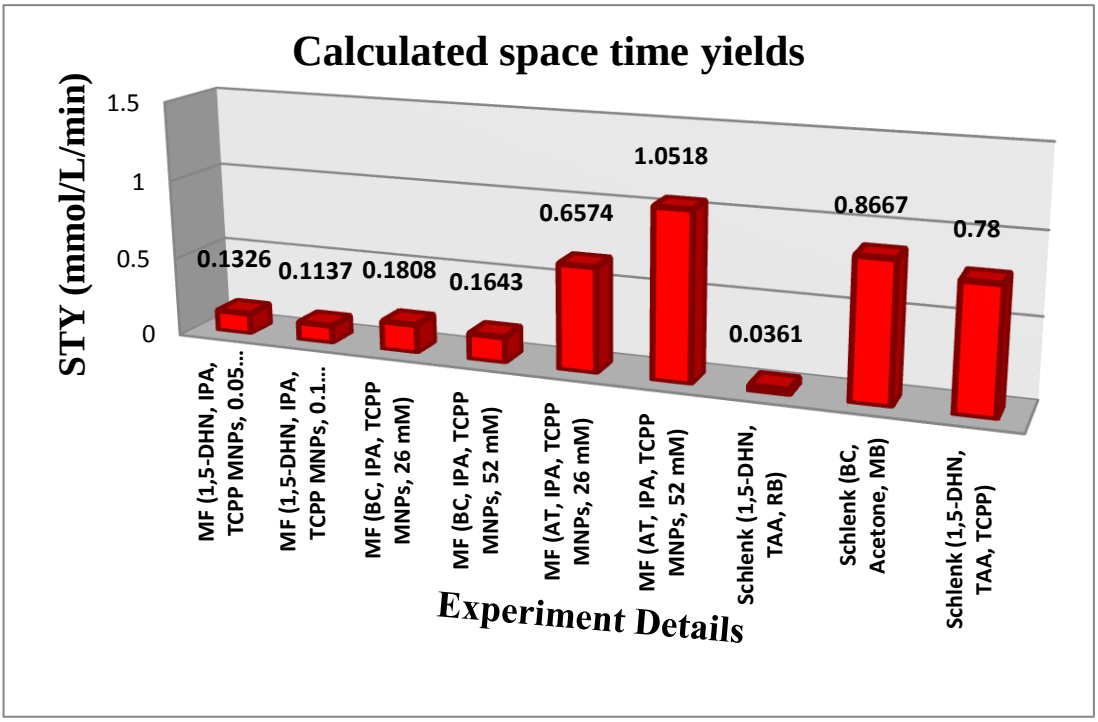

Figure 6.14: Calculated space time yields for the heterogeneous dye sensitized photooxygenations and optimised homogeneous photooxygenations of 1,5-DHN, β-citronellol and α-terpinene.

The results of Sections 6.2.1 and 6.2.3 clearly demonstrate that the TCPP functionalised SNPs provided superior yields over the TCPP functionalised MNPs. This may be attributed to two factors. 1) The concentration of the SNP stock solution was higher at 4 mg/ml compared to 2mg/ml for the MNPs. 2) The silica particles were white prior to functionalisation with TCPP. In contrast the MNPs were black. This may have resulted in the absorption of available light by the iron oxide nano particles, reducing the quantity of light available for sensitization.

However, it should be noted that in both cases sensitization to products was achieved. These were significant results as re-circulation of the reaction mixture through the microflow system would allow for complete conversion to products. As discussed previously the solid supported sensitizers could be removed by centrifugation or an external magnetic field. This would eliminate the requirement for column chromatography and associated wastes.

6.3 Conclusion

The synthesis and characterisation of TCPP functionalised iron oxide nano particles with an average diameter of ~20 nm was performed and described. These nano particles in addition to TCPP functionalised silica nano particles synthesised and characterised in Section 4.2 were used as nano structured solid support sensitizers for the heterogeneous dye sensitized photooxygenations of 1,5-DHN, β-citronellol and α-terpinene using the newly developed photochemical microflow reactor.

Initial results demonstrated that the novel TCPP functionalised SNPs and MNPs provided poor conversion of 1,5-DHN and β-citronellol to products in comparison to homogeneous dye sensitized photooxygenation using the photochemical microflow reactor. In contrast, the heterogeneous dye sensitized photooxygenation of a 26 mM solution of α-terpinene showed percent conversions of up to 97 % utilising TCPP SNPs as sensitizer. A percent conversion of 40 % was achieved for the same concentration of α-terpinene using TCPP functionalised MNPs. These superior percent conversions for α-terpinene, compared to both 1,5-DHN and β-citronellol, may be due to self sensitization and non Type II photooxygenation processes.

Despite the low percent conversions of the heterogeneous sensitised reactions in the photochemical microflow reactor, energy efficiency and space time yield calculations gave interesting results for these reactions.

These calculations demonstrated that for 1,5-DHN and α-terpinene, utilisation of TCPP functionalised SNPs and MNPs as solid support sensitizers in the photochemical microflow reactor was more efficient than homogeneous Schlenk flask systems. Calculations demonstrated that in the case of α-terpinene, the TCPP functionalised SNPs were ~13 times more efficient with respect to product formed per lamp power and ~ 4 times more efficient with respect to product formed per irradiated area. In addition calculated STYs were double that of results obtained from traditional Schlenk flask systems. Calculations also showed that in the case of 1,5-DHN the photochemical microflow reactor was ~19 times more efficient with respect to product formed per lamp power and ~ 6 times more efficient with respect

to product formed per irradiated area. STYs were more than double those calculated for Schlenk flask systems. In addition, STYs calculated for the homogeneous dye sensitized photooxygenations of 1,5-DHN and β-citronellol using flat bed reactor technology (Appendix D) show that results obtained from the photochemical microflow system with TCPP functionalised SNPs and MNPs are superior.

These results clearly illustrate that environmentally friendly; low energy demanding heterogeneous dye sensitized photooxygenations can be performed successfully using the newly developed photochemical microflow system. Despite low percent conversions compared to traditional homogeneous systems (both indoor and solar), the photochemical microflow reactor provides significantly superior energy efficiencies and STYs. In addition, by simply re-circulating the reaction mixture or by increasing the length of the capillary coil complete conversions could be achieved. Furthermore, column chromatography is eliminated and purification of the reaction mixtures is achieved by centrifugation or filtration thus allowing for the catalytic synthesis of several fine chemicals without the generation of any form of chemical waste.

6.4 Experimental

6.4.1 Dye sensitized photooxygenations using the photochemical microflow system and silica nano particles as solid support sensitizers

General procedure

TCPP-APTES SNPs synthesized in Section 4.2.3.1 were utilised as solid support sensitizers for the heterogeneous dye sensitized photooxygenations of 1,5-DHN, β-citronellol and α-terpinene using the photochemical microflow system. A stock solution of TCPP-APTES SNPs (4 mg/ml) was prepared in IPA. Next, solutions of 1,5-DHN, β-citronellol and α-terpinene of know concentration were made up in 5 ml volumetric flasks using the functionalised SNP stock solution in a dark room. These were covered in foil and pumped through the microflow system at a flow rate of 0.312 ml/min. The crude product was collected in amber Eppendorf vials and centrifuged at 9,000 rpm for 5 minutes. The supernatant was removed using a pipette and analysed by UV-Vis and/or ^{1}H NMR spectroscopy to determine percent conversion to product(s).

Experiment 106 Heterogeneous dye sensitized photooxygenation of 1,5-DHN

A solution of 1,5-DHN (10 mM) was prepared and pumped through the photochemical microflow system. ^{1}H NMR (acetone-d_6) confirmed a percent conversion of 16 %.

Experiment 107 Heterogeneous dye sensitized photooxygenation of 1,5-DHN

A solution of 1,5-DHN (20 mM) was prepared and pumped through the photochemical microflow system. ^{1}H NMR (acetone-d_6) confirmed a percent conversion of 7 %.

Experiment 108 Heterogeneous dye sensitized photooxygenation of β-citronellol

A solution of β-citronellol (26 mM) was prepared and pumped though the photochemical microflow system. ^{1}H NMR ($CDCl_3$) confirmed a 23 % conversion.

Experiment 109 ***Heterogeneous dye sensitized photooxygenation of β-citronellol***

A solution of β-citronellol (52 mM) was prepared and pumped though the photochemical microflow system. ^{1}H NMR ($CDCl_3$) confirmed a 16 % conversion.

Experiment 110 ***Heterogeneous dye sensitized photooxygenation of α-terpinene***

A solution of α-terpinene (26 mM) was prepared and pumped through the photochemical microflow system. UV-Vis spectroscopy confirmed a percent conversion of 97 %. ^{1}H NMR ($CDCl_3$) confirmed a *p*-cymene to ascaridole ratio of 12:88.

Experiment 111 ***Heterogeneous dye sensitized photooxygenation of α-terpinene***

A solution of α-terpinene (52 mM) was prepared and pumped through the photochemical microflow system. UV-Vis spectroscopy confirmed a percent conversion of 48 %. ^{1}H NMR ($CDCl_3$) confirmed a *p*-cymene to ascaridole ratio of 4:96.

6.4.2 Synthesis and functionalisation of iron oxide magnetic nano particles

6.4.2.1 Synthesis of benzyl alcohol stabilised iron oxide nano particles

A modified protocol of the method first developed by Pinna *et al* was used.[15] In a typical synthesis 1 g (2.832 mmol) of iron (III) acetylacetonate was weighed into a glass vial and then transferred to a three neck round bottom flask. 20 ml (0.193 mol) Of benzyl alcohol was transferred to the round bottom flask. A nitrogen flow system, a water cooled condenser and a high temperature thermometer (>300^{0}C) were attached to the three neck round bottom. The mixture was deoxygenated at room temperature by purging with N_2 for 15 minutes. A nitrogen atmosphere was maintained for the duration of the reaction. The heating mantle was turned to its highest settling and in all cases the reactions reached reflux at ~195 ^{0}C within 15 minutes. The reaction was allowed to reflux for 7 hours without stirring.

During the reaction, a colour change from red to black was observed. This suggests the formation of iron oxide nanoparticles. Following the reaction, the heating mantle was turned off and the reaction vessel was allowed to cool to room temperature gradually, while still under a N_2 atmosphere. The synthesised particles are known as benzyl alcohol stabilised iron oxide nanoparticles and hereby referred to as BA-MNPs. The suspensions were stored in a sealed container.

6.4.2.2 Functionalisation of benzyl alcohol stabilised iron oxide nano particles with APTES

Over time the BA-MNPs fall out of the mother liquor. They are visible as a black precipitate. The mother liquor was shaken using a vortex mixer until the precipitate was homogenous (~ 60 s). Typically 1.5 mL of the mother liquor was placed into a 1.5 mL Eppendorf™ centrifuge tube and centrifuged at 13200 rpm for 5 minutes using a tabletop Eppendorf Centrifuge 5415D. The BA-MNPs sedimented at the bottom of the flask and the resultant supernatant was removed. The centrifuge tube was filled with 1.5 mL of acetone and was mixed using a vortex mixer for 60 s. The mixture was re-centrifuged at 13200 rpm (16,100 rcf) for 5 minutes to sediment the BA-MNPs. The supernatant was removed and the above step was repeated once more. Following this all free benzyl alcohol was considered to be removed to afford bare MNPs.

APTES was added to the MNPs at 50 mg to every 20 mg MNP. To this 1.5ml of $CHCl_3$ was added and the sample was shaken for 4 hours. The excess APTES was removed by washing using methanol. Methanol was added in 3 fold excess to destabilise the APTES-MNP and collected using a magnet. This was repeated. To the washed APTES-MNP 37.5ul of 1M HCL was added to the solution and 1.5ml of water was added. Following overnight shaking the solution was centrifuged. The stabilised MNPs were centrifuged in multiple steps for 10 minutes at 13,200 rpm in order to remove aggregates. This is known as the concentrated stabilised MNP solution and was dark brown in colour; it is typically in the concentration range of 50 mM of Fe.

6.4.2.3 EDC/NHS coupling of TCPP to APTES MNPs (Experiment 112)

10 mg (0.0126 mmol) Of TCPP was dissolved in 4 ml of dry DMF and placed into a 25 ml 2-neck round bottomed flask under argon atmosphere. Four equivalents (0.05 mmol, 9.6 mg) of EDC were added in 1 ml dry DMF and the solution stirred for 20 minutes. Four equivalents (0.05 mmol, 5.8 mg) of NHS in 1 ml dry DMF was then added and the solution was stirred for a further 20 minutes. 1 ml Of the supplied APTES MNP (From Dr Dermot Brougham's group at DCU) solution in Milli-Q water was then added and the solution allowed to stir at room temperature for 24 hours. The resulting TCPP-APTES MNPs were collected by centrifugation (14,680 rpm, 10 minutes). The MNPs were then re-dispersed in ethanol and centrifuged again to remove any free porphyrin on the surface of the particles. This process was repeated 5 times. UV-Vis spectroscopic analysis of the final supernatant confirmed the absence of TCPP. The resulting TCPP-APTES MNPs were then analysed by FT-IR (KBr) and diffuse reflectance UV-Vis spectroscopy. FeSEM images were also obtained.

6.4.3 Dye sensitized photooxygenations using the photochemical microflow system and iron oxide nano particles as solid support sensitizers

General procedure

TCPP-APTES MNPs synthesized in Section 6.4.2 were utilised as solid support sensitizers for the heterogeneous dye sensitized photooxygenations of 1,5-DHN, β-citronellol and α-terpinene using the photochemical microflow system. A stock solution of TCPP-APTES MNPs (~2 mg/ml) was prepared in IPA. Next, solutions of 1,5-DHN, β-citronellol and α-terpinene of know concentration were made up in 5 ml volumetric flasks using the functionalised MNP stock solution in a dark room. These were covered in foil and pumped through the microflow system at a flow rate of 0.312 ml/min. The crude product was collected in amber Eppendorf vials and centrifuged at 14,680 rpm for 5 minutes. The supernatant was removed using a pipette and analysed by UV-Vis and/or ^{1}H NMR spectroscopy to determine percent conversion to product(s).

Experiment 113 Heterogeneous dye sensitized photooxygenation of 1,5-DHN

A solution of 1,5-DHN (10 mM) was prepared and pumped through the photochemical microflow system. ^{1}H NMR (acetone-d_6) confirmed a percent conversion of 21 %.

Experiment 114 Heterogeneous dye sensitized photooxygenation of 1,5-DHN

A solution of 1,5-DHN (20 mM) was prepared and pumped through the photochemical microflow system. ^{1}H NMR (acetone-d_6) confirmed a percent conversion of 9 %.

Experiment 115 Heterogeneous dye sensitized photooxygenation of α-terpinene

A solution of α-terpinene (26 mM) was prepared and pumped through the photochemical microflow system. UV-Vis spectroscopy confirmed a percent conversion of 40 %. ^{1}H NMR ($CDCl_3$) confirmed a *p*-cymene to ascaridole ratio of 12:88.

Experiment 116 Heterogeneous dye sensitized photooxygenation of α-terpinene

A solution of α-terpinene (52 mM) was prepared and pumped through the photochemical microflow system. UV-Vis spectroscopy confirmed a percent conversion of 32 %. ^{1}H NMR ($CDCl_3$) confirmed a *p*-cymene to ascaridole ratio of 4:96.

Experiment 117 Heterogeneous dye sensitized photooxygenation of β-citronellol

A solution of β-citronellol (26 mM) was prepared and pumped though the photochemical microflow system. ^{1}H NMR ($CDCl_3$) confirmed a 11 % conversion.

Experiment 118 Heterogeneous dye sensitized photooxygenation of β-citronellol

A solution of β-citronellol (52 mM) was prepared and pumped though the photochemical microflow system. ^{1}H NMR ($CDCl_3$) confirmed a 5 % conversion.

6.5 References

(1) Chikazumi, S.; Taketomi, S.; Ukita, M.; Mizukami, M.; Miyajima, H.; Setogawa, M.; Kurihara, Y. *J Magn Magn Mater* **1987**, *65*, 245-251.

(2) Hu, A.; Yee, G. T.; Lin, W. *J. Am. Chem. Soc.* **2005**, *127*, 12486-12487.

(3) Abu-Reziq, R.; Alper, H.; Wang, D.; Post, M. L. *J. Am. Chem. Soc.* **2006**, *128*, 5279-5282.

(4) Berry, C. B.; Curtis, A. S. G. *J. Phys. D* **2003**, *36*, R198.

(5) Cunningham, C. H.; Arai, T.; Yang, P. C.; McConnell, M. V.; Pauly, J. M.; Conolly, S. M. *Magnetic Resonance in Medicine* **2005**, *53*, 999-1005.

(6) Nitin, N.; LaConte, L. E. W.; Zurkiya, O.; Hu, X.; Bao, G. *Journal of Biological Inorganic Chemistry* **2004**, *9*, 706-712.

(7) Ethirajan, A., et al *Adv Mater* **2007**, *19*, 406-410.

(8) Roca, A. G.; Morales, M. P.; Serna, C. J. *Magnetics, IEEE Transactions on* **2006**, *42*, 3025-3029.

(9) Woo, K.; Hong, J.; Choi, S.; Lee, H.; Ahn, J.; Kim, C. S.; Lee, S. W. *Chemistry of Materials* **2004**, *16*, 2814-2818.

(10) Sun, S.; Zeng, H. *J. Am. Chem. Soc.* **2002**, *124*, 8204-8205.

(11) Sun, S.; Zeng, H.; Robinson, D. B.; Raoux, S.; Rice, P. M.; Wang, S. X.; Li, G. *J. Am. Chem. Soc.* **2004**, *126*, 273-279.

(12) Liu, Z. L.; Wang, X.; Yao, K. L.; Du, G. H.; Lu, Q. H.; Ding, Z. H.; Tao, J.; Ning, Q.; Luo, X. P.; Tian, D. Y. *Journal of Materials Science* **2004**, *39*, 2633.

(13) Lee, Y.; Lee, J.; Bae, C.J.; Park, J.; Noh, H.; Park, J.; Hyeon, T. *Advanced Functional Materials* **2005**, *15*, 503-509.

(14) Lu, A.; Salabas, E. L.; Schüth, F. *Angewandte Chemie International Edition* **2007**, *46*, 1222-1244.

(15).Pinna, N.; Grancharov, S.; Beato, P. *Chem. Mater.* **2005,** *17*, 3044-3049.

Thesis Conclusion

The homogeneous dye sensitized photooxygenations of 1,5-DHN, β-citronellol and α-terpinene were validated and optimised using a 500 W halogen lamp as the light source. The reactions were also optimized in terms of sensitizer and solvent utilised. These reactions were then assessed using the twelve principles of green chemistry. Water cooling and the high energy demand of the 500 W halogen lamp were identified as key factors that negatively impacted the overall "greenness" of the reactions. In addition, column chromatography was identified as a negative impact factor post irradiation.

Solar dye sensitized photooxygenations were then performed using both Schlenk flasks and custom built flat bed reactors designed to simultaneously irradiate large volumes of the reaction mixtures. These experiments proved that, on selected 'sunny' days, the synthesis of large quantities of fine chemicals is possible under Irish solar conditions with the direct saving of up to 1556.4 kJ/hr of electrical energy. However, the experiments still required water cooling and column chromatography post irradiation. In addition, the experiments also demonstrated that the rate of conversion was highly dependent on the quantity of solar irradiation available. Under Irish solar conditions the large quantities of global radiation required to achieve high rates of conversion were only achieved under exceptionally sunny days during the summer months of June, July and August. It is clear from the results of Chapter 2 that while solar dye sensitized photooxygenations provide an alternative energy free and cost free light source, the results are dramatically dependant on the weather conditions. The necessity of water cooling and a series of health and safety issues also outlined in Section 2.3.7.2 demonstrate that these solar reactions are not sufficiently "green" and that the setup of a pilot scale solar photochemical plant is not advisable in the Republic of Ireland.

In an attempt to eliminate column chromatography, from the above photooxygenations, a series of Merrifield resin beads were successfully functionalized with TCPP and RB in Chapter 3. It was found that complete conversion to products for the reaction of α-terpinene was achieved in under 6 hours when using 500 mg of the TCPP-MR beads in the batch Schlenck flask reactor. Interestingly, the beads also showed no loss of efficacy over 5 cycles indicating that they could be recycled a number of times. Complete conversion to product(s) provided a unique situation where purification of the reaction mixtures was achieved by simple filtration or centrifugation of TCPP-MR from the reaction mixture and the solvent removed under vacuum to afford the product in quantitative yields. Despite this advantageous result water cooling and the 500 W halogen lamp were still required.

To further investigate solid support sensitizers a series of monodisperse silica nano particles were synthesized. These were used to successfully perform the heterogeneous dye sensitized photooxygenation of α-terpinene under artificial light conditions (500 W halogen lamp). Both TCPP and TCPPZn SNPs proved to be inefficient solid support sensitizers. However, despite their lack of efficiency, it was noted that up to 83 % of the product formed was *p*-cymene. It is proposed that this increased selectivity for *p*-cymene formation is due to the close proximity of the sensitizer to the silica particles which results in the production of superoxide anions by the semi conducting silica particles. In order to increase the sensitizing efficiency of the SNPs the surface of a series of monodisperse APTES SNPs were functionalised with TCPP. Percent conversions of up to 54% and 45 %were realized with respect to TCPP-APTES SNPs and TCPP-Hex-APTES SNPs under batch conditions. The TCPP-APTES SNPs could also be removed from the reaction mixture via centrifugation, eliminating the requirement for column chromatography to remove the sensitizer. In addition, the SNP solid support sensitizers could be recycled. However, despite these results the 500 W halogen lamp and water cooling were still required. These issues were addressed by the design and implementation of a novel photochemical microflow reactor.

A new photochemical microflow reactor was designed. This photochemical microflow system utilised a single 8 W fluorescent lamp and incorporated an air inlet for dye sensitized photooxygenations. The reaction mixture was drawn through the capillary tubing via a peristaltic pump and it was this action that allowed for the introduction of air bubbles to create air slug conditions. The homogeneous dye sensitized photooxygenations of 1,5-DHN, β-citronellol and α-terpinene were performed successfully using this new microflow system. Energy efficiency calculations demonstrated that this new system was significantly more energy efficient than any previous syntheses utilizing artificial light sources. Space time yield calculations also showed that the new system was more efficient than previous solar syntheses. However, despite these promising results column chromatography was required to remove the sensitizer from the reaction mixture.

To eliminate column chromatography a combination of solid support sensitizers were applied to the photochemical microflow. The heterogeneous dye sensitized photooxygenations of 1,5-DHN, α-terpinene and β-citronellol were performed using TCPP functionalized silica and iron oxide nano particles. Despite moderate conversions for the 1,5-DHN and β-citronellol reactions, α-terpinene could be converted to ascariodole in 97% yields. The unique combination of the TCPP nano-functionalized solid supports and the photochemical microflow system provided comparable and/or superior energy efficiencies compared to previous syntheses utilising artificial light sources. In addition, calculated space time yields showed that this new combination was more efficient than solar syntheses, providing an energy efficient, low cost, controllable method for the year round synthesis of several fine chemicals via heterogeneous dye sensitized photooxygenations without the generation of chemical waste.

Appendix

A Singlet oxygen lifetimes in various solvents

Singlet oxygen lifetimes for various halogenated solvents obtained from literature. See Section 2.2.1.2 for references.

Table A1: Singlet oxygen life times in common halogenated solvents

Solvent	$^1O_2$ lifetime (μs)
CCl_4	59-900 μs
$CHCl_3$	75-265 μs
CH_2Cl_2	~100 μs

Singlet oxygen lifetimes for a selection of Pfizer's preferred solvents obtained from literature. See Section 2.2.1.2 for references.

Table A2: Singlet oxygen lifetimes in selected solvents

Solvent	$^1O_2$ Lifetimes (μs)
H_2O	4.0 – 4.2
Methanol	9-10
Ethanol	11-15
1-Butanol	18
2-Butanol	16-20
2-Propanol	22
Tert-butanol	34
Acetone	25-50
Ethyl acetate	45-50
Tert-amyl alcohol	--

B Electrical energy data

The energy usage of all equipment used in the photooxygenation of 1,5-dihydroxynaphthalene was determined using a plug in energy meter and is tabulated below.

Table B1: Energy consumption of lab equipment

Entry	Appliance	Model	Energy consumption (kW/hr)	Energy consumption (kJ/hr)
1	Halogen lamp	IQ group, 500W	0.4323	1556.4
2	Rayonet reactor	RPR200, 300 ±25 nm	0.1493	537.6
3	Medium pressure mercury lamp	Model 3040, 400 W	0.3730	1342.8
4	Heating mantle to 100°C	Yellowline MST	0.0840	302.4
5	Heating mantle maintained at 100 °C (1hr)	Yellowline MST	0.0540	194.4
6	White pump	Dymax 30, Charles Austin Pumps Ltd.	0.0200	72.0
7	Single pump A	Stellar S-20, Oscar Enterprises Inc.	0.0014	5.2
8	Single pump B	Hagen Elite 200	0.0020	7.3
9	Double pump	Hagen Elite 802	0.0035	12.6
10	Peristaltic pump	n/a	0.0217	78.12
11	Fluorescent lamp plus electric fan	n/a	0.011	39.6

C Emission spectra for lamps

Emission spectra for all lamps used in the work were obtained and are represented graphically in Figures C1-C5. Also included are the emission and absorption spectra of the 419 nm and “cool white” with the starting materials 1,5-DHN, α-terpinene and β-citronellol (Figures C6-C8).

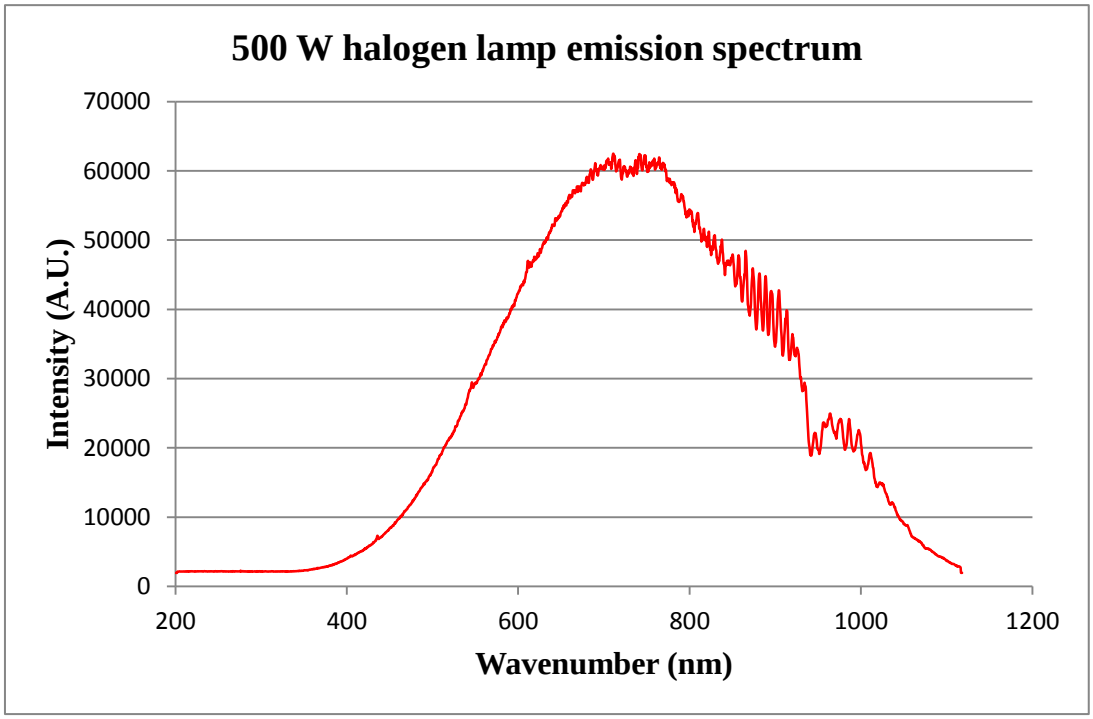

Figure C1: Emission spectrum of the 500 W halogen lamp.

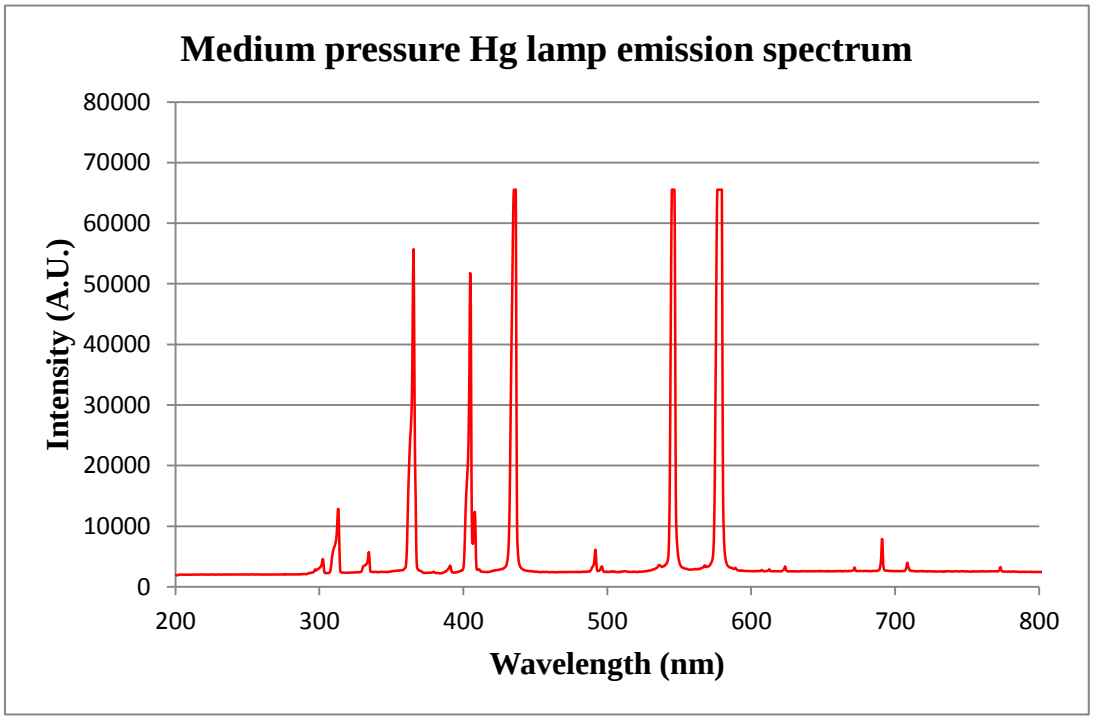

Figure C2: Emission spectrum of the medium pressure mercury lamp.

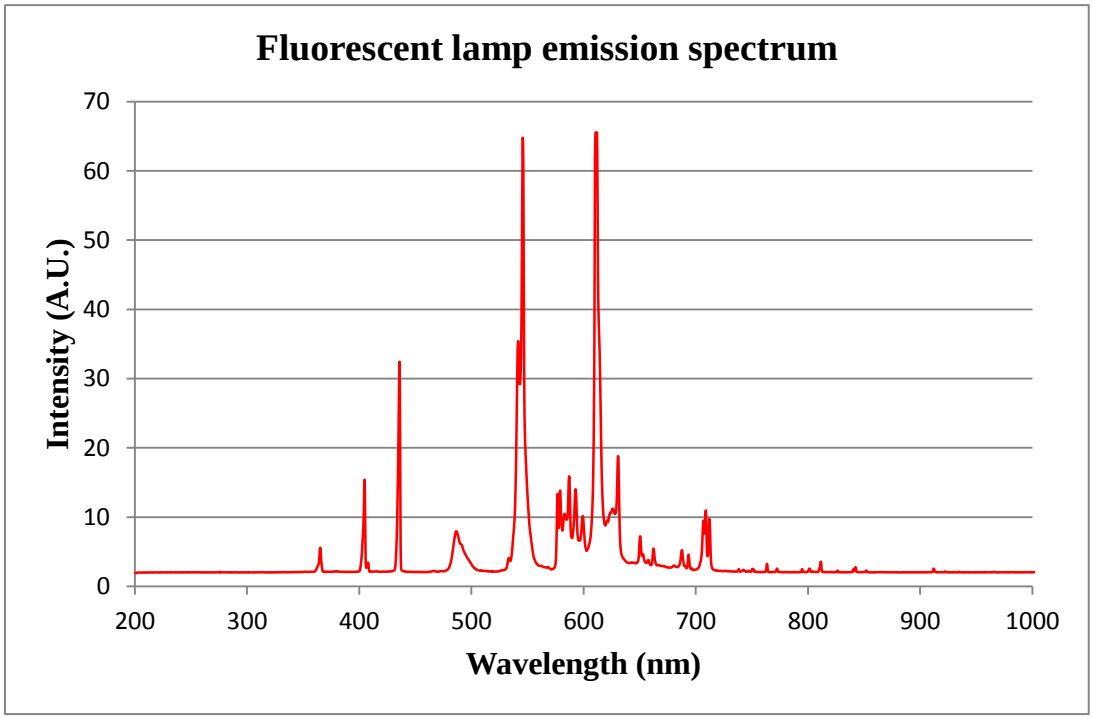

Figure C3: Emission spectrum of the fluorescent lamp.

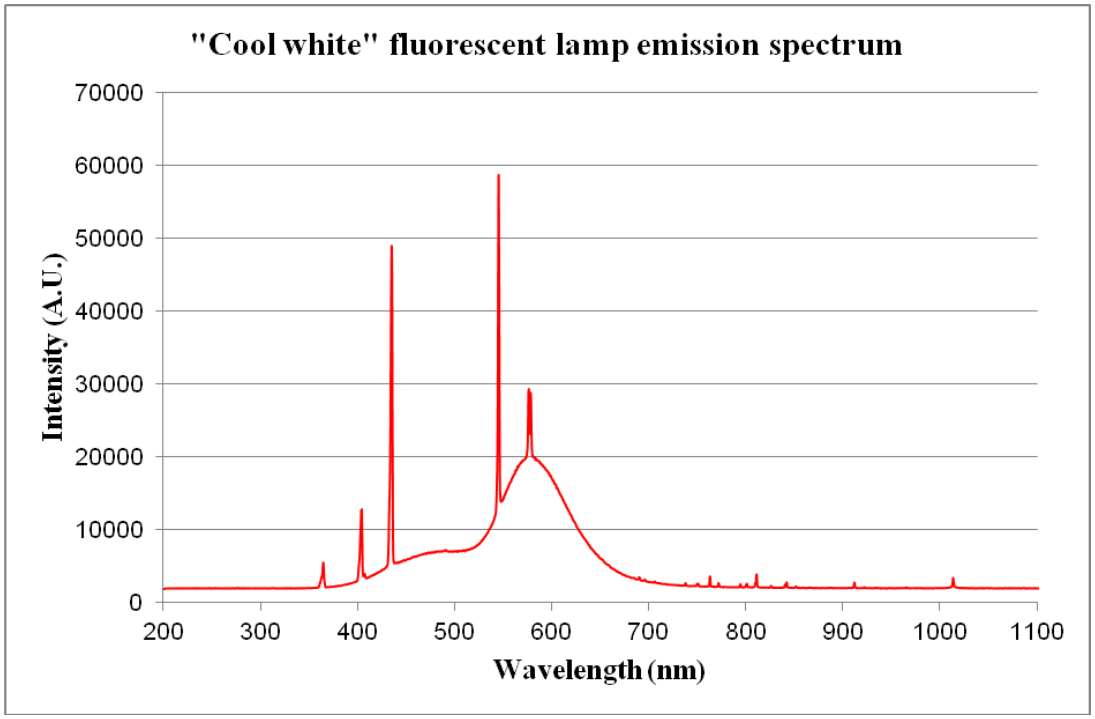

Figure C4: Emission spectrum of the "cool white" fluorescent lamp.

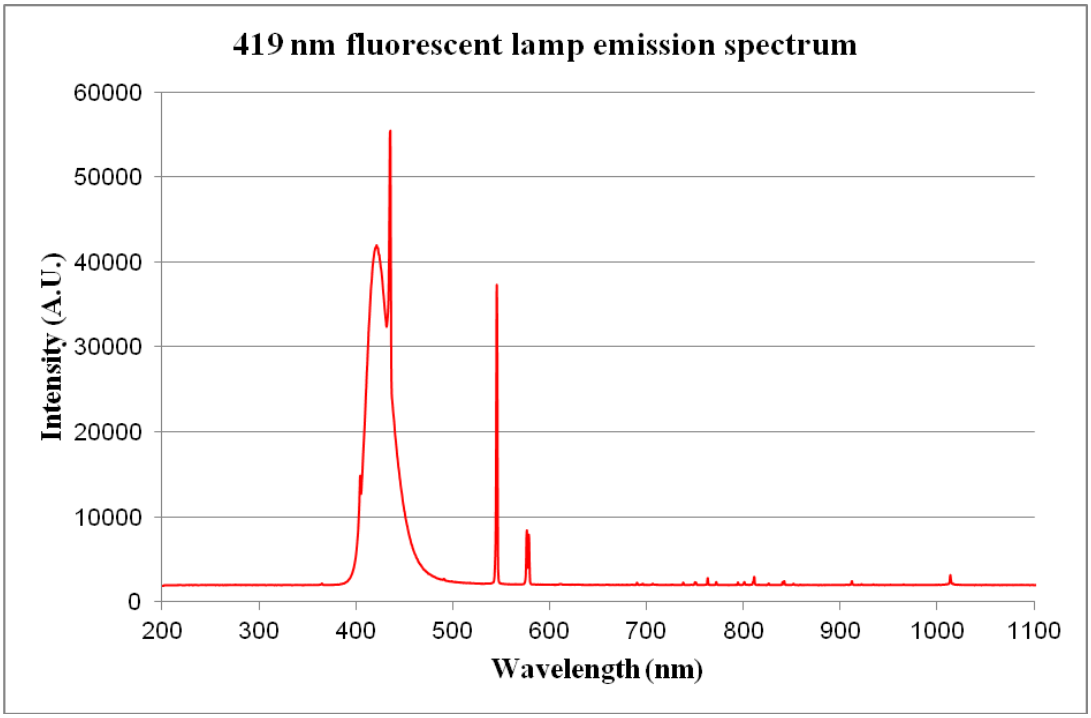

Figure C5: Emission spectrum of the 419 nm fluorescent lamp.

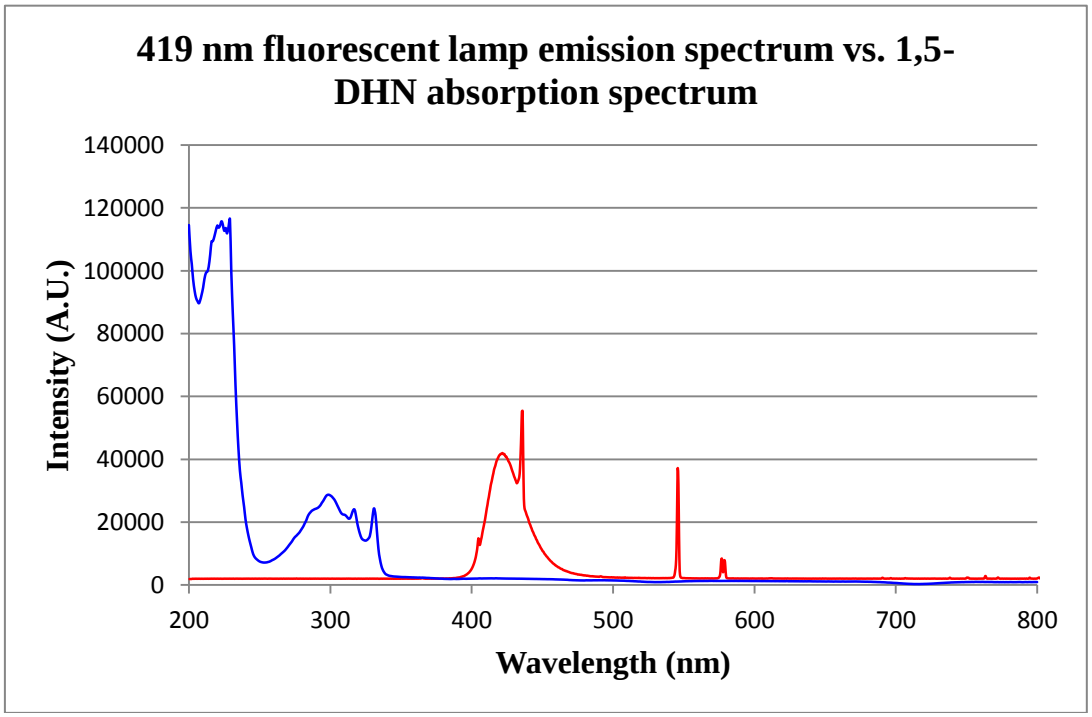

Figure C6: Emission spectrum of the 419 nm fluorescent lamp vs. absorption spectrum of 1,5-DHN.

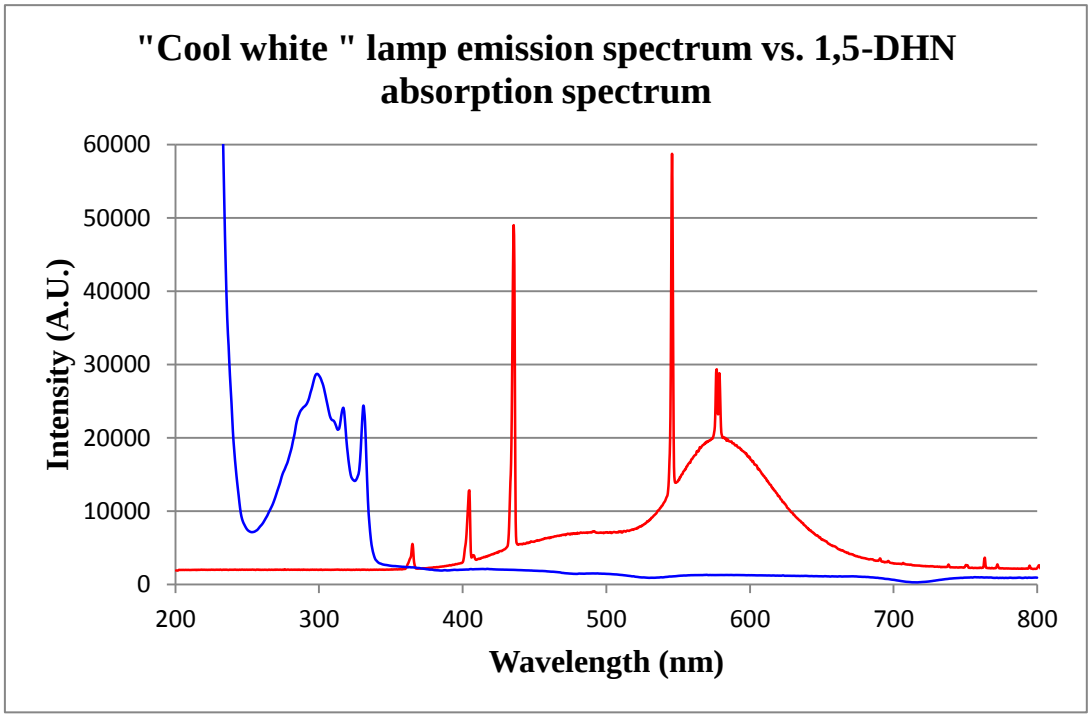

Figure C7: Emission spectrum of the "cool white" fluorescent lamp vs. absorption spectrum of 1,5-DHN.

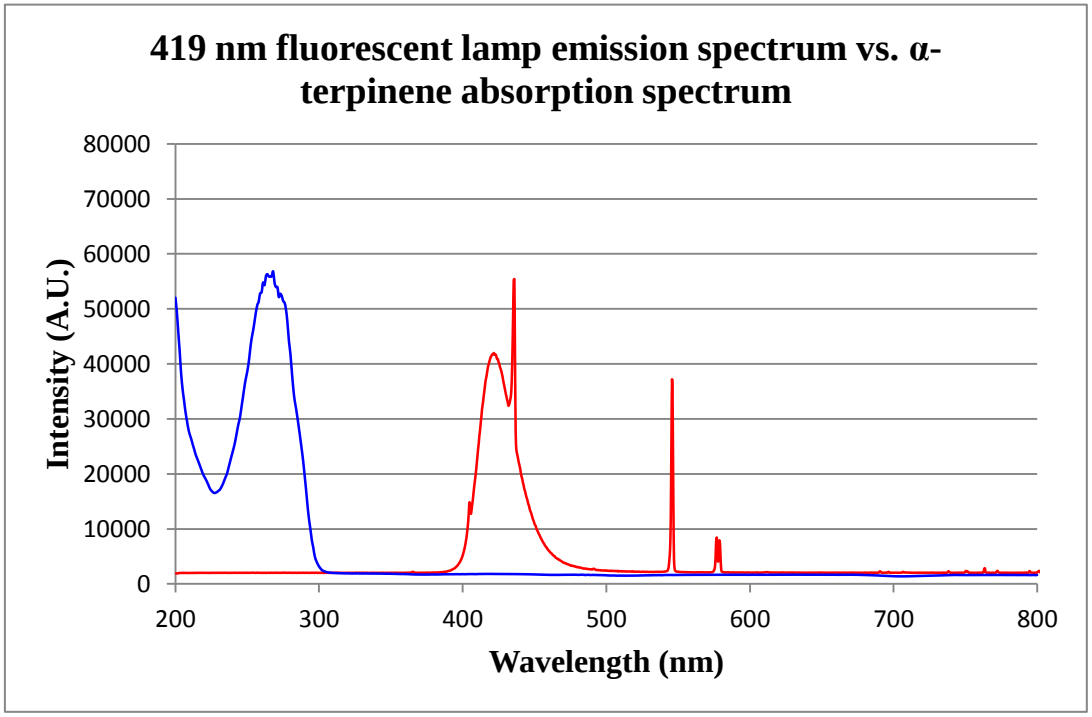

Figure C8 Emission spectrum of the 419 nm fluorescent lamp vs. absorption spectrum of α-terpinene.

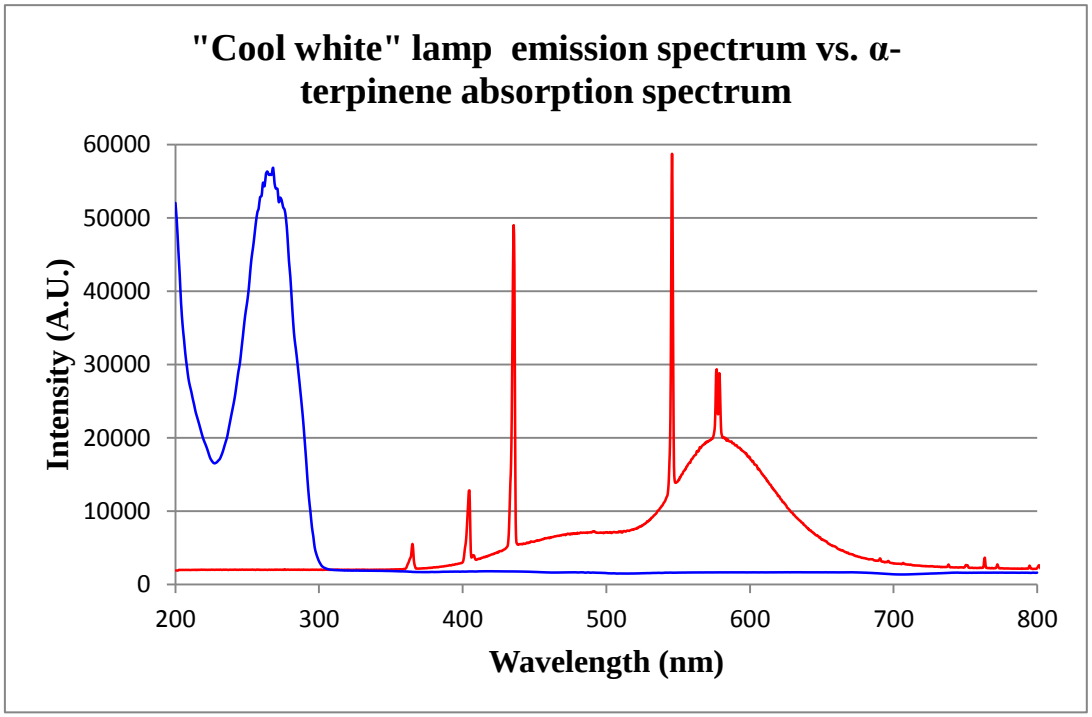

Figure C9: Emission spectrum of the "cool white" fluorescent lamp vs. absorption spectrum of α-terpinene.

D Schlenk flask and photochemical microflow system data

Table D1: Relevant data for the microflow system.

Microflow system	
Tube inner diameter	0.8 mm
Tuber inner radius	0.4 mm
Tube length	10,000 mm
Tube volume	5 ml
Tube surface area (irradiated)	251 cm^2
Irradiated area / volume (ratio)	50.2
Lamp power	8 W
Lamp power per irradiated area	0.032 $W.cm^{-2}$

Table D2: Relevant data for Schlenk flasks used in this work.

Schlenk Flasks		
	50 ml	**100 ml**
Irradiated area	85.41 cm^2	274.31 cm^2
Volume	50 ml	100 ml
Height of solvent	8.5 cm	27.3 cm
Irradiated area / volume (ratio)	1.71 $cm^2.cm^{-3}$	2.71 $cm^2.cm^{-3}$
Lamp power	500 W	500 W
Lamp power per irradiated area	5.85 $W.cm^{-2}$	1.82 $W.cm^{-2}$

D Calculated Energy Efficiencies

Energy efficiency calculations for 1,5-DHN in IPA using RB, MB and TCPP (MF reactor)

Exp No	1,5-DHN (mmol)	Sens	Area (cm2)	Lamp Power (W)	Volume (L)	Conversion (%)	Conv (mmol)	Res time (hr)	%/W/hr	%/W/hr/cm^2	mmol/W/hr	mmol/W/hr/cm^2
97a	0.09989	RB	251	8	0.005	30	0.0300	0.26	14.4231	0.0575	0.0144	5.73992E-05
97b	0.09989	MB	251	8	0.005	6	0.0060	0.26	2.8846	0.0115	0.0029	1.14798E-05
97c	0.09989	TCPP	251	8	0.005	89	0.0889	0.26	42.7885	0.1705	0.0427	0.000170284
95a	0.04995	RB	251	8	0.005	51	0.0255	0.26	24.5192	0.0977	0.0122	4.87942E-05
95b	0.04995	MB	251	8	0.005	19	0.0095	0.26	9.1346	0.0364	0.0046	1.81782E-05
95c	0.04995	TCPP	251	8	0.005	100	0.0500	0.26	48.0769	0.1915	0.0240	9.5675E-05
86	0.04995	none	251	8	0.005	0	0.0000	0.26	0.0000	0.0000	0.0000	0
89	0.04995	none	251	8	0.005	0	0.0000	0.26	0.0000	0.0000	0.0000	0

Energy efficiency calculation for 1,5-DHN in TAA using RB, MB and TCPP (MF reactor)

Exp No	1,5-DHN (mmol)	Sens	Area (cm2)	Lamp Power (W)	Volume (L)	Conversion (%)	Conv (mmol)	Res time (hr)	%/W/hr	%/W/hr/cm^2	mmol/W/hr	mmol/W/hr/cm^2
98a	0.09989	RB	251	8	0.005	21	0.0210	0.26	10.0962	0.0402	0.0101	4.01795E-05
98b	0.09989	MB	251	8	0.005	5	0.0050	0.26	2.4038	0.0096	0.0024	9.56654E-06
98c	0.09989	TCPP	251	8	0.005	100	0.0999	0.26	48.0769	0.1915	0.0480	0.000191331
96a	0.04995	RB	251	8	0.005	49	0.0245	0.26	23.5577	0.0939	0.0118	4.68807E-05
96b	0.04995	MB	251	8	0.005	5	0.0025	0.26	2.4038	0.0096	0.0012	4.78375E-06
96c	0.04995	TCPP	251	8	0.005	100	0.0500	0.26	48.0769	0.1915	0.0240	9.5675E-05
99	0.09989	TCPP	251	8	0.005	76	0.0759	0.081	117.2840	0.4673	0.1172	0.000466753

Energy efficiency calculation for 1,5-DHN in TAA using RB (Optimal Schlenk flask setup)

Exp No	1,5-DHN (mmol)	Sens	Area (cm2)	Lamp Power (W)	Volume (L)	Conversion (%)	Conv (mmol)	Res time (hr)	%/W/hr	%/W/hr/cm^2	mmol/W/hr	mmol/W/hr/cm^2
22	0.5	RB	85.41	500	0.05	65	0.325	3	0.0433	0.000507	0.000217	2.53678E-06

Energy efficiency calculations for BC in IPA using RB, MB and TCPP (MF reactor)

Exp No	BC (mmol)	Sens	Area (cm2)	Lamp Power (W)	Volume (L)	Conversion (%)	Conv (mmol)	Res time (hr)	%/W/hr	%/W/hr/cm^2	mmol/W/hr	mmol/W/hr/cm^2
102a	0.26	RB	251	8	0.005	77	0.2002	0.26	37.0192	0.1475	0.0963	0.000383466
102b	0.26	MB	251	8	0.005	49	0.1274	0.26	23.5577	0.0939	0.0613	0.000244024
102c	0.26	TCPP	251	8	0.005	74	0.1924	0.26	35.5769	0.1417	0.0925	0.000368526
100a	0.13	RB	251	8	0.005	83	0.1079	0.26	39.9038	0.1590	0.0519	0.000206673
100b	0.13	MB	251	8	0.005	45	0.0585	0.26	21.6346	0.0862	0.0281	0.000112052
100c	0.13	TCPP	251	8	0.005	100	0.13	0.26	48.0769	0.1915	0.0625	0.000249004

Energy efficiency calculation for BC in TAA using RB, MB and TCPP (MF reactor)

Exp No	BC (mmol)	Sens	Area (cm2)	Lamp Power (W)	Volume (L)	Conversion (%)	Conv (mmol)	Res time (hr)	%/W/hr	%/W/hr/cm^2	mmol/W/hr	mmol/W/hr/cm^2
103a	0.26	RB	251	8	0.005	100	0.26	0.26	48.0769	0.1915	0.1250	0.000498008
103b	0.26	MB	251	8	0.005	29	0.0754	0.26	13.9423	0.0555	0.0363	0.000144422
103c	0.26	TCPP	251	8	0.005	84	0.2184	0.26	40.3846	0.1609	0.1050	0.000418327
101a	0.13	RB	251	8	0.005	100	0.13	0.26	48.0769	0.1915	0.0625	0.000249004
101b	0.13	MB	251	8	0.005	58	0.0754	0.26	27.8846	0.1111	0.0363	0.000144422
101c	0.13	TCPP	251	8	0.005	100	0.13	0.26	48.0769	0.1915	0.0625	0.000249004

Energy efficiency calculation for BC in TAA and Acetone using RB, MB TPP and TCPP (Schlenk flask)

Exp No	BC (mmol)	Sens	Area (cm2)	Lamp Power (W)	Volume (L)	Conversion (%)	Conv (mmol)	Res time (hr)	%/W/hr	%/W/hr/cm^2	mmol/W/hr	mmol/W/hr/cm^2	Solvent
32	5.2	RB	85.41	500	0.05	44	2.288	2	0.0440	0.0005	0.0023	2.67884E-05	TAA
33	5.2	MB	85.41	500	0.05	52	2.704	2	0.0520	0.0006	0.0027	3.16591E-05	TAA
34	5.2	TCPP	85.41	500	0.05	51	2.652	2	0.0510	0.0006	0.0027	3.10502E-05	TAA
35	5.2	RB	85.41	500	0.05	62	3.224	2	0.0620	0.0007	0.0032	3.77473E-05	Acetone
36	5.2	MB	85.41	500	0.05	90	4.68	2	0.0900	0.0011	0.0047	5.47945E-05	Acetone
37	5.2	TCPP	85.41	500	0.05	60	3.12	2	0.0600	0.0007	0.0031	3.65297E-05	Acetone
38	5.2	TPP	85.41	500	0.05	86	4.472	2	0.0860	0.0010	0.0045	5.23592E-05	Acetone

Energy efficiency calculation for AT in IPA using RB, MB and TCPP (MF reactor)

Exp No	AT (mmol)	Sens	Area (cm2)	Lamp Power (W)	Volume (L)	Conversion (%)	Conv (mmol)	Res time (hr)	%/W/hr	%/W/hr/cm^2	mmol/W/hr	mmol/W/hr/cm^2
105a	0.26	RB	251	8	0.005	88	0.2288	0.26	42.3077	0.1686	0.1100	0.000438247
105b	0.26	MB	251	8	0.005	75	0.195	0.26	36.0577	0.1437	0.0938	0.000373506
105c	0.26	TCPP	251	8	0.005	86	0.2236	0.26	41.3462	0.1647	0.1075	0.000428287
104a	0.13	RB	251	8	0.005	100	0.13	0.26	48.0769	0.1915	0.0625	0.000249004
104b	0.13	MB	251	8	0.005	100	0.13	0.26	48.0769	0.1915	0.0625	0.000249004
104c	0.13	TCPP	251	8	0.005	100	0.13	0.26	48.0769	0.1915	0.0625	0.000249004
88	0.13	none	251	8	0.005	31	0.0403	0.26	14.9038	0.0594	0.0194	7.71912E-05
91	0.13	none	251	8	0.005	25	0.0325	0.26	12.0192	0.0479	0.0156	6.2251E-05

Energy efficiency calculation for AT in TAA and acetone using RB, MB, TPP and TCPP (Schlenk flask)

Exp No	AT (mmol)	Sens	Area (cm2)	Lamp Power (W)	Volume (L)	Conversion (%)	Conv (mmol)	Res time (min)	%/W/hr	%/W/hr/cm^2	mmol/W/hr	mmol/W/hr/cm^2	Solvent
29	5.2	RB	85.41	500	0.05	97	5.044	2	0.0970	0.0011	0.0050	5.90563E-05	TAA
30	5.2	MB	85.41	500	0.05	15	0.78	2	0.0150	0.0002	0.0008	9.13242E-06	TAA
31	5.2	TCPP	85.41	500	0.05	100	5.2	2	0.1000	0.0012	0.0052	6.08828E-05	TAA
24	5.2	RB	85.41	500	0.05	58	3.016	2	0.0580	0.0007	0.0030	3.5312E-05	Acetone
25	5.2	MB	85.41	500	0.05	42	2.184	2	0.0420	0.0005	0.0022	2.55708E-05	Acetone
26	5.2	TPP	85.41	500	0.05	61	3.172	2	0.0610	0.0007	0.0032	3.71385E-05	Acetone

Energy efficiency calculations for BC in IPA using TCPP SNPs (MF reactor)

Exp No	BC (mmol)	Sens	Area (cm2)	Lamp Power (W)	Volume (L)	Conversion (%)	Conv (mmol)	Res time (hr)	%/W/hr	%/W/hr/cm^2	mmol/W/hr	mmol/W/hr/cm^2
109	0.26	TCPP	251	8	0.005	16	0.0416	0.26	7.6923	0.0306	0.0200	7.96813E-05
108	0.13	TCPP	251	8	0.005	27	0.0351	0.26	12.9808	0.0517	0.0169	6.72311E-05

Energy efficiency calculations for AT in IPA using TCPP SNPs (MF reactor)

Exp No	AT (mmol)	Sens	Area (cm2)	Lamp Power (W)	Volume (L)	Conversion (%)	Conv (mmol)	Res time (hr)	%/W/hr	%/W/hr/cm^2	mmol/W/hr	mmol/W/hr/cm^2
111	0.26	TCPP	251	8	0.005	48	0.1248	0.26	23.0769	0.0919	0.0600	0.000239044
110	0.13	TCPP	251	8	0.005	97	0.1261	0.26	46.6346	0.1858	0.0606	0.000241534

Energy efficiency calculations for 1,5-DHN in IPA using TCPP SNPs (MF reactor)

Exp No	DHN (mmol)	Sens	Area (cm2)	Lamp Power (W)	Volume (L)	Conversion (%)	Conv (mmol)	Res time (hr)	%/W/hr	%/W/hr/cm^2	mmol/W/hr	mmol/W/hr/cm^2
106	0.04995	TCPP	251	8	0.005	16	0.007992	0.26	7.6923	0.0306	0.0038	1.5308E-05
107	0.09989	TCPP	251	8	0.005	7	0.006992	0.26	3.3654	0.0134	0.0034	1.33932E-05

Energy efficiency calculations for BC in IPA using TCPP MNPs (MF reactor)

Exp No	BC (mmol)	Sens	Area (cm2)	Lamp Power (W)	Volume (L)	Conversion (%)	Conv (mmol)	Res time (hr)	%/W/hr	%/W/hr/cm^2	mmol/W/hr	mmol/W/hr/cm^2
116	0.26	TCPP	251	8	0.005	5	0.013	0.26	2.4038	0.0096	0.0063	2.49004E-05
115	0.13	TCPP	251	8	0.005	11	0.0143	0.26	5.2885	0.0211	0.0069	2.73904E-05

Energy efficiency calculations for AT in IPA using TCPP MNPs (MF reactor)

Exp No	BC (mmol)	Sens	Area (cm2)	Lamp Power (W)	Volume (L)	Conversion (%)	Conv (mmol)	Res time (hr)	%/W/hr	%/W/hr/cm^2	mmol/W/hr	mmol/W/hr/cm^2
118	0.26	TCPP	251	8	0.005	32	0.0832	0.26	15.3846	0.0613	0.0400	0.000159363
117	0.13	TCPP	251	8	0.005	40	0.052	0.26	19.2308	0.0766	0.0250	9.96016E-05

Energy efficiency calculations for 1,5-DHN in IPA using TCPP MNPs (MF reactor)

Exp No	BC (mmol)	Sens	Area (cm2)	Lamp Power (W)	Volume (L)	Conversion (%)	Conv (mmol)	Res time (hr)	%/W/hr	%/W/hr/cm^2	mmol/W/hr	mmol/W/hr/cm^2
114	0.09989	TCPP	251	8	0.005	9	0.00899	0.26	4.3269	0.0172	0.0043	1.72198E-05
113	0.04995	TCPP	251	8	0.005	21	0.01049	0.26	10.0962	0.0402	0.0050	2.00917E-05

E Calculated Space Time Yields

STYs for 1,5-DHN in IPA using RB, MB and TCPP (Microflow system)

Exp No	1,5-DHN (mM)	1,5-DHN (mmol)	Sens	Solvent	Volume (L)	Conversion (%)	Conversion	Conv (mmol)	Res time (min)	STY (mmol.L^{-1}.min^{-1})
97a	20	0.09989	RB	IPA	0.005	30	0.3	0.0300	15.82	0.3788
97b	20	0.09989	MB	IPA	0.005	6	0.06	0.0060	15.82	0.0758
97c	20	0.09989	TCPP	IPA	0.005	89	0.89	0.0889	15.82	1.1239
95a	10	0.04995	RB	IPA	0.005	51	0.51	0.0255	15.82	0.3221
95b	10	0.04995	MB	IPA	0.005	19	0.19	0.0095	15.82	0.1200
95c	10	0.04995	TCPP	IPA	0.005	100	1	0.0500	15.82	0.6315
86	10	0.04995	None	IPA	0.005	0	0	0.0000	15.82	0.0000
89	10	0.04995	None	IPA	0.005	0	0	0.0000	15.82	0.0000

STYs for 1,5-DHN in TAA using RB, MB and TCPP (Microflow system)

Exp No	1,5-DHN (mM)	1,5-DHN (mmol)	Sens	Solvent	Volume (L)	Conversion (%)	Conversion	Conv (mmol)	Res time (min)	STY (mmol.L^{-1}.min^{-1})
98a	20	0.09989	RB	TAA	0.005	21	0.21	0.0210	15.82	0.2652
98b	20	0.09989	MB	TAA	0.005	5	0.05	0.0050	15.82	0.0631
98c	20	0.09989	TCPP	TAA	0.005	100	1	0.0999	15.82	1.2628
96a	10	0.04995	RB	TAA	0.005	49	0.49	0.0245	15.82	0.3094
96b	10	0.04995	MB	TAA	0.005	5	0.05	0.0025	15.82	0.0316
96c	10	0.04995	TCPP	TAA	0.005	100	1	0.0500	15.82	0.6315
99	20	0.09989	TCPP	TAA	0.005	76	0.76	0.0759	4.86	3.1241

STY for 1,5-DHN in TAA using RB (Schlenk flask)

Exp No	1,5-DHN (mM)	1,5-DHN (mmol)	Sens	Solvent	Volume (L)	Conversion (%)	Conversion	Conv (mmol)	Res time (min)	STY (mmol.L^{-1}.min^{-1})
22	10	0.5	RB	TAA	0.05	65	0.65	0.325	180	0.0361

STY for 1,5-DHN in TAA using RB (Solar Schlenk flask)

Exp No	AGR	1,5-DHN (mM)	1,5-DHN (mmol)	Sens	Solvent	Volume (L)	Conversion (%)	Conversion	Conv (mmol)	Res time (min)	STY (mmol.L^{-1}.min^{-1})
39	238	18.7	1.87	RB	TAA	0.1	69	0.69	1.2903	180	0.0717
40	183	18.7	1.87	RB	TAA	0.1	33	0.33	0.6171	180	0.0343
41	183	18.7	1.87	RB	TAA	0.1	34	0.34	0.6358	180	0.0353
42	130	18.7	1.87	RB	TAA	0.1	26	0.26	0.4862	300	0.0162

STY for 1,5-DHN in TAA and IPA using RB (2nd generation flatbed reactor)

Exp No	AGR	1,5-DHN (mM)	1,5-DHN (mmol)	Sens	Solvent	Volume (L)	Conversion (%)	Conversion	Conv (mmol)	Res time (min)	STY (mmol.L^{-1}.min^{-1})
48	190	10	80	RB	IPA	8	72	0.72	57.6000	360	0.0200
49	190	10	80	RB	TAA	8	85	0.85	68.0000	360	0.0236

STYs for BC in IPA using RB, MB and TCPP (Microflow system)

Exp No	BC (microL)	BC (mmol)	Sens	Solvent	Volume (L)	Conversion (%)	Conversion	Conv (mmol)	Res time (min)	STY (mmol.L^{-1}.min^{-1})
102a	52	0.26	RB	IPA	0.005	77	0.77	0.2002	15.82	2.5310
102b	52	0.26	MB	IPA	0.005	49	0.49	0.1274	15.82	1.6106
102c	52	0.26	TCPP	IPA	0.005	74	0.74	0.1924	15.82	2.4324
100a	26	0.13	RB	IPA	0.005	83	0.83	0.1079	15.82	1.3641
100b	26	0.13	MB	IPA	0.005	45	0.45	0.0585	15.82	0.7396
100c	26	0.13	TCPP	IPA	0.005	100	1	0.1300	15.82	1.6435
87	26	0.13	None	IPA	0.005	0	0	0.0000	15.82	0.0000
90	26	0.13	None	IPA	0.005	0	0	0.0000	15.82	0.0000

STYs for BC in TAA using RB, MB and TCPP (Microflow system)

Exp No	BC (microL)	BC (mmol)	Sens	Solvent	Volume (L)	Conversion (%)	Conversion	Conv (mmol)	Res time (min)	STY (mmol.L^{-1}.min^{-1})
103a	52	0.26	RB	TAA	0.005	63	0.63	0.1638	15.82	2.0708
103b	52	0.26	MB	TAA	0.005	29	0.29	0.0754	15.82	0.9532
103c	52	0.26	TCPP	TAA	0.005	84	0.84	0.2184	15.82	2.7611
101a	26	0.13	RB	TAA	0.005	100	1	0.1300	15.82	1.6435
101b	26	0.13	MB	TAA	0.005	58	0.58	0.0754	15.82	0.9532
101c	26	0.13	TCPP	TAA	0.005	100	1	0.1300	15.82	1.6435

STYs for BC in TAA and Acetone using RB, MB, TPP and TCPP (Schlenk flask)

Exp No	BC (mM)	BC (mmol)	Sens	Solvent	Volume (L)	Conversion (%)	Conversion	Conv (mmol)	Res time (min)	STY (mmol.L^{-1}.min^{-1})
32	104	5.2	RB	TAA	0.05	44	0.44	2.288	120	0.3813
33	104	5.2	MB	TAA	0.05	52	0.52	2.704	120	0.4507
34	104	5.2	TCPP	TAA	0.05	51	0.51	2.652	120	0.4420
35	104	5.2	RB	Acetone	0.05	62	0.62	3.224	120	0.5373
36	104	5.2	MB	Acetone	0.05	90	0.9	4.68	120	0.7800
37	104	5.2	TCPP	Acetone	0.05	60	0.6	3.12	120	0.5200
38	104	5.2	TPP	Acetone	0.05	86	0.86	4.472	120	0.7453

STYs for BC in TAA using RB (2nd generation flat bed reactor)

Exp No	BC (mM)	BC (mmol)	Sens	Solvent	Volume (L)	Conversion (%)	Conversion	Conv (mmol)	Res time (min)	STY (mmol.L^{-1}.min^{-1})
50	40	200	RB	TAA	5	100	1	200	240	0.1667

STYs for AT in IPA using RB, MB and TCPP (Microflow system)

Exp No	AT (microL)	AT (mmol)	Sens	Solvent	Volume (L)	Conversion (%)	Conversion	Conv (mmol)	Res time (min)	STY (mmol.L^{-1}.min^{-1})
105a	52	0.26	RB	IPA	0.005	88	0.88	0.2288	15.82	2.8925
105b	52	0.26	MB	IPA	0.005	75	0.75	0.1950	15.82	2.4652
105c	52	0.26	TCPP	IPA	0.005	86	0.86	0.2236	15.82	2.8268
104a	26	0.13	RB	IPA	0.005	100	1	0.1300	15.82	1.6435
104b	26	0.13	MB	IPA	0.005	100	1	0.1300	15.82	1.6435
104c	26	0.13	TCPP	IPA	0.005	100	1	0.1300	15.82	1.6435
88	26	0.13	none	IPA	0.005	31	0.31	0.0403	15.82	0.5095
91	26	0.13	none	IPA	0.005	25	0.25	0.0325	15.82	0.4109

STYs for AT in TAA and Acetone using RB, MB, TPP and TCPP (Schlenk flask)

Exp No	AT (mM)	AT (mmol)	Sens	Solvent	Volume (L)	Conversion (%)	Conversion	Conv (mmol)	Res time (min)	STY (mmol.L^{-1}.min^{-1})
24	104	5.2	RB	TAA	0.05	97	0.97	5.044	120	0.8407
25	104	5.2	MB	TAA	0.05	15	0.15	0.78	120	0.1300
26	104	5.2	TCPP	TAA	0.05	100	1	5.2	120	0.8667
29	104	5.2	RB	Acetone	0.05	58	0.58	3.016	120	0.5027
30	104	5.2	MB	Acetone	0.05	42	0.42	2.184	120	0.3640
31	104	5.2	TPP	Acetone	0.05	61	0.61	3.172	120	0.5287

STYs for AT in TAA RB (Solar Schlenk flask)

Exp No	AT (mM)	AT (mmol)	Sens	Solvent	Volume (L)	Conversion (%)	Conversion	Conv (mmol)	Res time (min)	STY (mmol.L^{-1}.min^{-1})
45	52	5.2	RB	TAA	0.1	66	0.66	3.432	300	0.1144
46	260	26	RB	TAA	0.1	45	0.45	11.7	180	0.6500

STYs for AT in IPA using TCPP SNPs (Microflow system)

Exp No	AT (microL)	AT (mmol)	Sens	Solvent	Volume (L)	Conversion (%)	Conversion	Conv (mmol)	Res time (min)	STY (mmol.L^{-1}.min^{-1})
111	52	0.26	TCPP SNP	IPA	0.005	48	0.48	0.1248	15.82	1.5777
110	26	0.13	TCPP SNP	IPA	0.005	97	0.97	0.1261	15.82	1.5942

STYs for BC in IPA using TCPP SNPs (Microflow system)

Exp No	BC (microL)	BC (mmol)	Sens	Solvent	Volume (L)	Conversion (%)	Conversion	Conv (mmol)	Res time (min)	STY (mmol.L^{-1}.min^{-1})
109	52	0.26	TCPP SNP	IPA	0.005	16	0.16	0.0416	15.82	0.5259
108	26	0.13	TCPP SNP	IPA	0.005	23	0.23	0.0299	15.82	0.3780

STYs for 1,5-DHN in IPA using TCPP SNPs (Microflow system)

Exp No	DHN (mg)	BC (mmol)	Sens	Solvent	Volume (L)	Conversion (%)	Conversion	Conv (mmol)	Res time (min)	STY (mmol.L^{-1}.min^{-1})
106	10	0.04995	TCPP SNP	IPA	0.005	16	0.16	0.0080	15.82	0.1010
107	20	0.09989	TCPP SNP	IPA	0.005	7	0.07	0.0070	15.82	0.0884

STYs for AT in IPA using TCPP MNPs (Microflow system)

Exp No	AT (microL)	AT (mmol)	Sens	Solvent	Volume (L)	Conversion (%)	Conversion	Conv (mmol)	Res time (min)	STY (mmol.L^{-1}.min^{-1})
118	52	0.26	TCPP MNP	IPA	0.005	32	0.32	0.0832	15.82	1.0518
117	26	0.13	TCPP MNP	IPA	0.005	40	0.4	0.0520	15.82	0.6574

STYs for BC in IPA using TCPP MNPs (Microflow system)

Exp No	BC (microL)	BC (mmol)	Sens	Solvent	Volume (L)	Conversion (%)	Conversion	Conv (mmol)	Res time (min)	STY (mmol.L^{-1}.min^{-1})
116	52	0.26	TCPP MNP	IPA	0.005	5	0.05	0.0130	15.82	0.1643
115	26	0.13	TCPP MNP	IPA	0.005	11	0.11	0.0143	15.82	0.1808

STYs for 1,5-DHN in IPA using TCPP MNPs (Microflow system)

Exp No	DHN (mg)	BC (mmol)	Sens	Solvent	Volume (L)	Conversion (%)	Conversion	Conv (mmol)	Res time (min)	STY (mmol.L^{-1}.min^{-1})
113	10	0.04995	TCPP MNP	IPA	0.005	21	0.21	0.0105	15.82	0.1326
114	20	0.09989	TCPP MNP	IPA	0.005	9	0.09	0.0090	15.82	0.1137